INVESTIGATION INTO FINE NON-COHESIVE SEDIMENT REMOVAL BY SWIRL/VORTEX SETTLING BASINS AT SMALL RIVER ABSTRACTION WORKS

Kuria Kiringu

Dissertation presented for the degree of
Doctor *of Philosophy in Civil Engineering*
in the Faculty of Engineering
at Stellenbosch University

Promotor: Prof. G.R. Basson

March 2020

The financial assistance of the South Africa Water Research Commission (WRC) towards this research is hereby acknowledged. Opinions expressed and conclusions arrived at, are those of the author and are not necessarily to be attributed to the WRC.

DECLARATION

By submitting this dissertation electronically, I declare that the entirety of the work contained therein is my own, original work, that I am the authorship owner thereof (unless to the extent explicitly otherwise stated), that reproduction and publication thereof by Stellenbosch University will not infringe any third-party rights and that I have not previously in its entirety or in part submitted it for obtaining any qualification.

March 2020

ABSTRACT

The often fine non-cohesive and cohesive nature of sediments in South African rivers makes sediment management at river abstraction works rather complex. Sediment removal at river abstraction works is essential for the protection of the pumps and pipelines. A wide range of sediment control design guidelines for large abstraction works are available, but these are not applicable for small abstraction works with a duty pump capacity of less than 100 l/s (7.2 Ml/d at 20 h/d), which is typical for rural potable water schemes in Africa.

For sediment removal of fine non-cohesive sediment at small abstraction works, Vortex settling basins (VSBs) offer a promising alternative to conventional sediment settling structures such as sand traps, settlers, hoppers with jet pumps or primary settling tanks. VSBs have a small footprint, no moving parts, require no chemical dosing and continuously flush sediment back to the river. This study seeks to furnish the hydraulic designers with parameters for an optimized design of a VSB.

Numerous computational fluid dynamics (CFD) model simulations were carried out using the software package ANSYS FLUENT and validated against two physical VSB models: 0.48 m diameter and 0.7 m high, as well as 0.68 m diameter and 1.0 m high. These tests indicated that non-cohesive sediment removal in a VSB is mainly gravity driven and centrifugal forces play an essential role in keeping particles in suspension near the outer wall, thus increasing residence time.

The inlet velocity, the diameter and height of the VSB, underflow, deflectors, sediment size and concentration, the location and type of outlet structure all play important roles in controlling the sediment trap efficiency. The cone angle and the angle of inlet effects are minimal.

The following design ratios are recommended: $\frac{\text{Underflow}(Q_u)}{\text{Inflow}(Q_i)}$ = 0.05-0.10, $\frac{\text{position of inlet}(H_i)}{\text{cylinder height }(H_t)}$ = 0.50-0.88, $\frac{\text{Cylinder height }(H_t)}{\text{cylinder diameter }(D)}$>0.5, $\frac{\text{Cylinder diameter}(D)}{\text{Inlet diameter }(D_i)}$ = 8.2 and inlet velocity of 0.26 m/s. Deflectors of length = Di extending 180° clockwise and 70° anticlockwise, inclined at an angle 1:2 (H:V), just above the inlet were found to give maximum efficiency combined with a rectangular central outlet length =1.28 Di, width=Di and height =Di, located at 180° opposite the inlet. With these findings two VSB designs are proposed: (a) for an inflow of 5 l/s with 5% water loss at a 99% trapping efficiency for sediment particles as small as 75µm in diameter and maximum inflow sediment concentration of 10,000 mg/l, and (b) for an inflow of 10 l/s with 8% water loss at a 91% trapping efficiency for sediment particles 75 µm in diameter and maximum inflow sediment concentration of 10,000 mg/l.

A possible river abstraction works layout incorporating VSBs is suggested for abstraction discharges smaller than 100 l/s for use by rural small local authorities for potable use.

OPSOMMING

Die aard van fyn nie-kohesiewe en kohesiewe sediment in Suid Afrikaanse riviere maak sediment bestuur vir water onttrekking uit riviere gekompliseerd. Verwydering van sediment vir wateronttrekking uit riviere is belangrik vir die beskerming van pompe en pyplyne. ‘n Wye reeks sedimentbeheer riglyne vir groot wateronttrekking skemas uit riviere is beskikbaar, maar dit is nie die geval vir riglyne vir klein wateronttrekkingskemas (kleiner as 100 l/s of 7.2 Ml/d) nie – soos vir tipiese wateronttrekking hoeveelhede in die platteland in Afrika.

“Vortex” besinkings-bakke (VSB’s) is ‘n aantreklike alternatief vir konvensionele sediment besinking-strukture soos “sand traps”, “settlers”, “hoppers” met “jet pumps”, of primêre sedimenttenke. VSBs het ‘n klein omgewingsvoetspoor, het geen bewegende dele nie, benodig geen chemikalieë nie en spoel voortdurend sediment terug na die rivier. Hierdie studie poog om ontwerpriglyne vir VSB’s daar te stel.

Verskeie “CFD” model simulasies is in hierdie studie uigevoer met die numeriese model “ANSYS FLUENT” en gekontroleer teen twee fisiese VSB modelle: 0.48 m diameter met ‘n hoogte van 0.7 m, asook 0.68 m diameter met ‘n hoogte van 1.0 m. Die resultate van die toetse het aangedui dat nie-kohesiewe sediment verwydering in ‘n VSB is hoofsaaklik gravitasie gedrewe en sentrifugale kragte speel ‘n belangrike rol om die partikels in suspensie te hou naby die buitewand van die VSB om so die “residence” tyd van sediment te verleng.

Die inlaat snelheid, diameter en hoogte van die VSB, onderuitlaat, deflektors, sedimentgroottes en konsentrasie, posisie en tipe uitlaat struktuur speel ‘n belangrike rol in die sediment besinkings- effektiwiteit. Die invloed van die keëlhoek en die hoek van die inlaat is minimaal.

Die volgende verhoudings word voorgestel: $\frac{\text{onderloop}(Q_u)}{\text{inlaat vloei}(Q_i)}$ = 0.05-0.10, $\frac{\text{posisie van inlaat}(H_i)}{\text{silinder hoogte }(H_t)}$ = 0.50-0.88, $\frac{\text{silinder hoogte }(H_t)}{\text{silinder diameter }(D)}$>0.5, $\frac{\text{silinder diameter }(D)}{\text{inlaat diameter }(D_i)}$ = 8.2 en ‘n inlaat snelheid van 0.26 m/s.

Die studie het getoon dat deflektor lengte = Di wat 180° kloksgewys en 70° antikloksgewys verleng is, met ‘n helling van 1:2 (H:V) net bo die inlaat, die maksimum effektiwiteit gee as dit gekombineer word met ‘n reghoekige sentrale uitlaatlengte van 1.28 Di, wydte=Di and hoogte =Di, geplaas 180° oorkant die inlaatVanuit die studie se bevindinge word twee VSB ontwerpe voorgestel: (a) met ‘n inlaat vloeitempo van 5 l/s met 5 % waterverliese met ‘n 99 % sediment besinkings-effektiwiteit vir sedimentpartikels tot so klein as 75µm in diameter en maksimum inlaatvloei sediment konsentrasie van 10,000 mg/l, en (b) met ‘n inlaat vloeitempo van 10 l/s met 8% waterverliese met 91 % sediment besinkings-effektiwiteit vir sedimentpartikels 75 µm in diameter en maksimum inlaat vloei sediment konsentrasie van 10,000 mg/l.

‘n Potensiële VSB geïnkorporeerde uitleg word voorgestel vir wateronttrekking uit riviere vir vloeitempo’s kleiner as 100 l/s.

ACKNOWLEDGEMENTS

The financial assistance of the South Africa Water Research Commission (WRC) towards this research is hereby acknowledged and the Council for Scientific and Industrial Research (CSIR) for access to Centre for High Performance (CHPC). Opinions expressed and conclusions arrived at, are those of the author and are not necessarily to be attributed to the WRC and CSIR.

In addition, the following people deserve acknowledgement for their assistance in making this dissertation project possible:

- Prof GR Basson, my supervisor and Mr Eddie D E Bosman, for guidance throughout my study program;
- My family, colleagues and friends for the incredible support.

TABLE OF CONTENTS

DECLARATION I
ABSTRACT II
OPSOMMING III
ACKNOWLEDGEMENTS IV
TABLE OF CONTENTS V
LIST OF FIGURES IX
LIST OF TABLES XVIII
ACRONYMS XX
1 Introduction 1
1.1 Background 1
1.2 Motivation for this study 2
2 Literature study and theoretical background 3
2.1 Overview of sediment removal mechanisms 3
2.2 Conventional settler 3
2.3 Hydro-cyclones 6
2.4 Vortex settling basin 8
2.4.1 Basin diameter (D) 10
2.4.2 Cone slope 11
2.4.3 Underflow 11
2.4.4 Flow depth to diameter ratio 11
2.4.5 Geometric configuration and deflectors 11
2.4.6 Centroid outlet 13
2.4.7 Efficiency removal prediction 15
2.4.8 Design example 15
2.5 Sediment characteristics in South African river abstraction works 16
2.6 Abstraction location and secondary flow 16
2.7 Numerical modelling 17
2.7.1 Introduction 17
2.7.2 Summary of governing equations. 18

3 Research Methodology 23
3.1 Justification for parameters selected 27
3.2 Laboratory model setup 30
3.3 Physical model test procedure 33
3.4 Numerical modelling 33
3.5 Parameters to be tested 38
4 Results and analysis 39
4.1 Overview of the Chapter 39
4.2 Influence of underflow, Qu 41
4.2.1 Introduction 41
4.2.2 Sediment trapping efficiency 42
4.2.3 Flow field 45
4.2.4 Turbulent kinetic energy, TKE 51
4.2.5 Conclusion on underflow 52
4.3 Location and size of the outlet 54
4.3.1 Introduction 54
4.3.2 Sediment trapping efficiency 55
4.3.3 Flow field 58
4.3.4 Conclusion on outlet location, outlet sector size 65
4.4 Inlet velocity, Vi 66
4.4.1 Introduction 66
4.4.2 Sediment trapping efficiency 66
4.4.3 Flow field 68
4.4.4 Turbulent kinetic energy, TKE 71
4.4.5 Conclusion on inlet velocity 72
4.5 Inflow rate influence, Qi 73
4.6 Inlet position to cylinder height, Hi/Ht 74
4.6.1 Introduction 74
4.6.2 Sediment trapping efficiency 74
4.6.3 Flow field 75
4.6.4 Conclusion on inlet position 79
4.7 Angle of inlet 80

4.7.1 Introduction 80
4.7.2 Sediment trapping efficiency 80
4.7.3 Flow field 81
4.7.4 Conclusion on the angle of inlet 84
4.8 Cylinder height to cylinder diameter, Ht/D 85
4.8.1 Introduction 85
4.8.2 Sediment trapping efficiency 85
4.8.3 Conclusion on cylinder height 87
4.9 Cone angle 88
4.9.1 Introduction 88
4.9.2 Sediment trapping efficiency 88
4.9.3 Conclusion on the cone angle 89
4.10 Cylinder diameter influence, D 90
4.10.1 Introduction 90
4.10.2 Sediment trapping efficiency 90
4.10.3 Flow field 94
4.10.4 Turbulent kinetic energy, TKE 98
4.10.5 Conclusion on cylinder diameter 98
4.11 Deflectors 99
4.11.1 Introduction 99
4.11.2 Deflector 1 optimisation 100
4.11.3 Deflector 1-2 optimization 101
4.11.4 Deflector 1-2-3 optimization 102
4.11.5 Deflector 1-2-3-4-5 optimization 103
4.11.6 Limitation of Model 1 configuration 105
4.11.7 Conclusion on Model 1 deflectors 106
4.12 Outlet structure 106
4.12.1 Introduction 106
4.12.2 Configuration II 107
4.12.3 Configuration III 112
4.12.4 Conclusion on outlet structure configuration 119
5 Proposed layout based on VSB parameter study 120

5.1 Introduction 120
5.2 Sediment trapping efficiency 125
5.3 Axial velocity 125
5.4 Tangential velocity 127
5.5 Turbulent kinetic energy, TKE 128
5.6 Conclusion on the proposed layout 129
6 Practical considerations 130
7 Final conclusion and recommendations 138
8 References 140
9 Appendix A 144
9.1 Experimental data 144
9.2 Experimental data results 150
9.3 Design of drop inlet 157

LIST OF FIGURES

Figure 2-1: Several options available to remove sediment particles (adapted from Green and Southard (2019)) 3

Figure 2-2: Settling velocity of natural sand (Interagency Committee, 1957) 4

Figure 2-3: Illustration of settling basin principles (adapted from NPTEL (2018)) 5

Figure 2-4: Batchwise washout settler (Bouvard, 1992) 6

Figure 2-5: Illustration of hydro-cyclone mechanism (adapted from MULTOTEC (2018) and Richardson et al. (2002)) 7

Figure 2-6: Illustration of typical velocity distribution in hydro-cyclone (LZVV is locus of zero axial velocity) (adapted from Richardson et al. (2002)) 7

Figure 2-7: Illustration of sediment particle motion path coloured by average hydraulic retention time 8

Figure 2-8: Forces acting on a sediment particle in Fluid motion (adapted from Gronowska (2012)) 9

Figure 2-9: Different model configuration (adapted from Athar et al. (2002b); Jan et al. (2016); Luyckx & Berlamont (2004); Ogihara & Sakaguchi (1984) and Paul et al. (1991)) 12

Figure 2-10: Illustration of StormKing overflow HDVS (adapted from Andoh and Saul (2003)) 13

Figure 2-11: Illustration of patented Grit King and TeaCup separators (adapted from GritKing (2019) and TeaCup (2019)) 14

Figure 2-12: Various outlet considered by Veerapen et al. (2005) 14

Figure 2-13: CFD typical flow chart 17

Figure 2-14: Reynolds Averaged Navier-Stokes Simulation turbulence models available in ANSYS FLUENT 18

Figure 2-15: Graph of velocity u against distance y from y at point x showing the logarithmic-based wall functions (adapted from ANSYS (2018)) 19

Figure 2-16: A graph of logarithmic dimensionless value y+ against velocity u* showing subdivisions of the near-wall zones (adapted from ANSYS (2018)) 20

Figure 2-17: Calculation procedure for steady flow discrete phase model (adapted from ANSYS (2018)) 21

Figure 2-18: Calculation procedure for un-steady flow discrete phase model (adapted from ANSYS (2018)) 21

Figure 2-19: Sediment particle packing in DEM model 22

Figure 3-1: Models 1 and 2 schematic diagram 24

Figure 3-2: Illustration of progressive optimisation of Model 1 deflectors and parameters considered..... 25

Figure 3-3: Illustration of different outlet configurations considered and parameters optimised 26

Figure 3-4: Illustration of inclined deflector and parameters optimised..... 27

Figure 3-5: Model 1 and 2 longitudinal, floor plan and schematic setup incorporating vortex settling basin..... 31

Figure 3-6: Models 1 side and top view as constructed in the laboratory..... 32

Figure 3-7: ANSYS FLUENT model flowchart 33

Figure 3-8: VSB meshing comparison between tetrahedron and hexahedron 34

Figure 3-9: Graph showing simulation results grid dependency (physical model not affected by element number thus dashed for illustration)..... 35

Figure 3-10: Inflation layer implemented to capture boundary layer 35

Figure 3-11: Simulated ANSYS FLUENT Particle tracking..... 37

Figure 4-1: Chapter 4 overview 40

Figure 4-2: Summary of various authors' findings on underflow effect on sediment removal efficiency (Curi, Esen, & Velioglu, 1979; Mashauri, 1986; Paul et al., 1991) 41

Figure 4-3: Model 1 numerical (continuous line) and the physical model (dotted) ratio of underflow to inflow impact on trapping (sediment removal) efficiency 43

Figure 4-4: Modified equation Model 1 numerical (continuous line) and the physical model (dotted) ratio of underflow to inflow impact on sediment removal efficiency 43

Figure 4-5: 75 µm probable particle path coloured by average hydraulic retention time of a) Qu/Qi = 0.05, b) Qu/Qi = 0.08 and c) Qu/Qi = 0.16 top and side view..... 44

Figure 4-6: Numerical model average velocity magnitude contours of a) Qu/Qi = 0.05, b) Qu/Qi = 0.08 and c) Qu/Qi = 0.16 on plane y-x, z-x at y = 0.288 m, y = 0.5 m, y = 0.7 m and y = 0.92 m..... 45

Figure 4-7:Numerical model average axial velocity contours of a) Qu/Qi = 0.05, b) Qu/Qi = 0.08 and c) Qu/Qi = 0.16 on plane y-x, z-x at y = 0.288 m, y = 0.5 m, y = 0.7 m and y = 0.92 m (cyan: downward movement of water, yellow/red: rising water) 46

Figure 4-8: Numerical model average axial velocity profile of a) Qu/Qi = 0.05, b) Qu/Qi = 0.08 and c) Qu/Qi = 0.16 along lines A-B and C-D at y = 0.228 m 47

Figure 4-9:Numerical model average tangential velocity contours of a) Qu/Qi = 0.05, b) Qu/Qi = 0.08 and c) Qu/Qi = 0.16 on plane y-x, z-x at y = 0.288 m, y = 0.5 m, y = 0.7 m and y = 0.92 m..... 48

Figure 4-10: Numerical model average tangential velocity profile of a) Qu/Qi = 0.05, b) Qu/Qi = 0.08 and c) Qu/Qi = 0.16 along lines A-B and C-D at y = 0.228 m 48

Figure 4-11: Numerical model average radial velocity contours of a) Qu/Qi = 0.05, b) Qu/Qi = 0.08 and c) Qu/Qi = 0.16 on plane y-x, z-x at y = 0.288 m, y = 0.5 m, y = 0.7 m and y = 0.92 m 49

Figure 4-12:Numerical model average radial velocity profile of a) Qu/Qi = 0.05, b) Qu/Qi = 0.08 and c) Qu/Qi = 0.16 along lines A-B and C-D at y = 0.228 m 50

Figure 4-13: Numerical model vorticity and velocity vectors of a) Qu/Qi = 0.05, b) Qu/Qi = 0.08 and c) Qu/Qi = 0.16..... 51

Figure 4-14: An illustration of air-core formation in the laboratory..... 51

Figure 4-15: Numerical model turbulence kinetic energy for a) Qu/Qi = 0.05, b) Qu/Qi = 0.08 and c) Qu/Qi = 0.16 on the z-x plane at y = 0.288 m, y = 0.5 m, y = 0.7 m and y = 0.92 m..... 52

Figure 4-16: Possible plan layout of clustered VSBs..... 53

Figure 4-17: 60° and 120 ° sector outlets..... 54

Figure 4-18: Influence of outlet location on sediment removal efficiency Model 1 numerical (continuous line) and physical model results 56

Figure 4-19: Influence of outlet location on sediment removal efficiency Model 2 numerical (continuous line) and physical model results 56

Figure 4-20: Influence of outlet size on sediment removal efficiency Model 1 numerical (continuous line) and physical model results 57

Figure 4-21: Influence of outlet size on sediment removal efficiency Model 2 numerical (continuous line) and physical model results 58

Figure 4-22: Model 1 numerical model average axial velocity profile of 35 °, 60° and 120° sector on the z-x plane along lines A-B at y = 0.228 m..... 59

Figure 4-23: Model 1 numerical model average axial velocity profile of 35 °, 60° and 120° sector on the z-x plane along line C-D at y = 0.228 m 59

Figure 4-24: Model 1 numerical model minimum average axial velocity profile of 35° and 60° sector at 0° and 30° on the z-x plane along lines A-B at y = 0.228 m 60

Figure 4-25: Model 2 numerical model average axial velocity profile of 35° and 60° sector on the z-x plane along lines A-B at y= 1.208 m..... 61

Figure 4-26: Model 2 numerical model average axial velocity profile of 35° and 60° sector on the z-x plane along line C-D at y= 1.208 m 61

Figure 4-27: Model 1 numerical model average tangential velocity profile of 35 °, 60° and 120° sector on the z-x plane at lines A-B at y = 0.228 m 62

Figure 4-28: Model 1 numerical model average tangential velocity profile of 35 °, 60° and 120° sector on the z-x plane at line C-D at y = 0.228 m..... 63

Figure 4-29: Model 2 numerical model average tangential velocity profile of 35° and 60° sector on the z-x plane at lines A-B at y= 1.208 m..... 64

Figure 4-30: Model 2 numerical model average tangential velocity profile of 35° and 60° sector on the z-x plane at line C-D at y= 1.208 m 64

Figure 4-31: Model 1 numerical model (continuous lines) and physical model (markers) show the impact of inlet velocity on sediment removal efficiency 66

Figure 4-32: Numerical model average velocity magnitude contours of a) 0.198 m/s, b) 0.220 m/s, c) 0.257 m/s and d) 0.295 m/s on the z-x plane at y = 0.288 m, y = 0.5 m, y = 0.7 m and y = 0.92 m 68

Figure 4-33: Numerical model average axial velocity contours of a) 0.198 m/s, b) 0.220 m/s, c) 0.257 m/s and d) 0.295 m/s on the z-x plane at y = 0.288 m, y = 0.5 m, y = 0.7 m and y = 0.92 m (cyan/blue: downward movement of water, yellow: rising water)..... 69

Figure 4-34: Numerical model average axial velocity profile of a) 0.198 m/s, b) 0.220 m/s, c) 0.257 m/s and d) 0.295 m/s along lines A-B and C-D at y = 0.288 m 69

Figure 4-35: Numerical model average tangential velocity contours of a) 0.198 m/s, b) 0.220 m/s, c) 0.257 m/s and d) 0.295 m/s on the z-x plane at y = 0.288 m, y = 0.5 m, y = 0.7 m and y = 0.92 m 70

Figure 4-36: Numerical model average tangential velocity profile of a) 0.198 m/s, b) 0.220 m/s, c) 0.257 m/s and d) 0.295 m/s along lines A-B and C-D at y= 0.288m..... 70

Figure 4-37: Numerical model average radial velocity of a) 0.198 m/s, b) 0.220 m/s, c) 0.257 m/s and d) 0.295 m/s along lines A-B and C-D at y= 0.288m..... 71

Figure 4-38: Numerical model average turbulence kinetic energy of a) 0.198 m/s, b) 0.220 m/s, c) 0.257 m/s and d) 0.295 m/s on the z-x plane at y = 0.288 m, y = 0.5 m, y = 0.7 m and y = 0.92 m..... 71

Figure 4-39: Influence of flow rate on sediment removal efficiency Model 1 numerical (continuous line) and physical model results 73

Figure 4-40: Influence of inlet position on sediment removal efficiency Model 1 numerical (continuous line) and physical model results 74

Figure 4-41: Influence of inlet position on sediment removal efficiency Model 2 numerical model (continuous line) and physical model results 75

Figure 4-42: Numerical model effect of inlet location on the z-x plane average axial velocity contour (cyan/blue: downward movement of secondary currents, yellow/red: rising water).... 76

Figure 4-43: Numerical model effect of inlet location on average axial velocity profile along lines A-B and C-D..... 76

Figure 4-44: 75 µm 10 seconds particle tracking..... 77

Figure 4-45: Effect of inlet location on numerical model average tangential velocity contours on inlet z-x plane 77

Figure 4-46: Effect of inlet location on numerical model average tangential velocity profile on inlet z-x plane along lines A-B and C-D 78

Figure 4-47: Effect of inlet location on the vortex core region and velocity vectors 78

Figure 4-48: Effect of inlet location on 75 µm particle movement..... 79

Figure 4-49: Influence of downward angle of the inlet on sediment removal efficiency Model 2 numerical results 80

Figure 4-50: Influence of angle of the inlet on 75 µm sediment particle tracking coloured by hydraulic retention time 81

Figure 4-51: Numerical model average axial velocity contours of a) 0° b) 11.3° and c) 15° inlet angles on the z-x plane at y = 0.4 m, y = 0.63 m and y = 1.208 m 81

Figure 4-52: Numerical model average axial velocity profile of a) 0° b) 11.3° and c) 15° inlet angles along lines A-B and C-D at y= 1.208m 82

Figure 4-53: Numerical model average tangential velocity profile of a) 0° b) 11.3° and c) 15° inlet angles on the z-x plane at y = 0.4 m, y = 0.63 m and y = 1.208 m 82

Figure 4-54: Numerical model average tangential velocity profile of a) 0° b) 11.3° and c) 15° inlet angles along lines A-B and C-D at y= 1.208m 83

Figure 4-55: Numerical model average radial velocity profile of a) 0° b) 11.3° and c) 15° inlet angles on the z-x plane at y = 0.4 m, y = 0.63 m and y = 1.208 m 83

Figure 4-56: Numerical model average radial velocity profile of a) 0° b) 11.3° and c) 15° inlet angles along lines A-B and C-D at y= 1.208m 84

Figure 4-57: Influence of cylinder height on sediment removal efficiency Model 1 numerical (continuous line) and physical model results 86

Figure 4-58: Influence of cylinder height on sediment removal efficiency Model 2 numerical results 87

Figure 4-59: Influence of cone angle on sediment removal efficiency Model 2 numerical model results 88

Figure 4-60: An illustration of a 46° (left) and 60° (right) cone influence on the height of VSB 89

Figure 4-61: Influence of cylinder diameter on sediment removal efficiency model 1 numerical (continuous line) and physical model results 91

Figure 4-62: Influence of cylinder diameter on sediment removal efficiency Model 2 numerical and physical model results 91

Figure 4-63: Effect of diameter on effective height (all units in mm) 92

Figure 4-64: Influence of cylinder diameter/inlet diameter on sediment removal efficiency and residence time Model 2 numerical results..... 94

Figure 4-65: Numerical model average axial velocity contours in VSB of diameter: a) 0.634 m b) 1.0 m and c) 1.5 m on the z-x plane at y = 1.073 m, y = 1.256 m and y = 1.506 m 94

Figure 4-66: Numerical model average axial velocity profile in VSB of diameter: a) 0.634 m b) 1.0 m and c) 1.5 m on the z-x plane along lines A-B and C-D, Note: the dimensionless distance = the distance/ the VSB radius 95

Figure 4-67: Numerical model result showing probable particle path for 75 µm sediment coloured by 10 and 15 seconds hydraulic retention time in VSB with a diameter of: a) 0.634 m b) 1.0 m and c) 1.5 m 95

Figure 4-68: Numerical model average tangential velocity contours with VSB diameters of: a) 0.634 m b) 1.0 m and c) 1.5 m, on the z-x plane at y = 1.073 m, y = 1.256 m and y = 1.506 m96

Figure 4-69: Numerical model average tangential velocity profile in VSB of diameter: a) 0.634 m b) 1.0 m and c) 1.5 m on the z-x plane along lines A-B and C-D, Note: the dimensionless distance = the distance/ the VSB radius 96

Figure 4-70: Numerical model average radial velocity contours for a VSB of diameter: a) 0.634 m b) 1.0 m and c) 1.5 m on the z-x plane at y = 1.073 m, y = 1.256 m and y = 1.506 m 97

Figure 4-71: Numerical model helical vorticity and velocity vectors for a VSB of diameter: a) 0.634 m b) 1.0 m and c) 1.5 m 97

Figure 4-72: Numerical model average turbulent kinetic energy contours for a VSB of diameter: a) 0.634 m b) 1.0 m and c) 1.5 m on the z-x plane at y = 1.073 m, y = 1.256 m and y = 1.506 m 98

Figure 4-73: Optimization parameters considered 99

Figure 4-74: Deflector 1 optimisation parameters considered 100

Figure 4-75: Effect of deflector 1 on sediment removal efficiency Model 1 numerical and physical model 100

Figure 4-76: Deflector 1 and 2 general layout 101

Figure 4-77: Effect of deflector 1-2 on sediment removal efficiency Model 1 numerical and physical model 101

Figure 4-78: Deflector 1, 2 and 3 general layout 102

Figure 4-79: Effect of deflector 1-2-3 on sediment removal efficiency Model 1 numerical and physical model 102

Figure 4-80: Deflector 1-2-3-4 and 5 general layout 103

Figure 4-81: Effect of deflector 1-2-3-4-5 on sediment removal efficiency Model 1 numerical and physical model 103

Figure 4-82: Deflectors particle tracking comparison showing different residence times 104

Figure 4-83: An illustration showing sediment concentration comparing physical and numerical models 104

Figure 4-84: Numerical model results showing the effect of inlet location on the plane z-x average axial velocity contour (cyan/blue: downward movement of secondary currents, yellow/red: rising water) 105

Figure 4-85: Physical Model 1 observed sediment settled on the deflectors 105

Figure 4-86: Illustration of Model 2 side outlet and sediment particle tracks coloured by hydraulic retention time (configuration I) side and top view 106

Figure 4-87: Illustration of a central circular outlet with pipe outlet at the top (configuration II) side and top view 107

Figure 4-88: Influence of outlet configuration II on sediment removal efficiency optimised numerical model results 108

Figure 4-89: Numerical model effect of outlet configuration II on the z-x plane average axial velocity contour (cyan/blue: downward movement of water, yellow/red: rising water) 109

Figure 4-90: Numerical model average axial velocity profile of outlet configuration II on the z-x plane along lines A-B and C-D at y = 1.236 m 109

Figure 4-91: Numerical model effect of outlet configuration II on the z-x plane average tangential velocity contour at y = 1.236 m 110

Figure 4-92: Numerical model average tangential velocity profile of outlet configuration II on the z-x plane along lines A-B and C-D at y = 1.236 m 110

Figure 4-93: Effect of outlet configuration II on 75 µm particle tracking coloured by hydraulic retention time 111

Figure 4-94: Configuration II numerical model turbulent kinetic energy contours on the z-x plane at y = 1.236 m 111

Figure 4-95: Illustration of numerical model central rectangular and circular outlet with pipe outlet at the bottom (configuration III) side and top view 112

Figure 4-96: Types of free surface vortex classification and definitions of D and S (Hydraulic Institute, 2012) 113

Figure 4-97: 90 mm shaft rating curve 114

Figure 4-98: 90 mm shaft and inlet mouth outline 114

Figure 4-99: Illustration of physical model with vortex and aeration core in preliminary analysis 115

Figure 4-100: Illustration of laboratory physical model outlet configuration II with and without a low weir 115

Figure 4-101: Influence of outlet configuration II and III on sediment removal efficiency optimised numerical model results 116

Figure 4-102: Numerical model effect of outlet configuration III on the z-x plane average axial velocity contour (cyan/blue: downward movement of water, yellow/red: rising water) 117

Figure 4-103: Numerical model average axial velocity profile of outlet configuration III on the z-x plane along lines A-B and C-D at y = 1.236 m 117

Figure 4-104: Numerical model effect of outlet configuration III on the z-x plane tangential velocity contour at y = 1.236 m 118

Figure 4-105: Numerical model average tangential velocity profile of outlet configuration III on the z-x plane along lines A-B and C-D at y = 1.236 m 118

Figure 4-106: Configuration III numerical model turbulent kinetic energy contours on the z-x plane at y = 1.236 m 119

Figure 5-1: Proposed VSB configuration 120

Figure 5-2: Chapter 5 overview 122

Figure 5-3: Proposed VSB Model 1 dimensions 124

Figure 5-4: Proposed VSB Model 2 dimensions 124

Figure 5-5: Numerical Models 1 and 2 average axial velocity contours on the z-x plane (cyan/blue: downward movement of water, yellow/red: rising water) 125

Figure 5-6: Numerical Models 1 and 2 axial velocity profile on the z-x plane along dimensionless lines A-B and C-D 126

Figure 5-7: Models 1 and 2 numerical 75 µm probable particle path coloured by hydraulic retention time 126

Figure 5-8: Numerical Models 1 and 2 average tangential velocity contours on the z-x plane127

Figure 5-9: Numerical Models 1 and 2 average tangential velocity profile on the z-x plane along dimensionless lines A-B and C-D 128

Figure 5-10: Models 1 and 2 numerical model turbulent kinetic energy contours on the z-x plane at y= 1.318 m and y = 1.46 m 128

Figure 6-1: Conventional flume/canal type settler numerical model a) 75 µm sediment particle tracking coloured by hydraulic retention time, b) velocity contours and c) turbulent kinetic energy contours 131

Figure 6-2: Possible river abstraction works layout with VSBs in parallel to meet the required demand 132

Figure 6-3: Numerical model sand volume fraction at inlet concentration a) 5,149 mg/l and b) 10,000 mg/l at the z-x plane y = 0.42 m, y = 0.80m and y = 1.318 m 135

Figure 6-4: Numerical model sediment removal efficiency over varying sediment sizes 135

Figure 6-5: Model 1 numerical model sediment removal efficiency over varying sediment sizes and underflow 136

Figure 6-6: Model 2 numerical model sediment removal efficiency over varying sediment sizes and underflow 136

Figure 6-7: Model 1 numerical model sediment removal efficiency over varying sediment sizes and inflow 137

Figure 6-8: Model 2 numerical model sediment removal efficiency over varying sediment sizes and inflow..... 137

LIST OF TABLES

Table 2-1: Sediment removal mechanisms and examples 3

Table 2-2: Sediment range used and efficiency achieved by various authors 10

Table 2-3: Possible factors affecting VSB performance 10

Table 2-4: Range of parameters used by different investigators (Athar et al., 2005) 15

Table 3-1: Model parameters 24

Table 3-2: Approximate time taken by a natural sediment particle to settle in 1 m water depth 27

Table 3-3: Typical river sediment transport calculation based on Van Rijn (1993, 2007) 29

Table 3-4: ANSYS FLUENT mesh metric parameters to check the quality of the mesh (ANSYS, 2018) 35

Table 3-5: Summary of other ANSYS FLUENT setting parameters 36

Table 4-1: Influence of underflow VSB base model parameters 42

Table 4-2: Influence of outlet location on trapping efficiency VSB base model parameters 55

Table 4-3: Influence of inlet velocity VSB base model parameters 66

Table 4-4: Summary of Figure 4-3 numerical and physical model correlation statistical analysis 67

Table 4-5: Summary of minimum velocity needed to initiate sediment motion in pipes according to Equation 4-3 67

Table 4-6: Summary of Figure 4-39 numerical and physical model correlation statistical analysis 73

Table 4-7: Effect of inlet position on sediment removal efficiency base model parameters 74

Table 4-8: Summary of Figure 4-41 numerical and physical model correlation statistical analysis for Model 2 75

Table 4-9: Influence of cylinder height on sediment removal trapping efficiency base model parameters 85

Table 4-10: Influence of cone angle on sediment removal efficiency base model parameters 88

Table 4-11: Influence of cylinder diameter on sediment removal trapping efficiency base model parameters 90

Table 4-12: Rate of incremental change of residence time with D/Di 93

Table 4-13: Influence of outlet structure on sediment removal trapping efficiency base model parameters 107

Table 4-14: Influence of outlet configuration II on sediment removal efficiency optimised numerical model results 108

Table 4-15: Summary of critical submergence depth required for various outlet diameters according to Equation 4-5 113

Table 4-16: Influence of outlet configuration III on sediment removal efficiency optimised numerical model results 116

Table 5-1: A comparison of proposed model parameters 123

Table 5-2: Summary of optmised proposed VSB dimension..... 123

Table 5-3: Proposed optimised VSB dimension sediment trapping efficiency 123

Table 6-1: Dimensions and energy requirements of a conventional settler, hydro-cyclone and VSB required to settle 75 µm sediment particles at 50l/s 130

Table 6-2: VSB sediment mass balance..... 134

Table 6-3: Concrete channel sediment transport calculations per sediment size based on (Van Rijn, 1993, 2007)..... 134

ACRONYMS

1D	One dimensional
2D	Two dimensional
3D	Three dimensional
C	Concentration
CFD	Computational Fluid Dynamics
CHPC	Centre for High-Performance Computing
D	Cylinder diameter
d50	Sediment median diameter
DDPM	Dense Dispersed Phase Model
DEM	Discrete Element Method
Di	Inlet diameter
DNS	Direct Numerical Simulation
DPM	Discrete Phase model
Du	Underflow diameter
Hc	Cone height
Hi	Inlet height
Ho	Outlet height
HPP	Hydro Power plant
Ht	Cylinder height
LES	Large EddySimulation
Qi	Inlet flow
RANS	Reynolds Averaged Navier Stokes Simulation
SA	South Africa
SHP	Small hydropower plant
TKE	Turbulent kinetic energy
VOF	Volume of Fluid
VSB	Vortex settling basin
WL	Water Lever

1 Introduction

1.1 Background

The South African government is now supplying water to nearly 100% of households in the country. The large storage dams store huge volumes of runoff and supply over the year storage during droughts, but many of the smaller water supply schemes rely on the abstraction of water from rivers.

In the semi-arid climate of South Africa, the river flows oscillate between drought and flood. The flows are seasonal with floods lasting from a few minutes to hours, and low flows during droughts even lasting for years. The sediment transport which is a natural phenomenon is highly variable in South African rivers due to the semi-arid climate. Because of this seasonal flow variation as well as other factors, the river sediment loads vary greatly and generally contain about 80% to 90 % silt and clay (0.98 µm - 62.5 µm) (Brink, Basson, & Denys, 2006).

Diverted or abstracted sediments cause a wide range of problems which lead to increased operational costs and downtimes such as abrasion of turbines/pumps at hydraulic structures and blocking of intakes and outlets. The fine sediments that are typical of South African rivers require a considerable hydraulic retention time to settle under gravity only. As an example, to settle 60 µm sediment particles through 1 m water depth, approximately 30 minutes are required. Also, if cohesive sediment is allowed to compact, it becomes challenging to flush out.

A wide range of river abstraction works designs are available but, in South Africa, river abstraction with a low weir, or even without a weir, is promoted as the costs are less prohibitive and these designs are less environmentally degrading.

Although these types of designs have successfully been implemented, the design of smaller cheaper river abstraction works with a duty pump capacity of say less than 100 l/s (7.2 ML/d at 20 h/d) has not successfully been covered in guidelines. There is a great need for this type of abstraction works for small scale potable use in rural water schemes.

A Vortex Settling Basin (VSB) is a promising alternative to conventional sediment settling structures in the removal of fine non-cohesive sediment (>75 µm). The VSB is mainly gravity driven but due to the tangential location of the inlet, centrifugal forces assist in sustaining the sediment particles near the wall and with the outlet located at the centre, the hydraulic retention time is increased considerably thus achieving higher sediment trapping efficiency. A small footprint, no moving parts, no chemical dosing, low energy requirements, high sediment removal and continuous flushing of sediment back to the river makes the VSB an attractive option.

Hydraulic design development for VSBs will be the main focus of this research. Numerical and physical modelling will be the methodology used to actualise a proposed river abstraction works layout. Although each abstraction works is unique with many factors influencing the optimum configuration, the concepts developed for low flow VSBs will provide specialised design information to hydraulic engineers tailor-made for African conditions.

1.2 Motivation for this study

Although VSBs offer a good alternative to traditional large river abstraction works, lack of specific design guidelines for small river abstraction works has hindered their adoption. VSBs have been extensively used in wastewater treatment and in grit removal from stormwater, where the design requirements are more or less similar but where the target particle diameters are in the order of 1000 µm or larger. This research seeks to improve the hydraulic understanding and propose design concepts of VSBs for use in small river abstraction works.

To achieve this, the following activities will be conducted:

I. Identify the important hydraulic parameters that influence the performance of a VSB in the removal of fine sediment ≈ 75 µm.
II. Carry out detailed numerical and physical model validation analysis with the aim of developing hydraulic design guidelines of VSBs for African conditions.
III. Propose river abstraction works layouts incorporating VSBs with a duty pump capacity of less than 100 l/s (7.2 ML/d at 20 h/d).

2 Literature study and theoretical background

2.1 Overview of sediment removal mechanisms

There are in general four mechanical sediment removal mechanisms, these are summarised in **Table 2-1**.

Table 2-1: Sediment removal mechanisms and examples

Removal mechanism	Examples
Gravity	Sand traps, settlers, tunnel type excluders
Gravity + weak centrifugal forces	VSBs
Gravity + high centrifugal forces	Hydro cyclones and centrifuges
High pressure	Filters

The selection of one type mainly depends on the acceptable allowable sediment size in the scheme. As an example, Brekke, Wu, and Cai (2003) noted that Pelton turbines subjected to sediment where 77.0% of particles were finer than 63 microns and 99.0% finer than 125 microns operated at a high pumping-head of 920 m suffered severe damage after 600 hours of operation. **Figure 2-1** below gives a summary of the appropriate sediment removal type according to sediment size. They are briefly discussed in the followingsubsections:

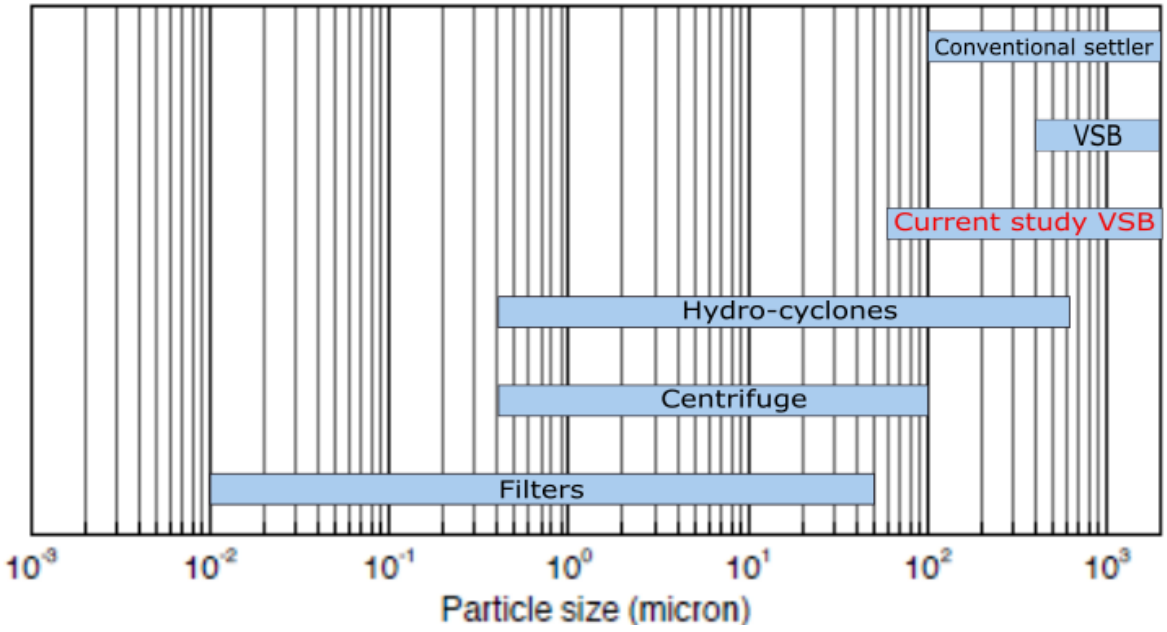

Figure 2-1: Several options available to remove sediment particles (adapted from Green and Southard (2019))

2.2 Conventional settler

Sediment particles can only be transported in suspension if their settling velocity is less than the vertical component of hydraulic turbulence; thus a reduction in flow velocity causes the sediments to settle out. The settling or fall velocity of sediments is dependent on grain size, shape, density, temperature and salinity (of the fluid) and sediment concentration. For comparison between different sediments, the standard fall diameter of a sphere having the same

specific weight is used (Interagency Committee, 1957). For clays and silts with discrete particles large enough to overcome Brownian motion, Stokes' law is used (**Equation 2-1**). Stokes' law is only valid for Reynolds numbers Re < 0.4 and particle sizes < 76µm (Gibbs, Matthews & Link, 1971). To cater for effects of concentration, flocculation and hindered settling, corrections need to be done (Morris & Fan, 1998).

For coarse grains under the full range of laminar flow **Equation 2-2** can be used and under turbulent flow **Figure 2-2** can be used to estimate the fall velocity.

$$\omega = \frac{d^2(\rho_s - \rho)}{18\mu} \qquad \text{Equation 2-1}$$

$$\omega^2 = \frac{4gd}{3C_d}\left(\frac{\gamma_s - \gamma}{\gamma}\right) \qquad \text{Equation 2-2}$$

Where ω: fall velocity (m/s), d: particle diameter (m), ρ_s: particle density (kg/m^3), ρ: fluid density (kg/m^3), µ: dynamic viscosity (N.s/m^2), g: gravity constant (m/s^2), γ_s, γ: specific weight of particle and liquid, C_d: drag coefficient=24/Re for laminar flow

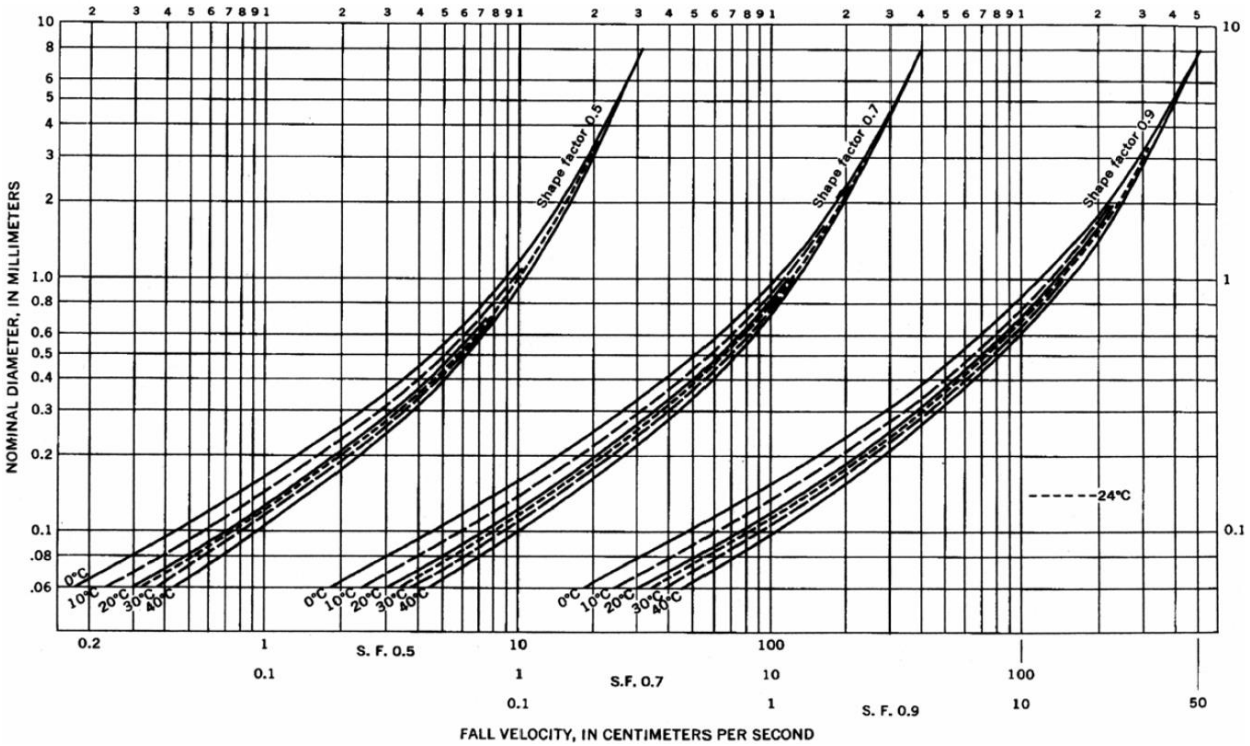

Figure 2-2: Settling velocity of natural sand (Interagency Committee, 1957)

Equation 2-2 is a generalised equation and much more detailed equations to cater for different conditions are briefly explained:

i. (Rubey, 1933)

$$\omega = \frac{[1636(\rho_s - \rho)d^3 + 9\mu^2]^{0.5} - 3\mu}{500d} \qquad \text{Equation 2-3}$$

Where ω: fall velocity (m/s), d: particle diameter (m), ρ_s: particle density (kg/m^3), ρ: fluid density (kg/m^3), µ: dynamic viscosity (N.s/m^2)

The equation is simplified to enable programmable calculations but cannot be applied to natural sediment particles as it does not consider the shape of sediment.

ii. (Zhiyao, Tingting, Fumin, & Ruijie, 2008)

Zhiyao et al. (2008) suggested a simplified equation applicable to natural sediment for Reynolds numbers less than 2 x 10^5 :

$$\omega = \frac{v}{d} d_*^3 \left[38.1 + 0.93 d_*^{12/7}\right]^{-7/8} \quad \text{Equation 2-4}$$

$$d_* = d\left[\frac{\left(\frac{\rho_S - \rho}{\rho}\right)g}{v^2}\right]^{\frac{1}{3}} \quad \text{Equation 2-5}$$

ω: fall velocity(m/s), d: particle diameter (m), v: kinematic viscosity (m^2/s), g: gravity constant (m/s^2), ρs, ρ: particle and fluid density(kg/m^3), d_*: dimensionless particle diameter.

For the gravity-driven system, hydraulic retention time needs to be adequate for the particles to travel the entire water depth. For the same residence time, decreasing the basin depth and increasing the length reduces the time required to settle the particles, but turbulence leads to the possibility of resuspension as illustrated in **Figure 2-3a**. In **Figure 2-3b** it can be observed that baffles increase the surface contact area which improves the performance, and the height has no impact on the throughput.

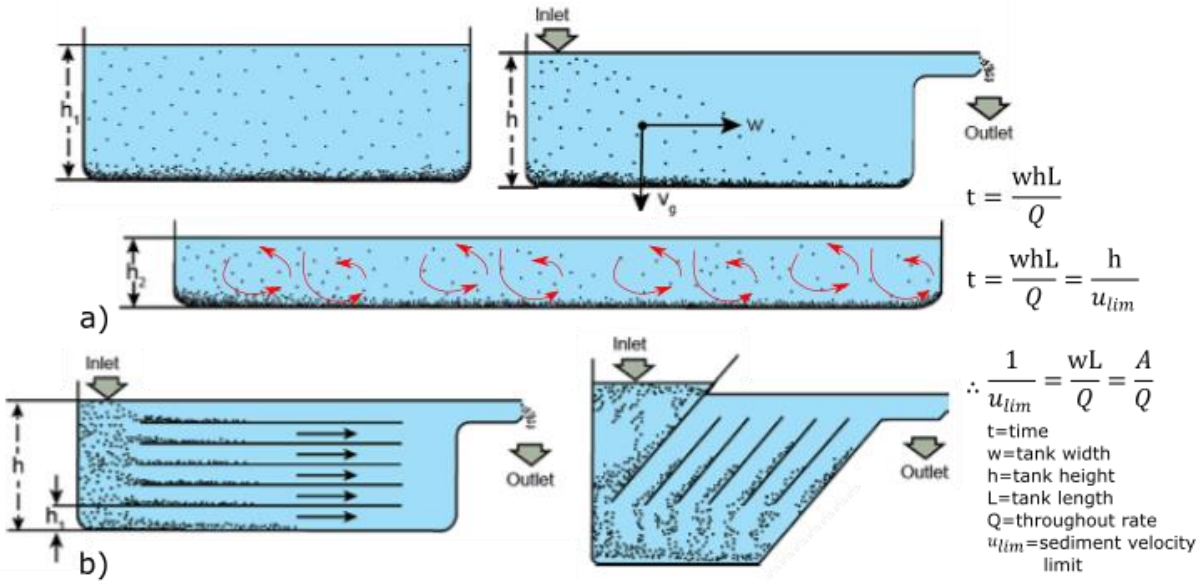

Figure 2-3: Illustration of settling basin principles (adapted from NPTEL (2018))

Settlers with intermittent flushing are ideally suited for South African systems with a throughput of 4 to 6 m^3/s. They consist of a channel, as shown in **Figure 2-4**, operating with a mean velocity of 0.1 to 0.2 m/s (Basson, 2006). They can be utilised to remove particles > 100 µm but require large basins thus are primarily used to remove coarse sediment > 300 µm achieving 100% trapping efficiency.

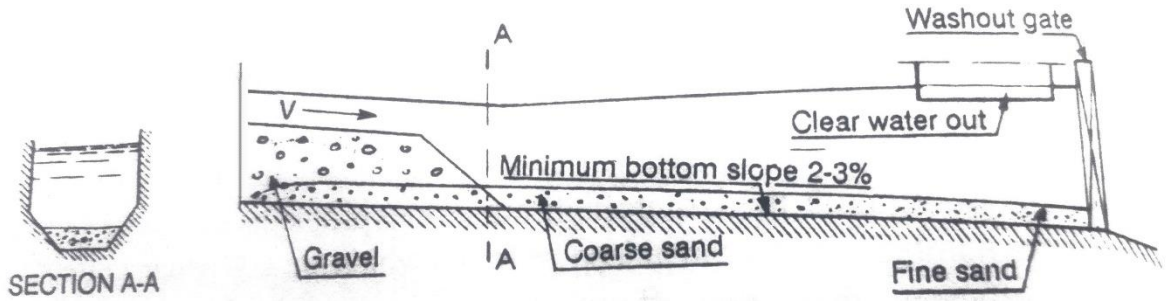

Figure 2-4: Batchwise washout settler (Bouvard, 1992)

During normal operation, the settler fills gradually from upstream with coarse material with fines settling further downstream. At critical sediment load, flushing is carried out. Settler sizing is according to **Equation 2-6** and **Equation 2-7** (Basson, 2006):

$$T = {V}/{G_s} \qquad \text{Equation 2-6}$$

$$S_o = {0.44d^{(9/7)}}/{q^{(6/7)}} \qquad \text{Equation 2-7}$$

T: period between successive washouts (s), V: volume of settler that can be occupied by deposited sediments, G_S: volume of inflow sediment, S_o: slope, d: sediment diameter (m), q: unit discharge (m^2/s)

Sand traps are designed with continuous flushing and sizing is according to **Equation 2-8** to **Equation 2-10** (Basson, 2006).

$$v_{cr} = 10\omega R^{1/6} \qquad \text{Equation 2-8}$$

$$L = v \times \frac{h}{\omega - u^*} \qquad \text{Equation 2-9}$$

$$u^* = \frac{4.2v}{100} \times \frac{1}{R^{1/6}} \qquad \text{Equation 2-10}$$

v_{cr}: critical velocity (m/s), v: mean flow velocity (m/s), ω: sediment settling velocity (m/s), R: hydraulic radius, h: flow depth (m), L: trap length (m), u*: shear velocity (m/s). recommended: $v < v_{cr}$, width ≈ 2h, v≈ 0.07 m/s to remove 100 µm and 0.35 m/s to remove 300 µm

2.3 Hydro-cyclones

Hydro-cyclones comprise mechanical equipment utilising gravity and high centrifugal forces to achieve high separation efficiency over a small surface area (loading). Flow under high pressure enters the flow domain at the top tangentially and causes the flow to spin creating two opposing forces:

a) Centrifugal forces which accelerate heavier particles towards the outer wall settling towards the underflow and
b) Drag force acting inwards at the zone of low pressure near the centre axis where finer particles spiral upwards towards the overflow as illustrated in **Figure 2-5** (Richardson, Harker, & Backhurst, 2002).

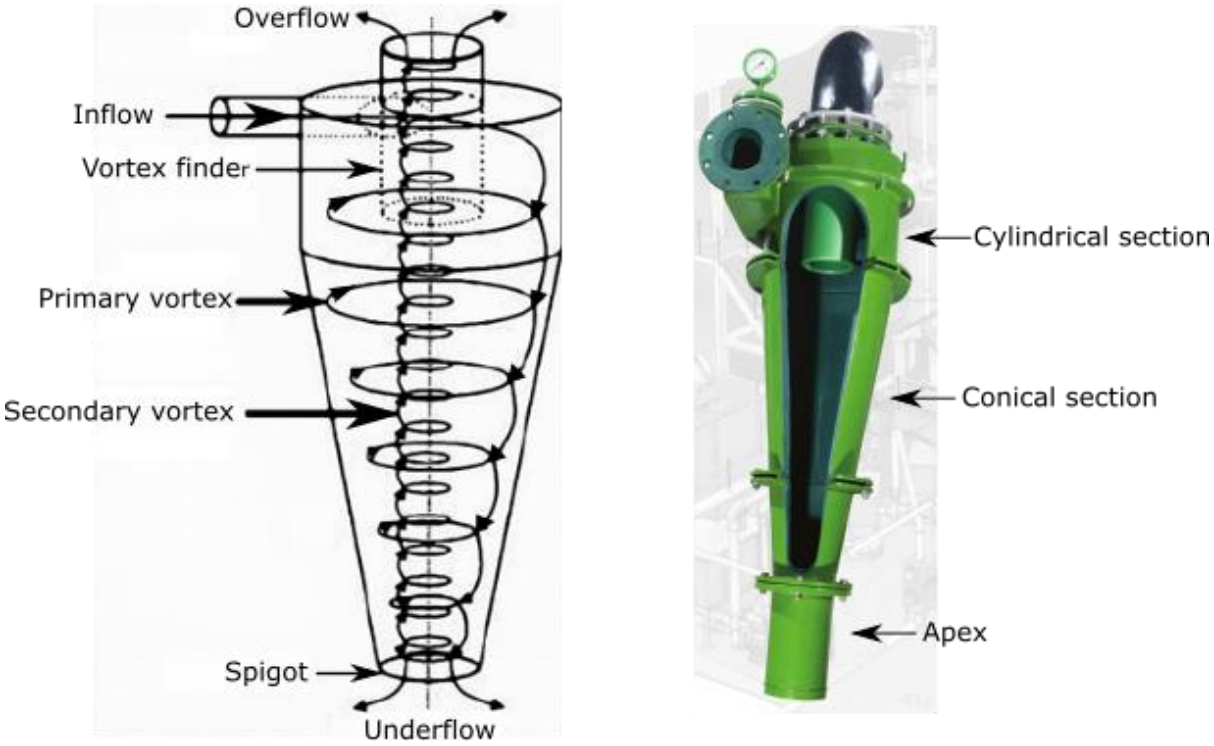

Figure 2-5: Illustration of hydro-cyclone mechanism (adapted from MULTOTEC (2018) and Richardson et al. (2002))

The effectiveness of separation is dependent on tangential (u_t), radial (u_r) and axial (u_a) velocity components throughout the flow domain. The tangential velocity component is the most influential, and if fluid friction is assumed to be absent, the relationship between the tangential component and radius (r) is as follows:

a) Free/irrotational vortex (frictionless fluid would swirl), in which: $u_t r = \text{constant}$
b) Forced/rotational vortex, in which: angular velocity, $\omega = \frac{u_t}{r} = \text{constant}$

In hydro-cyclones, friction is present thus both free and forced vortices are present (Rankine's vortex) as illustrated in **Figure 2-6**.

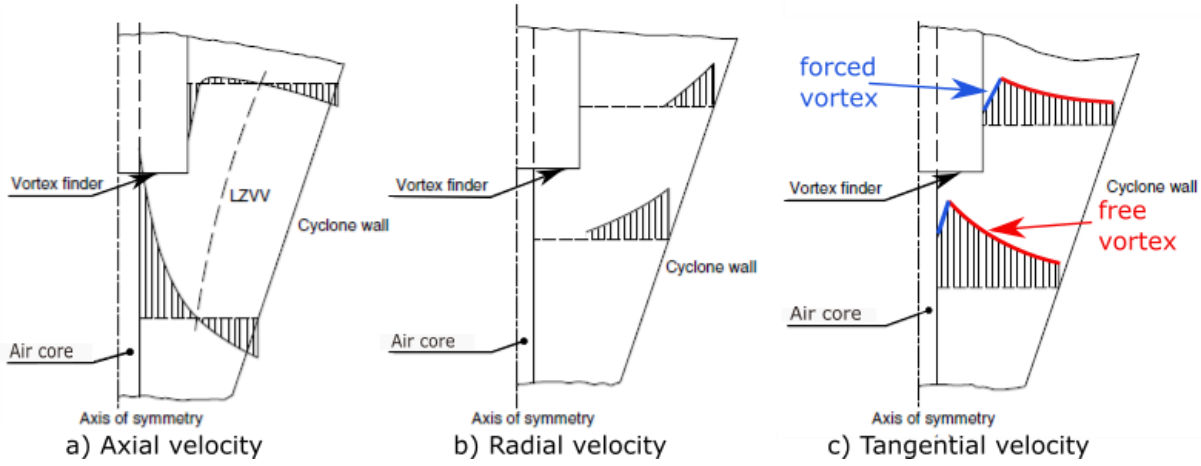

Figure 2-6: Illustration of typical velocity distribution in hydro-cyclone (LZVV is locus of zero axial velocity) (adapted from Richardson et al. (2002))

Hydro-cyclones are compact but have high energy demands and stringent manufacture and operating conditions. They are appropriate for 4 µm to 500 µm particles with performance evaluated by:

- Pressure drop,
- Efficiency and
- Cut diameter.

Appendix A1 provides a chart illustrating cyclone cut off diameter (sediment diameter that a particle has equal chances of moving to overflow or underflow) and throughput flow rate for the selected cyclone diameter.

2.4 Vortex settling basin

A Vortex Settling Basin (VSB) is a cylindrical fluidic device with a conical base where the sediment-laden flow enters tangentially to the flow domain and relying on gravity, and centrifugal forces, more concentrated flow (underflow) exits at the bottom outlet and more clear water as overflow. This is illustrated in **Figure 2-7** below showing the sediment particle path coloured by average retention time in the VSB flow domain.

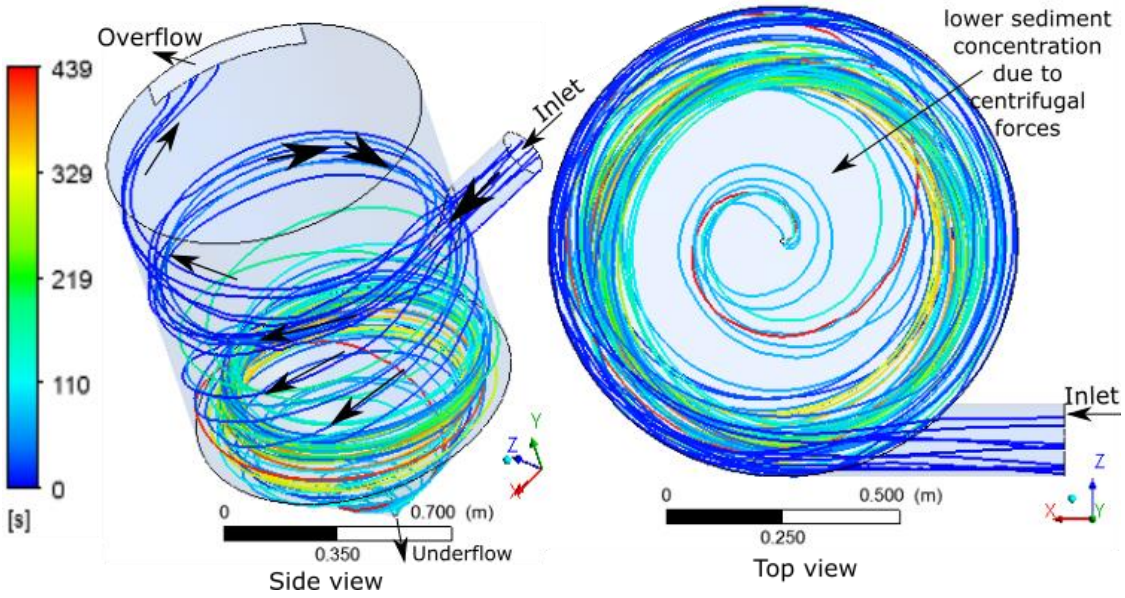

Figure 2-7: Illustration of sediment particle motion path coloured by average hydraulic retention time

Particles entering the VSB with a water stream follow a circular motion and a particle in this motion is subjected to the following forces summarised in **Figure 2-8**:

- Drag force, F_D

$$F_D = C_D S_p \frac{\rho|u - v_p|(u - v_p)}{2} \qquad \text{Equation 2-11}$$

- Force of inertia, F_i

$$F_i = \rho_p V_p \frac{dv_p}{dt} \qquad \text{Equation 2-12}$$

- Mass force, F_{AM}

$$F_{Am} = a_r \rho_p V_p \frac{d(u - v_p)}{dt} \qquad \text{Equation 2-13}$$

- Gravity force, F_G
- Hydrostatic force, F_A
- Centrifugal force, F_C

$$F_C = m_p \frac{u_t^2}{r} = \rho_p V_p \frac{u_t^2}{r} \qquad \text{Equation 2-14}$$

- Buoyancy force, F_{TP}

$$F_{TP} = -V_p \frac{dp}{dr} \qquad \text{Equation 2-15}$$

Neglecting Saffman, Magnus and Basset forces which describe velocity gradients around the particle, possible particle rotary motion if it occurs and change of particle motion conditions in time respectively, it has been shown that the particle motion can be described as follows (Gronowska-Szneler & Sawicki, 2014; Gronowska, 2012; Slattery, 1999; Soo, 1990):

$$\rho_p V_p \frac{dv_p}{dt} = a_r \rho V_p \frac{d(u - v_p)}{dt} + (\rho_p - \rho) V_p g + C_D S_p \frac{\rho |u - v_p| (u - v_p)}{2} + m_p \frac{u_t^2}{r} - V_p \frac{dp}{dr} \qquad \text{Equation 2-16}$$

Sp: cross-sectional area of particle, ρ: water density, u: water velocity, v_p: particle velocity, V_p: volume of particle, ρ_p: particle density, a_r: associated mass coefficient, m_p: mass of particle, i, t: radial and tangential versors, r,φ,z : cylindrical coordinates

Moreover, a particle will be removed from the underflow provided **Equation 2-17** at the overflow section is fulfilled, or the gravitational force is so high that the particles are out of range of the overflow stream,

$$F_C \geq F_D + F_{TP} \qquad \text{Equation 2-17}$$

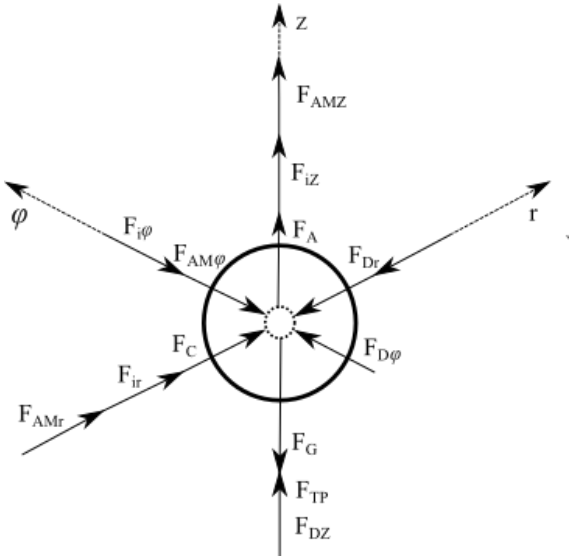

Figure 2-8: Forces acting on a sediment particle in Fluid motion (adapted from Gronowska (2012))

Several authors have investigated VSBs. Sullivan (1972) undertook extensive research on swirl as illustrated in **Appendix A3** for the removal of sediment sizes >200µm. Paul et al. (1991) proposed simple empirical formulas for sizing various components of VSBs and their effectiveness as shown in **Figure 2-9(i)**. Athar, Kothyari, and Garde (2002a, 2002b) investigated various configuration designs and their efficiency. Jan, Hsu, Lin, & Zeng (2011) and Truong (2011) examined the effects of deflectors on removal efficiency while Singh and Kumar (2016) studied performance evaluation of settling basins and VSBs constructed at SHP stations.

Most of these studies were site-specific and used a wide range of configurations and sediment sizes. **Table 2-2** which is of relevance for SA conditions with fine sediment sizes shows the sediment sizes used by various authors and the trapping efficiencies achieved.

Table 2-2: Sediment range used and efficiency achieved by various authors

Authors	Range of sediment size (mm)	Trapping efficiency (%)
Mashauri (1986)	0.063–0.250	31-90
Paul et al. (1991)	0.050-7.640	76-100
Athar et al. (2002b)	0.055-0.931	25-86
Keshavarzi and Gheisi (2006)	0.183	68

Table 2-3 summarises several parameters that affect VSB performance. They are classified as the dimension, operation regime, sediment and water properties. From the literature, the physical aspects that are of relevance to SA conditions are explored further.

Table 2-3: Possible factors affecting VSB performance

Dimensions	Sediment properties	Water properties	Others
VSB diameter	Density	Inlet velocity	Wall roughness
VSB height	Shape factor	Density	Operation regime
Underflow diameter	Sediment size	Temperature	Energy loss
Location of outlet	Sediment distribution	Viscosity	
Size of outlet	Mass loading		
Location of inlet	Angle of repose		
Size of inlet	Cohesive sediment		
Angle of inlet			
Cone angle			
Deflectors			

2.4.1 Basin diameter (D)

From different studies, the basin diameter with the highest efficiency has been experimentally determined to be 5 to 6 times the channel width (B). In most cases, the D= 5B has been chosen as larger diameters only increase the residence time without a significant increase in efficiency (Mashauri, 1986; Paul, 1988; Paul et al., 1991; Sullivan, 1972).

2.4.2 Cone slope

The cone chamber is necessary for the removal of coarse sediments and limiting of sediment settling. However, an increase in cone slope increases the underflow discharge (Paul et al., 1991). Most investigators have proposed a slope of 1:10 (V: H) to be ideal. Due to cohesive and fine sediment in South African rivers, steeper slopes shall be considered.

2.4.3 Underflow

The ratio of underflow to inflow is maintained at less than 15%. Higher values lead to the formation of air-cores thus reducing the efficiency. A ratio of 10% is optimal so as to minimise water wastage (Alquier, Delmas, & Pellerej, 1982; Cecen, 1977; Paul et al., 1991; Salakhov, 1975).

2.4.4 Flow depth to diameter ratio

Chrysostomou (1983) and Mashauri (1986) have shown that $\frac{\mathrm{Ht}}{\mathrm{D}} > 0.26$ where Ht is the flow depth and D is the basin diameter The efficiency increases with increase in the ratio, with an optimal value of 0.6 being suggested (Sullivan, 1972; Veerapen, Lowry, & Couturier, 2005).

Most of the previous work carried out was geared towards the removal of coarse sediment, thus the optimal 0.6 value is to limit the construction cost. In this study, deep-depth VSBs will be investigated with $\frac{\mathrm{Ht}}{\mathrm{D}} > 1$ since Jan, Hsu, Lin, and Zeng (2016) have suggested higher ratios to remove fine sediment sizes.

2.4.5 Geometric configuration and deflectors

Various VSB design configurations by different investigators are shown in **Figure 2-9**. Two types of layouts have widely been utilised, Athar et al. (2002b) configuration 3 and Paul et al. (1991). For removal of particles <500 µm Paul et al. (1991) recommended configuration **Figure 2-9 (i)** while Athar et al. (2002b) investigated configurations 1 to 3 (**Figure 2-9 e, f, g**) and found out that 3 gives the highest efficiency. Three small hydropower desilting basins were constructed based on this setup and Singh and Kumar (2016) reviewed their performance and concluded 90% trapping efficiency for particles > 250 µm is achieved in the field. The difference in configuration promoted investigation on the optimum location of the outlet thus Model 1 configuration is investigated in chapter 4.

To avoid short-circuiting of sediment into the overflow, Mashauri (1986) and Paul et al. (1991) recommended the use of horizontal deflectors placed at $\frac{\mathrm{h1}}{3}$ extending 20 to 50h1 as shown in **Figure 2-9 (d, i)Error! Reference source not found.**.

In deep-depth VSBs, Jan et al. (2011) and Truong, (2011) noted that deflectors play a significant role in removal efficiency and proposed configuration **Figure 2-9 (i)**. The wide options of deflector configurations promoted the investigation of deflectors in Model 1 investigated in section 4.11. In this current study, after intensive investigation of Model 1 configuration with deflectors, it was found that at a flow of 1 l/s, >99 % efficiency for 100 µm was achieved. At increased flow, the trapping efficiency decreased significantly <40% and settling of particles on the deflectors (see section 4.11.6) promoting the Model 1

discontinuation. An alternative configuration with centroid configuration were investigated and for the purpose of deflector usage, a brief literature review of such configuration is discussed below.

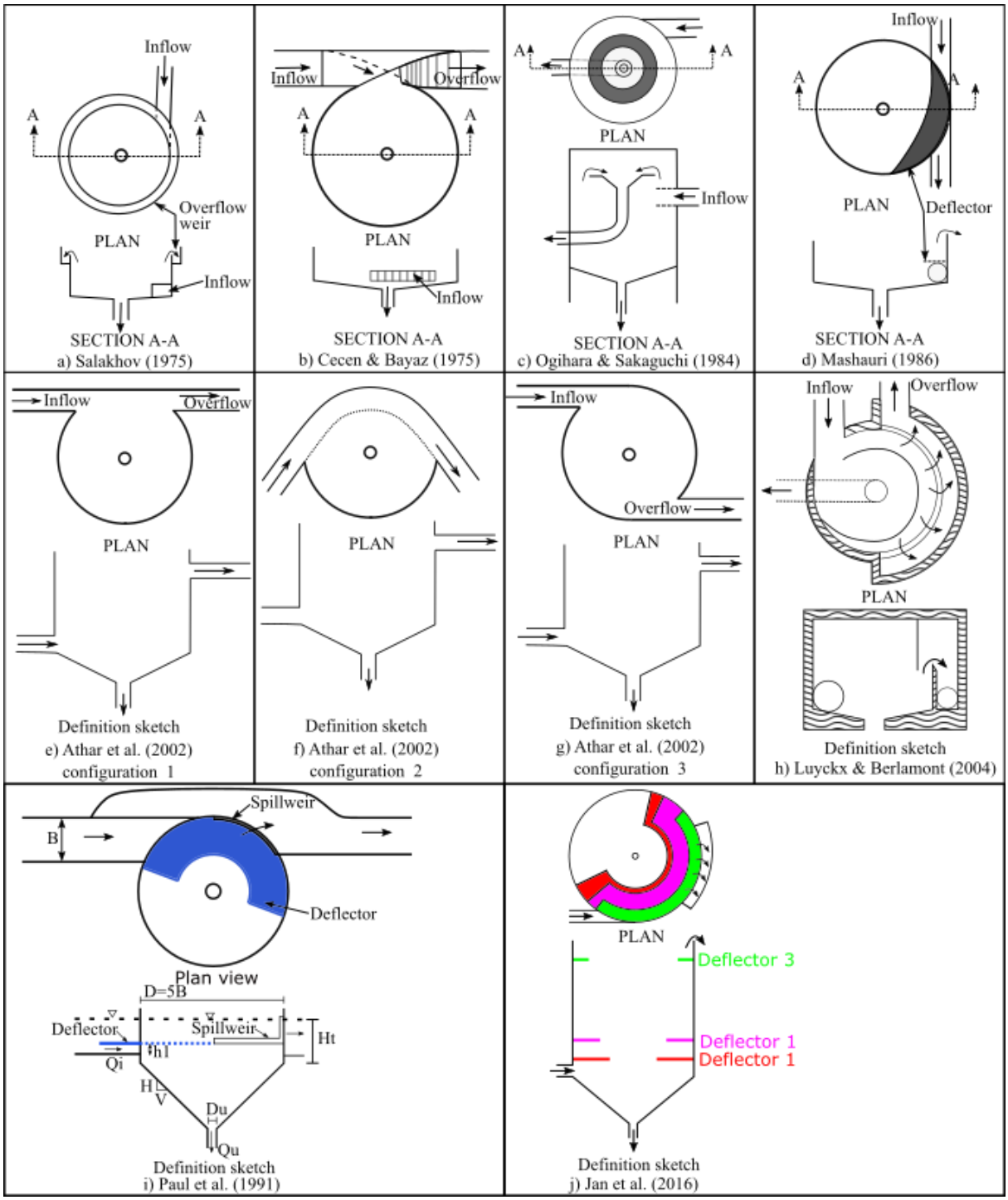

Figure 2-9: Different model configuration (adapted from Athar et al. (2002b); Jan et al. (2016); Luyckx & Berlamont (2004); Ogihara & Sakaguchi (1984) and Paul et al. (1991))

Where Qi: Inflow (l/s), Qu: underflow (l/s), h1: height between the base of cone and deflector (m), Du: diameter of underflow (m), B: canal width (m), D: VSB diameter (m), Ht: height between the base of cone and water level (m)

In the combined sewer, deflectors have been utilised in patented Hydrodynamic Vortex Separators (HDVS) shown in **Figure 2-10**. The StormKing with inlet deflectors and top baffles achieves a trapping efficiency of 95% for particles >105 µm (Andoh & Saul, 2003). The orientation, size and location are patented or are not well documented in literature and will be investigated in section 5.

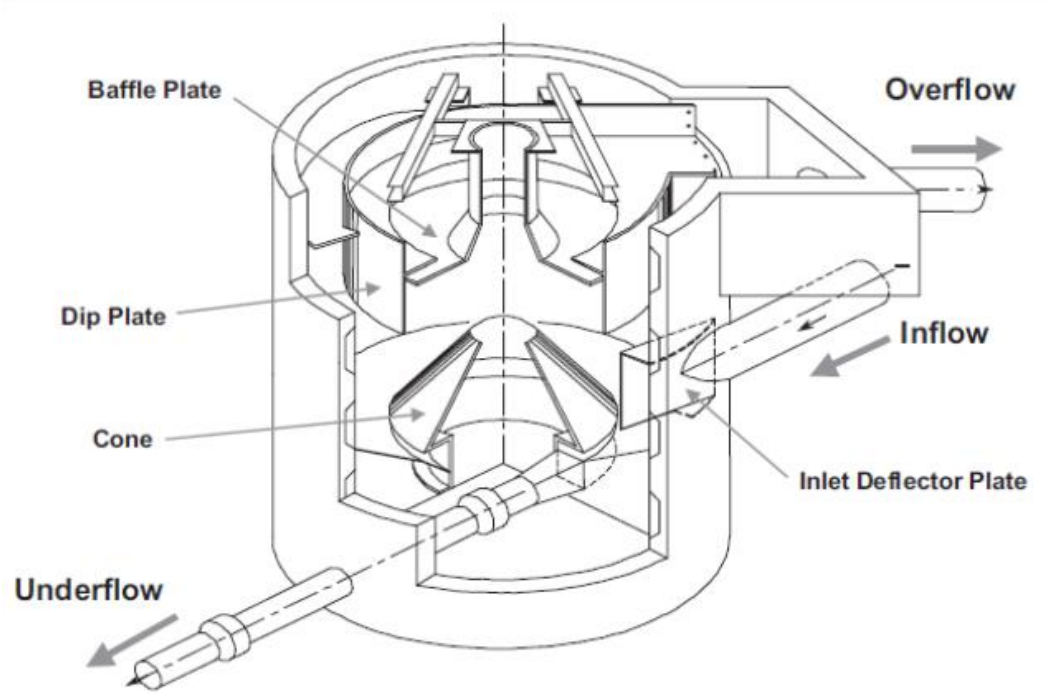

Figure 2-10: Illustration of StormKing overflow HDVS (adapted from Andoh and Saul (2003))

2.4.6 Centroid outlet

In the current study, optimisation of Model 1 configuration was undertaken, although side outlets have been utilised extensively by various authors in the removal of particles >300 µm. It was concluded that it underperforms in the removal of sediment particles >75µm. The study of other outlet configurations is undertaken in section 4.12 and a summary of various outlet configuration considered is discussed below.

In the combined sewer, centroid outlet has been utilised in patented GritKing and TeaCup separators shown in **Figure 2-11**. The TeaCup (2019) is optimised for removal of particles larger than 75 µm at a 95% efficiency at flows greater than 4.4 l/s with head loss less than 0.31 m. The GritKing (2019) has been optimised for removal of sediment particles larger than 106 µm at a 95% efficiency at flows greater than 11 l/s. Veerapen et al. (2005) in aquaculture solid waste removal, considered various outlet (**Figure 2-12)**:

a) ½ inch pipe outlet,
b) ¾ inch pipe outlet,
c) ¾ inch reversed pipe outlet,
d) Disc outlet,

e) Side outlet,
f) Centroid pipe with side outlet and

concluded that **Figure 2-12 (b)** is optimum for fish waste removal. With these options from literature, various centroid configurations are considered in section 4.12 that are optimum for river abstraction works.

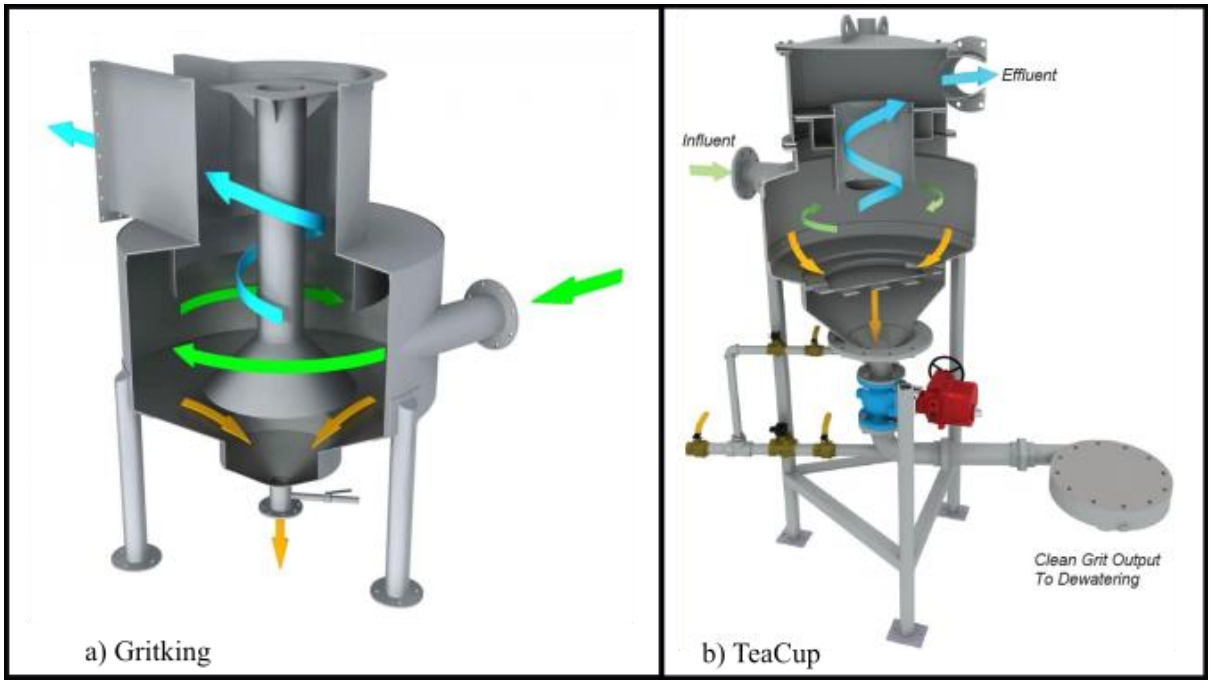

Figure 2-11: Illustration of patented Grit King and TeaCup separators (adapted from GritKing (2019) and TeaCup (2019))

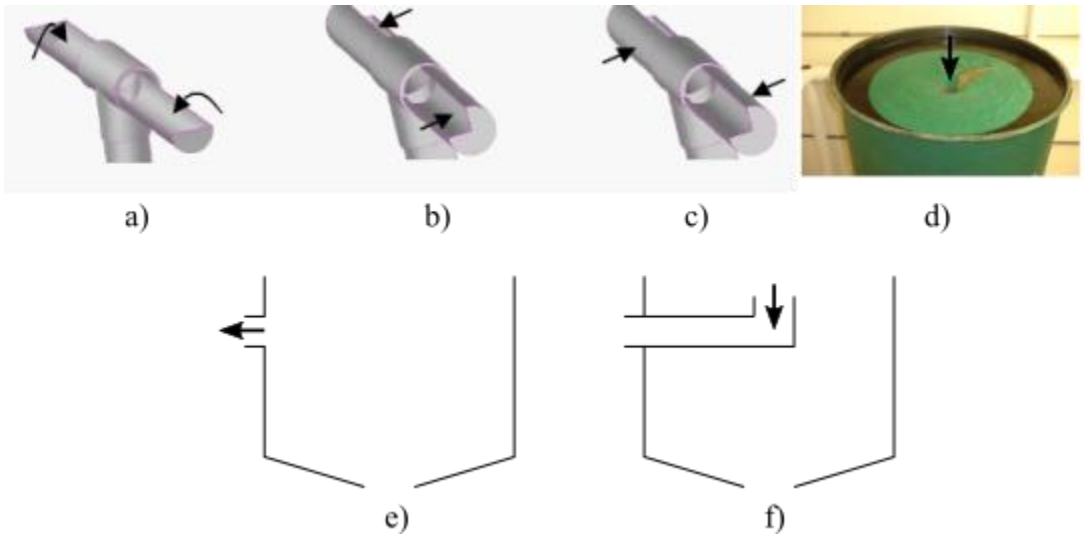

Figure 2-12: Various outlet considered by Veerapen et al. (2005)

2.4.7 Efficiency removal prediction

Athar, Jamil, and Ashfaq (2005) incorporated all the results from different authors and suggested the use of **Equation 2-18**. The equation has a margin error of ∓40% and is only valid for a range of parameters, as shown in **Table 2-4.**

$$n = 0.40\left[\left(\frac{Qu}{Qi}\right)^{0.27}\left(\frac{Di}{D_u}\right)^{0.1}\left(\frac{\omega d50}{v}\right)^{0.12}\left(\frac{Ht}{Du}\right)^{0.35}\right] \quad \text{Equation 2-18}$$

Where n: trapping efficiency, Qu: underflow (m^3/s) ,Qi: inflow (m^3/s), Di: diameter of inflow, Du: diameter of underflow, ω:particle fall velocity (m/s), d50: mean particle size (m), v:kinematic viscosity (m^2/s), Ht: depth of flow (m)

Table 2-4: Range of parameters used by different investigators (Athar et al., 2005)

Investigator	**PARAMETERS**								
	Qi l/s	**Qu l/s**	**Di cm**	**Du cm**	**d50 mm**	**Hi cm**	**B cm**	**Ht cm**	**ω cm/s**
Curi et al. (1975)	4.46-12.13	0.22-1.1	90	2.17-5.08	0.8-3.40	5.0	18.0	5.78-20.08	2.0-16.04
Mashauri M-1 (1986)	6.8 - 17.0	0.15-1.09	50	1.5-2.0	0.38-1.80	8.5	5.5	10.02-10.06	0.332-6.70
Mashauri M-11 (1986)	2.42-3.50	0.152-0.182	50	1.0-2.0	0.19-0.75	8.0	5.0	10.08-10.12	2.27-11.15
Athar et al. (2002)	8.0-22.0	0.589-2.90	100	100	0.06-0.93	5.0-12.5	20.0	15.9-25.9	0.267-13.68
Athar et al. (2002)	8.0-17.0	0.62-2.90	100	10	0.06-0.22	5.0-12.5	20.0	17.9 28.1	0.267-2.86

Where: Qi: inflow (m^3/s), Qu: underflow (m^3/s), Di: diameter of inflow (m), Du: diameter of underflow (m), d50: particle mean diameter (m), Hi: length between cone base and inlet (m), B: Inlet channel width (m), Ht: depth of flow (m), ω:particle fall velocity (m/s)

2.4.8 Design example

To summarise the literature an example of configuration **Figure 2-9 (i)** shallow VSB ($Ht/D < 1$) is illustrated below:

i. Inlet discharge Qi, mean sediment size d50, sediment fall velocity ω, canal width B need to be known prior.
ii. From section **2.2.1**, the basin diameter is determined from equation D=5B, with a cone slope 1:10 as in section **2.2.2**.
iii. From section 2.4.3, (Qu/Qi) is taken to be between 8 to 13%. Thus, the underflow can be determined.
iv. Section **2.4.4** gives the cylinder height, which can be determined from the equation; $(Ht/D \approx 0.6)$.
v. The expected efficiency determined from **Equation 2-18**

These equations can be used up to flows of about 60 m^3/s to remove sediment sizes d50 >30mm

2.5 Sediment characteristics in South African river abstraction works

South Africa's semi-arid climate oscillates between drought and flood, and so do the river flows. The flows can be said to be seasonal with floods lasting for a few minutes/hours and low flows even lasting for years during drought periods.

The majority of river abstraction works in South Africa are found in alluvium rivers (Rooseboom, 2002). Typically, the sediment median grain size (d50) of river beds after floods is 0.2 mm to 0.5 mm. As noted by Brink et al. (2006) the sediment transported in suspension during floods is relatively fine with about 40% clay (0.98 µm –3.9 µm), 40% silt (3.9 µm – 62.5 µm) and 20% sand (62.5 µm-2 mm). However, the mountainous reaches of the Western Cape differ with more bedload transport. The fines in South African rivers make the vertical distribution of sediments more uniform, which is unique for South African rivers.

The fine sediment load of South African rivers is highly variable, influenced by the availability in the catchments rather than the transport capacity of rivers. During the first storm of the year, the fine sediment will all be transported, but in subsequent storms, sediment in the catchment will have been depleted thus the sediment transported in the river is less than the river's transport capacity. Bedload, on the other hand, is influenced by transport capacity (Brink et al., 2006).

High variability of sediment loads over time coupled with a near-uniform vertical distribution makes the designs in South Africa rather complex.

2.6 Abstraction location and secondary flow

The principle of diverting as little sediment as possible from the main channel and removing the deposited sediments from the abstraction works with the most inexpensive available method is recommended. Helicoidal flow created at river bends can aid in diverting little sediment. Sediment-laden bottom flow moves towards the inside of the bend while the upper flow with less suspended sediment moves towards the outer bend where diversion works should be located.

With approximately 60 to 80% of sediments transported in South African rivers being fine, the principle of sediment rejection is not applicable when considering total load due to the near-uniform lateral and vertical distribution of fine sediments. However, coarse sediment can utilise this principle as an important consideration in the design, since pumps and pipelines are generally sensitive to these grain sizes (Basson, 2006).

Generally, abstraction works should be located at stable banks, preferably just below the vertex of concave banks with caution taken with meandering rivers (Tan, 1996). Use of numerical and physical modelling is recommended to ascertain the location as well as various aspects of design as empirical equations have inherent uncertainty.

2.7 Numerical modelling

2.7.1 Introduction

Computational Fluid Dynamics (CFD) of fluid flow has in the recent past become an integral tool in adding and complementing otherwise expensive and time-consuming physical modelling. Reduction in lead times, ability to carry out automatic/assisted optimisation, easy tweaking of scenario and parameters, the unparalleled in-depth study of details and possible large volumes of configurations and data make CFD an attractive option.

Fitting of the physical world into numerical algorithms comes with a cost and greater responsibility. Over time there has been a significant uptake of numerical modelling and demand for more realistic approximated results. Gradually, initial simplifying assumptions have been incorporated into the main equations and so has been the demand of computing power. So far, the technological computing demand has kept up with more powerful computers being availed or so cloud computing has caught up.

With computing power not being a limiting factor any more and more assumptions incorporated, a proper understanding of underlying principles and assumptions are needed. This chapter will try to introduce the basic principles used for this study and will not dwell into CFD as a topic. If a more detailed understanding of computational numerical analysis is needed, ANSYS (2018) user guide and Versteeg and Malalasekera (2007) offer a clear in-depth study on this topic.

To unlock the potential of CFD, the following essential steps are undertaken and are summarised in **Figure 2-13** below:

i. Pre-processing:
   - The identification of goals
   - Identification of possible assumptions and bounding of the domain
   - Setting up domain and mesh generation keeping in mind the accuracy needed, computational resources and lead time
   - Sound boundary conditions
   - Definition of material properties
   - Selection of appropriate physics

ii. Solving, calibration and verification

iii. Post-processing

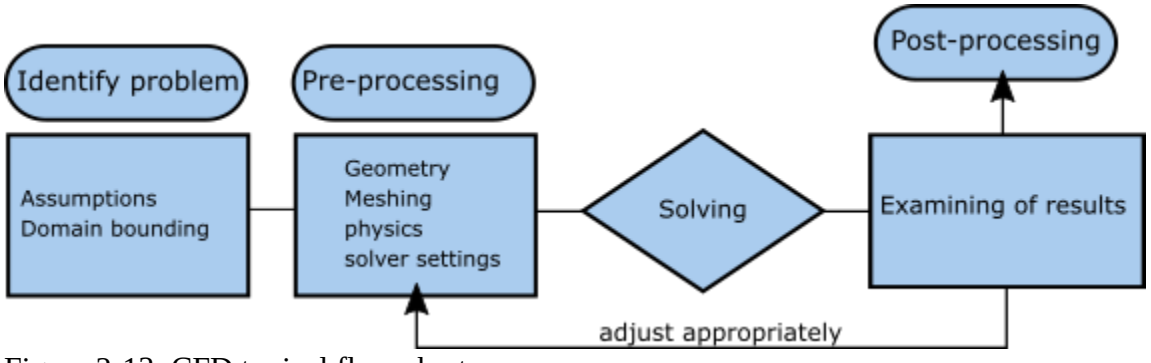

Figure 2-13: CFD typical flow chart

In this study, ANSYS FLUENT version 18.2 pre-processor, solver and post-processor engine is used (ANSYS, 2018). ANSYS FLUENT being a commercial leader in CFD application, having well-proven modelling capabilities and availability of student license plus access to the computers of The Centre for High-Performance Computing (CHPC) in South Africa made it an easy choice and it was deemed unnecessary to develop custom codes for this project.

2.7.2 Summary of governing equations.

In this study, water is the fluid medium and is assumed to be incompressible. Thus incompressible continuity, momentum and energy Navier-Stokes equations are utilised. Finite Volume Method in FLUENT is used to discretise equations. The discretisation strategy of these equations is not considered in this study; instead, the focus is on implementation. The reader is advised to refer to the ANSYS FLUENT User Guide (ANSYS, 2018) and Versteeg and Malalasekera (2007).

A discussion regarding parameters that influence the results is presented in the following Sections.

2.7.2.1 Turbulence model

Flow in a VSB is of swirling nature and turbulent. How to computationally deal with it is of importance. The following choices are available in ANSYS FLUENT (2018):

i. Direct Numerical Simulations (DNS)
   - The whole spectrum of unsteady Navier-Stokes equations is solved over space and time solving the turbulence indirectly.
   - Fine mesh is required and practically cost prohibitive.

ii. Large Eddy Simulation (LES)
   - Unsteady Navier-Stokes equation is partially solved; in that small-scale turbulence is solved and large-scale turbulence is resolved.

iii. Reynolds Averaged Navier-Stokes Simulation (RANS)
   - The whole turbulence Unsteady Navier-Stokes equations are solved by considering time averages.
   - A wide range of RANS models are available as summarised in **Figure 2-14**.

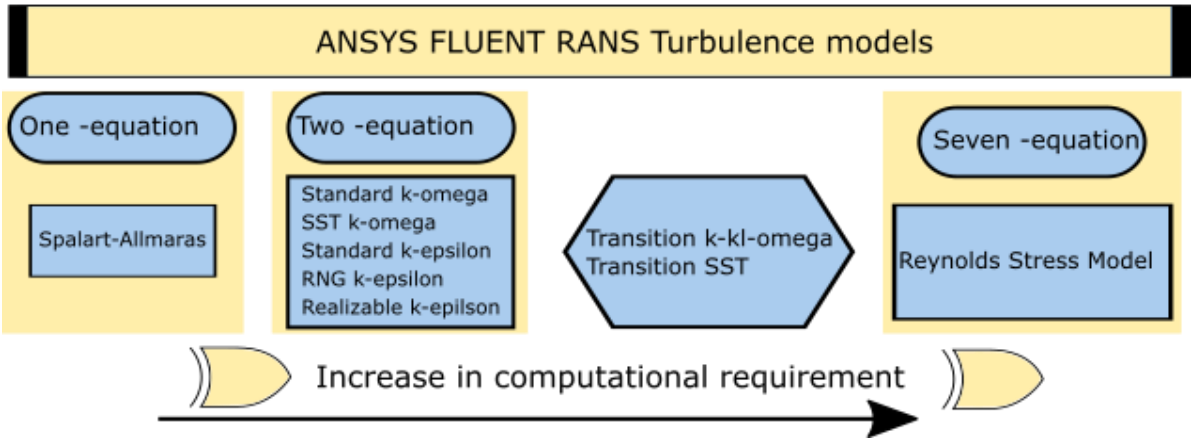

Figure 2-14: Reynolds Averaged Navier-Stokes Simulation turbulence models available in ANSYS FLUENT

ANSYS (2018) has recommended the use of the realisable k -epsilon (k- ε) turbulence model for moderate swirling flows. Boysan, Ayers, & Swithenbank (1982) and Cullivan, Williams, Dyakowski, & Cross, (2004) have analysed gas cyclones using the k-ε model and concluded that it does not give satisfactory results. In particular, Griffiths and Boysan (1996) noted that a 12% deviation with physical modelling results could be expected. Fredriksson (1999) attributed this to the model overestimating the pressure drop and tangential velocity and underestimating the axial velocity variation.

Various authors have recommended the use of LES and Reynolds Stress Model (RSM) models (Chu, Wang, Xu, Chen, & Yu, 2011; Gimbun, Chuah, Choong, & Fakhru'l-Razi, 2005; Hoekstra, Derksen, & Van Den Akker, 1999; Slack, Prasad, Bakker, & Boysan, 2000)

The LES model has the disadvantage of requiring significant computational resources than RSM utilised in this study.

An important consideration is how the wall velocities are numerically handled. In a flow field at a distance x it is known the velocity at a wall is zero and increases to a maximum value in the mainstream flow at a distance y from the wall. In turbulent flow, a viscous sub-layer exists near the wall, a buffer/transition layer and turbulent/log boundary layer. This boundary is illustrated in **Figure 2-15**.

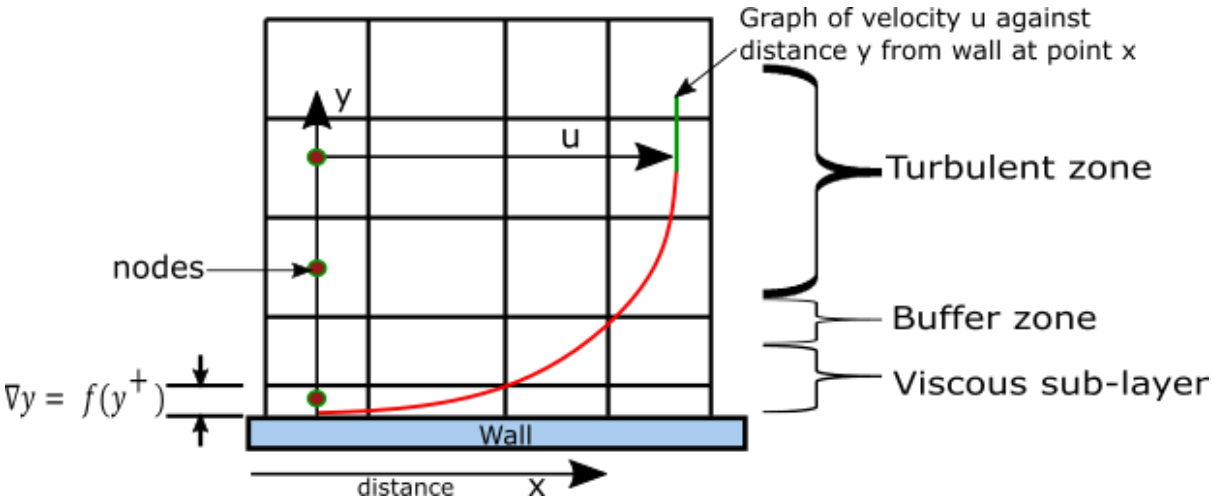

Figure 2-15: Graph of velocity u against distance y from y at point x showing the logarithmic-based wall functions (adapted from ANSYS (2018))

A CFD mesh has to be adequate to capture the velocity profile. ANSYS FLUENT handles this by either utilising:

i. Wall functions or
ii. Resolving the viscous sub-layer.

Ideally, we would want to resolve the whole viscous sublayer layer, but this requires a very fine mesh and consequently, more computational resources and thus not utilised in this study.

ANSYS (2018) noted that if a logarithmic plot of dimensionless value y+ against u is plotted, the graph obtained is more predictable and can be utilised to predict the minimum value of the

first cell. This is the wall function approach, and **Figure 2-16** below illustrates the line of fit for typical velocity profiles.

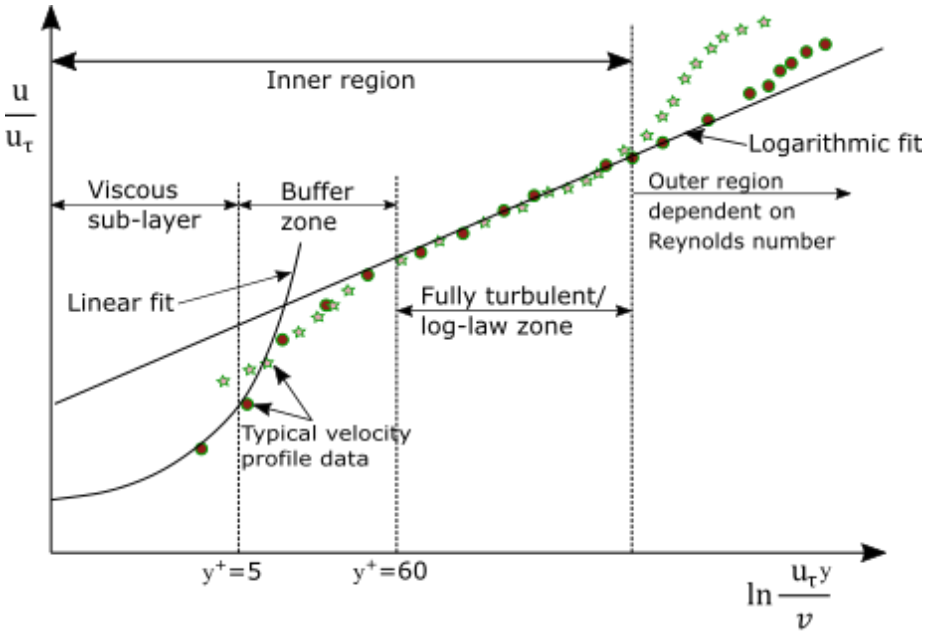

Figure 2-16: A graph of logarithmic dimensionless value y+ against velocity u* showing subdivisions of the near-wall zones (adapted from ANSYS (2018))

Where u_τ: shear /friction velocity, u: velocity parallel to the wall, ν: kinematic viscosity (m^2/s)

Standard wall functions will be utilised in this study, where the first cell is recommended to be in the predictable logarithmic region, that is valid for $30<y^+<300$. At first, the velocity is not known. Hence an approximate y^+ value is used, and the mesh iteratively sized to give desirable results.

2.7.2.2 Multiphase flow

In this study, water, air and sediment are the materials under consideration. The interaction between these three phases can be classified as:

i. Free surface flow indicating the interaction between water and air.
ii. Particle-laden flow indicating the interaction between water and sediment particles.

Two strategies of modelling multiphase flow exist, namely:

a) Euler-Lagrange: where the fluid phase is solved as a continuum, and the solid phase is tracked through the liquid phase. It assumes that the volume occupied by the solids is negligible, and thus, concentration by volume should be less than 10%. The particle trajectories are calculated at specified durations during Fluid iterations. Therefore, it is assumed the particles do not influence the liquid phase calculation. In ANSYS FLUENT, the one coupling Discrete Phase Model (DPM) is utilised, and a brief introduction of the module is discussed in section **2.7.2.2.1** below. A modified DPM module: Dense Discrete Phase Model (DDPM) that enables two-way coupling, thus

interaction between the fluid and sediment particles, is also utilised and is discussed in section **2.7.2.2.2** below.

b) Euler-Euler: all the phases are mathematically treated to be interacting with each other. It is the most mathematically sound and can be used to compute any multiphase flow but requires more computing resources. In this study, ANSYS FLUENT Volume of Fluid (VOF), which incorporates the Euler-Euler approach, will be utilised. A brief introduction to this module is introduced in section **2.7.2.2.3** below.

2.7.2.2.1 Discrete phase model (DPM)

This module enables the simulation of a dispersed phase using the Lagrangian method and the continuous phase using the Eulerian method.

Because of turbulence in the fluid stream, sediment particles try to follow the eddies as they are crossing it. A random walk or stochastic model is used to track the dispersion of particles with the Gaussian probability density function keeping track of particle concentration in the trajectory. The stochastic tracking has the advantage of accounting for local variation in the flow properties (i.e. concentration and velocity) but has the downside of requiring a large number of tries making it computationally intensive.

The discrete phase has no direct impact on turbulence in the continuous phase. The manner in which it is modelled in ANSYS FLUENT for both steady and unsteady flow is summarised in **Figure 2-17** and **Figure 2-18**.

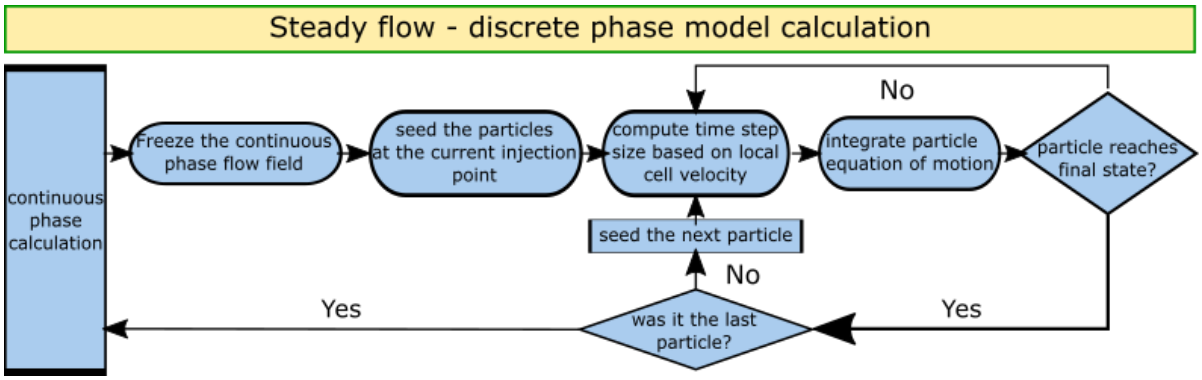

Figure 2-17: Calculation procedure for steady flow discrete phase model (adapted from ANSYS (2018))

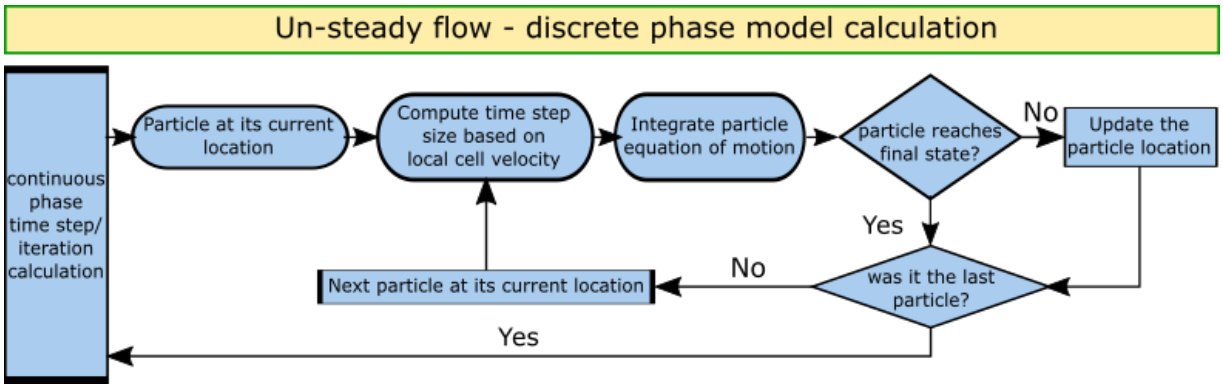

Figure 2-18: Calculation procedure for un-steady flow discrete phase model (adapted from ANSYS (2018))

The module has the following limitations:

a) The sediment particles have to be in a discrete phase,
b) Sediment particle concentration has to be less than 10-12% by volume,
c) Sediment particles have to have well-defined entry/exit boundary conditions and not remain in suspension indefinitely,
d) Sediment particles are modelled as spheres and if other properties, i.e. dynamic drag forces and shape factor are to be taken into account other submodels have to be activated,
e) There is no particle-particle sediment interaction and
f) Grid dependency for fine meshes.

2.7.2.2.2 Dense Discrete Phase Model-Discrete Element method (DDPM-DEM)

DDPM-DEM is a more enhanced DPM model where particle to particle interaction is explicitly resolved using DEM method, and dense particulate flows can be solved taking away the 10-12% volume limitation of the discrete phase. Further two-way coupling is enabled, thus the effect of sediment particles in the Fluid is resolved.

It is resource-intensive to track each sediment particle individually, and ANSYS FLUENT uses a representative particle in a pack where the mass in the in-collision calculation is the mass of the entire pack, the diameter is full pack diameter and density as particle density. A sample of particle packing is illustrated in **Figure 2-19** below. This is the module extensively utilised in this study.

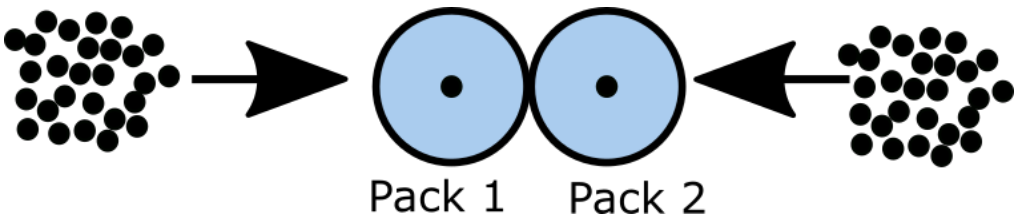

Figure 2-19: Sediment particle packing in DEM model

2.7.2.2.3 Volume of Fluid (VOF)

This module handles fluids that have clearly defined boundaries and are immiscible (e.g. water and air).

Effects of surface tension and drag are modelled in this study; this is as a result of the formation of an air-core at higher underflow discharge ($Qu/Qi>0.15$).

The phase continuity equations can either be explicitly or implicitly solved. However, in this study, the implicit scheme is used as it does not have Courant number restrictions and can take advantage of larger time steps and better adaptability to a poor mesh. An explicit interface between air and water is not well defined, but this shortcoming is acceptable as it does not affect the model trapping efficiency estimation.

3 Research Methodology

Investigating the use of a vortex settling basin (VSB) to remove sediments from coarse to fine non-cohesive sediment (down to approximately 75 µm) at small abstraction works (approximately smaller than 100 l/s) is the primary objective of this study. The target users are small-scale rural farmers, small municipalities and irrigation schemes. The investigation of the VSB was selected because it is an inexpensive method with low maintenance.

To achieve this, the following methodology was applied:

i. A review of the literature on sediment control focusing on:
   - Location, orientation and components of the works
   - Sand traps/settlers
   - Hydro-cyclones
   - Vortex settling basin
ii. Identifying possible significant parameters that affect the performance of VSB from the literature review and preliminary numerical simulations
iii. Use of physical modelling and numerical modelling with software ANSYS FLUENT (2018) to carry out tests evaluating suitable hydraulic designs for South African alluvial river sediment
iv. Reconciling the identified parameters and optimising a suitable design
v. Recommending a suitable design option and layout for cheaper sustainable abstraction works for potable water use.

Because of the complex nature of flow in VSBs and limitations in cost and time, numerical modelling was extensively used, and physical modelling used more as a validation tool for the numerical model. For the validation of the numerical model, the numerical model was set up to simulate the physical model's dimensions, flow rates and sediment characteristics on a 1:1 scale.

Two basic types of VSB were investigated, i.e. Model 1 with its tangential injection location near the bottom and Model 2 with its tangential injection point near the top of the VSB. **Figure 3-1** below illustrates the various parameters and symbology that are of concern for both Models 1 and 2 in this study and the multiple dimensions that were varied as summarised in **Table 3-1**.

With these two basic setups, the following parameters were investigated in-depth:

a) The impact of underflow to inflow ratio to achieve minimum water loss.
b) Optimal location and sizing of outlet structure to reduce turbulence and short-circuiting of sediments.
c) The impact of inlet flow rate and average velocity on removal efficiency enabling in determining the optimal inlet velocity in scaling up of the model.
d) The impact of inlet location (Hi) and tilting of the inlet on trap efficiency.
e) The impact of cylinder height (Ht) as African rivers have high variability in water levels between floods and droughts. The VSB has to be in operation in both high flows and low flows.

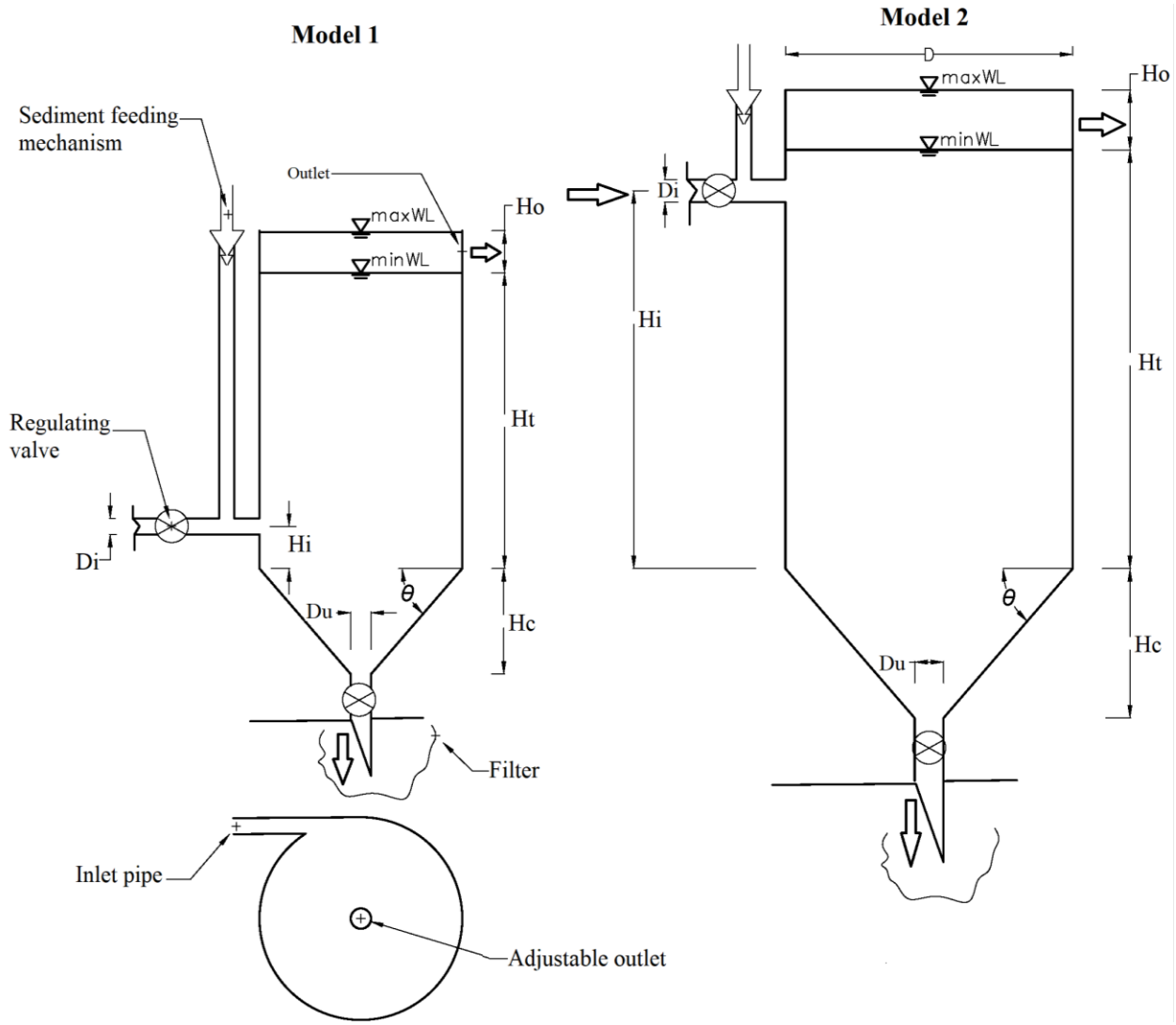

Figure 3-1: Models 1 and 2 schematic diagram

Table 3-1: Model parameters

Parameter	Symbol and unit	Model 1	Model 2
Inlet flow	Qi (l/s)	1-3	3-5
Cylinder diameter	D (mm)	480-1500	634
Inlet diameter	Di (mm)	30-100	90-156
Cone height	Hc (mm)	250-1570	330
Cylinder height	Ht (mm)	240-1530	700-1000
Outlet height	Ho (mm)	80	80
Inlet height	Hi (mm)	11.5-525	11.5-800
Underflow diameter	Du (mm)	0-53	0-53
Sediment particle diameter	d50 (µm)	75-112	75-112
Sediment concentration in inflow	C (mg/l)	10,000-50,000	10,000-50,000
Cone angle	Ø	≈46	≈46

f) The impact of cone angle (Ø) on sediment removal. African rivers sediment is cohesive in nature and if allowed to compact, the flushing becomes difficult necessitating mechanical removal.
g) The impact of cylinder diameter on trap efficiency.
h) The optimal location and sizing of deflectors, Model 1 shown in **Figure 3-1** was modified to **Figure 3-2**. The illustration shows the progressive optimisation of deflector 1 to 5 and parameters considered during optimisation. From this setup, high trapping efficiencies were achieved (>90% for 75 µm) at low flows of 1 l/s but no so when the model was scaled up to higher flows of 5 l/s. From sensitivity analysis, having the outlet closer to the outlet as shown in Model 2 in **Figure 3-1** had a more considerable influence in controlling sediment removal. This necessitated optimising Model 2 and modifying it to allow deflectors to be used.

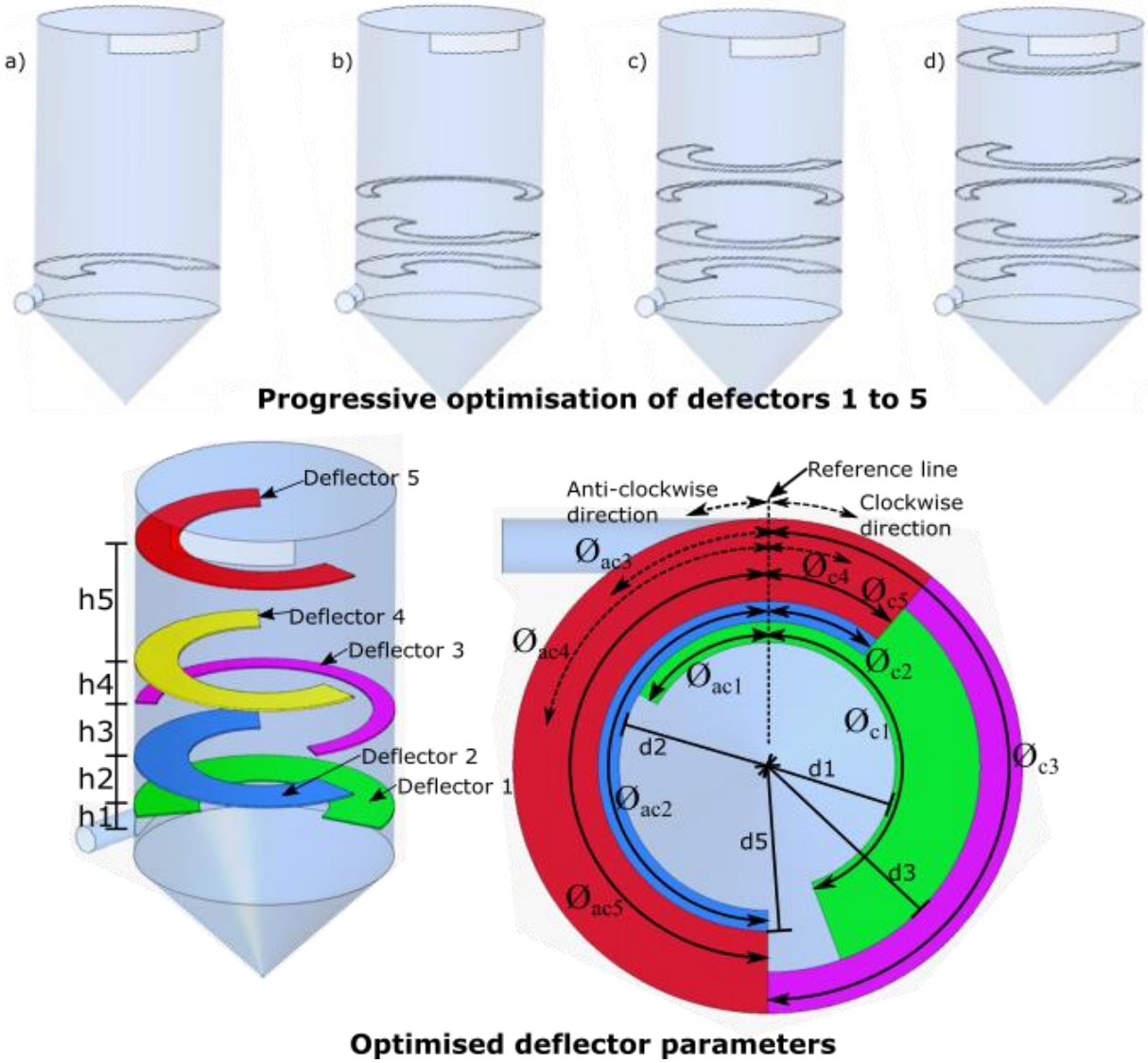

Figure 3-2: Illustration of progressive optimisation of Model 1 deflectors and parameters considered

i) To allow the use of deflectors in Model 2, the optimal parameters identified from a) to h) above were used in this setup. Impacts of different outlet configurations shown in **Figure 3-3** below on sediment removal were investigated.

j) With optimal outlet configuration, the impact of inclined deflector shown in **Figure 3-4** was investigated.

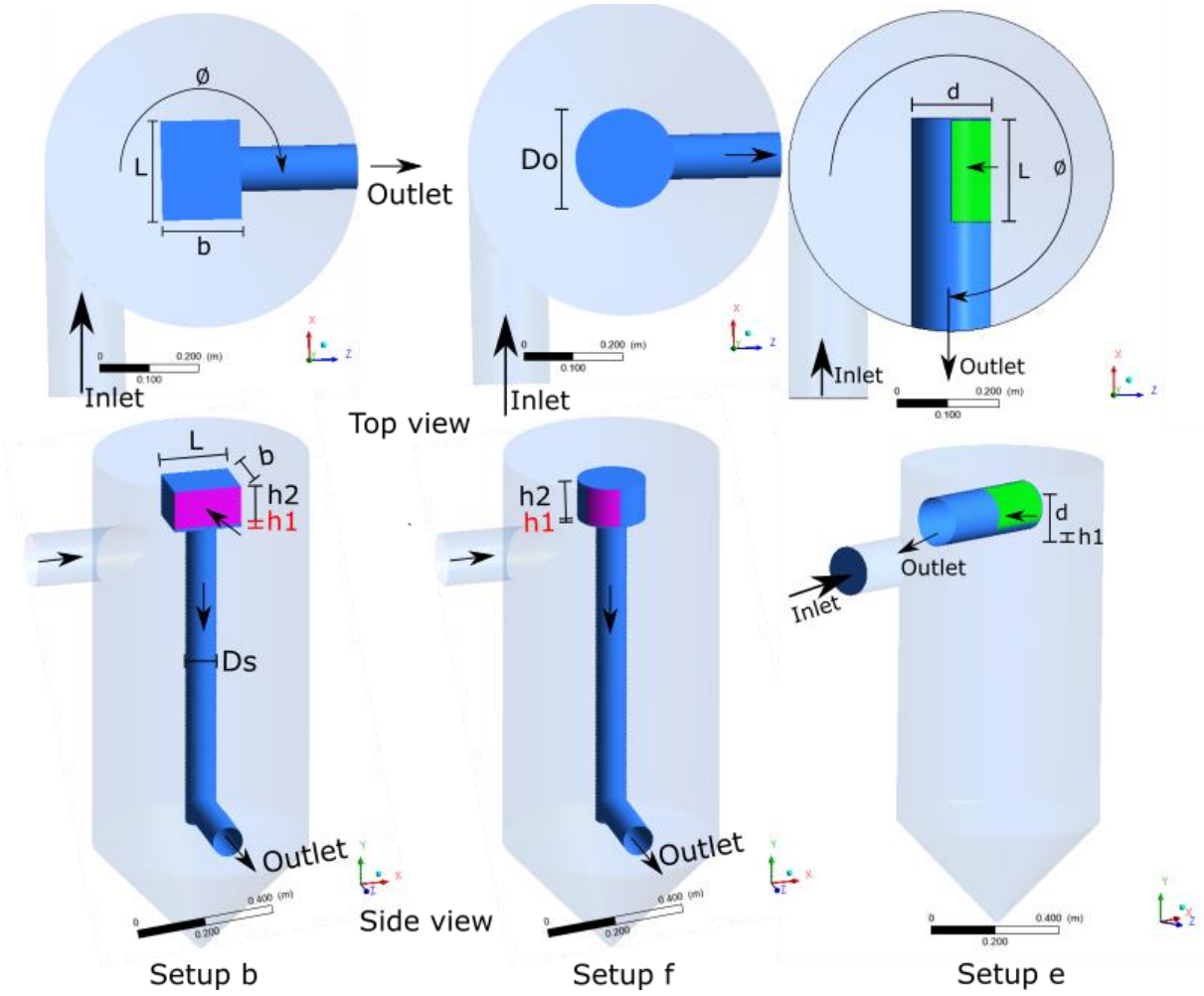

Figure 3-3: Illustration of different outlet configurations considered and parameters optimised

k) With optimal parameters selected, an optimised configuration was investigated and proposed.

l) Practical considerations were investigated to identify the applicability of the proposed schemes under different conditions not investigated in this study

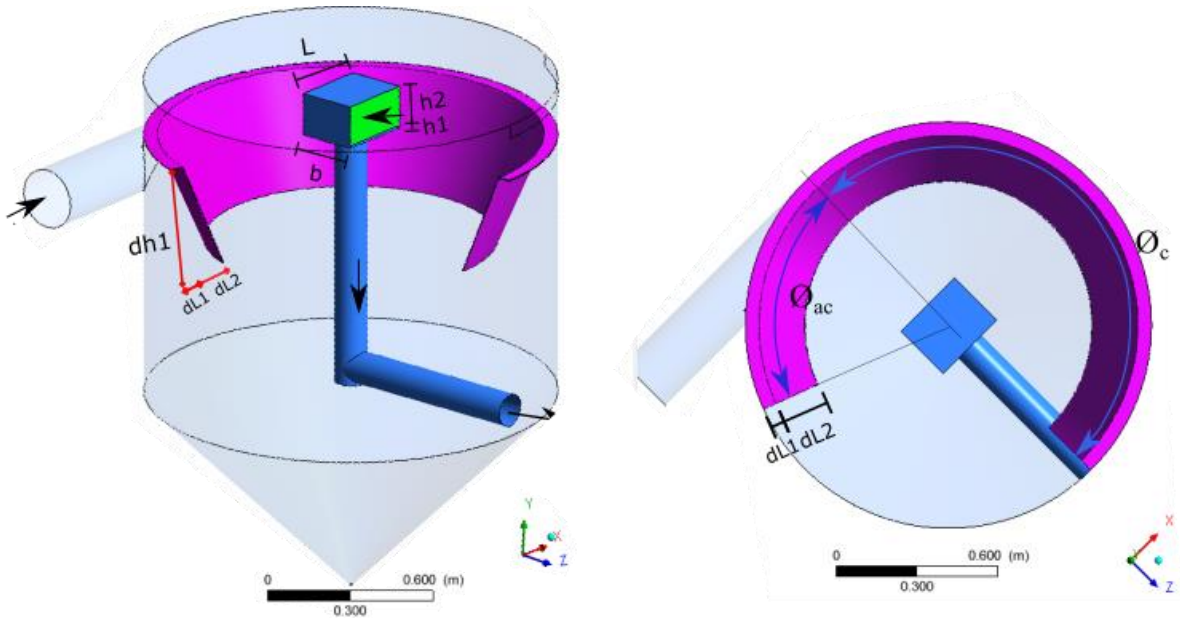

Figure 3-4: Illustration of inclined deflector and parameters optimised

3.1 Justification for parameters selected

I. Sediment size

Settling was identified as the primary sediment removal mechanism in VSB. **Table 3-2** gives a summary of settling velocity and time taken for various sediment particles to settle in 1 m water depth. Settling particles <75 µm would require a considerable retention time in the VSB and thus was deemed not practical in VSB.

Secondary currents caused by centrifugal forces help in keeping sediment particles in suspension near the outer wall increasing the retention time considerably. With this in mind, smaller particles <75 µm are susceptible to turbulence/eddies and destructive secondary currents and easily carried towards the overflow outlet.

Table 3-2: Approximate time taken by a natural sediment particle to settle in 1 m water depth

Particle size (µm)	**Settling velocity (m/s) (Equation 2-4) (Zhiyao et al., 2008)**	**Time (minutes)**
300	0.0362	0.46
100	0.0061	2.73
75	0.0035	4.77
60	0.0023	7.25
30	0.0006	27.77

II. Sediment concentration

In ungauged sites, Bosman, Prestedge, Rooseboom, and Slatter (2002) recommended, from experience, the following concentrations for design purposes:

- 20,000 mg/l: this may be exceeded during a flood event
- 40,000 mg/l: this may be exceeded during times of extremely heavy rainfall in the catchment
- 60,000 mg/l: expected only in rivers with heavy sediment load but rare

Considering a typical wide river (200 m) with bed roughness of ks of 3.084 m and mean sediment particle size of d50 =75 µm and a channel slope of 1:1000 and normal flow depth of 15 m to mimic 100 ARI flow, calculations were carried out yielding a flow of 11,681 m^3/s (**Equation 3-1**) $\left(18\log\left(\frac{12*15}{3.084}\right)*200*15*\sqrt{15*0.001}\right)$. Based on the same flow, normal depth was calculated on a flatter slope and sediment transport calculated based on Van Rijn, (1993, 2007) sediment transport **Equation 3-2** and **Equation 3-3**.

$$Q = bh * 0.18\log\left(\frac{12R}{ks}\right)\sqrt{RS} \qquad \text{Equation 3-1}$$

$$q_b = 0.015buh\left(\frac{d50}{h}\right)^{1.2} M_e{}^{1.5} \qquad \text{Equation 3-2}$$

$$q_s = 0.012buM_e{}^{2.4}D_*^{-0.6} \qquad \text{Equation 3-3}$$

With Q: flow (m^3/s), b: channel width (m), h: flow depth (m), R: hydraulic radius (m) (≈h in wide rivers), Ks: roughness coefficient, representing the size of irregularities on bed and sides (m), S: slope(-), q_b: bedload transport (kg/s), u: depth-averaged flow velocity (m/s), d50: mean particle diameter (m), $M_e = (u_e-u_{cr})/([\frac{\rho_s}{\rho_w}-1]gd50)^{0.5}$: mobility parameter (-), ρ_s: particle density (kg/m^3), ρ_w: water density (kg/m^3), $u_e = u + \gamma u_w$: effective velocity (m/s) with γ=0.4 for irregular waves (and 0.8 for regular waves), $u_w = \pi H_s/(T_p \sinh[kh])$: peak orbital velocity (m/s) based on linear wave theory, H_s: significant wave height (m), T_p: peak wave period (s), $u_{cr} = \beta u_{cr,c} + (1-\beta)u_{cr,w}$: critical velocity (m/s) with $\beta = u/(u+u_w)$, $u_{cr,c}$: critical velocity (m/s) for currents based on Shields initiation of motion with $u_{cr,c} = 0.19(d50)^{0.1}\log(12h/3(d90))$ for $0.0001<d50<0.0005$ m, $u_{cr,w}$: critical velocity (m/s) for waves with $u_{cr,w} = 0.24[(\frac{\rho_s}{\rho_w}-1)g]^{0.66}(d50)^{0.33}Tp^{0.33}$ for $0.0001<d50<0.0005$ m, q_s: suspended load transport (kg/s), $D_* = d50([\frac{\rho_s}{\rho_w}-1]g/\nu^2)^{1/3}$= dimensionless particle size (m), ν: kinematic viscosity (m^2/s)

Table 3-3 summarises the results. In these calculations, a maximum total load concentration of 6,853 mg/l was calculated thus, a maximum laboratory concentration of 10,000 mg/l is acceptable.

Table 3-3: Typical river sediment transport calculation based on Van Rijn (1993, 2007)

Slope(m/m)	0.001	0.00065	0.00037
d50 (µm)	75	75	75
Water density (kg/m^3) (ρ_w)	1000	1000	1000
Sand density(kg/m^3) (ρ_s)	2650	2650	2650
Channel width (m) (b)	200	200	200
Water depth(m) (h)	15.0	17	20.0
Kinematic viscosity(m^2/s) (ν)	1.14E-06	1.14E-06	1.14E-06
Ks(m)	3.1	3.1	3.1
Depth-averaged flow velocity (m/s) ($v = 0.18\log\left(\frac{12R}{ks}\right)\sqrt{RS}$)	3.89	3.89	3.89
Discharge (m^3/s)(Q=vbh)	11681	11681	11681
Critical velocity (m/s) ($u_{cr,c} = 0.19(d50)^{0.1}\log(12h/3(6*d50)$	0.41	0.42	0.42
Dimensionless particle size (m) ($D_* = d50([\frac{\rho_s}{\rho_w}-1]g/\nu^2)^{1/3}$)	1.89	1.890	1.89
Mobility parameter (-)($M_e = (u_e-u_{cr})/([\frac{\rho_s}{\rho_w}-1]gd50)^{0.5}$)	99.93	86.67	71.73
Bed load (m^3/s) (**Equation 3-2)**	0.080	0.053	0.033
Suspended. load (m^3/s) (**Equation 3-3**)	30.13	18.89	10.20
Total load(m^3/s) (q_b+q_s)	30.21	18.94	10.23
Sand transport (kg/s) ($Qs=\rho_s(q_b+q_s)$)	80053	50204	27111
Concentration (mg/l)	6853	4298	2321

Note: d90 taken as 6*d50, u_e taken as v

III. Inflow

From preliminary analysis, it was observed that there exists a specific large diameter where the VSB operates like a settler or a small diameter where it operates like a hydro-cyclone. **Section 4.10** discusses this in detail. Based on the limited perspex VSB diameter that could be manufactured, the laboratory inflow was limited to 5l/s, and larger inflows were only tested numerically.

IV. VSB dimensions and sediment size

The objective was to use minimum VSB dimensions while achieving high sediment removal efficiencies. Literature review and preliminary numerical modelling formed the basis of the initial proportions, which were modified as lessons were learnt. It should be noted works from literature focused on sediment sizes > 300 µm (see summary in **Table 2-4)** which easily settles while this study objective was to remove sediment > 75 µm. It was observed in **Table 3-2** above to settle sediment <75 µm would require a considerable hydraulic retention time for a gravity-driven mechanism. VSB is mainly gravity-driven thus; 75 µm was deemed as a practical sediment size.

3.2 Laboratory model setup

Two laboratory model setup configurations as shown in **Figure 3-5**, **Figure 3-6** and **Appendix A2** were used in the physical model investigation. One consisted of a 480 mm internal diameter, 1000 mm tall clear Perspex cylinder and the other a 634 mm internal diameter, 700 mm tall clear perspex cylinder, each had an approximately 46° concrete cone base chosen to minimise fine sediment settling in the cone. The cone base was connected in each case to a 38 mm PVC pipe with a valve controlling the rate of the underflow.

The inflow was supplied from a 0.7 m^3 tank regulated by a valve and monitored on the flow meter. Sediment was injected into the flow stream after the valve using an hourglass type mechanism.

Both inflow and outflow sediments were captured in separate filters and sediment-free water in separate marine ply tanks and repumped to the supply tank. **Figure 3-5** below illustrates this.

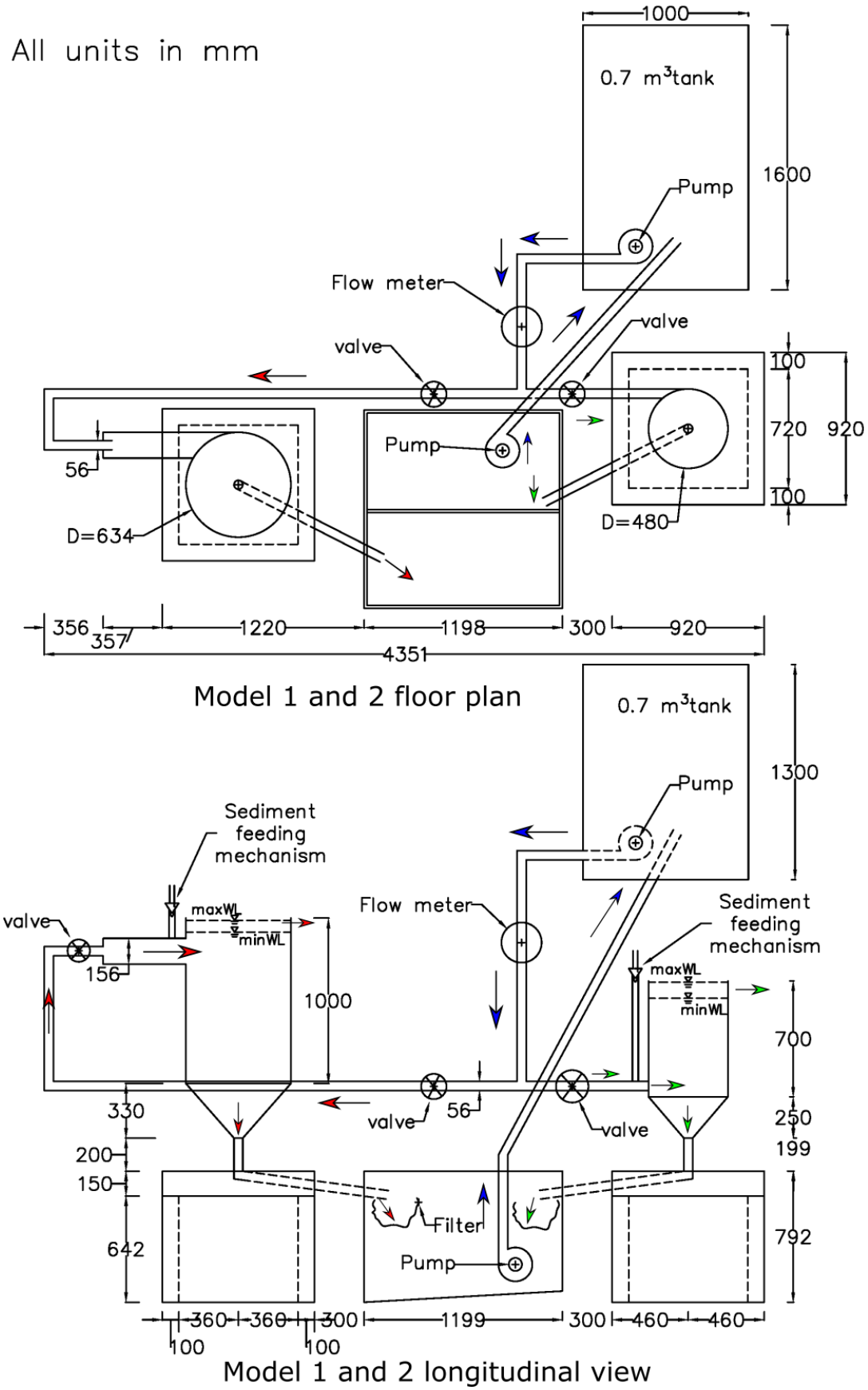

Figure 3-5: Model 1 and 2 longitudinal, floor plan and schematic setup incorporating vortex settling basin

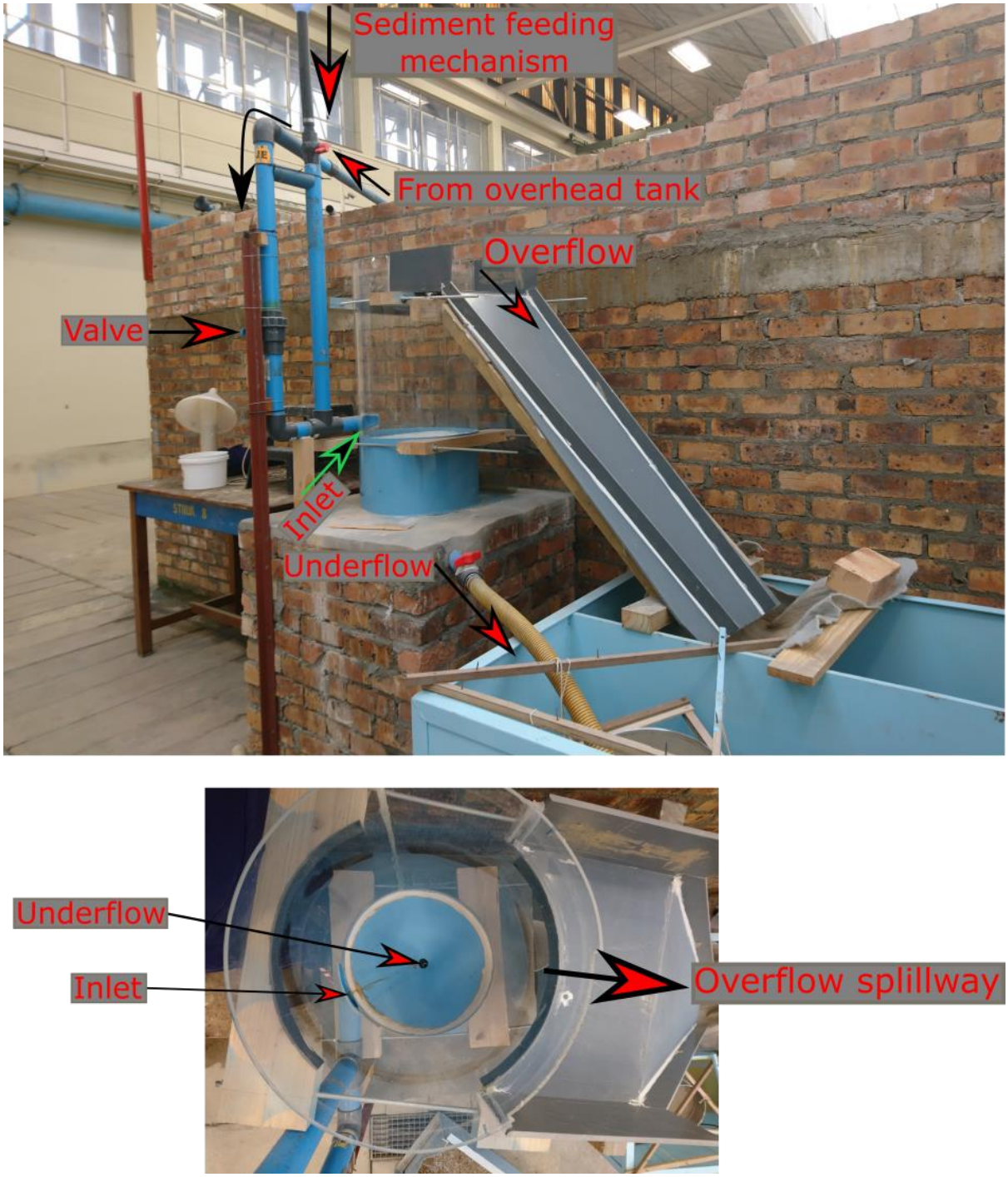

Figure 3-6: Models 1 side and top view as constructed in the laboratory

3.3 Physical model test procedure

For each run test, clean water was first injected into the VSB until stabilisation conditions met. With stable states, a predetermined mass of sediment was injected at a constant flow rate achieving a specific concentration.

The setup was allowed to run for about 3 minutes until there was no visible sediment in the VSB, while all the sediment particles at inflow and outflow were collected at filters located at both ends. The sediment was dried in an oven operated at 100 ℃ for 2 hours and mass balance determined for trapping efficiency calculations.

Each test scenario was repeated three times, and an average was taken as the result after ensuring there was no considerable deviation between the outcomes.

3.4 Numerical modelling

To complement the physical modelling, ANSYS FLUENT version 18.2 (ANSYS, 2018) was used to optimise the design and carry out preliminary tests. Section **2.7** above gives a detailed clarification as to why some modules were implemented. In all numerical simulation cases of the physical model a 1:1 scale was used without scaling.

To successfully utilise ANSYS FLUENT various tasks were undertaken and the flowchart in **Figure 3-7** below summarises this.

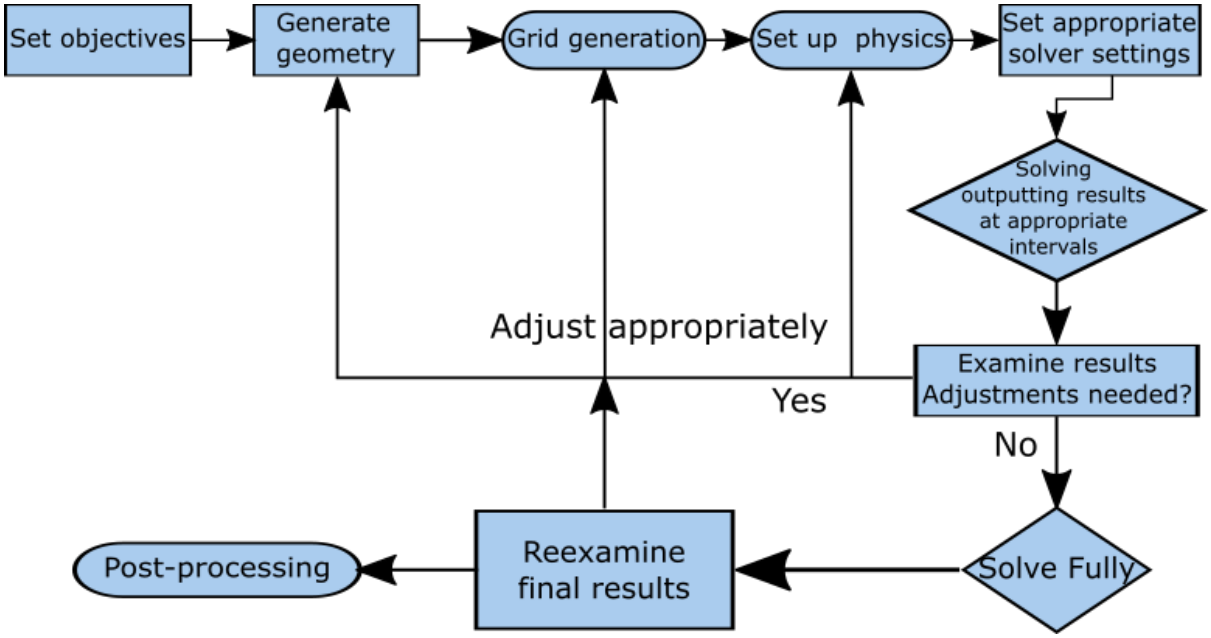

Figure 3-7: ANSYS FLUENT model flowchart

In accordance with the objective, as an example to compare the influence of underflow diameter on VSB trapping efficiency in the physical model, all the other parameters were held constant and only the underflow diameter was made a variable.

The type of mesh and grid size have a considerable influence on the convergence, stability, accuracy and run times of the model. **Figure 3-8** shows a generated tetrahedral and hexahedron

mesh type of the laboratory model setup. Although the cell sizes have the same settings, there is a significant discrepancy between the number of elements; the tetrahedral meshing generates about six times more elements increasing the runtime considerably. This study utilised both types of mesh with hexahedron meshing being dominant and tetrahedral mesh only used at zones of non-uniform/complex geometry locations.

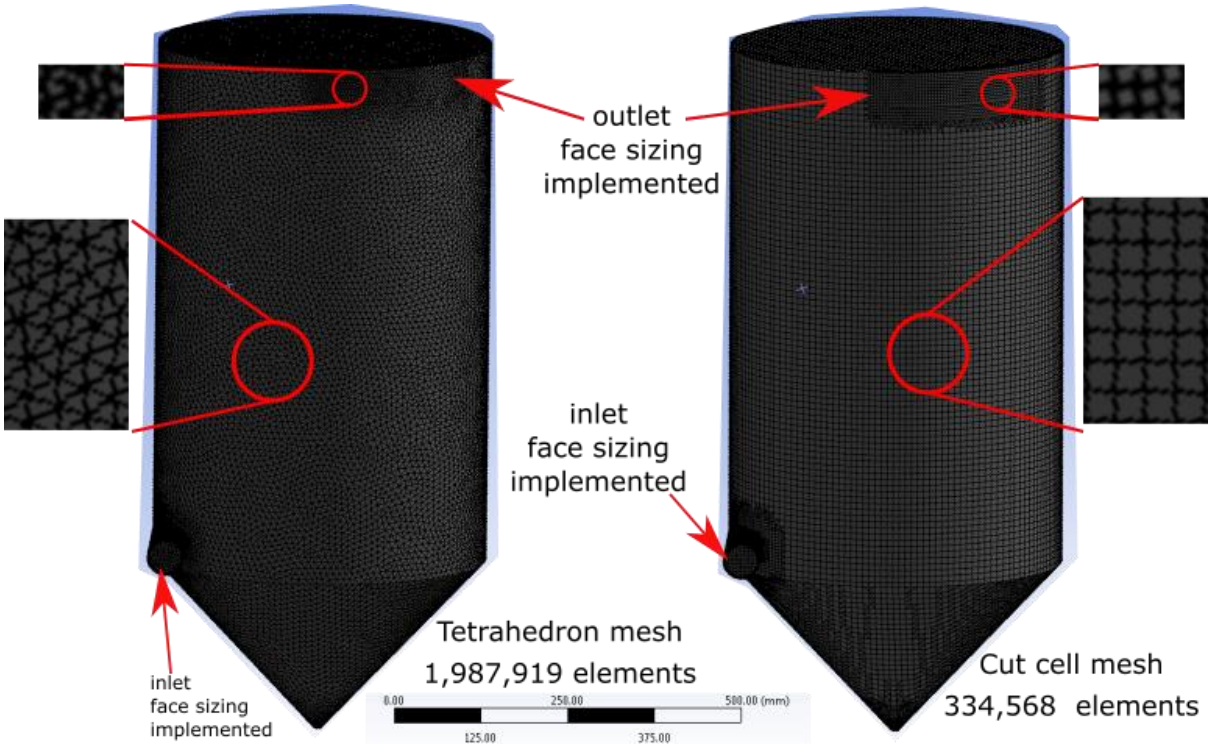

Figure 3-8: VSB meshing comparison between tetrahedron and hexahedron

Sensitivity analysis was conducted to scrutinise the influence of the mesh and grid refinement to ensure computed results were independent of the mesh characteristics. **Figure 3-9** below shows a graph illustrating different cell sizes and corresponding numerical model trapping efficiency plus the corresponding physical model result for validation. The physical models' results were used to establish the mesh size at which the numerical model results closely agree. It was concluded that the simulated results become grid-independent at a value higher than 455,903 which is almost equivalent to a maximum hexahedron size of 8 mm. As discussed under section **2.7**, fine mesh elements lead to grid dependency when the DDPM module is utilised. Fixing the minimum element size at 0.3 mm, which is two times larger than the smallest sediment particle (0.150 mm) injected in the flow stream, avoided this.

At the boundary location, the grid size has to be adequate to capture the flows. Face sizing the element achieved this and is illustrated in **Figure 3-8** above where the inlet and outlet boundary sizes were fixed at 4 mm.

There are various parameters summarised in **Table 3-4** suggested by ANSYS FLUENT to check the quality of the mesh. For all the setups these values were achieved.

Table 3-4: ANSYS FLUENT mesh metric parameters to check the quality of the mesh (ANSYS, 2018)

Parameter	**Acceptable value**
Element quality	>0.2
Orthogonality quality	>0.2
Skewness	< 0.8
Aspect ratio	Not more than 5:1.

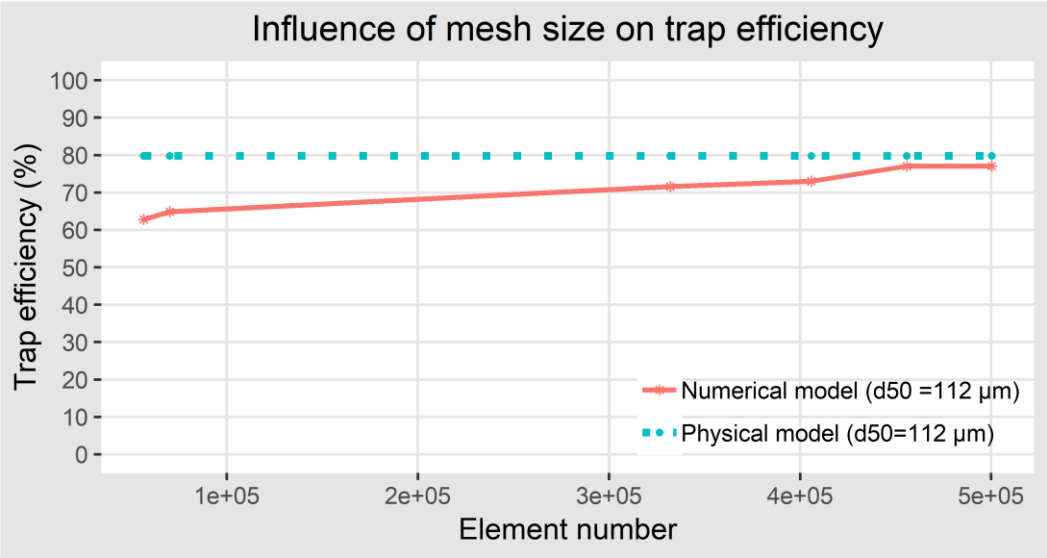

Figure 3-9: Graph showing simulation results grid dependency (physical model not affected by element number thus dashed for illustration)

Grid setup and generation is iterative in that the cell bordering the wall has to be adequate to capture the boundary layer. More details on this have been discussed in section **2.7.2**. The standard wall function y+ value was maintained between 30<y+<300. Adjusting the Inflation layer length near the wall, achieved this.

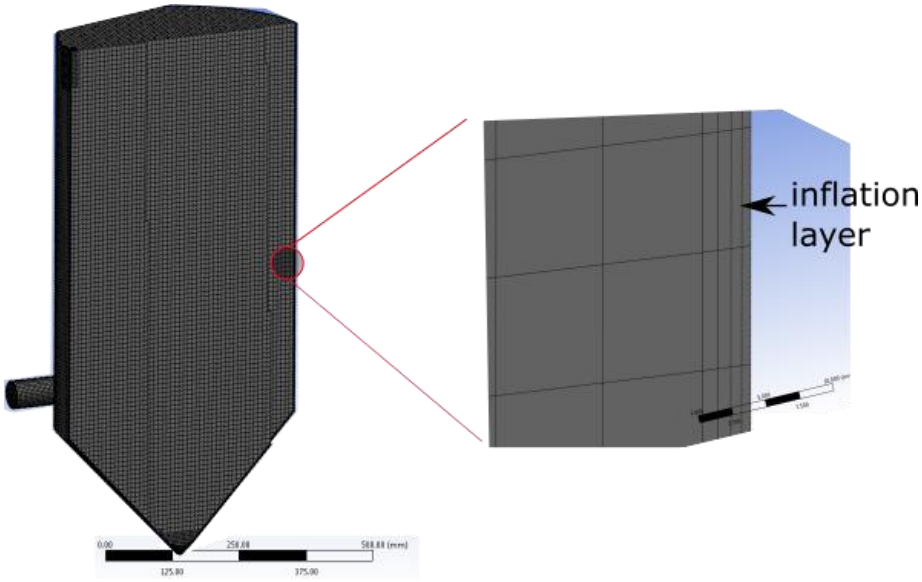

Figure 3-10: Inflation layer implemented to capture boundary layer

The Volume of Fluid (VOF) module was implemented in this study with two Eulerian phases, namely air and water. The surface tension force modelling was enabled with a constant surface tension of 0.072 N/m applied. As the level of detail between the interfaces was not of importance, a dispersed explicit scheme was implemented.

It was noted from gas-solid hydro-cyclone literature and simulations that the Reynolds Stress Model (RSM) and Large Eddy Simulation (LES) are better suited than the standard k- ε model. Although VSB operates at a lower Reynolds number, the RSM model with standard wall function was implemented in this study.

Other ANSYS FLUENT parameters implemented for this study are summarised in **Table 3-5** below.

Table 3-5: Summary of other ANSYS FLUENT setting parameters

Solver setting	
Pressure based	
Gravity	9.81 m/s^2
Operating density	1.225 kg/m^3
Boundary condition	
Inlet	Velocity inlet/inlet and hydraulic diameter turbulence
Overflow outlet	Pressure outlet/inlet and hydraulic diameter turbulence
Underflow outlet	Pressure outlet/inlet and hydraulic diameter turbulence
Solution methods	
Pressure-velocity coupling	Coupled
Gradient	Least Square cell-based
Pressure	PRESTO!
Momentum	Second-Order Upwind
Volume Fraction	Compressive
Turbulent Kinetic Energy	Second-Order Upwind
Turbulent Dissipation Rate	Second-Order Upwind
Reynolds Stresses	Second-Order Upwind
Pseudo-transient	
Warped-Face-Gradient Correction	
Default under-relaxation factors	

With appropriate CFD model setup, simulations were conducted, and the level of convergence monitored. Equations Residual was set at $1x10^{-5}$ which is more than ANSYS FLUENT default convergence criterion value of $1x10^{-3}$. Further, the mass balance was monitored.

For steady simulations implementing DPM method, particle injection was executed once steady flow conditions were achieved. Sediment particles flowing through the overflow were taken as escaped particles, underflow as trapped with the walls reflecting the particles. In some situations, there are ≈1-5 particles tracked as incomplete in the large VSB; these are particles

that remain in suspension after the simulation time and it was deemed unnecessary to increase the simulation time as to know their eventual fate.

Figure 3-11 below shows the numerical model particle tracking DPM module sample results, with the efficiency calculated from **Equation 3-4**.

$$\text{Numerical model trap efficiency} = \frac{\text{number of particles trapped}}{\text{number of particles injected} - \text{number of incomplete}} \qquad \text{Equation 3-4}$$

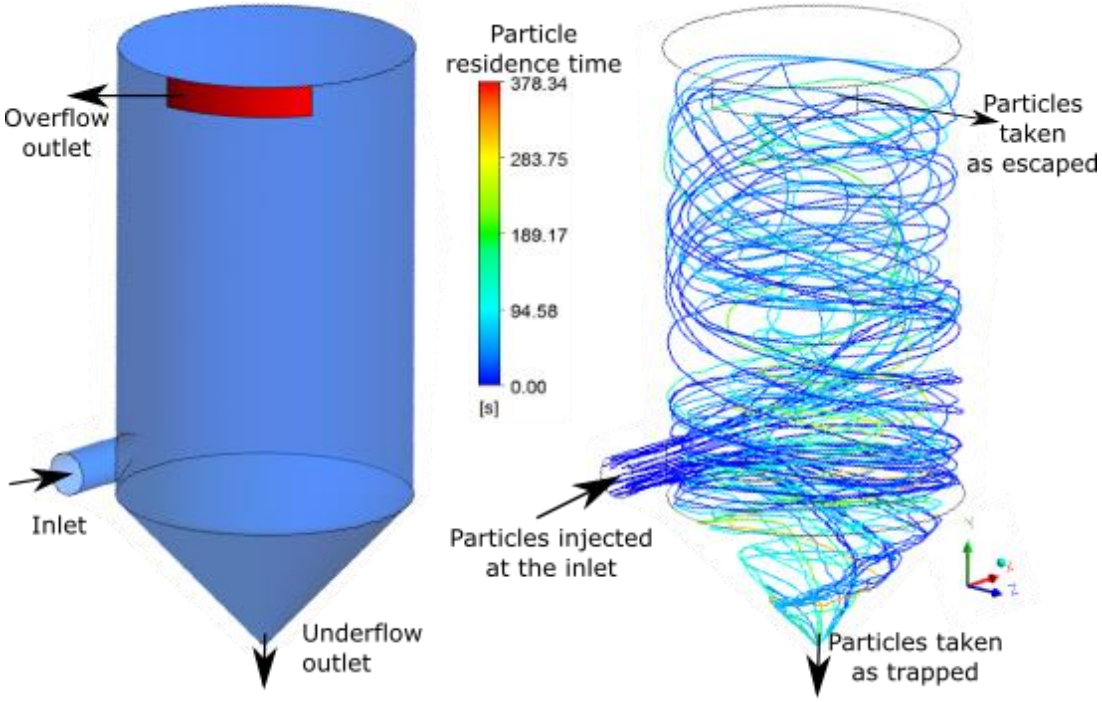

Figure 3-11: Simulated ANSYS FLUENT Particle tracking

3.5 Parameters to be tested

Various parameters affect the efficiency of a VSB, and the physical model trapping efficiency is defined as; $\text{physical model trap efficiency} = \frac{\text{sediment mass of size x in the underflow}}{\text{the mass of inflow sediment}}$ where x is sediment of size d50 =112 µm for example, however, of particular interest in this study are:

i. The impact of inlet flow rate and average velocity on removal efficiency enabling determination of the optimal inlet velocity in scaling-up of the model.
ii. The impact on inlet location, Hi, on trapping efficiency.
iii. The impact of cylinder height to diameter (H/D) ratio. Preliminarily results have shown that this ratio plays a significant role in the removal of fine sediment. In previous studies done, $\frac{H}{D}$ ratio was maintained at a ratio of less than one. In this study, the $\frac{H}{D} > 1$ thus we have assumed a deep-depth VSB.
iv. Optimal location and sizing of the outlet structure to reduce turbulence and short-circuiting of sediments.
v. The impact of underflow to inflow ratio in deep-depth VSB.
vi. Location and sizing of deflectors. Numerical modelling shall mainly aid in determining the flow fields and impacts for optimal design.
vii. The impact of cylinder diameter on trapping efficiency.
viii. Energy requirements.

4 Results and analysis

4.1 Overview of the Chapter

Various parameters summarised in **Table 3-1** influencing the sediment trapping efficiency of VSB were investigated and are reported in this chapter. **Figure 4-1** below gives a schematic overview of model optimisation. Three classes of sediment sizes were considered: single-particle sizes of 75 µm and 100 µm and median particle size (d50) of 112 µm.

Physical and numerical modelling were conducted on Model 1 and Model 2. The main difference between the two models being the position of inlet location, cylinder diameter and Model 2 optimised for higher flows (3 l/s to 5 l/s). The impact of the following parameters on sediment removal efficiency were investigated:

i. Influence of underflow,
ii. Influence of location and sizing of side outlet,
iii. Influence of inlet velocity,
iv. Influence of inflow rate,
v. Influence of inlet position,
vi. Influence of angle of the inlet,
vii. Influence of cylinder height,
viii. Influence of cone angle and
ix. Influence of cylinder diameter.

From the above, optimal parameters that gave the maximum trapping efficiency were summarised. Model 1 was further modified with flat deflectors and optimisation of the orientation, sizing and positioning of deflectors carried out on physical and numerical modelling.

With optimised parameters, scaling of Model 1 to Model 2 was investigated. With the flat deflectors modification on Model 2, numerical modelling was intensively undertaken to optimise the fine sediment removal. From this investigation, it was concluded that the use of flat deflectors was not feasible due to:

- Sediment particles were settling on the deflectors. Due to the cohesive nature of African Rivers sediment, the design is unsustainable.
- Low trapping efficiencies with flows > 3 l/s.

The use of flat deflectors was not investigated further and Model 1 discontinued from additional optimisation. Three significant insights were learnt that led to a different design:

- Having the inlet closer to the outlet gave better trapping efficiency.
- Deflectors improved sediment trapping significantly.
- Motivated by the design of inclined hoppers for cohesive sediment, inclined deflectors were investigated.

For the utilisation of inclined deflectors and the inlet closer to the outlet, the use of centroid outlet was investigated. Optimal parameters (i to ix above) were utilised and numerical and physical modelling undertaken. Rectangular centroid outlet with a shaft was found to give maximum trapping efficiency. This outlet design with inclined deflectors were investigated further and the results discussed in chapter 5.

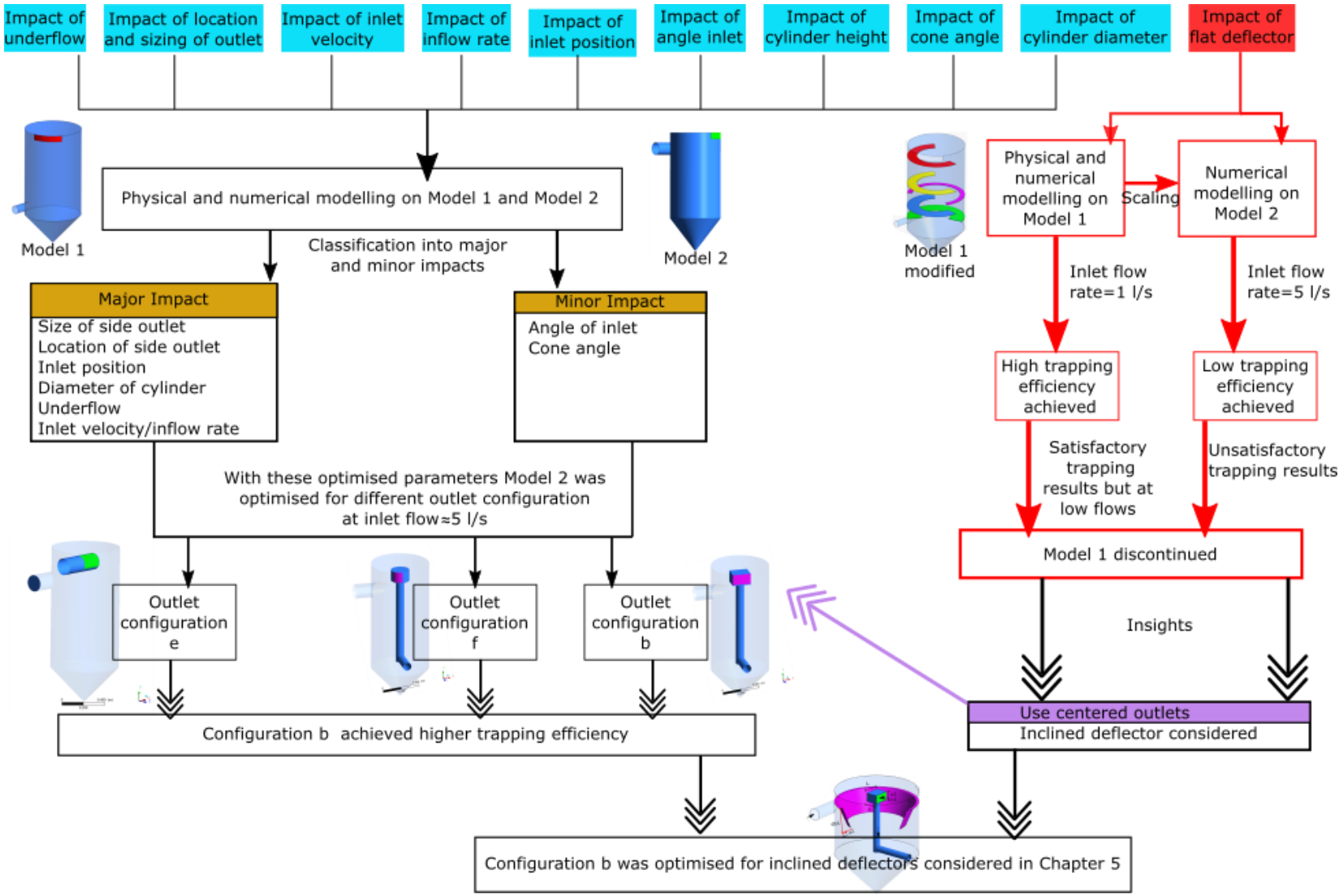

Figure 4-1: Chapter 4 overview

4.2 Influence of underflow, Qu

4.2.1 Introduction

The underflow is sediment-laden and flows back to the river. It is desirable to minimise the amount of water lost through the underflow while giving the optimum sediment removal efficiency. **Figure 4-2** below illustrates a summary of the variation of efficiency with $\frac{\text{underflow}}{\text{inflow}}$ as investigated by various authors utilising different VSB configurations. From the data, no apparent trend is observed but most reviews have kept a rate of $0.03 \leq Qu/Qi \leq 0.1$

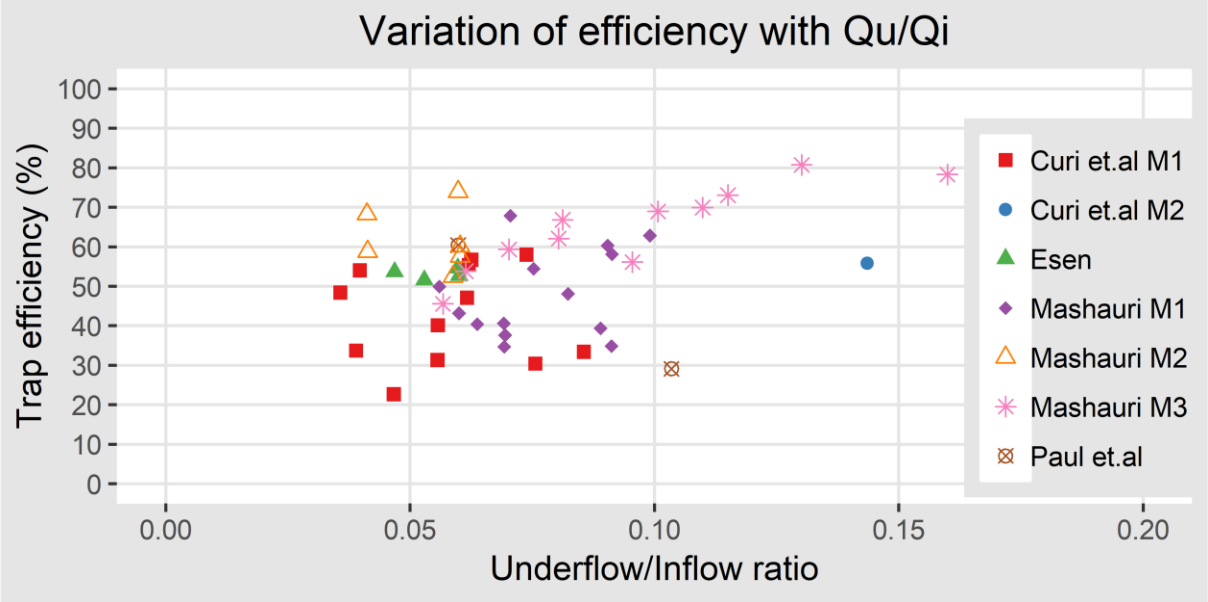

Figure 4-2: Summary of various authors' findings on underflow effect on sediment removal efficiency (Curi, Esen, & Velioglu, 1979; Mashauri, 1986; Paul et al., 1991)

Although a ratio of less than 10% is recommended, the studies utilised sediment particles greater than 200 µm with the exception of Mashauri (1986) model 3 which used 60 µm to 250 µm sediment particles.

This section describes the numerical and physical investigation of the effect of underflow on the removal of fine sediment: for single-particle sizes of 75 µm and 100 µm and a median particle size of $d50 \approx 112$ µm. In addition, the velocity and flow field patterns are numerically examined. To accomplish this, all other model parameters summarised in **Table 4-1** below were held constant with the underflow only varied.

Table 4-1: Influence of underflow VSB base model parameters

Parameter	Symbol and unit	Model 1
Inlet flow	Qi (l/s)	1.04
Cylinder diameter	D (mm)	480
Inlet diameter	Di (mm)	53
Cone height	Hc (mm)	250
Cylinder height	Ht (mm)	700
Outlet height	Ho (mm)	80
Inlet height	Hi (mm)	11.5
Underflow diameter	Du (mm)	0-53
Sediment particle diameter	d50 (µm)	75-112
Sediment concentration in inflow	C (mg/l)	10,000

4.2.2 Sediment trapping efficiency

Figure 4-3 below is a plot of $\frac{\text{Underflow}}{\text{Inflow}}$ ratio against efficiency. One set of results is the physical model with a d50 ≈ 112 µm and three sets of numerical modelling (continuous line with the varying single-particle size of 75 µm and 100 µm and the median diameter of d50 ≈ 112 µm).

From these results, there was a 5% difference between the physical model and numerical model. This can be attributed to the RSM turbulence model and one-way coupling between phases, in that the particle motion does not affect the water phase and the lack of particle-particle interaction. It is resource-intensive to undertake two-way coupling in that sediment particle, water and air phases interact with each other. Numerical modelling was used as a tool to aid in identifying key parameters that influence sediment particle trapping efficiency and, for this purpose, the accuracy was deemed good enough. In section **2.7.2.2.1** Discrete Phase Model and inherent assumptions are discussed.

A ratio of $0.05 < \frac{\text{Underflow}}{\text{Inflow}} < 0.1$ gives acceptable results with maximum efficiency at 0.08. Rates higher than 0.1 lead to air core formation and a slight dip in efficiency which further recovers as more water is lost through the underflow. The increase in efficiency cannot be attributed to better performance, but due to mass balance. **Equation 4-1** shows this. If the underflow sediment load is equal to inflow, the efficiency will be 100%.

$$\text{Physical model trapping efficiency} = \frac{\text{sediment mass of size} \geq \text{x in the underflow}}{\text{the total mass of inflow sediment}} \quad \text{Equation 4-1}$$

Where x is sediment of size d50 =112 µm for example.

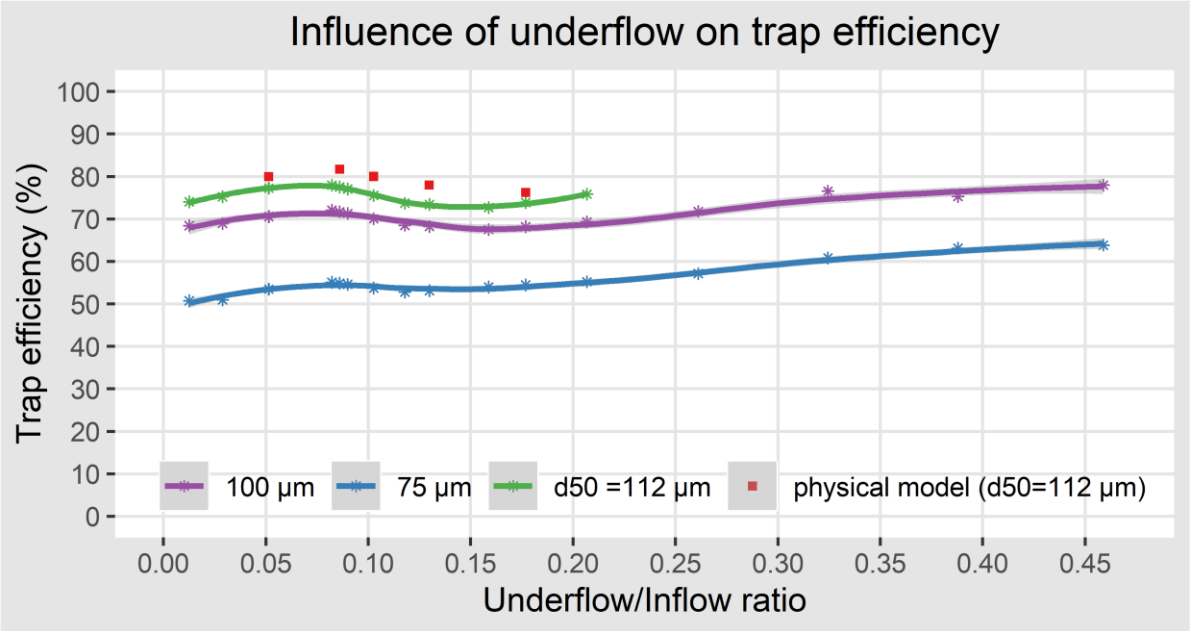

Figure 4-3: Model 1 numerical (continuous line) and the physical model (dotted) ratio of underflow to inflow impact on trapping (sediment removal) efficiency

A modified **Equation 4-2** considering the ratio of underflow to inflow was used to compare efficiency to rectify the impression, efficiency increases after the dip. In this case, if the mass of the underflow sediment load is equal to the inflow sediment load the efficiency will be 0%. **Figure 4-4** illustrates the resulting graph.

$$\text{Physical model modified trap efficiency} = \frac{\eta - {}^{Qu}/_{Qi}}{1 - {}^{Qu}/_{Qi}} \qquad \text{Equation 4-2}$$

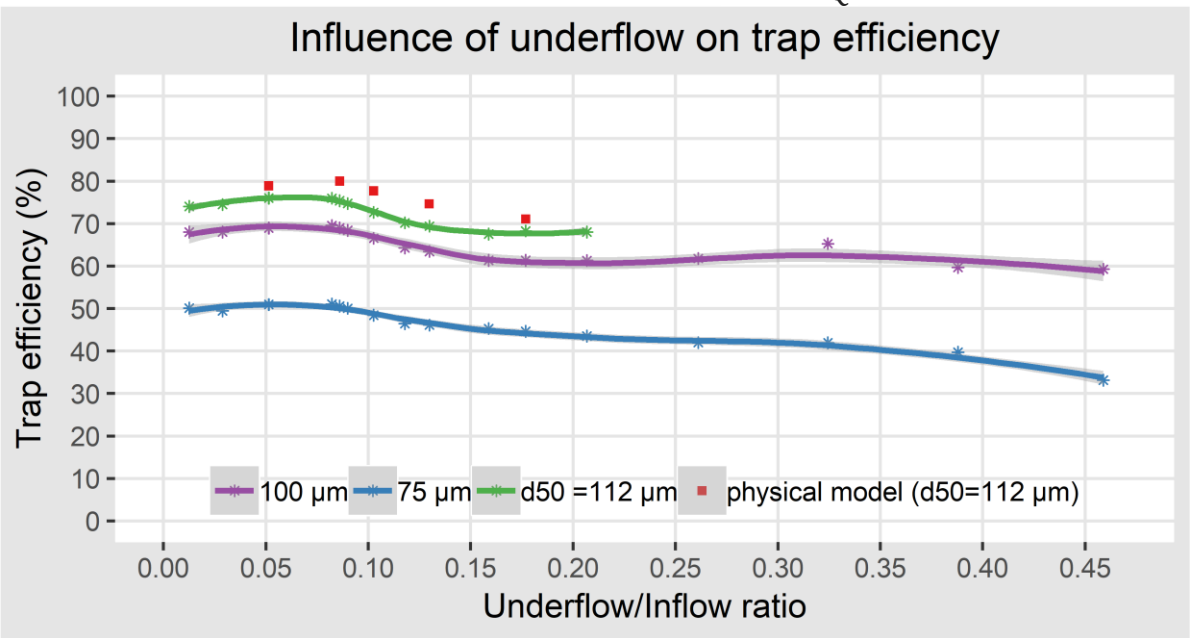

Figure 4-4: Modified equation Model 1 numerical (continuous line) and the physical model (dotted) ratio of underflow to inflow impact on sediment removal efficiency

A DPM method was implemented to track the most likely path particles of size 75 µm follow and **Figure 4-5** illustrates results for three $\frac{\text{underflow}}{\text{inflow}}$ ratios. For the ease of illustration, only fifteen paths are shown coloured by average hydraulic retention time.

The following was observed:

a) The hydraulic retention time decreased with an increase in $\frac{\text{underflow}}{\text{inflow}}$ ratios.

b) At scenario $\frac{Qu}{Qi} = 0.08$ particles are held in suspension closer to the underflow explaining why it has a higher trapping efficiency despite having a slightly lower hydraulic retention time than $\frac{Q_u}{Q_i} = 0.05$.

c) The particles tend to be carried towards the overflow outlet even with the inlet being closer to the underflow. These observations do not clarify the hydraulic behaviour but nevertheless give an insight into how the particles tend to move. The average velocity and particles vectors discussed below give a better understanding.

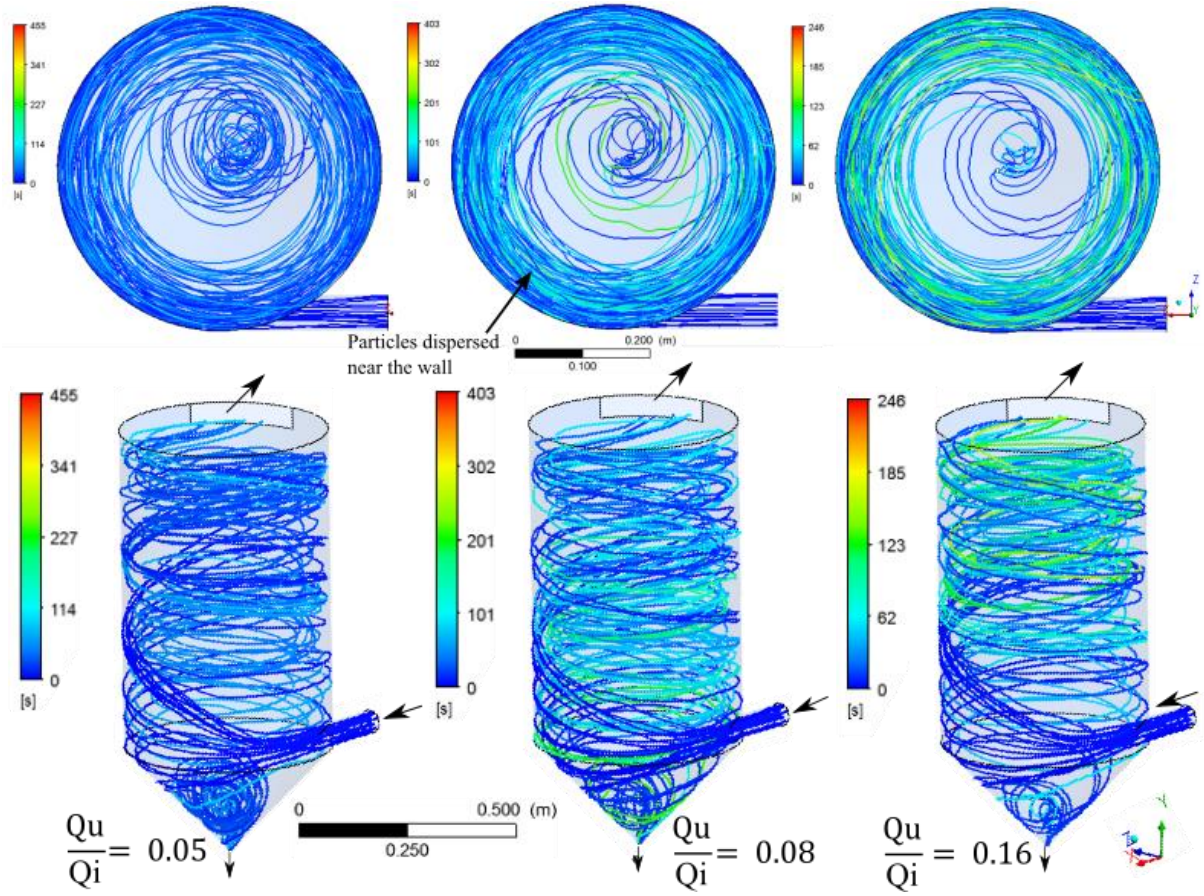

Figure 4-5: 75 µm probable particle path coloured by average hydraulic retention time of a) Qu/Qi = 0.05, b) Qu/Qi = 0.08 and c) Qu/Qi = 0.16 top and side view

4.2.3 Flow field

The velocity flow field indicates the hydraulic behaviour of VSB. **Figure 4-6** below illustrates numerical model average velocity magnitude contours over time for underflow ratios of $\frac{Qu}{Qi} = 0.05, 0.08$ and 0.16 on various contours (various heights above the cone). It was observed that:

a) The velocities are highest at the inlet.
b) There is a vortex core with low velocities at the centre.
c) The vortex core velocities decreased with the decrease in $\frac{Qu}{Qi}$ ratios.

From this observation, it would be expected $\frac{Qu}{Qi} = 0.05$ would give the maximum efficiency, but it is not the case. Richardson et al. (2002) noted cyclone flow velocities need to be reported in tangential, axial and radial velocity components. This is discussed below.

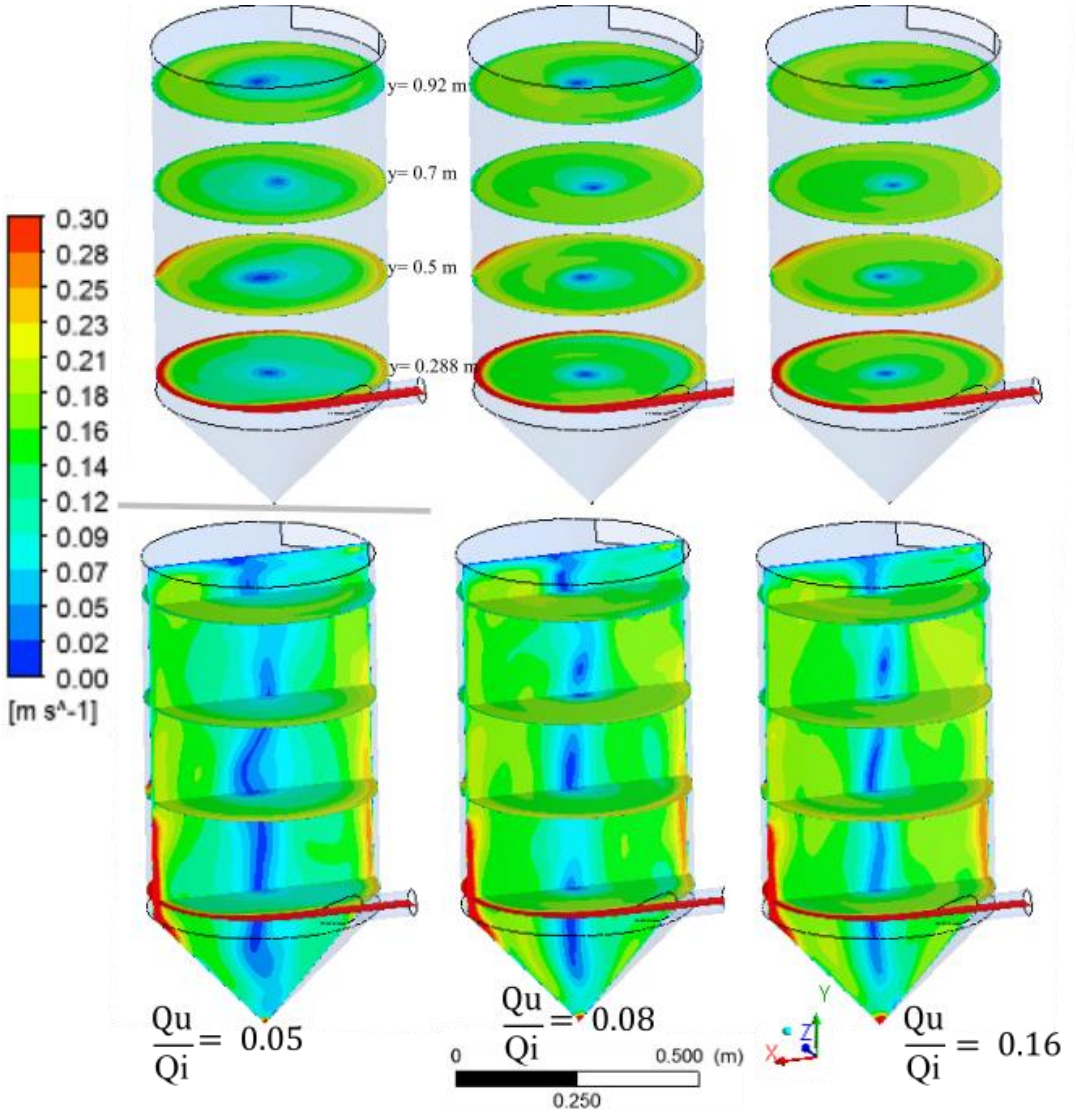

Figure 4-6: Numerical model average velocity magnitude contours of a) Qu/Qi = 0.05, b) Qu/Qi = 0.08 and c) Qu/Qi = 0.16 on plane y-x, z-x at y = 0.288 m, y = 0.5 m, y = 0.7 m and y = 0.92 m

4.2.3.1 Axial velocity

Axial velocity represents flow field moving up and down in the direction of the axis of gravity. **Figure 4-7** below illustrates the numerical model average axial velocity contours for underflow $\frac{Qu}{Qi} = 0.05, 0.08$ and 0.16 on various planes and velocity profiles along lines A-B and C-D in **Figure 4-8**. It was noted just after the entry there is a downstream flow and an immediate flow upwards which transports sediment downward or upwards.

Salakhov (1975) and Veerapen et al. (2005) noted that a VSB is mainly gravity-driven and in **Figure 4-8** it can be seen $\frac{Qu}{Qi} = 0.08$ (blue line) has a higher percentage of water moving downwards especially just at the entrance where the sediment is immediately carried to the underflow.

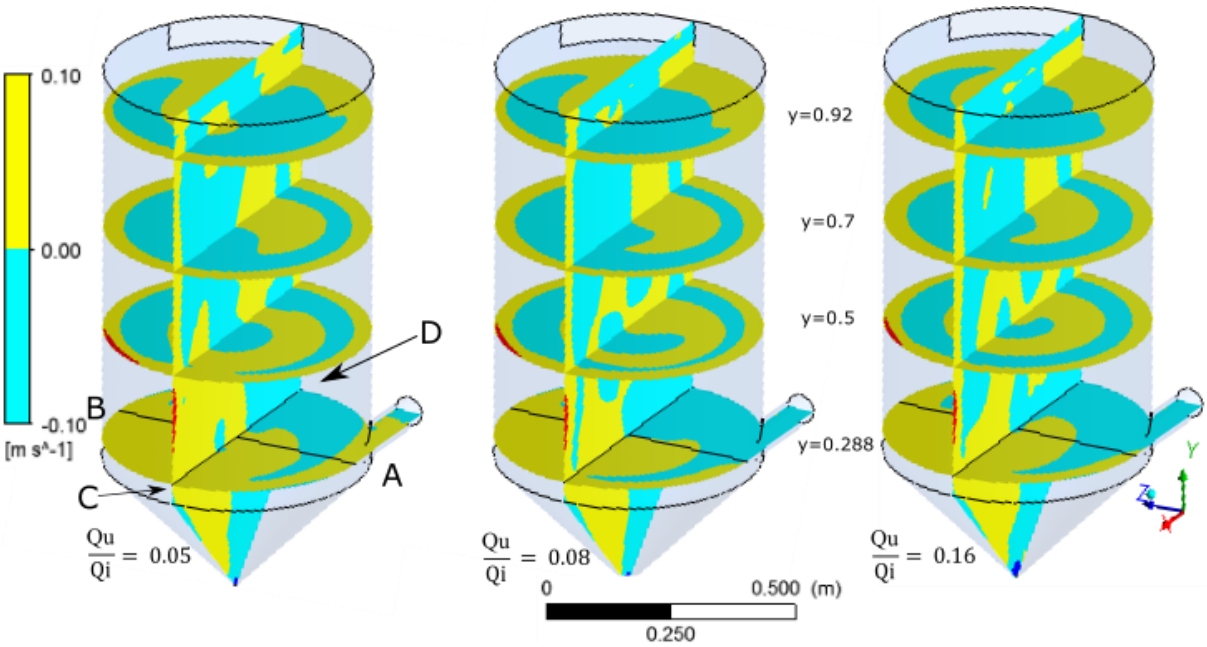

Figure 4-7:Numerical model average axial velocity contours of a) Qu/Qi = 0.05, b) Qu/Qi = 0.08 and c) Qu/Qi = 0.16 on plane y-x, z-x at y = 0.288 m, y = 0.5 m, y = 0.7 m and y = 0.92 m (cyan: downward movement of water, yellow/red: rising water)

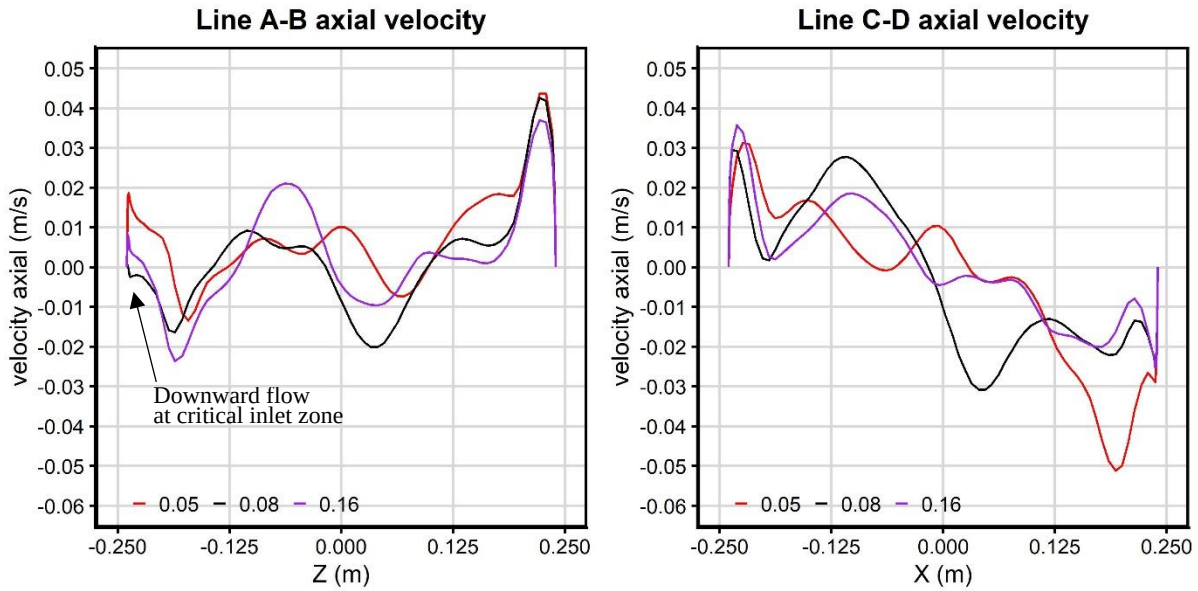

Figure 4-8: Numerical model average axial velocity profile of a) Qu/Qi = 0.05, b) Qu/Qi = 0.08 and c) Qu/Qi = 0.16 along lines A-B and C-D at y = 0.228 m

4.2.3.2 Tangential velocity

The tangential flow component represents centrifugal forces due to swirling flow. **Figure 4-9** below illustrates the numerical model average tangential velocity contours for underflow $\frac{\text{Qu}}{\text{Qi}} =$ 0.05, 0.08 and 0.16 on various planes and an extracted profile along lines A-B and C-D in **Figure 4-10**. It was observed that:

a) The tangential velocity component is the highest amongst the axial and radial component.
b) The highest values are located near the wall and lowest at the centre exhibiting a Rankine's type of profile.
c) There is no significant variation in shape and magnitude among the underflows explaining why despite it being the most significant component in magnitude, not much difference can be noted regarding efficiency.

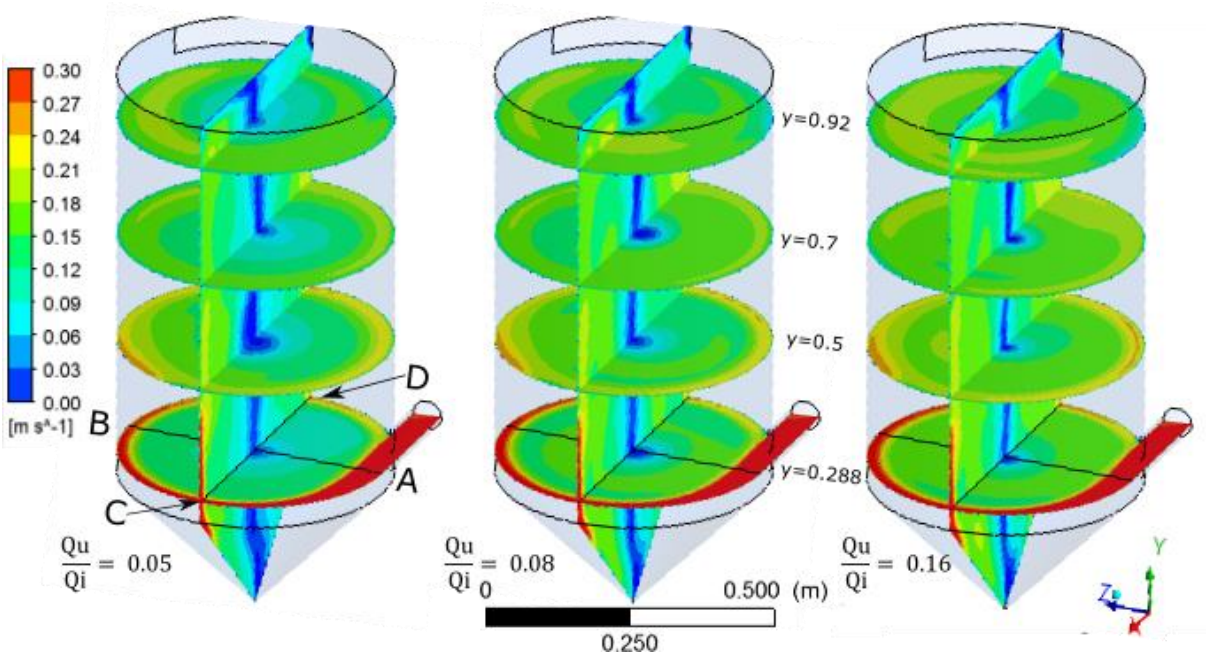

Figure 4-9:Numerical model average tangential velocity contours of a) Qu/Qi = 0.05, b) Qu/Qi = 0.08 and c) Qu/Qi = 0.16 on plane y-x, z-x at y = 0.288 m, y = 0.5 m, y = 0.7 m and y = 0.92 m

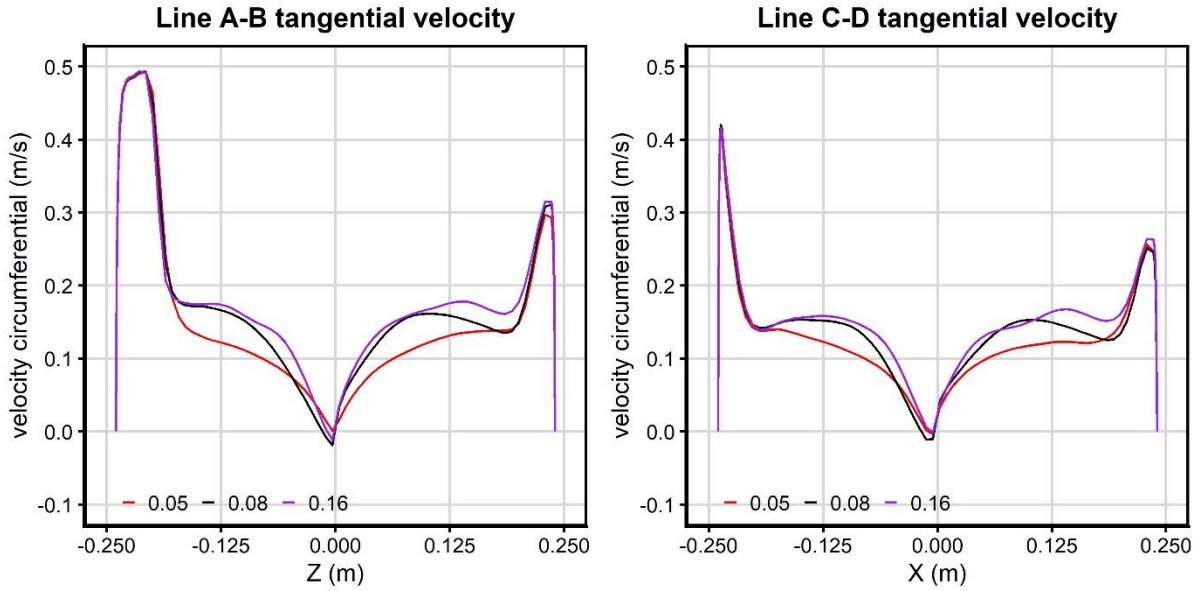

Figure 4-10: Numerical model average tangential velocity profile of a) Qu/Qi = 0.05, b) Qu/Qi = 0.08 and c) Qu/Qi = 0.16 along lines A-B and C-D at y = 0.228 m

4.2.3.3 Radial velocity

Radial velocity describes the velocity component that transports and distributes sediment towards the wall. **Figure 4-11** below illustrates the numerical model average radial velocity contours for underflow $\frac{Qu}{Qi} = 0.05, 0.08$ and 0.16 on various planes and an extracted profile along lines A-B and C-D in **Figure 4-12**. It was observed that:

a) The radial is slightly higher than the axial component, confirming that VSB flow is gravity driven and centrifugal force helps in keeping the particles in suspension near the wall. Thus, explaining why in particle tracking illustrated in **Figure 4-5**, the paths are dispersed near the wall.
b) The gravity component should be enhanced to increase efficiency.
c) In $\frac{Qu}{Qi} = 0.08$ the radial component in **Figure 4-12** below is the highest at the middle of VSB. This coupled with high axial velocity as noted above explains why better trapping efficiencies are realised. It should be noted the radial velocity of a sediment particle with respect to the centre of VSB taken on y-x or z-x plane is moving towards the wall from the middle and towards the middle from the wall.

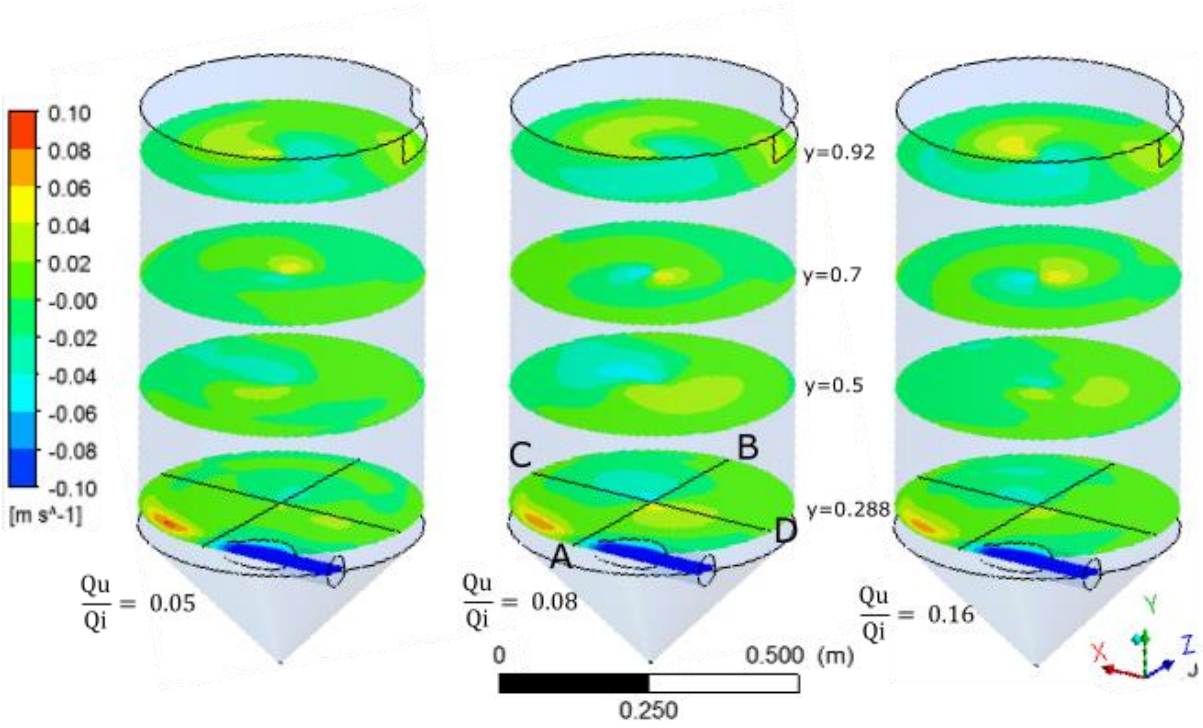

Figure 4-11: Numerical model average radial velocity contours of a) Qu/Qi = 0.05, b) Qu/Qi = 0.08 and c) Qu/Qi = 0.16 on plane y-x, z-x at y = 0.288 m, y = 0.5 m, y = 0.7 m and y = 0.92 m

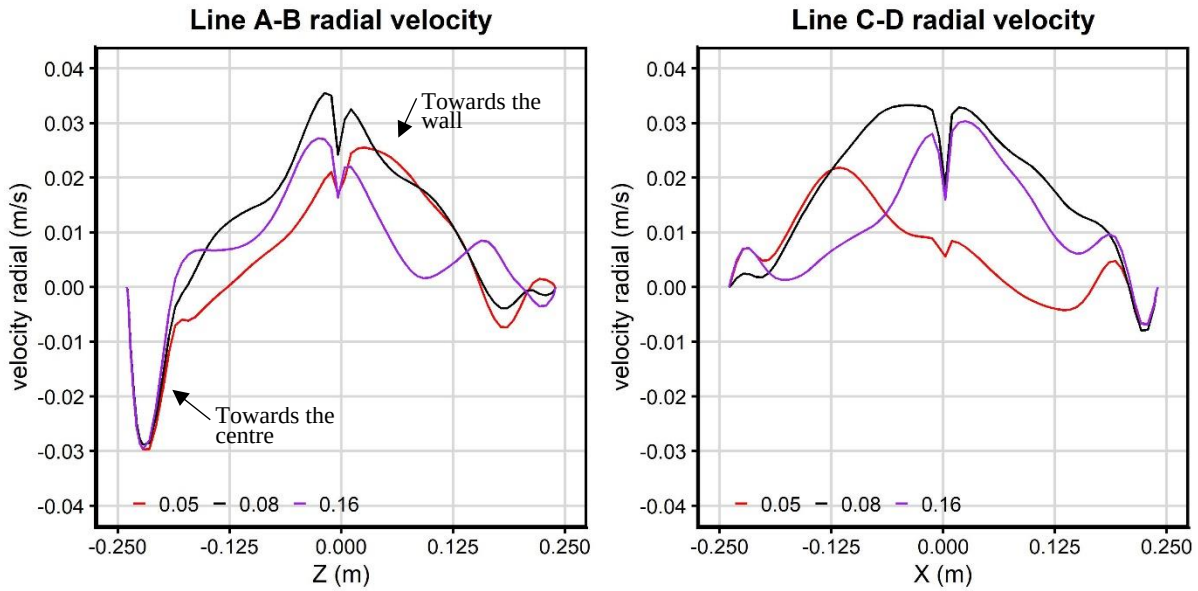

Figure 4-12:Numerical model average radial velocity profile of a) Qu/Qi = 0.05, b) Qu/Qi = 0.08 and c) Qu/Qi = 0.16 along lines A-B and C-D at y = 0.228 m

4.2.3.4 Vorticity

Vorticity is the measure of fluid rotational motion on a reference axis taken as the centre of the VSB. Helicity which is a dot product of (velocity vector and vorticity) gives a better understanding of vorticity associated with the fluid stream. **Figure 4-13** below is an illustration of vorticity clipped at 4.49 s^{-1} to enable visualisation of the air-core for underflow ratios $\frac{Qu}{Qi} = 0.05, 0.08$ and 0.16. The clipping time was arbitrarily taken as vorticity is a dynamic process and it was not the intention of this study to make animated plots. It was observed that:

a) A helical flow towards the overflow and underflow and a downward central helical flow toward the underflow is generated.
b) The central core is developed due to high swirling strength.
c) Due to high swirling strength experienced at $\frac{Qu}{Qi} > 0.15$, the axial pressure is sufficiently lower than atmospheric pressure causing the formation of central air core illustrated in **Figure 4-14** below.
d) The air core formation develops from the underflow contrary to earlier assumptions that it originated from the top. Cullivan et al. (2004) affirm this observation.
e) Vortex core and particle trajectory are asymmetrical due to the tangential inlet.
f) Vorticity decreases with decreasing $\frac{Qu}{Qi}$ ratio.
g) At $\frac{Qu}{Qi} = 0.08$ at the inlet, a higher percentage of sediment particles are dispersed outwards towards the underflow.

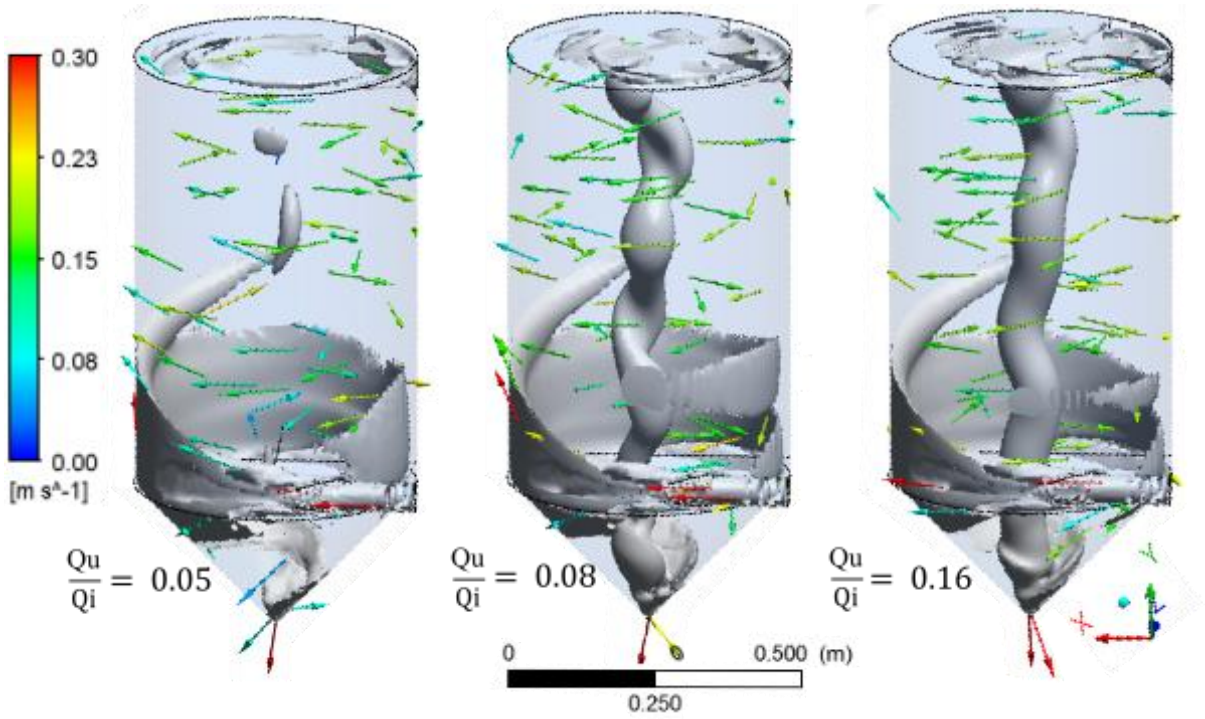

Figure 4-13: Numerical model vorticity and velocity vectors of a) Qu/Qi = 0.05, b) Qu/Qi = 0.08 and c) Qu/Qi = 0.16

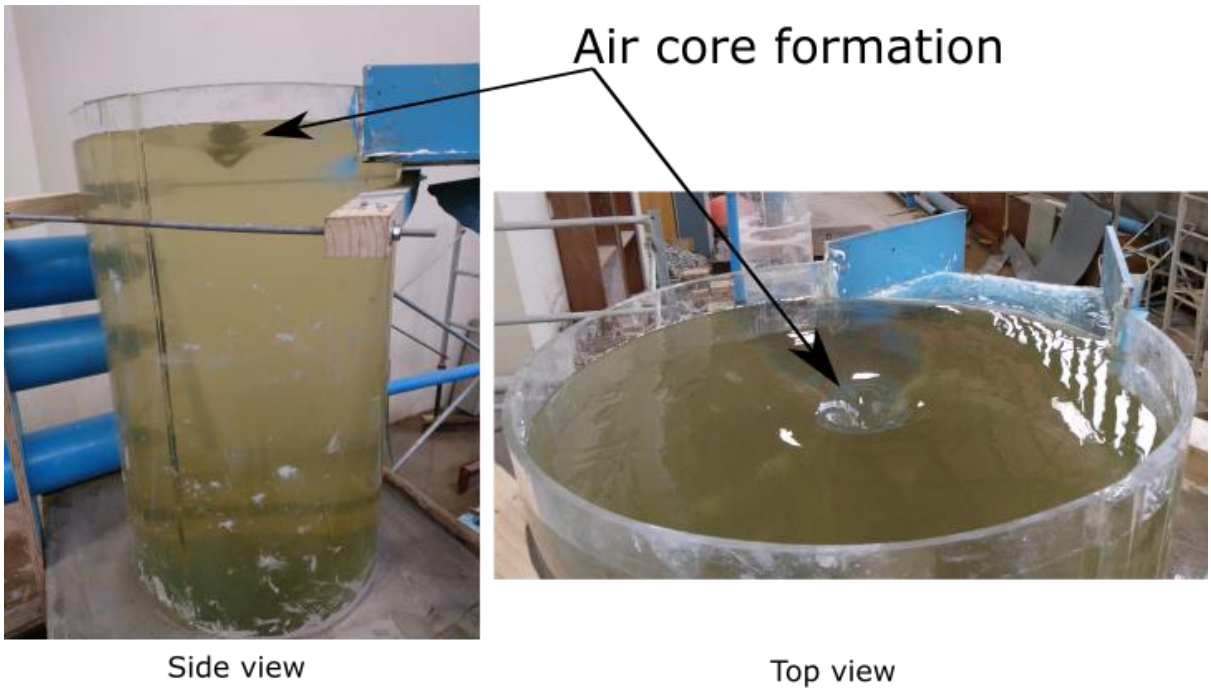

Figure 4-14: An illustration of air-core formation in the laboratory

4.2.4 Turbulent kinetic energy, TKE

TKE (Turbulent Kinetic Energy) best describes the intensity of turbulence in a flow field. The lower the magnitude of TKE (m^2/s^2), the higher the flow recirculation and vice versa is true.

Figure 4-15 below illustrates the numerical model average TKE contours for underflow $\frac{Qu}{Qi} = 0.05$, 0.08 and 0.16 on the z-x plane. It was observed that:

a) High TKE values are experienced near the inlet, outlet and near the wall.
b) Minimum values are recorded near the central core.
c) TKE decreases with an increase in $\frac{Qu}{Qi}$ ratios.
d) At underflow ratio $\frac{Qu}{Qi} = 0.16$, low values TKE at plane y = 0.288 m in the z-x plane were observed. High recirculation at the entrance plane is detrimental to gravity-driven mechanism, thus low trapping efficiency.

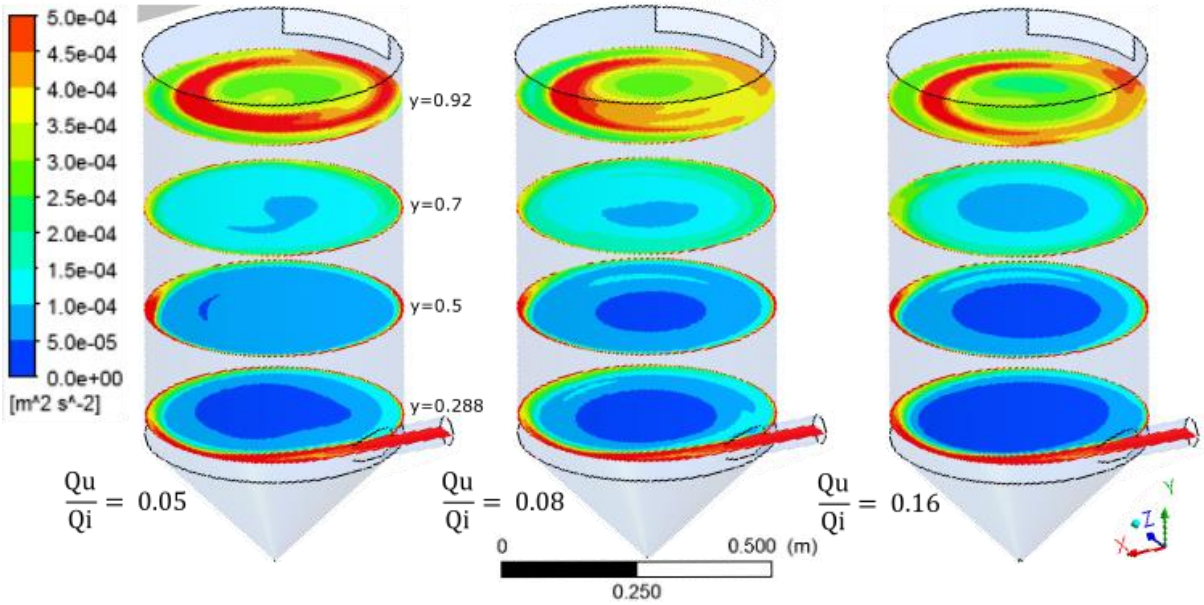

Figure 4-15: Numerical model turbulence kinetic energy for a) Qu/Qi = 0.05, b) Qu/Qi = 0.08 and c) Qu/Qi = 0.16 on the z-x plane at y = 0.288 m, y = 0.5 m, y = 0.7 m and y = 0.92 m

4.2.5 Conclusion on underflow

The Volume of Fluid (VOF) and the Discrete Element Method (DEM) numerical models and physical modelling were conducted to investigate the influence of underflow on sediment removal, and it was concluded that:

- Increasing the underflow greater than a ratio of $\frac{Qu}{Qi} = 0.1$ leads to more water loss without necessarily increasing the trapping efficiency significantly. A ratio $\frac{Qu}{Qi} = 0.08$ gives the maximum efficiency with less water loss and is recommended.
- As concluded by other investigators, VSB is mainly gravity-driven, but the centrifugal force plays an essential role in dispersing sediment particles and keeping them near the wall.
- Increasing the centrifugal forces does not improve the removal efficiency as VSB is not designed as a hydro cyclone.

- To achieve a better efficiency settling should be enhanced.

If an economic analysis is carried out, and it is found to be cheaper to construct clustered VSBs in series as shown in **Figure 4-16**. Under section 6, in performance evaluation, it was concluded that sediment loading does not influence VSB performance. A ratio of $\frac{Q_u}{Q_i} = 0.05$ can be used for both VSBs effectively increasing the combined trapping efficiency from 80% to ≈ 96% with a total water loss of 10% (Taking inflow load=10,000 mg/l, inflow into VSB2= (100% -80%)*10,000=2,000 mg/l. VSB2 overflow load = (100% -80%)*2,000=400 mg/l which translates to 96 % trapping efficiency). This option is more attractive than having one VSB with an 8% water loss and 82% trapping efficiency.

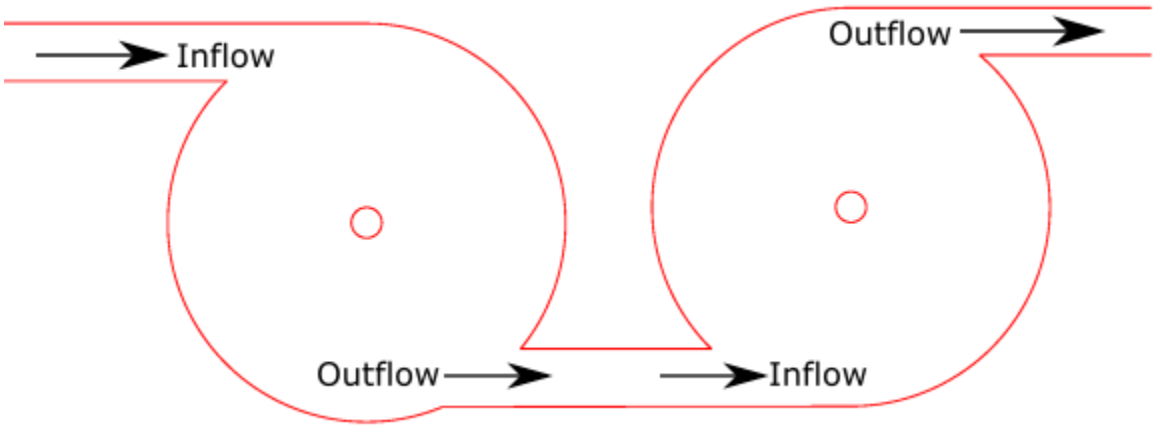

Figure 4-16: Possible plan layout of clustered VSBs

4.3 Location and size of the outlet

4.3.1 Introduction

Location and sizing of the outlet play a crucial role in sediment removal efficiency. Different VSB configurations have been suggested (see **Figure 2-9**) but their applications were mainly in wastewater, combined sewer, hydropower and aquaculture. The requirements in abstraction works are slightly different necessitating a different approach.

From the literature review, it was found that information on sizing is inadequate, and this study investigated the influence of location and outlet sizing on sediment removal efficiency through physical and numerical modelling. A side outlet is investigated in this chapter and other outlet structure configurations in section **4.12**.

Three scenarios were considered:

- An outlet with a 60° sector and a varying incremental orientation of the face of 30° (0°, 30°, 60°, 90°, 120°, 150°, 180°, 210°, 240°, 270°, 300°, 330°). **Figure 4-17**(a) illustrates an example of 60° sector sector with 210° incremental angle.
- An outlet with a 120° sector and a varying incremental orientation of the face of 60° (0°, 70°, 130°, 190°, 250°). **Figure 4-17**(b) shows an example of 120° sector with 190° incremental angle.
- An outlet with a 35° sector and a varying incremental orientation of the face of 30° to 60°.

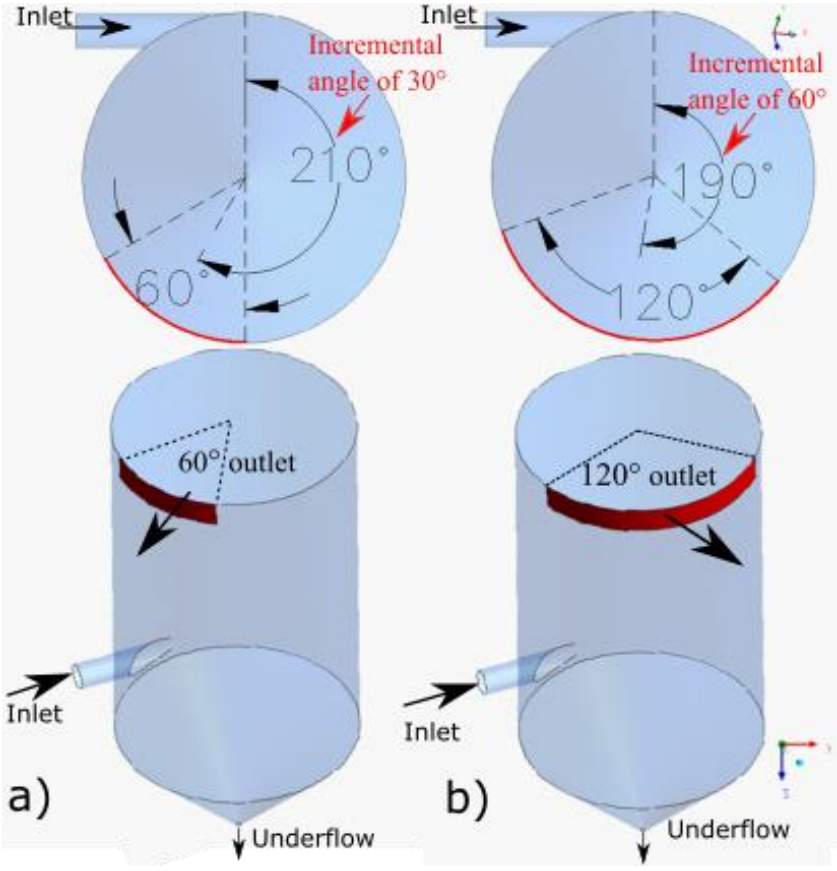

Figure 4-17: 60° and 120 ° sector outlets

Table 4-2 below gives a summary of the base parameters used for this investigation.

Table 4-2: Influence of outlet location on trapping efficiency VSB base model parameters

Parameter	Symbol and units	Model 1	Model 2
Inlet flow	Qi (l/s)	1.04	5
Cylinder diameter	D (mm)	480	634
Inlet diameter	Di (mm)	53	156
Underflow/Inflow	Qu/Qi	0.19	0.11
Cylinder height	Ht (mm)	700	1000
Cone height	Hc (mm)	250	330
Inlet height	Hi (mm)	11.5	800
Sediment concentration in inflow	C (mg/l)	10,000	10,000

4.3.2 Sediment trapping efficiency

4.3.2.1 Outlet sector location

Figure 4-18 below illustrates Model 1 numerical simulation and physical model results with a summary in **Appendix A7**. Model 2 simulation results are in **Figure 4-19**. The graphs show how the efficiency varies with a varying incremental angle and with various outlet sectors.

From results with Models 1 and 2, a suitable validation was shown since the physical models agree with the simulated results.

- At an angle 210° with 60° sector, Model 1 numerical efficiency is 77% with the physical model at 80%.
- At an angle 150° with 60° sector, Model 2 numerical efficiency is 72% with the physical model at 74%.

It should be noted that only two physical models could be tested, as testing other scenarios would require reconstructing the model and the prefabricated clear Perspex cylinder was outsourced which prevented this flexibility. Therefore the 0° incremental angle for Model 1 and 150° for Model 2 is the ideal place to have the outlet for this type of configuration. This is discussed further in combination with outlet size in the next chapter.

It was observed that Models 1 and 2 results do not follow a similar trend; this is a caution showing that graphs and equations developed are more or less only valid for the type of model used to generate the result. The main difference between the two models was the cylinder diameter and position of the inlet. These parameters are investigated in sections **4.6** and **4.10**.

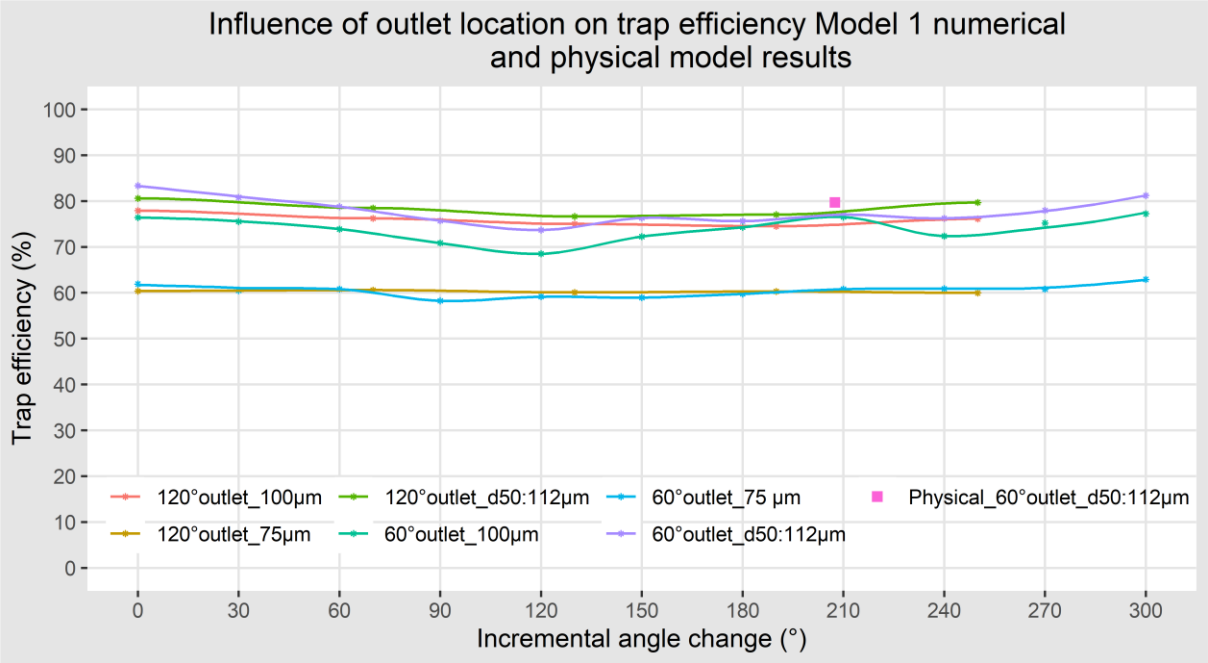

Figure 4-18: Influence of outlet location on sediment removal efficiency Model 1 numerical (continuous line) and physical model results

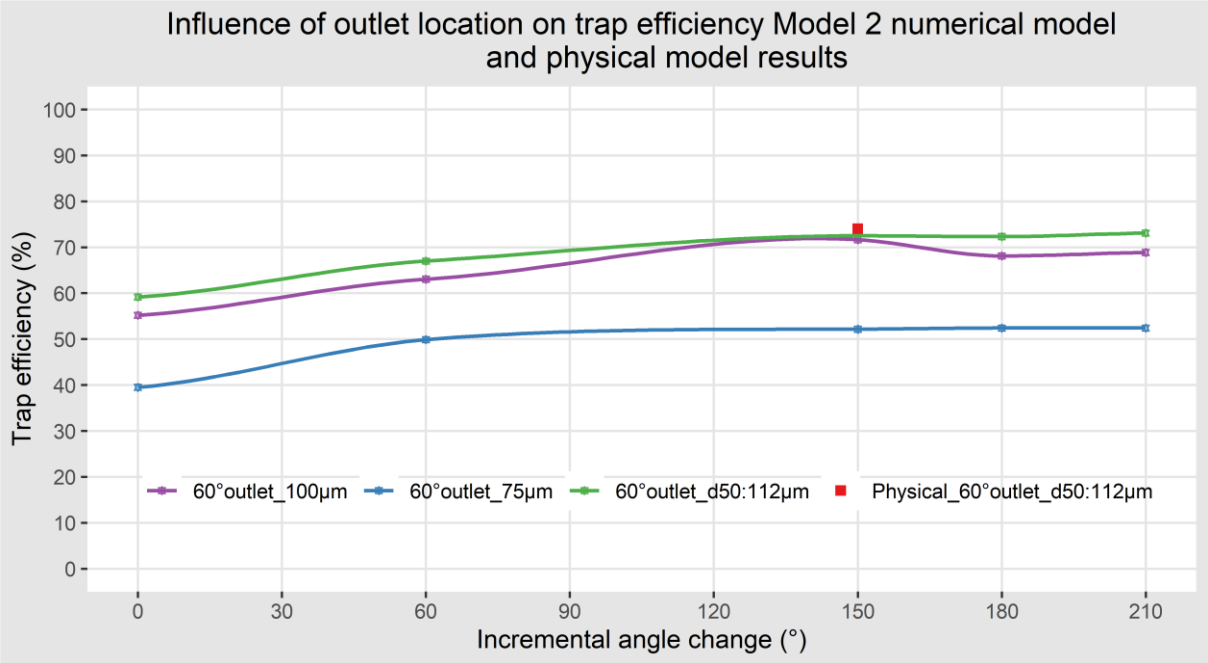

Figure 4-19: Influence of outlet location on sediment removal efficiency Model 2 numerical (continuous line) and physical model results

4.3.2.2 Outlet sector size

Initially, preliminary analysis had been carried out, and an outlet that is ≈ 0.17πD was found to be most appropriate. This preliminary analysis was carried out using ANSYS FLUENT supervised automatic calibration. It is a data-intensive and resource-intensive undertaking thus only one output was saved at the end of simulations. In total 288 possible simulations were

carried out. Regarding simulations, the sector sizes were limited to (30° to 70°) this is 40/5 possible sectors * $\frac{360°}{10}$ possible locations of outlet = 288.

Figure 4-20 below illustrates Model 1 comparison between 35° sector (≈ 0.1πD), 60° sector (≈ 0.17πD) and 120° sector (≈ 0.33πD) using numerical and physical model results. The incremental angle was varied for each sector to yield the graph illustrated. Two sediment particles were considered that is 75 µm and d50 = 112 µm.

It was noted that the maximum trapping efficiency was achieved for:

- 75 µm sediment size at 0° incremental angle with an outlet of 35° sector.
- d50 = 112 µm sediment size at 0° incremental angle with 60° sector.

Thus, it was concluded that the 60° sector gave better efficiency than the 35° and 120° sectors for a wide range of sediment sizes, and it is desirable to adopt this for the Model 1 setup.

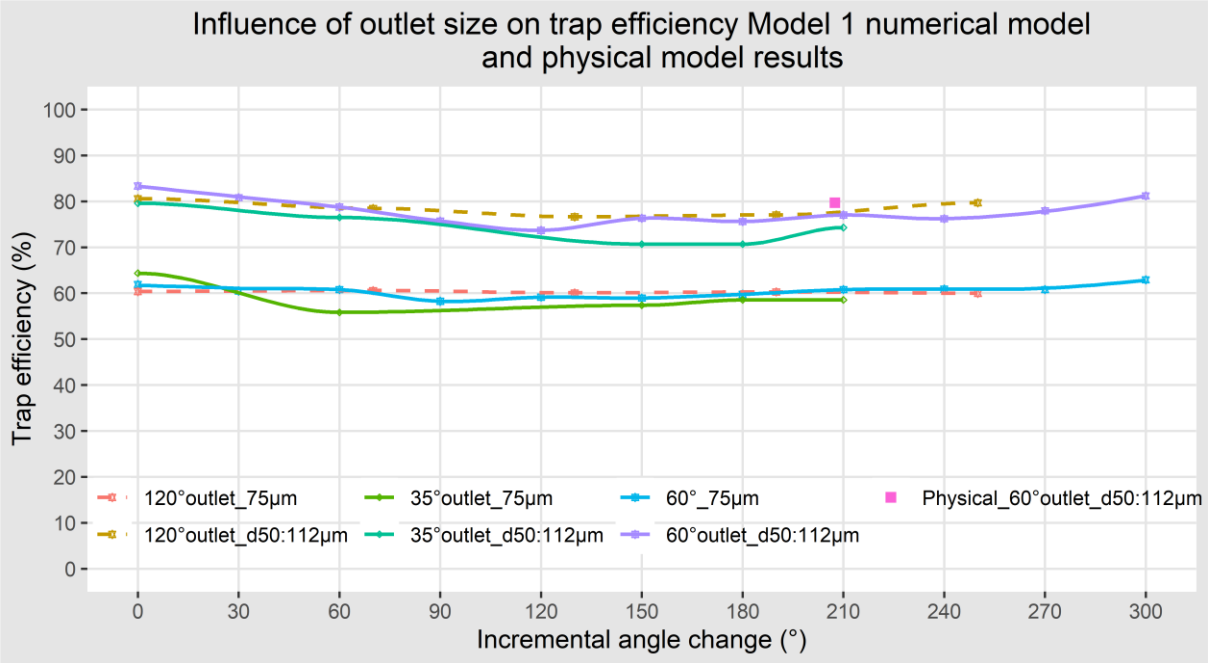

Figure 4-20: Influence of outlet size on sediment removal efficiency Model 1 numerical (continuous line) and physical model results

Figure 4-21 below illustrates Model 2 numerical and physical model results. The graph shows a comparison of the 35° sector (≈ 0.1πD) and 60° sector (≈ 0.17πD) effect on sediment trapping efficiency with an incremental angle of change. Three sediment sizes were used: 75 µm, 100 µm and d50 = 112 µm and the maximum efficiencies are listed below:

- For 75 µm sediment size maximum efficiency was found at 180° incremental angle with 35° sector outlet.
- For 100 µm sediment size maximum efficiency was observed at 150° incremental angle with 60° sector outlet.
- For d50 = 112 µm sediment size, the maximum efficiency was at 210° incremental angle with 60° sector outlet.

From these results, it was concluded that a 60° sector outlet at 150° incremental angle has a higher overall efficiency over a wide range of sediment sizes.

For the removal of fine sediment (≈ 75 µm) the outlet positioning and size play a significant role in influencing the trapping efficiency and an outlet of 60° sector (≈ 0.17πD) with an incremental angle between 150° and 210° is recommended.

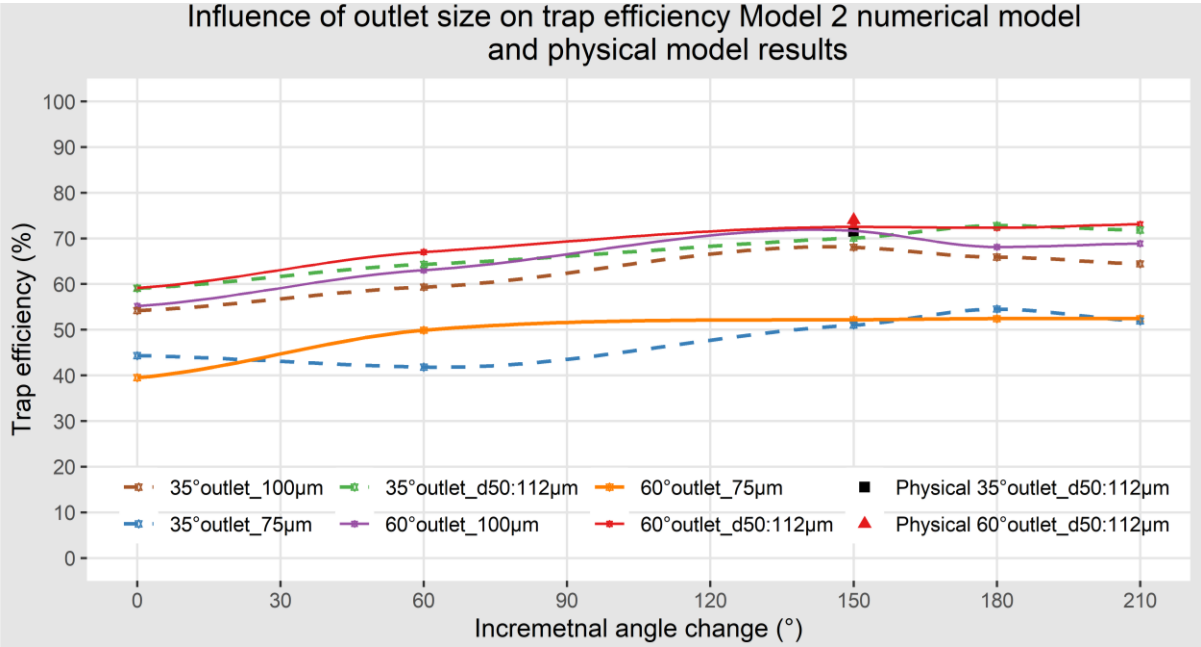

Figure 4-21: Influence of outlet size on sediment removal efficiency Model 2 numerical (continuous line) and physical model results

4.3.3 Flow field

4.3.3.1 Axial velocity

Appendix A14, **Appendix A15** and **Appendix A16** illustrate Model 1 numerical model snapshot of average axial velocity contours of the 60° sector, 120° sector and 35° sector respectively on the z-x plane at y = 0.288 m, y = 0.5 m, y = 0.7 m and y = 0.92 m. It was observed that:

a) There is an upward flow near the wall and a downward movement at the centre of VSB.
b) There is a downward current at the inlet.

In section **4.2.3.1** it was identified that VSBs are gravity-driven and the magnitude of axial velocity at the inlet is critical in determining the efficiency. Using the numerical model, the average axial velocity profile has been plotted along lines A-B and C-D and is illustrated in **Figure 4-22** and **Figure 4-23** below. To avoid data overplotting, only scenarios that gave the minimum axial velocity at the inlet region are summarised in **Figure 4-24**.

It was observed that 35° and 60° sector at 0° (see the image a and q in **Appendix A14** and **Appendix A16)** had the minimum positive axial velocity thus assisting in sediment settling. This corresponds to the location that was identified to be the most ideal for Model 1 type of configuration.

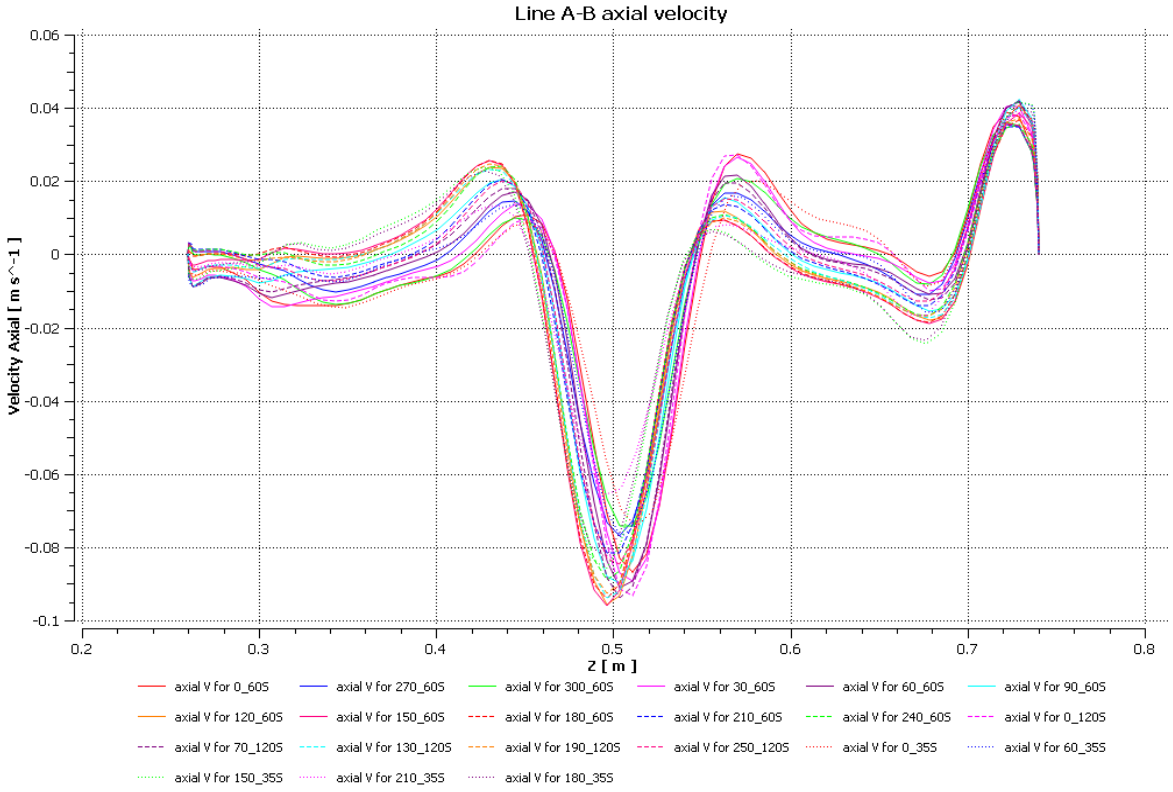

Figure 4-22: Model 1 numerical model average axial velocity profile of 35 °, 60° and 120° sector on the z-x plane along lines A-B at y = 0.228 m

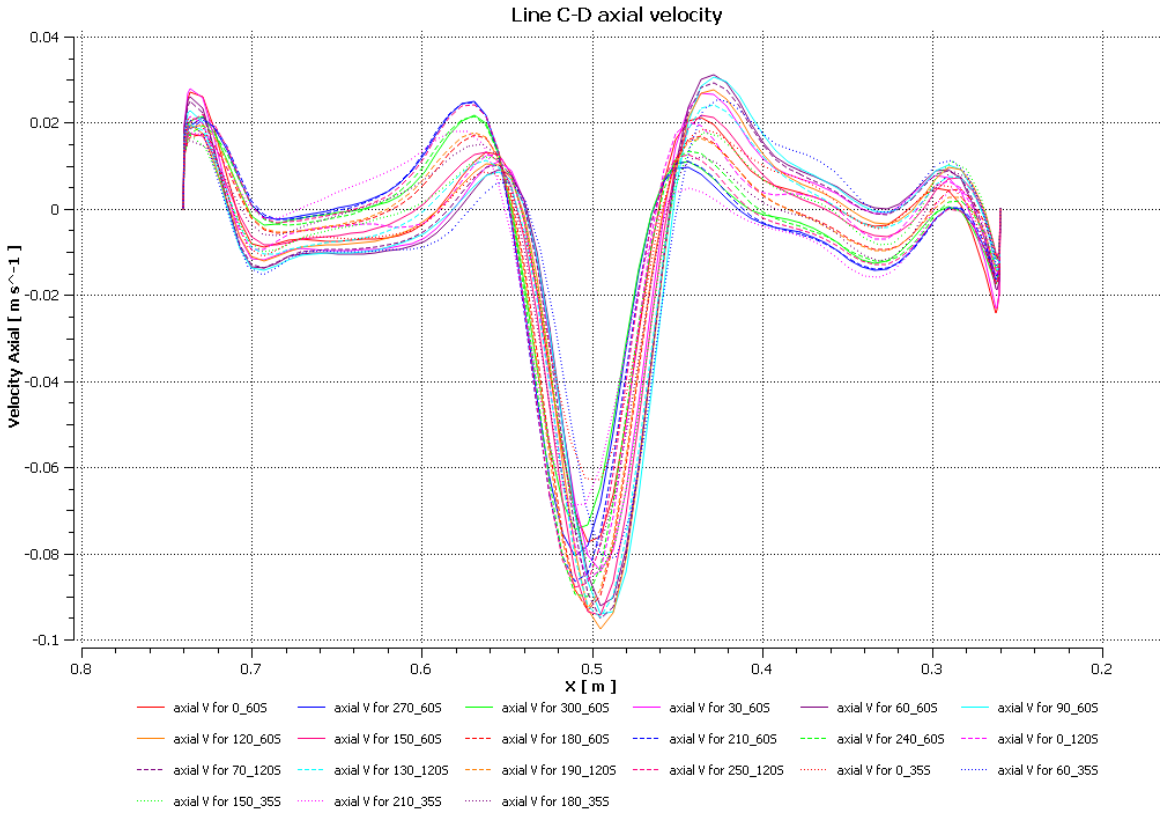

Figure 4-23: Model 1 numerical model average axial velocity profile of 35 °, 60° and 120° sector on the z-x plane along line C-D at y = 0.228 m

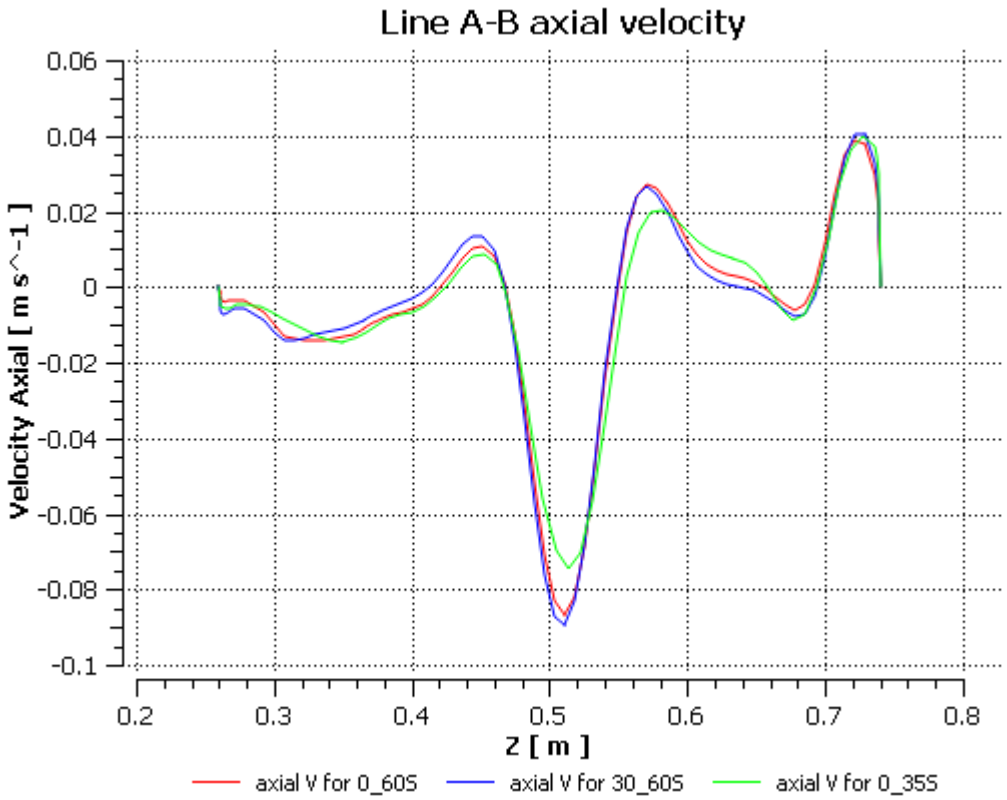

Figure 4-24: Model 1 numerical model minimum average axial velocity profile of 35° and 60° sector at 0° and 30° on the z-x plane along lines A-B at y = 0.228 m

Appendix A17 and **Appendix A18** illustrate Model 2 numerical snapshot of average velocity contours of 60° sector and 35° sector respectively on the z-x plane at y = 0.33 m, y = 0.62 m, y = 0.91 m and y = 1.208 m. It was observed that depending on the outlet location there is an upward or downward current near the inlet and from section **4.2.3.1**, it was determined that a downward axial current at the inlet is more desirable.

A graph of the numerical model, axial velocity profiles, was plotted along lines A-B and C-D and is illustrated in **Figure 4-25** and **Figure 4-26** below. It was observed that a 35° sector at 150° angle and 60° sector at 150° angle had the minimum axial velocity at the crucial inlet zone, and this corresponds to the best efficiency and is recommended.

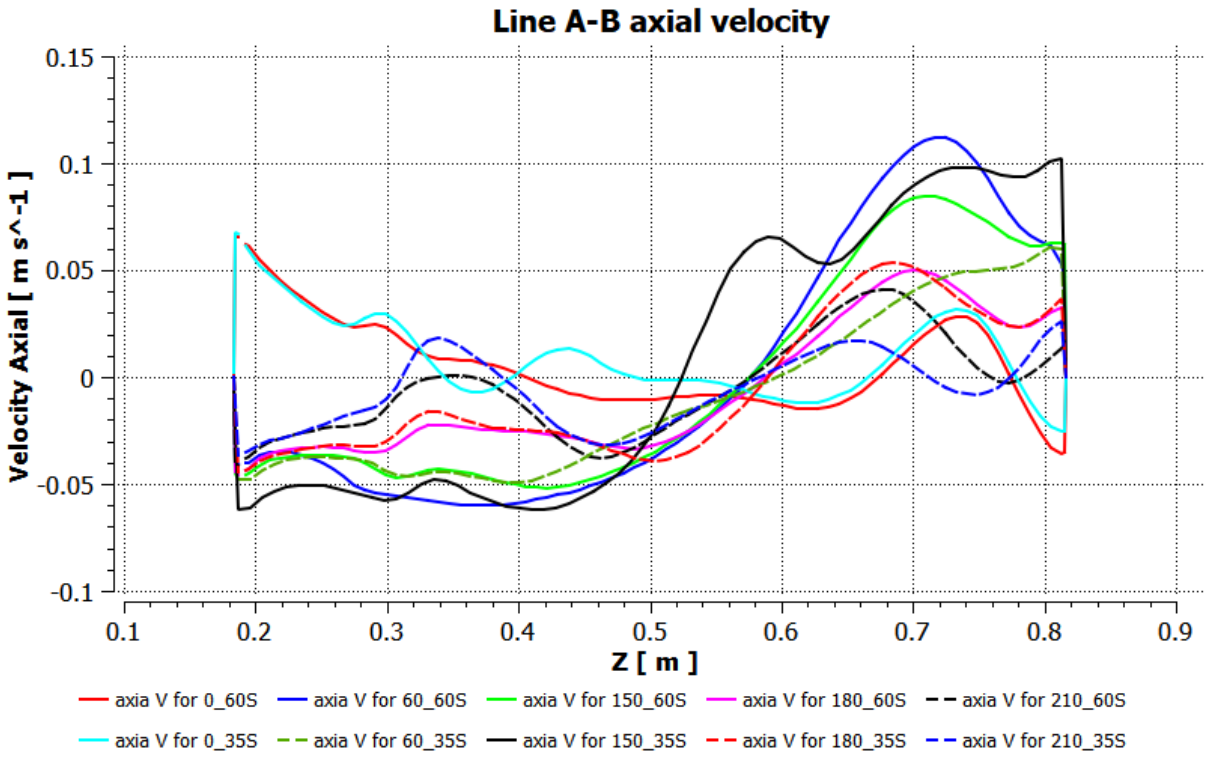

Figure 4-25: Model 2 numerical model average axial velocity profile of 35° and 60° sector on the z-x plane along lines A-B at y= 1.208 m

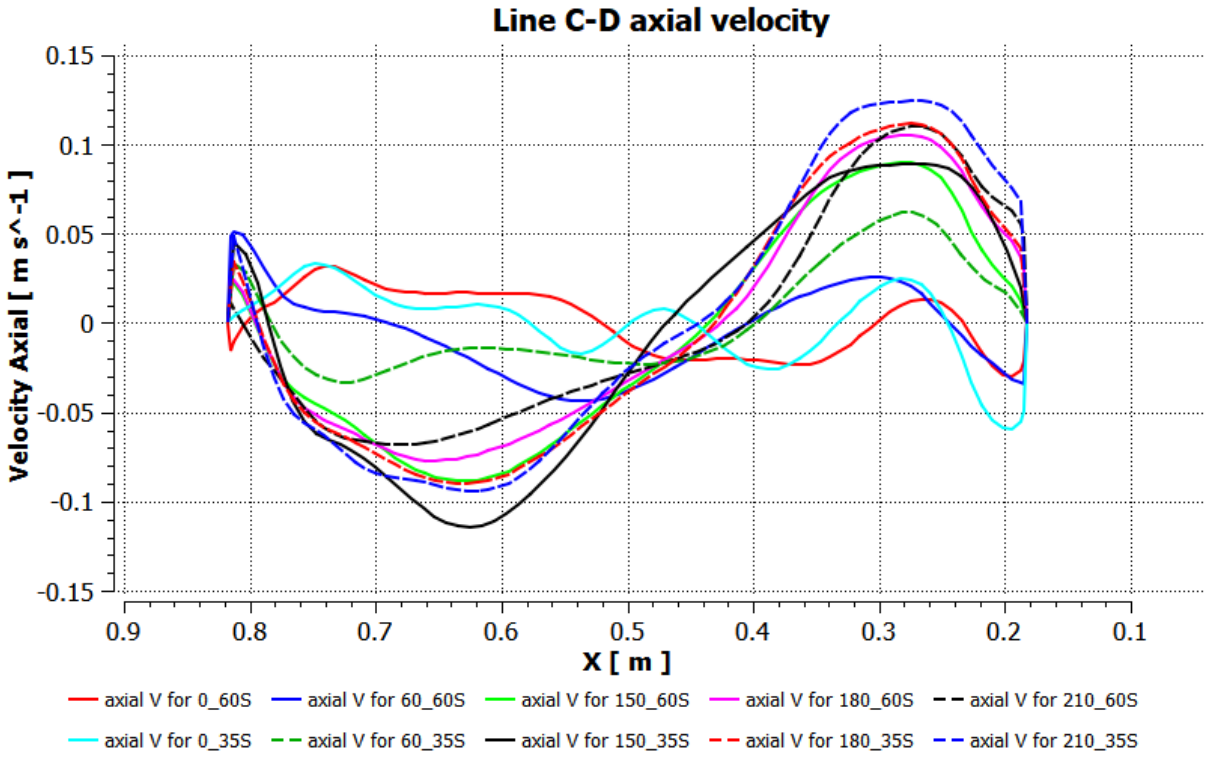

Figure 4-26: Model 2 numerical model average axial velocity profile of 35° and 60° sector on the z-x plane along line C-D at y= 1.208 m

4.3.3.2 Tangential velocity

Figure 4-27 and **Figure 4-28** below illustrate Model 1 numerical model snapshot of average tangential velocity profiles on the z-x plane at lines A-B and C-D. It was observed for all scenarios that:

a) The tangential velocity was highest at the inlet.
b) A Rankine's type of profile was exhibited.
c) The magnitude did not vary significantly and thus not much efficiency difference can be attributed to centrifugal forces.

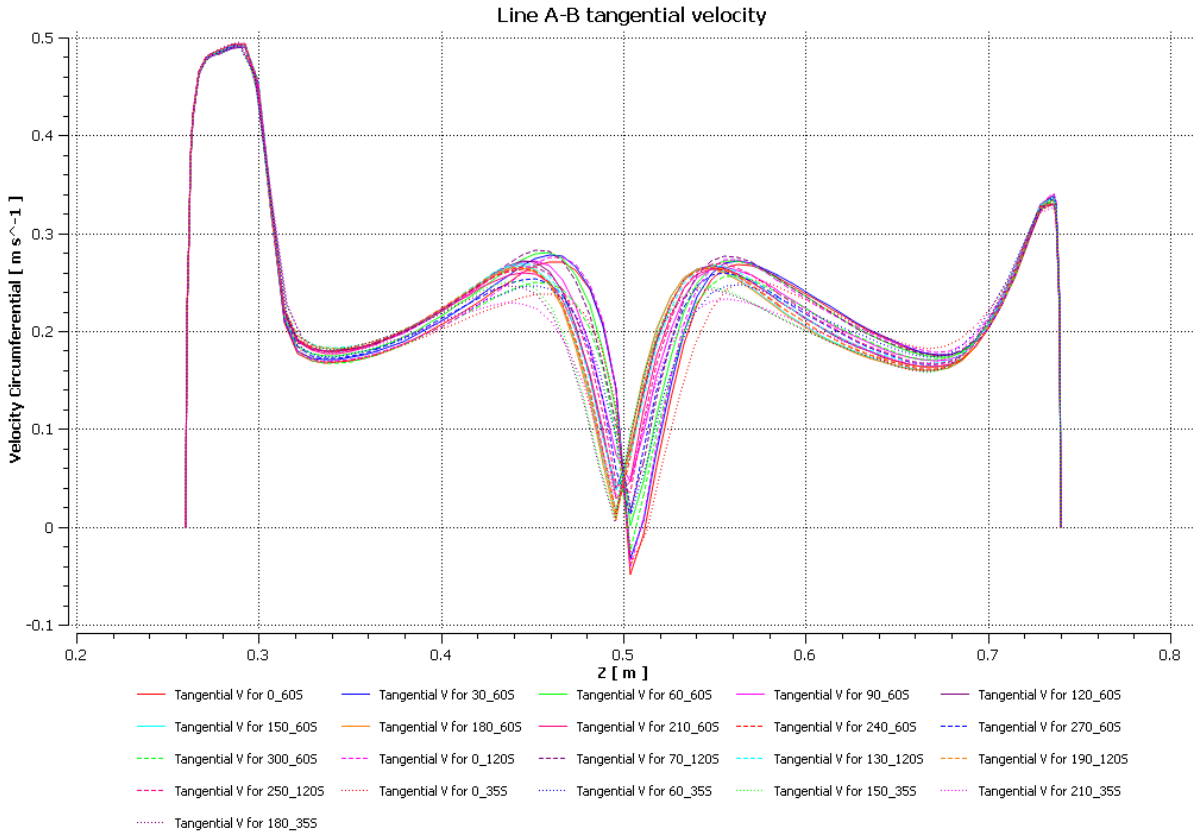

Figure 4-27: Model 1 numerical model average tangential velocity profile of 35 °, 60° and 120° sector on the z-x plane at lines A-B at y = 0.228 m

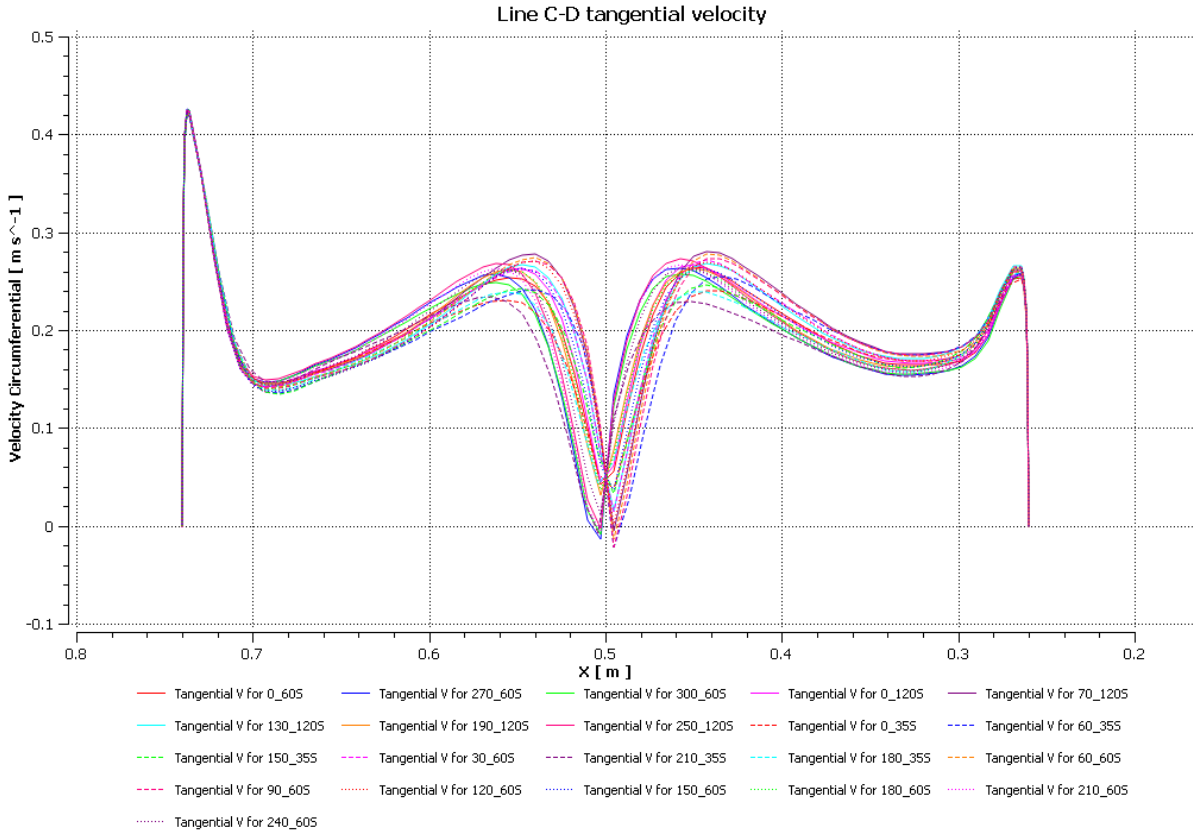

Figure 4-28: Model 1 numerical model average tangential velocity profile of 35 °, 60° and 120° sector on the z-x plane at line C-D at y = 0.228 m

Figure 4-29 and **Figure 4-30** below illustrate Model 2 numerical model average tangential velocity profile on the z-x plane at lines A-B and C-D. It was observed that:

a) A Rankine's type of profile was exhibited.
b) The profiles varied in magnitude.
c) The outliers at 0° angle had the highest tangential velocity and lowest trapping efficiency and it can be concluded that high tangential velocities are detrimental to sediment removal.

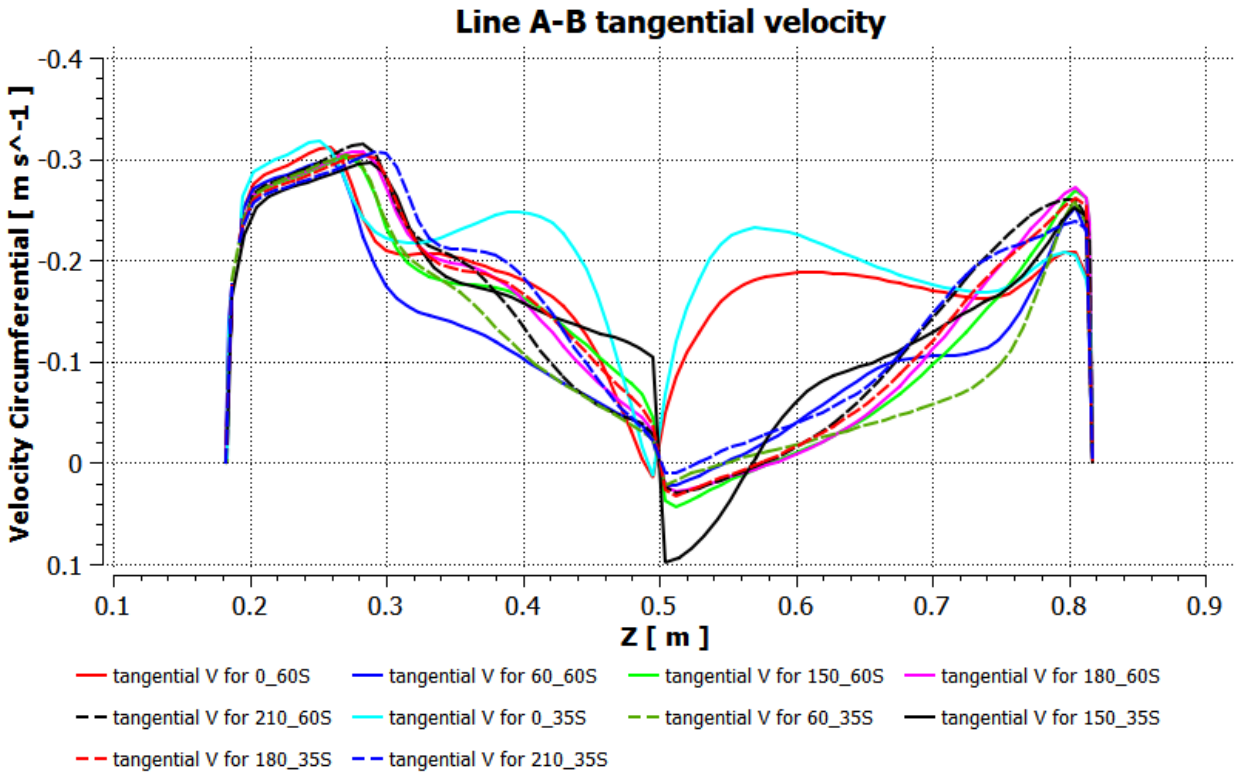

Figure 4-29: Model 2 numerical model average tangential velocity profile of 35° and 60° sector on the z-x plane at lines A-B at y= 1.208 m

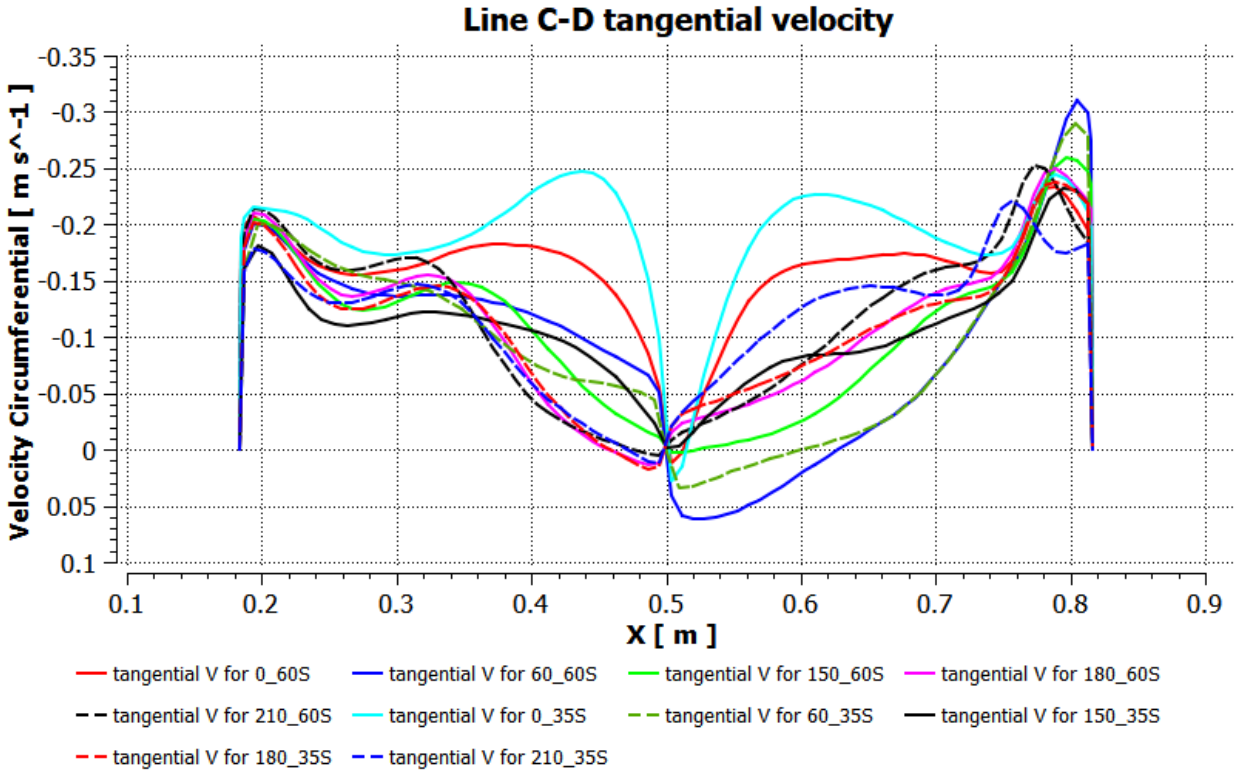

Figure 4-30: Model 2 numerical model average tangential velocity profile of 35° and 60° sector on the z-x plane at line C-D at y= 1.208 m

4.3.4 Conclusion on outlet location, outlet sector size

The Volume of Fluid (VOF) and the Discrete Element Method (DEM) numerical models and physical modelling were conducted to investigate the influence of outlet location and size on sediment removal and it can be concluded that:

- Outlet location positioning plays a significant role in the removal of fine sediment in Model 1 configuration.
- 60° sector at 0° in Model 1 is recommended. The configuration has been recommended in other industries, but it was observed to have shortcomings (an upward current draft carrying sediment) for use in water abstraction works.
- Model 2 with an outlet at 60° sector and an incremental angle between 150° and 210° is recommended for use in water abstraction works and is investigated in detail. It should be noted as the study progressed a centroid outlet is utilised and side outlets become obsolete.

4.4 Inlet velocity, Vi

4.4.1 Introduction

Inlet velocity is a critical consideration in hydraulic design. Richardson et al. (2002) established that hydro-cyclones are centrifugal driven and require a high inlet velocity for efficient removal of fine sediment and can be in the order of 5 m/s or more hence have high energy requirements.

On the other hand, settlers which are gravity-driven need low velocity in the order < 0.02 m/s to remove fine sediment. In the VSB under consideration, the sediment removal mechanism is gravity driven but takes advantage of weak centrifugal forces allowing a higher inlet velocity hence having low energy requirements. To study the effect of inlet velocity on trapping efficiency, Model 1 was used and **Table 4-3** summarises base parameters.

Table 4-3: Influence of inlet velocity VSB base model parameters

Parameter	Symbol and units	Model 1 range
Inlet flow	Qi (l/s)	1-2
Cylinder diameter	D (mm)	480
Inlet diameter	Di (mm)	30-100
Cone height	Hc (mm)	250
Cylinder height	Ht (mm)	700
Outlet height	Ho (mm)	80
Inlet height	Hi (mm)	11.5
Underflow/Inflow	Qu/Qi	0.3
Sediment particle diameter	d50 (µm)	75-112
Sediment concentration in inflow	C (mg/l)	10,000

4.4.2 Sediment trapping efficiency

Figure 4-31 illustrates Model 1 physical and numerical results. The graph is a plot of varying inlet velocities against 75 µm, 100 µm and d50 =112 µm sediment trapping efficiencies.

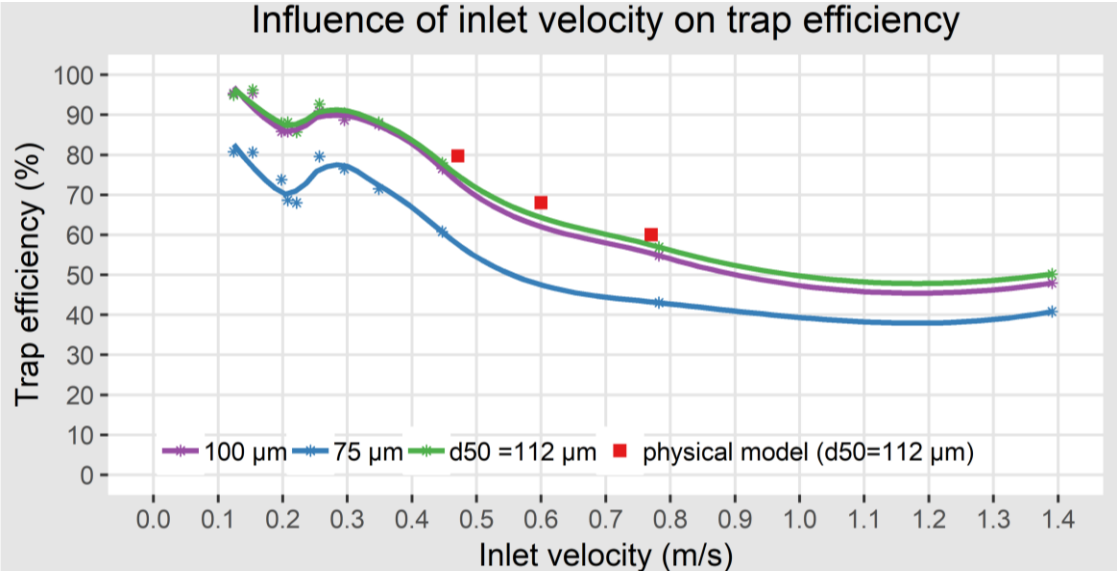

Figure 4-31: Model 1 numerical model (continuous lines) and physical model (markers) show the impact of inlet velocity on sediment removal efficiency

Statistical analysis was undertaken on the data, and it was observed that there is a good correlation between the simulated and physical model results. **Table 4-4** below summarises the analysis with a correlation of 0.998 calculated with the average difference being 3.3% and a maximum difference of 4%.

Table 4-4: Summary of Figure 4-3 numerical and physical model correlation statistical analysis

Inlet velocity(m/s)	**Trapping efficiency (%)**			**Correlation**
	Physical model	**Numerical model**	**Difference**	
0.47	79.7	76.1	3.6	0.998
0.60	68.0	64.0	4.0	
0.77	60.0	57.7	2.3	
Average difference			3.3	

The inlet velocity plays a vital role in controlling sediment removal efficiency. It was observed that the sediment trapping efficiencies decline with an increase in inlet velocities.

High inlet velocities cause disturbances in the VSB leading to sediment resuspension towards the outlet and short-circuiting. Further confirming that sediment removal is gravity driven and centrifugal forces influences are minimal. The centrifugal forces help in keeping the particles in suspension thus increasing the residence time of particles. Hence it can be concluded a low inlet velocity increases the trapping efficiency. However, at inlet velocities of between 0.15 to 0.25 m/s, there was a reduction in efficiency. This phenomenon was investigated in more detail in section **4.4.3**.

It is tempting to use lower inflow velocities < 0.15 m/s but this will lead to inlet blockage in the long run due to sediment deposition in the pipe, thus unsustainable design. Novak and Nalluri (1984) suggested **Equation 4-3** which can predict the incipient motion of sediment particles in pipes. The equation is more suitable than using equations which predict self-cleaning velocity as the objective in this circumstance is to minimise the velocity but not to the detriment of sustainability.

As an example: taking maximum sediment sizes that could get into the system to be about ≈ 1 mm, the velocity should be ≥ 0.20 m/s for a 156 mm internal diameter to have a sustainable design. An assumption was made that there is a boulder/gravel trap and trash rack to exclude larger sediment particles ensuring that the maximum sediment size getting in the VSB is 1 mm, but for other sediment sizes, the minimum velocity required to achieve a sustainable design are summarised in **Table 4-5**.

Table 4-5: Summary of minimum velocity needed to initiate sediment motion in pipes according to Equation 4-3

Sediment size (mm)	0.075	0.100	0.500	1.000	1.500	20.000	30.000	40.000
Inlet pipe diameter (m)	0.156	0.156	0.156	0.156	0.156	0.156	0.156	0.156
Minimum velocity (m/s)	0.115	0.123	0.178	0.209	0.229	0.416	0.456	0.487

$$v = 0.61\sqrt{gd50\left(\frac{\rho_s-\rho_w}{\rho_w}\right)}\left(\frac{d50}{R}\right)^{-0.27} \quad (m/s) \qquad \text{Equation 4-3}$$

V = velocity (m/s), g = acceleration due to gravity (m/s^2), d50 = sediment median diameter (m), ρ_s = sediment density (kg/m^3), ρ_w = water density (kg/m^3), R = hydraulic radius

4.4.3 Flow field

Velocity contours of VSB flows give a better understanding of hydraulic performance. To avoid data over-plotting, four inlet velocities 0.198, 0.220, 0.257 and 0.295 m/s were considered. They were selected based on the need:

a) To explain the dip in efficiency.
b) To use the recommended inlet velocity.

Figure 4-32 below illustrates the Model 1 numerical model impact of inlet velocity on average velocity magnitude contours on different z-x planes. It was observed that:

a) At the inlet velocity, 0.220 m/s which coincides with the dip in efficiency, there was a high core velocity.
b) Apart from this anomaly, the core velocities decreased with a decrease in inlet velocity. For better understanding, the velocities were resolved into their components and are discussed further.

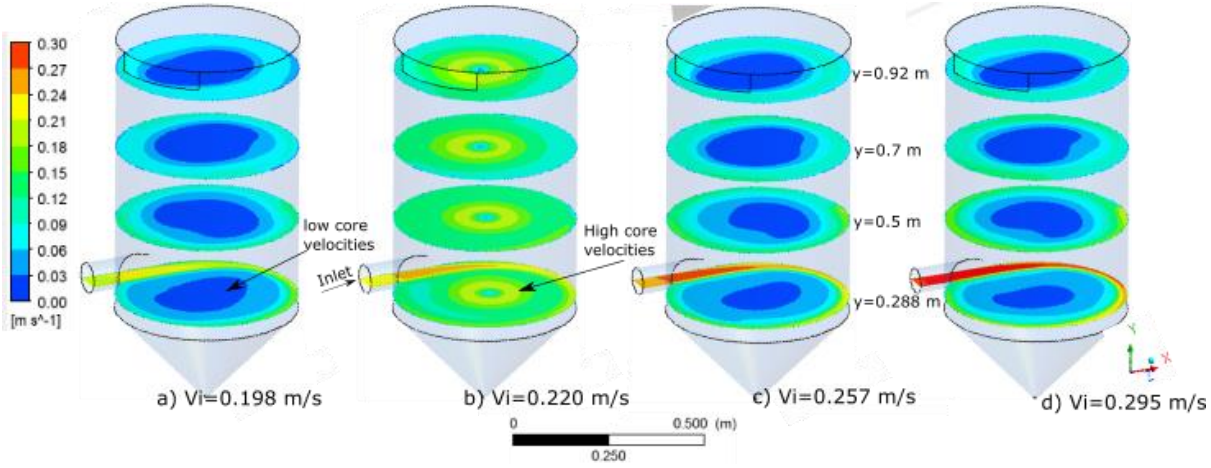

Figure 4-32: Numerical model average velocity magnitude contours of a) 0.198 m/s, b) 0.220 m/s, c) 0.257 m/s and d) 0.295 m/s on the z-x plane at y = 0.288 m, y = 0.5 m, y = 0.7 m and y = 0.92 m

4.4.3.1 Axial velocity

Figure 4-33 below illustrates the Model 1 numerical model effect of inlet velocity on average axial velocity contours on the different z-x planes and **Figure 4-34** shows axial profiles along lines A-B and C-D. It was observed that:

a) There was a rising current at the inlet carrying sediment with it.

b) Scenario b with inlet velocity at 0.220 m/s has the highest rising water stream thus explaining the dip in efficiency.
c) Scenarios a, c and d, had a similar axial velocity profile shape but varying magnitude.

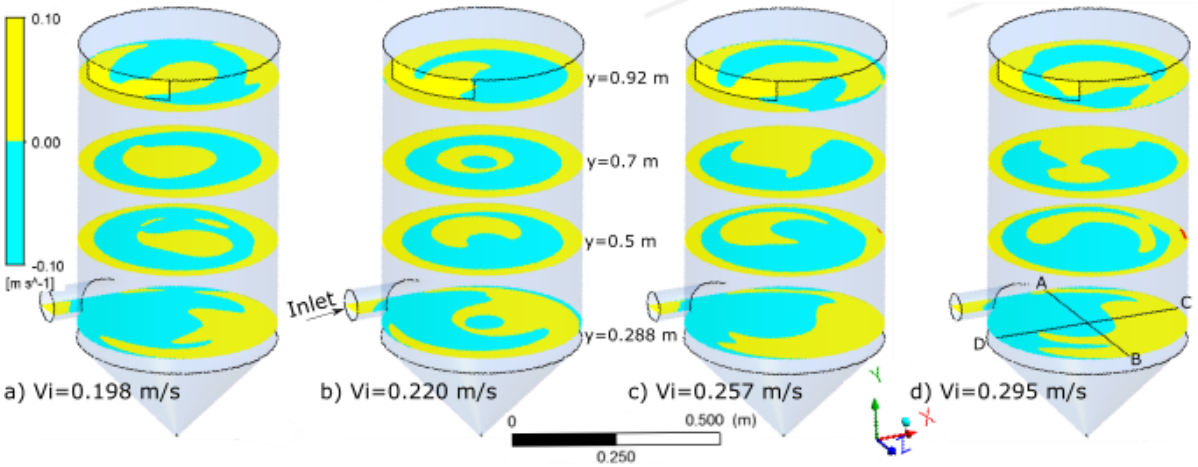

Figure 4-33: Numerical model average axial velocity contours of a) 0.198 m/s, b) 0.220 m/s, c) 0.257 m/s and d) 0.295 m/s on the z-x plane at y = 0.288 m, y = 0.5 m, y = 0.7 m and y = 0.92 m (cyan/blue: downward movement of water, yellow: rising water)

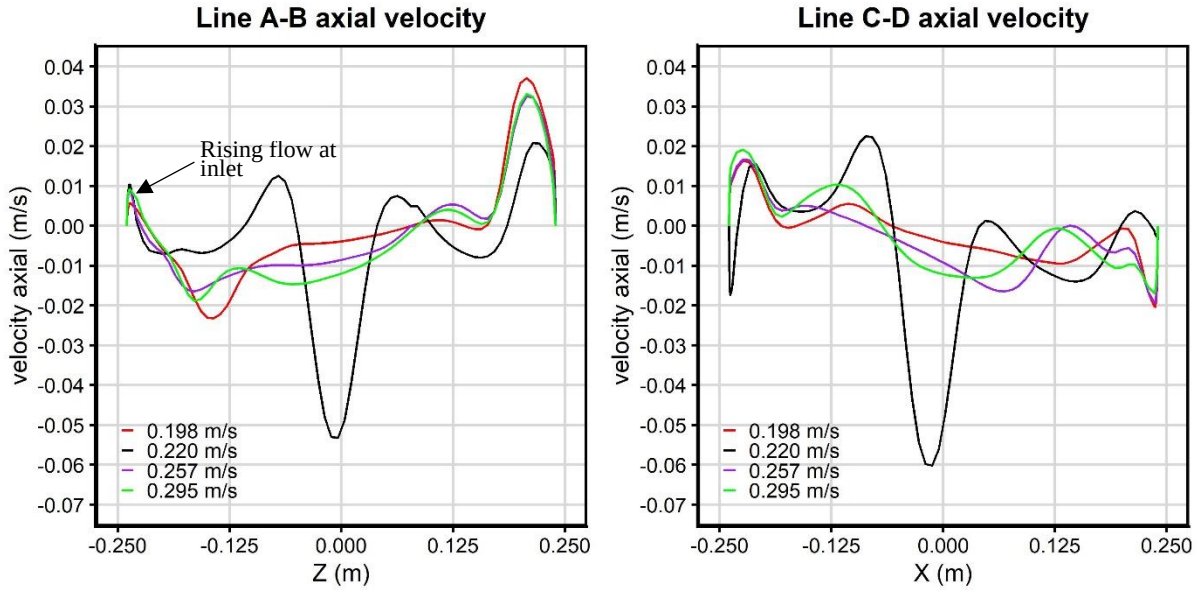

Figure 4-34: Numerical model average axial velocity profile of a) 0.198 m/s, b) 0.220 m/s, c) 0.257 m/s and d) 0.295 m/s along lines A-B and C-D at y = 0.288 m

4.4.3.2 Tangential velocity.

Figure 4-35 below illustrates Model 1 numerical model effect of inlet velocity on average tangential velocity contours on different z-x planes and profiles extracted along lines A-B and C-D in **Figure 4-36**. It was observed that:

a) High inlet tangential velocities are recorded near the inlet and near the walls.
b) A Rankine's type of profile is exhibited.

c) Scenario b (0.220m/s inlet velocity) had high tangential velocity throughout the VSB and it corresponds with the lowest efficiency.
d) The tangential velocity increases with an increase in inlet velocity thus lower trapping efficiency.

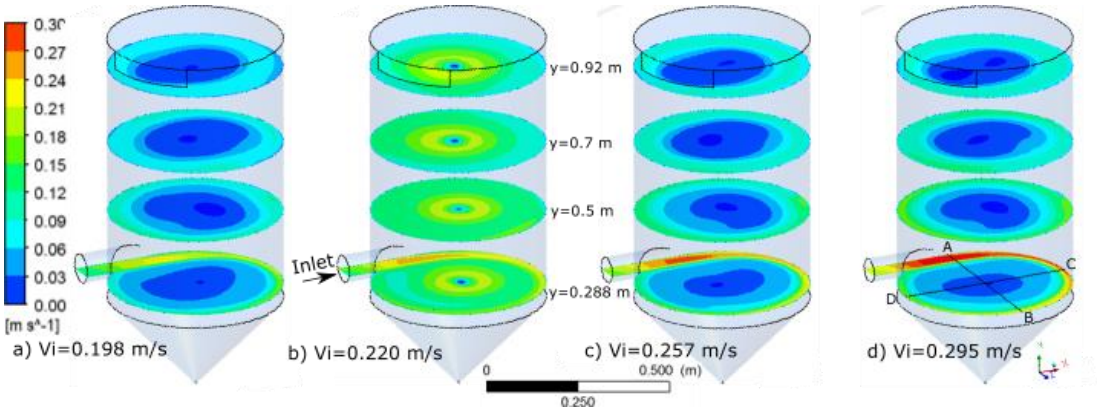

Figure 4-35: Numerical model average tangential velocity contours of a) 0.198 m/s, b) 0.220 m/s, c) 0.257 m/s and d) 0.295 m/s on the z-x plane at y = 0.288 m, y = 0.5 m, y = 0.7 m and y = 0.92 m

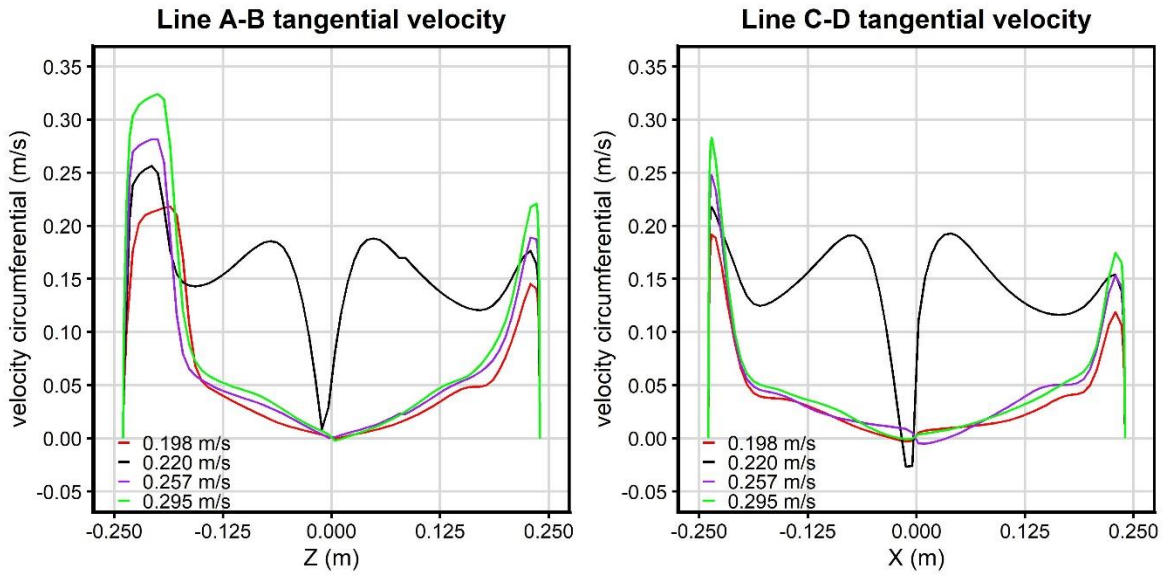

Figure 4-36: Numerical model average tangential velocity profile of a) 0.198 m/s, b) 0.220 m/s, c) 0.257 m/s and d) 0.295 m/s along lines A-B and C-D at y= 0.288m

4.4.3.3 Radial velocity

Figure 4-37 below illustrates numerical model average radial velocity along lines A-B and C-D. It was observed that:

a) Scenario b (0.220 m/s inlet velocity) had high radial velocity throughout the VSB hence settling is hindered,
b) The radial velocity increased with increase in inlet velocity thus decline in efficiency.

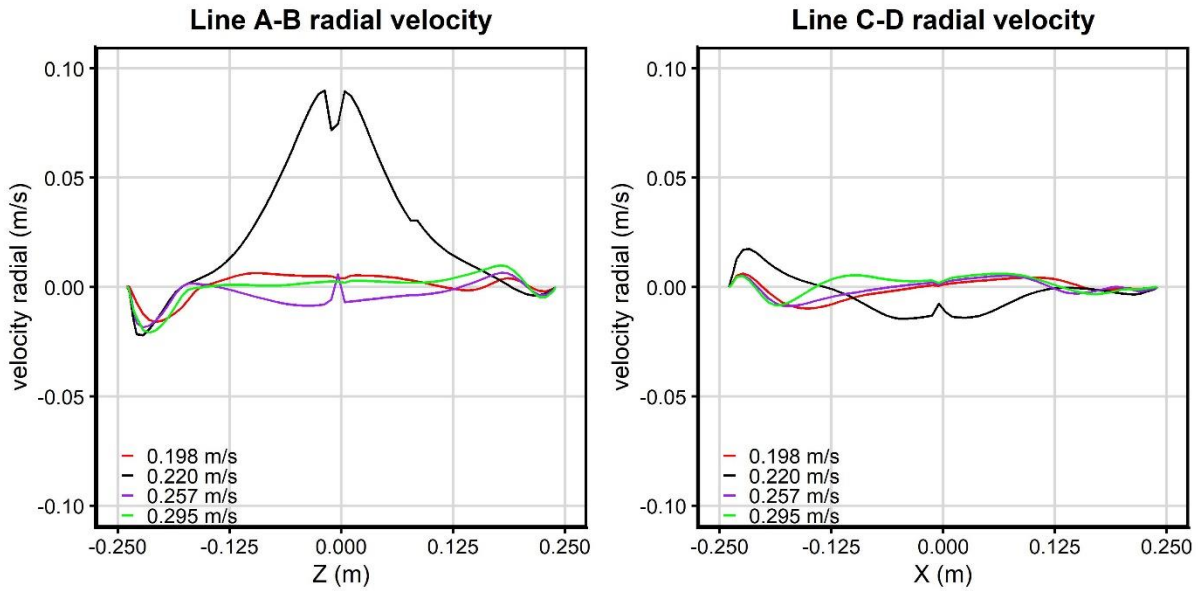

Figure 4-37: Numerical model average radial velocity of a) 0.198 m/s, b) 0.220 m/s, c) 0.257 m/s and d) 0.295 m/s along lines A-B and C-D at y= 0.288m

4.4.4 Turbulent kinetic energy, TKE

Figure 4-38 below illustrates Model 1 numerical model effect of inlet velocity on average TKE contours on the different z-x planes. It was observed that:

a) In scenarios a, b and c TKE decreased with a decrease in inlet velocity,
b) High TKE values were recorded at scenario b (Vi=0.220 m/s) thus; it can be concluded the ratio of $\frac{Qu}{Qi}$=0.3 and inlet velocity 0.220 m/s enhance tangential velocities leading to a turbulent flow.

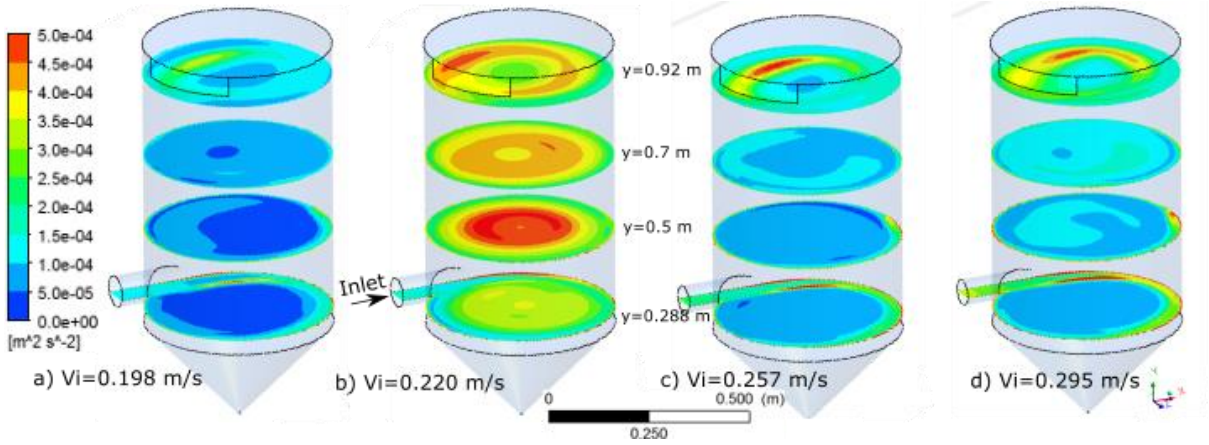

Figure 4-38: Numerical model average turbulence kinetic energy of a) 0.198 m/s, b) 0.220 m/s, c) 0.257 m/s and d) 0.295 m/s on the z-x plane at y = 0.288 m, y = 0.5 m, y = 0.7 m and y = 0.92 m

4.4.5 Conclusion on inlet velocity

The Volume of Fluid (VOF) and the Discrete Element Method (DEM) numerical models and physical modelling were conducted to investigate the influence of inlet velocity on sediment removal. It was concluded that:

- Low inlet velocities are desirable for the removal of fine sediment.
- Velocities less than 0.26 m/s are recommended to minimise the effect of centrifugal forces. The flow in the main supply line should be at a higher velocity to limit settling of sediment; **Equation 4-3** can be used to calculate minimum velocity in the pipe.
- One should ensure $\frac{Qu}{Qi}$ ratio and inlet velocity combination does not resonate increasing the tangential/ radial velocity component. Model 1 ratio of $\frac{Qu}{Qi} = 0.3$ was used due to the physical model limitation of measuring 0.08 l/s. (see section **4.2.5**; a ratio of $0.05 < \frac{\text{Underflow}}{\text{Inflow}} < 0.1$ has been recommended).

4.5 Inflow rate influence, Qi

The effect of inflow rate on trapping efficiency was investigated, and **Table 4-3** summarises Model 1 base parameters. The inlet flow rate was varied, and **Figure 4-39** illustrates the resultant effect on trapping efficiency. The graph is a plot of inflow against trapping efficiency for the numerical and physical modelling of 75 µm, 100 µm and d50 = 112µm sediment sizes.

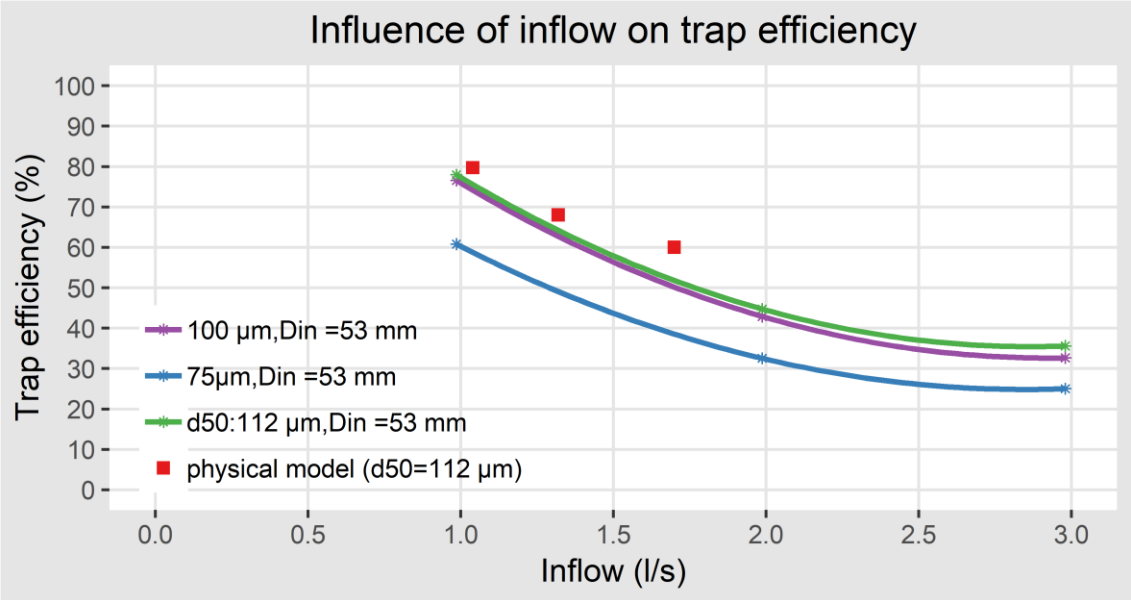

Figure 4-39: Influence of flow rate on sediment removal efficiency Model 1 numerical (continuous line) and physical model results

A statistical analysis of the physical models and the corresponding numerical model results was calculated and summarised in **Table 4-6** below. It was deduced that there is a good correlation between the numerical and physical modelling results. A correlation of 0.991 was calculated with the average difference being 5.2% and a maximum difference of 8%.

Table 4-6: Summary of Figure 4-39 numerical and physical model correlation statistical analysis

Inflow (l/s)	**Inlet velocity (m/s)**	**Trapping efficiency (%)**			**Correlation**
		Physical model	Numerical model	difference	
1.04	0.47	79.7	75.7	4.0	0.991
1.32	0.60	68.0	64.4	3.6	
1.70	0.77	60.0	52.0	8.0	
Average difference				5.2	

The inflow has a direct relationship with inlet velocity, low inflow/inlet velocities increase the trapping efficiency, but it is desirable to have higher flow rates. Increasing the inflow diameter reduces inlet velocity and increases the flow.

4.6 Inlet position to cylinder height, Hi/Ht

4.6.1 Introduction

The impact of inlet height on sediment removal has been studied for the removal of coarse sediment. Sullivan (1972) and Veerapen et al. (2005) recommended a ratio of $\frac{Hi}{Ht} > 0.5$ for the removal of course sediment particles. Not much work has been undertaken on the removal of fine sediment particles with gravity being the dominant removal mechanism.

Models 1 and 2 were used to investigate the effect of inlet positioning, and **Table 4-7** summarises the base model parameters.

Table 4-7: Effect of inlet position on sediment removal efficiency base model parameters

Parameter	Symbol and units	Model 1	Model 2
Inlet flow	Qi (l/s)	1	5
Cylinder diameter	D (mm)	480	634
Inlet diameter	Di (mm)	53	156
Cone height	Hc (mm)	250	330
Cylinder height	Ht (mm)	700	1000
Outlet height	Ho (mm)	50	80
Inlet height	Hi (mm)	11.5-525	100-800
Underflow/Inflow	Qu/Qi	0.3	0.1
Sediment particle diameter	d50 (µm)	75-112	75-112
Sediment concentration in inflow	C (mg/l)	10,000	10,000

4.6.2 Sediment trapping efficiency

Due to different model dimensions (Model 1 and 2), the ratio: $\frac{\text{height between cone base and inlet pipe (Hi)}}{\text{cylinder height (Ht)}}$ was deemed as an appropriate parameter for comparison. Models 1 and 2 were modelled in numerical and physical models using sediment sizes of 75 µm, 100 µm and d50 = 112 µm. Resulting sediment trapping efficiency results are plotted in **Figure 4-40** and **Figure 4-41** respectively.

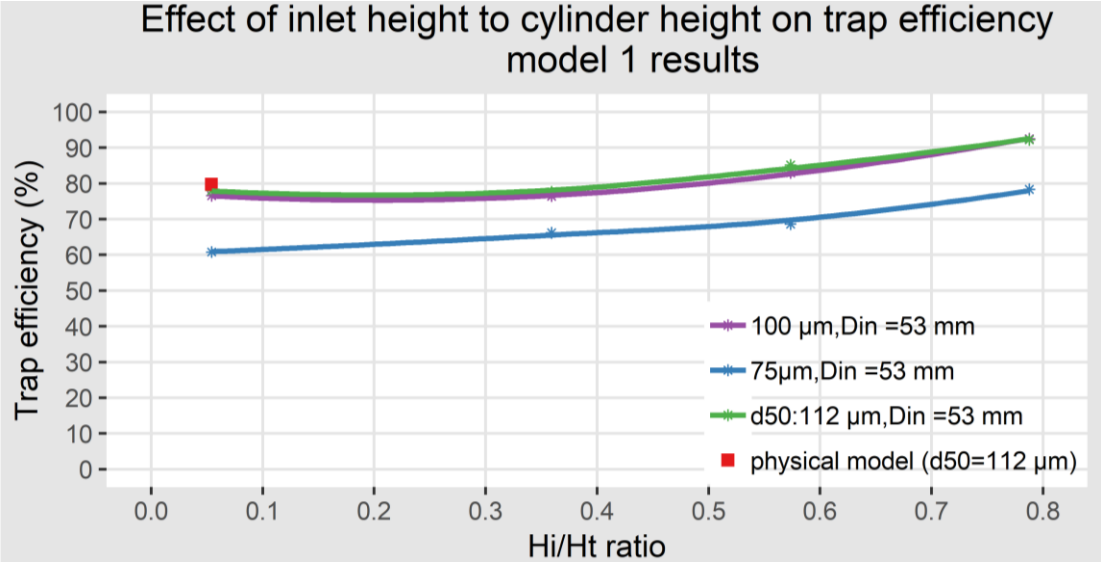

Figure 4-40: Influence of inlet position on sediment removal efficiency Model 1 numerical (continuous line) and physical model results

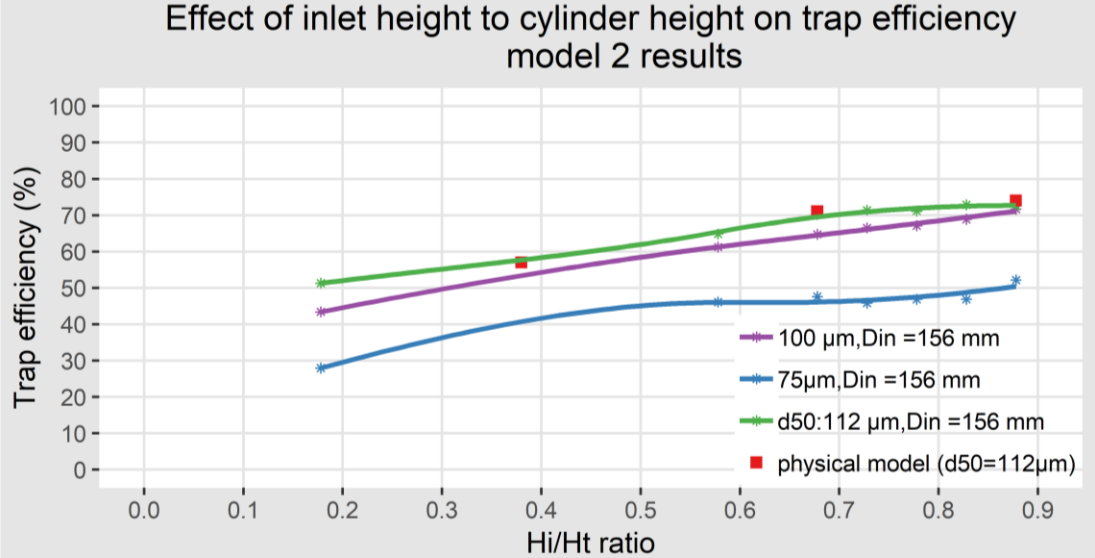

Figure 4-41: Influence of inlet position on sediment removal efficiency Model 2 numerical model (continuous line) and physical model results

It was noted there was a good correlation between the numerical and physical model results and **Table 4-8** below summarises the Model 2 statistical calculation.

Table 4-8: Summary of Figure 4-41 numerical and physical model correlation statistical analysis for Model 2

$\frac{Hi}{Ht}$	**Trapping efficiency (%)**			**Correlation**
	Physical model	Numerical model	difference	
0.88	74.00	72.49	1.51	0.999
0.68	71.00	70.19	0.81	
0.38	57.00	58.00	-1.00	
Average difference			0.44	

It was concluded that trapping efficiency increases with the inlet closer to the outlet and $\frac{Hi}{Ht} = 0.88$ gave the maximum efficiency. The value cannot be one as the flow would flow directly to the outlet. This observation is counter-intuitive as it would be expected having the inlet further away from the outlet would give maximum efficiency. To answer this peculiarity Model 2 numerical results flow fields were investigated and are discussed below.

4.6.3 Flow field

4.6.3.1 Axial velocity

Average axial velocities were plotted on the z-x plane normal to the centre of inlet diameter, as shown in **Figure 4-42** and velocity profiles along lines A-B and C-D summarised in **Figure 4-43**. Two major distinct regions were observed:

a) Regions with water flowing down towards the underflow (blue and cyan) which facilitates settling of particles hence increasing trapping efficiency and

b) The region with water flowing upwards toward the outlet (red and yellow) which reduces the efficiency.

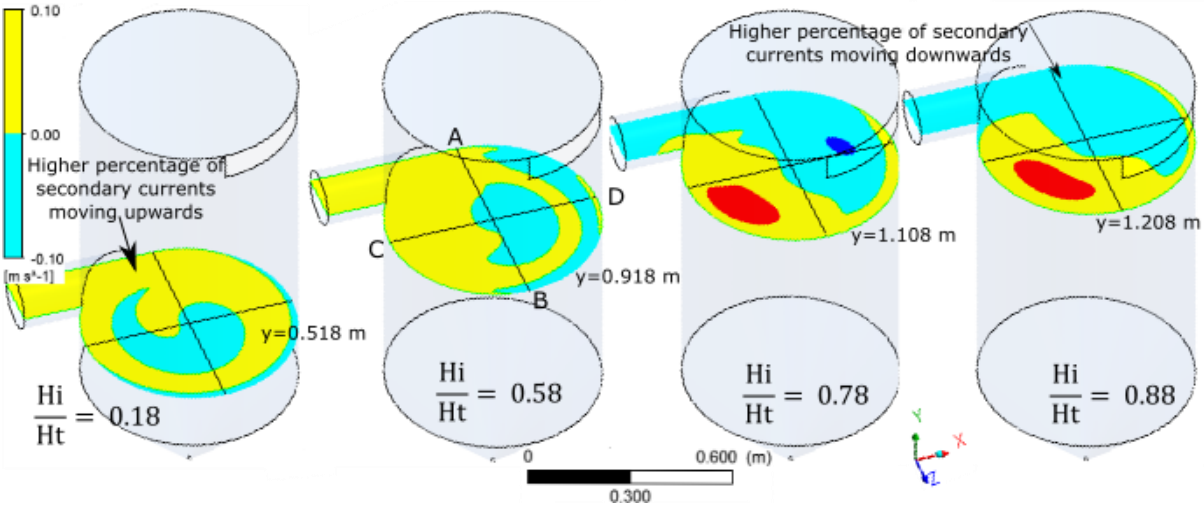

Figure 4-42: Numerical model effect of inlet location on the z-x plane average axial velocity contour (cyan/blue: downward movement of secondary currents, yellow/red: rising water)

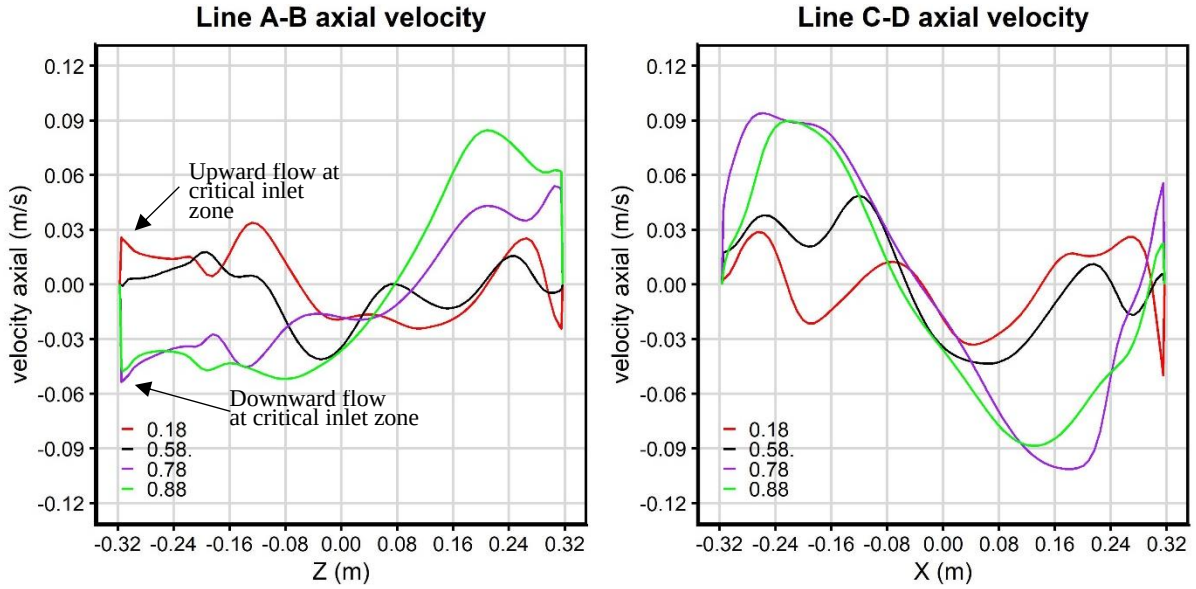

Figure 4-43: Numerical model effect of inlet location on average axial velocity profile along lines A-B and C-D

$\frac{\text{Hi}}{\text{Ht}} = 0.88$ has a higher percentage of water moving downwards explaining why higher trapping efficiency is achieved in such a configuration. A plot of 10 s numerical model particle tracking confirms this. The particle tracking gives the most probable paths particles will follow. **Figure 4-44** illustrates the resultant numerical model particle tracks. The majority of particles in the $\frac{\text{Hi}}{\text{Ht}} = 0.18$ model setup tend to move towards the overflow outlet, and in $\frac{\text{Hi}}{\text{Ht}} = 0.88$ the particles immediately after entry meet a region with secondary currents moving downwards thus settle towards the underflow although at a tilted angle.

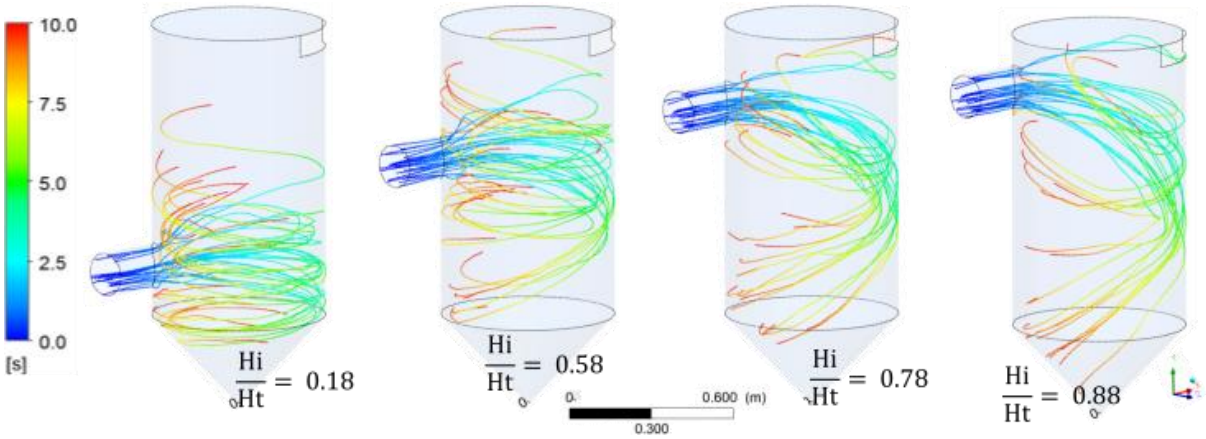

Figure 4-44: 75 µm 10 seconds particle tracking

4.6.3.2 Tangential velocity

Numerical model average tangential velocity contours were plotted at cross-section z-x normal to the centre of inlet diameter, as shown in **Figure 4-45** and velocity profiles along lines A-B and C-D summarised in **Figure 4-46**. It was observed that:

a) Tangential velocity at inlet z-x plane declines with an increase in $\frac{Hi}{Ht}$ ratio. $\frac{Hi}{Ht} = 0.88$ had the lowest tangential velocity validating that it needs to be minimised for improved efficiency.

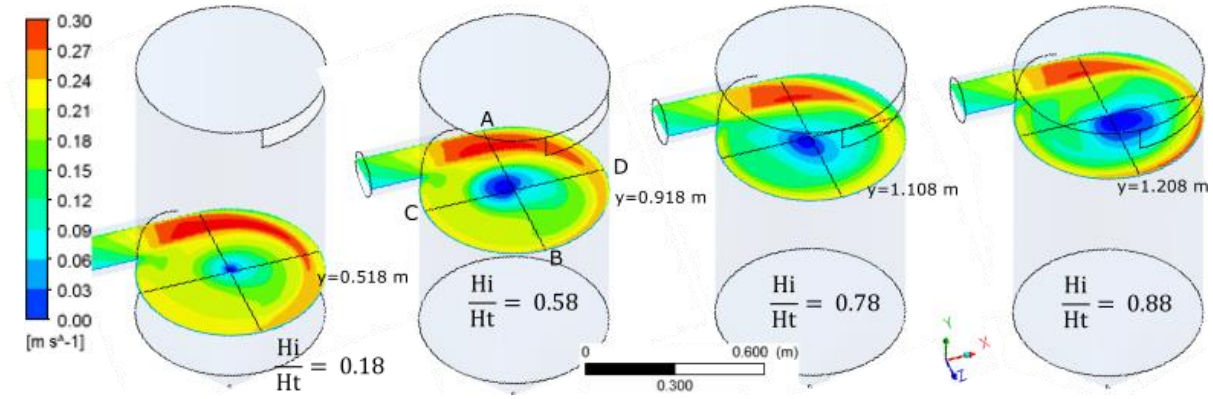

Figure 4-45: Effect of inlet location on numerical model average tangential velocity contours on inlet z-x plane

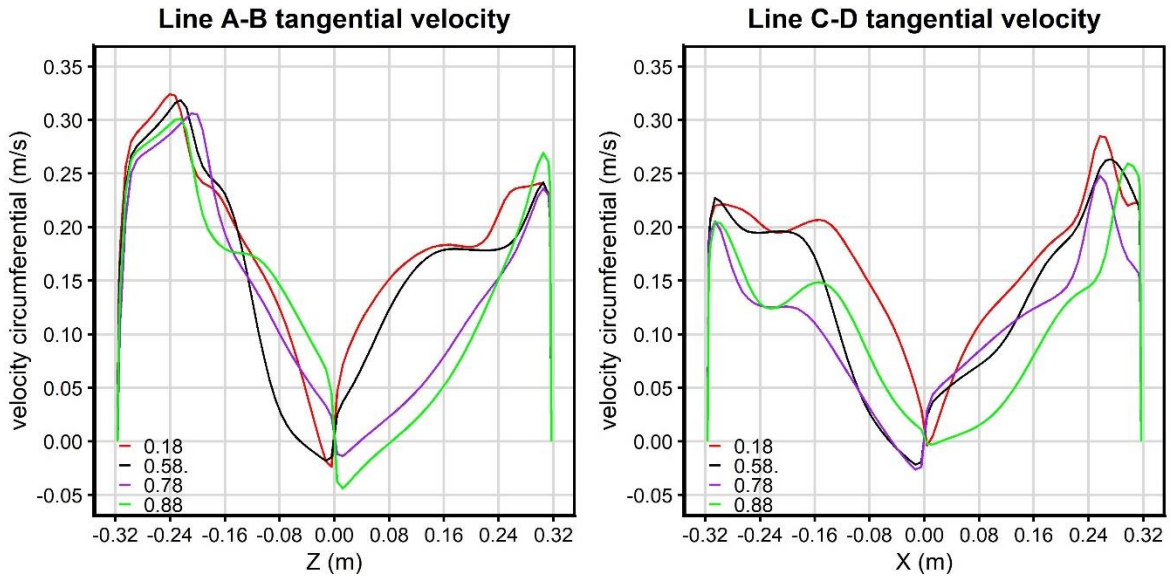

Figure 4-46: Effect of inlet location on numerical model average tangential velocity profile on inlet z-x plane along lines A-B and C-D

4.6.3.3 Vorticity and velocity vectors

The numerical model velocity vectors and vortex core region were plotted having a swirling strength of 0.0021. It was observed that having the inlet closer to the outlet forces the core region to tilt at an angle which can be observed in **Figure 4-47**. The core circulation is tilted at an angle such that particles at the inlet are accelerated downward towards the downflow, **Figure 4-48** illustrates this. Further due to this tilting of this core region the residence time of particles is increased to 345 s in the case of $\frac{\text{Hi}}{\text{Ht}} = 0.88$ from 108 s in the case of $\frac{\text{Hi}}{\text{Ht}} = 0.18$, hence the increased trapping efficiency.

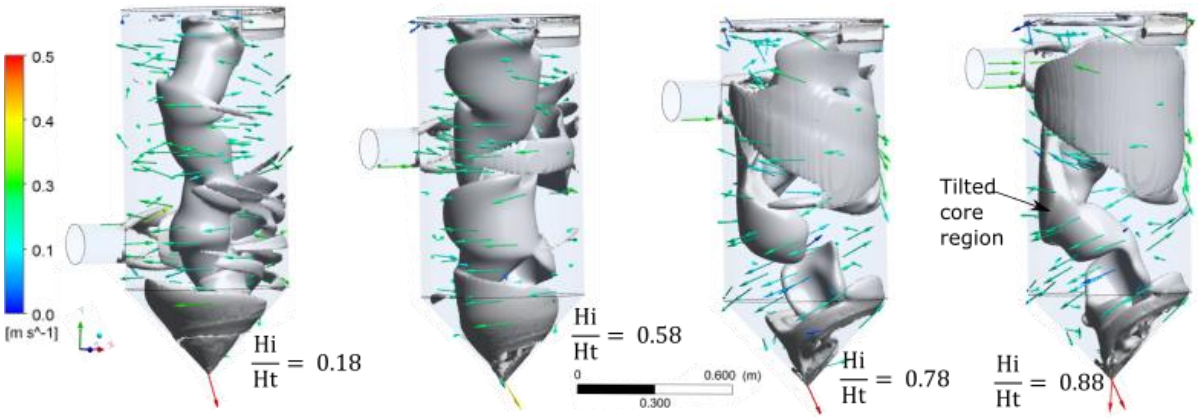

Figure 4-47: Effect of inlet location on the vortex core region and velocity vectors

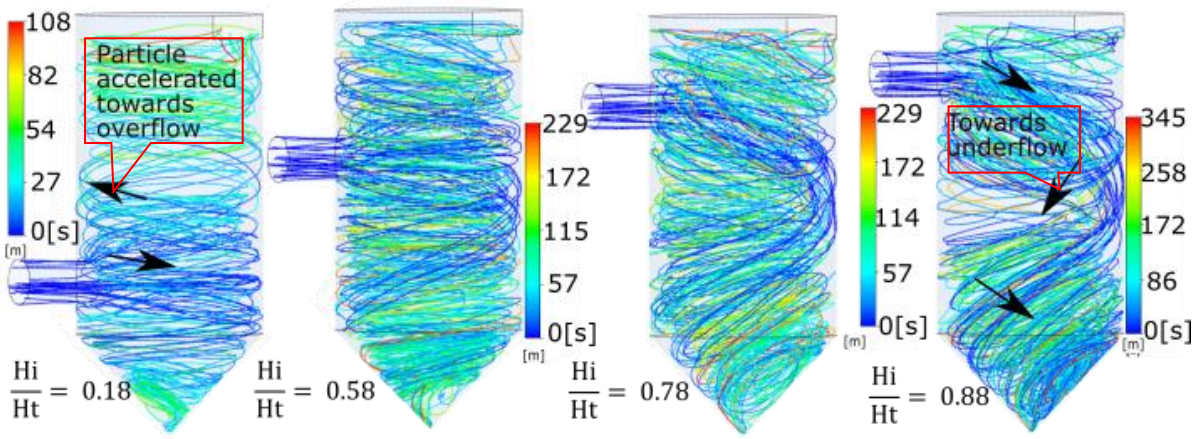

Figure 4-48: Effect of inlet location on 75 µm particle movement

4.6.4 Conclusion on inlet position

The Volume of Fluid (VOF) and the Discrete Element Method (DEM) numerical models and physical modelling were conducted to investigate the influence of underflow on sediment removal. It was concluded that:

- For gravity-driven VSB, axial velocity is an important parameter controlling the sediment removal efficiency. An axial velocity flowing towards the underflow at the crucial inlet zone should be enhanced for improved trapping efficiency.
- For removal of fine sediment, $\frac{\text{Hi}}{\text{Ht}} > 0.7$ is recommended.

4.7 Angle of inlet

4.7.1 Introduction

In **section 4.6**, it was observed that at $\frac{Hi}{Ht} = 0.88$, due to the location of outlet and inlet, secondary currents accelerated particles at the entrance towards the underflow. By tilting the inlet (downwards) at a certain angle, this could possibly be enhanced. Numerical modelling was used to investigate, and the findings are discussed below.

4.7.2 Sediment trapping efficiency

Figure 4-49 below illustrates the effect of inlet angle on Model 2 using numerical and physical modelling to predict sediment removal. It was observed that:

a) A downwards angle of 11.3° to the horizontal gave maximum efficiency, but the effects of tilting the inlet are minor.
b) Tilting the inlet at an angle greater than 11.3° leads to short-circuiting of sediment particles directly to the outlet, **Figure 4-50** below illustrates this. The number of paths illustrated has been limited to 5 to avoid overplotting.

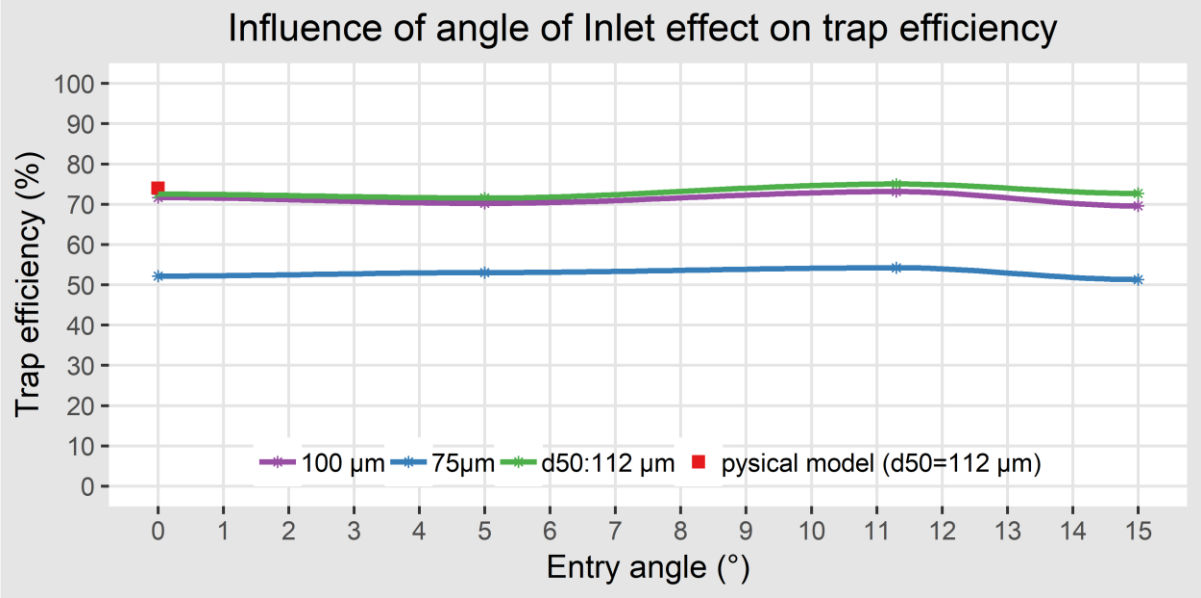

Figure 4-49: Influence of downward angle of the inlet on sediment removal efficiency Model 2 numerical results

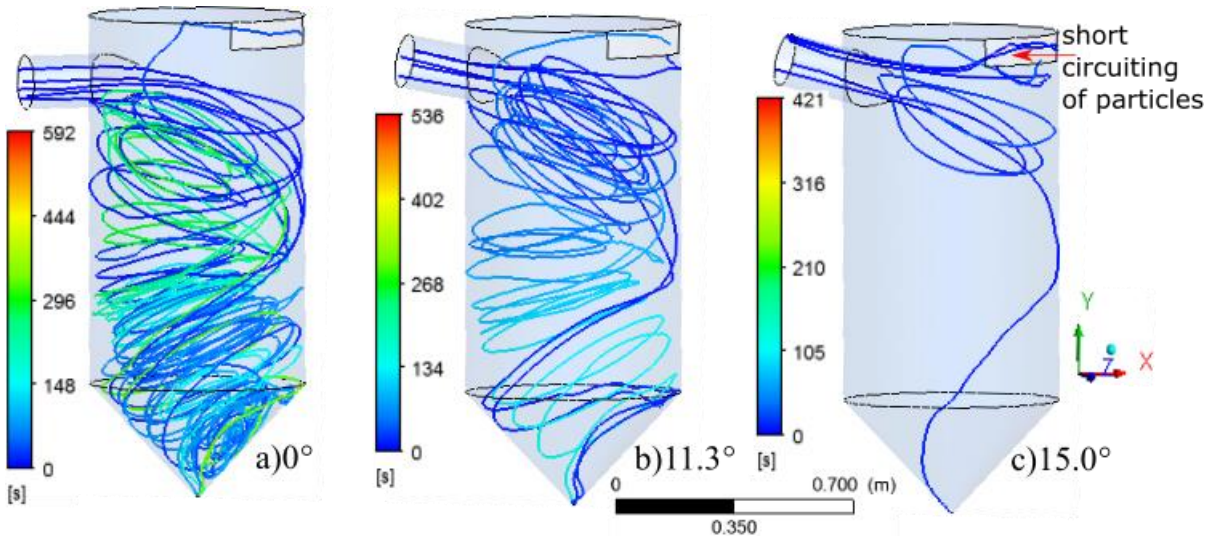

Figure 4-50: Influence of angle of the inlet on 75 µm sediment particle tracking coloured by hydraulic retention time

To have a better understanding of the angle effect, numerical model velocity flow fields were studied and the findings are summarised below.

4.7.3 Flow field

4.7.3.1 Axial velocity

Figure 4-51 below illustrates the numerical model effect of inclining the inlet on average axial velocity contours on the z-x plane at y = 0.4 m, y = 0.63 m and y = 1.208 m. Axial velocity profiles extracted along lines A-B and C-D are shown in **Figure 4-52**. It was observed that:

a) As the angle of inlet increased, the negative axial velocity at the crucial zone increased leading to assisted settling hence better efficiency.
b) At an inlet angle of 15°, the negative axial velocity at the crucial inlet zone was marginally higher than 11.3° inlet angle.

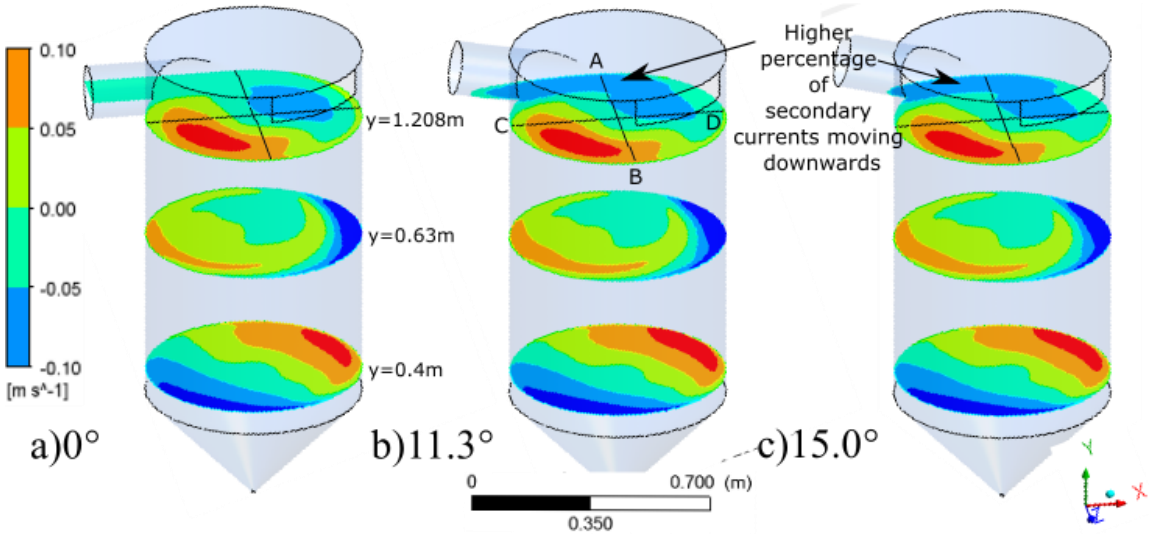

Figure 4-51: Numerical model average axial velocity contours of a) 0° b) 11.3° and c) 15° inlet angles on the z-x plane at y = 0.4 m, y = 0.63 m and y = 1.208 m

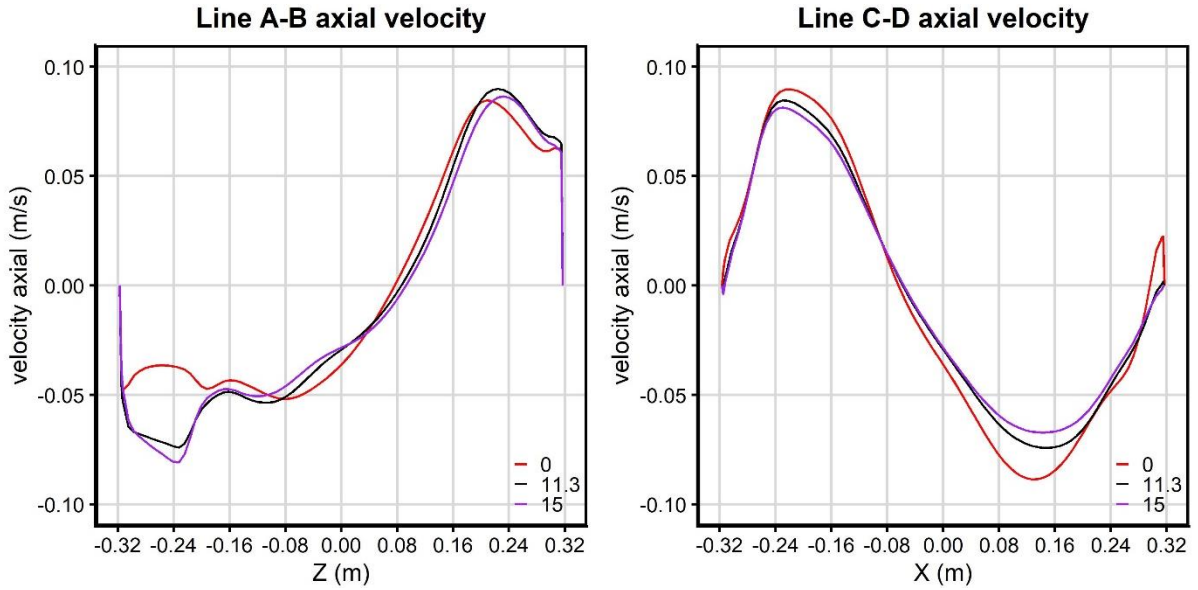

Figure 4-52: Numerical model average axial velocity profile of a) 0° b) 11.3° and c) 15° inlet angles along lines A-B and C-D at y= 1.208m

4.7.3.2 Tangential velocity

Figure 4-53 below illustrates the numerical model effect of inclining the inlet on average tangential velocity contours on the z-x plane at y = 0.4 m, y = 0.63 m and y = 1.208 m. **Figure 4-54** shows the tangential velocity profiles extracted along lines A-B and C-D. It was observed that:

a) The highest values are near the wall and lowest at the centre exhibiting a Rankine's type of profile.
b) There was not much difference in tangential velocity magnitude between the 3 cases.

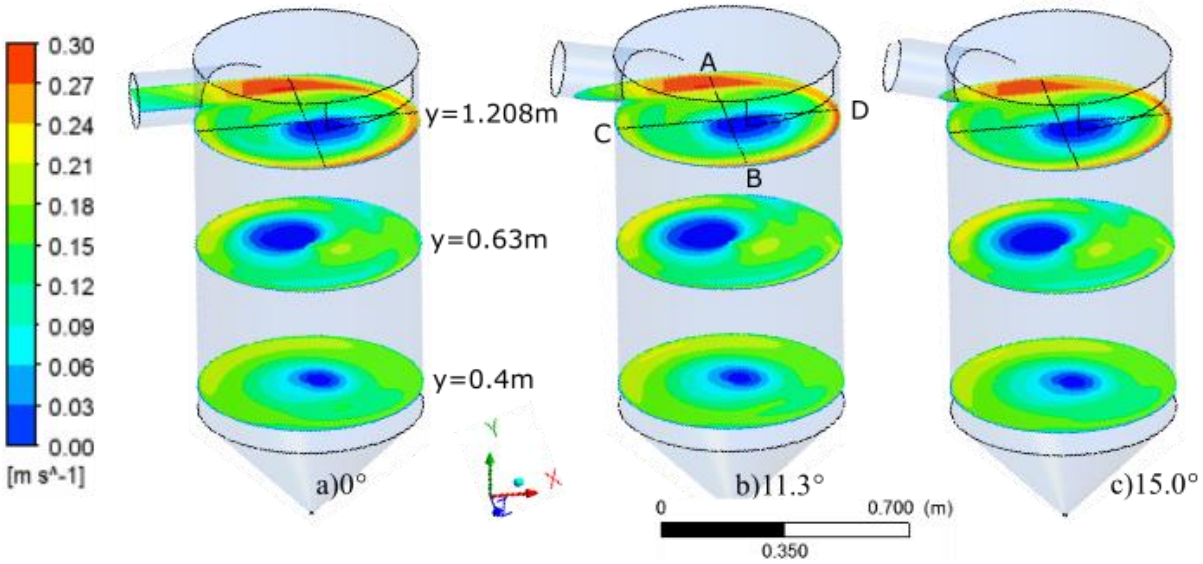

Figure 4-53: Numerical model average tangential velocity profile of a) 0° b) 11.3° and c) 15° inlet angles on the z-x plane at y = 0.4 m, y = 0.63 m and y = 1.208 m

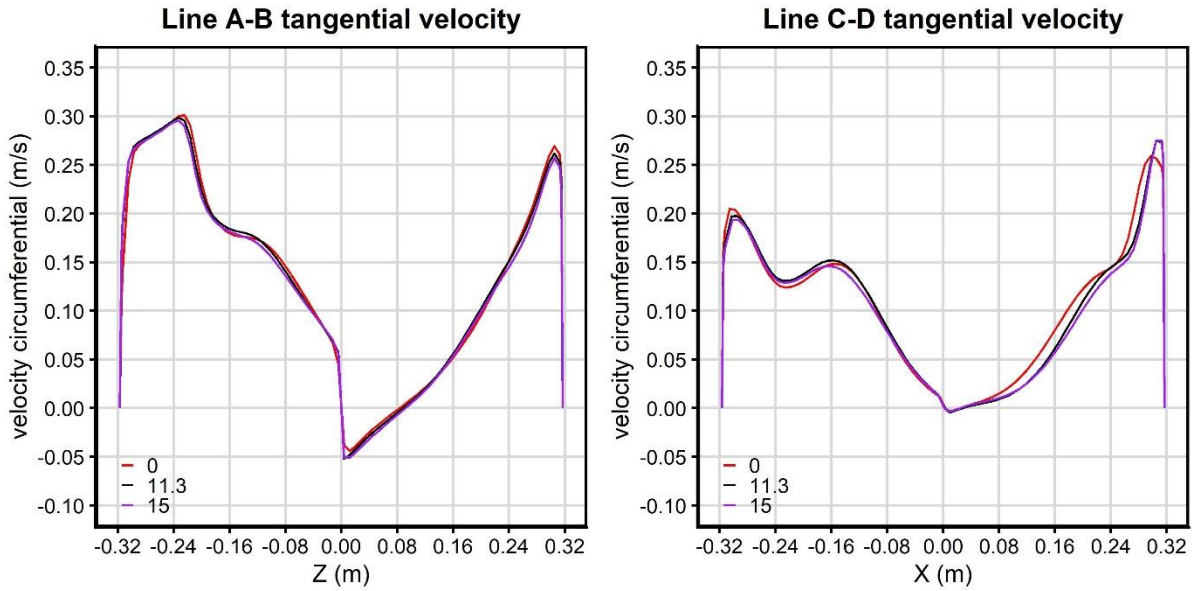

Figure 4-54: Numerical model average tangential velocity profile of a) 0° b) 11.3° and c) 15° inlet angles along lines A-B and C-D at y= 1.208m

4.7.3.3 Radial velocity

The radial velocity component influences sediment distribution towards the wall/centre of VSB. **Figure 4-55** below illustrates numerical model average radial velocity contours on different z-x planes and profiles extracted along lines A-B and C-D in Figure 4-56. It was concluded that:

a) The least amount of sediment is transported towards the centre of VSB at the crucial inlet zone in the scenario 15° incline. With recirculation towards the outlet being the highest, the probability of short-circuiting increases significantly hence low trapping efficiency is expected.
b) The radial component at inlet angle 11.3° promotes settling.

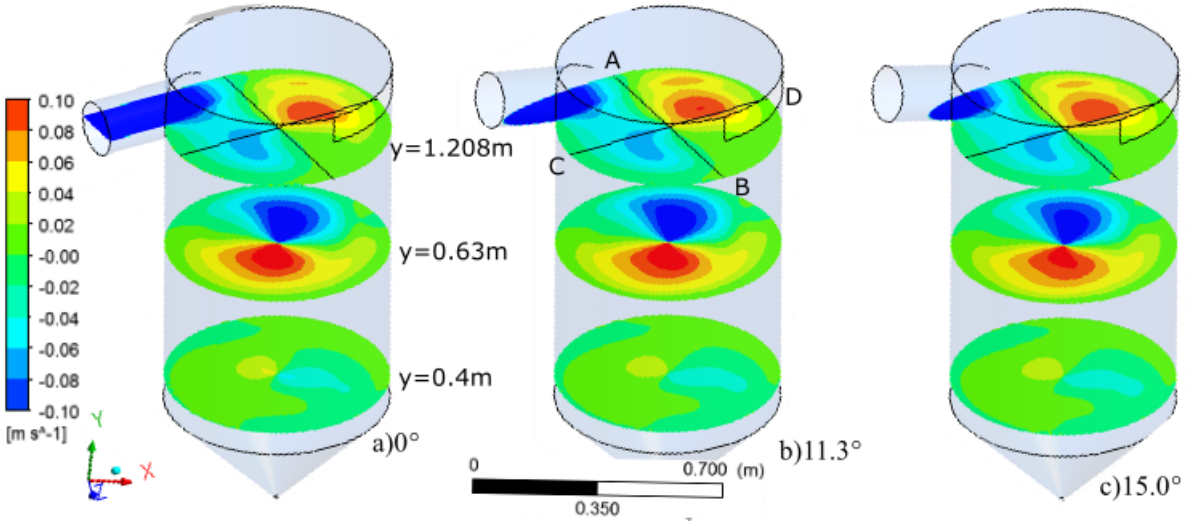

Figure 4-55: Numerical model average radial velocity profile of a) 0° b) 11.3° and c) 15° inlet angles on the z-x plane at y = 0.4 m, y = 0.63 m and y = 1.208 m

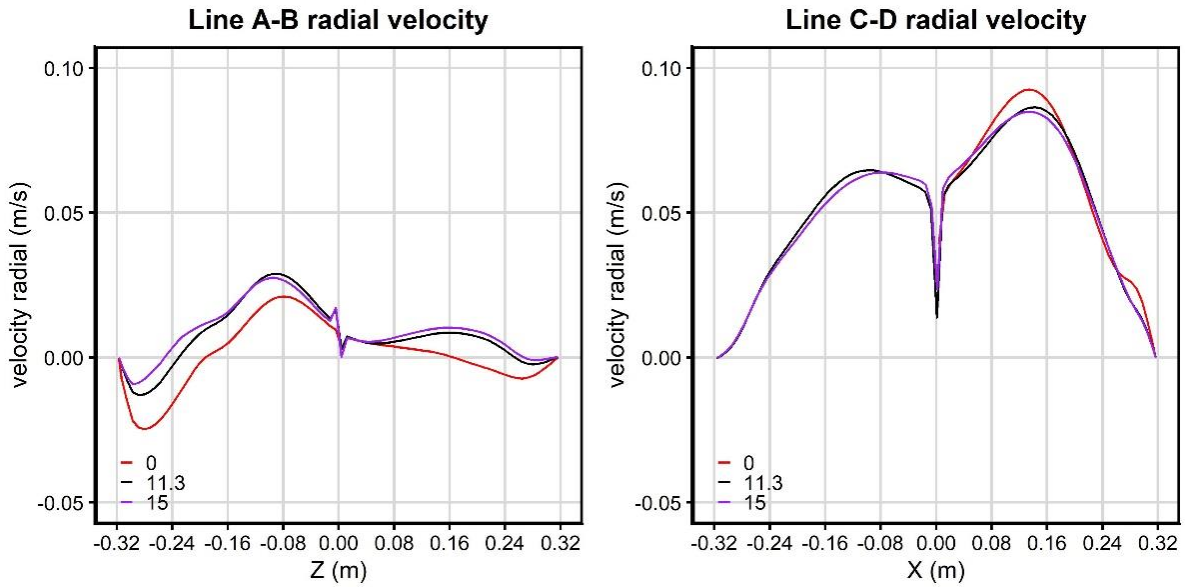

Figure 4-56: Numerical model average radial velocity profile of a) 0° b) 11.3° and c) 15° inlet angles along lines A-B and C-D at y= 1.208m

4.7.4 Conclusion on the angle of inlet

The Volume of Fluid (VOF) and the Discrete Element Method (DEM) numerical models and physical modelling were conducted to investigate the influence of inclining the inlet on sediment removal. It was concluded that:

- Tilting the inlet has minor effects on sediment removal efficiency.
- Although inlet inclined at 11.3° downwards has a better trapping efficiency, the inherent risks of short circuiting are high to justify the slight increase in trapping efficiency, thus it is recommended the inlet should not be inlined.

4.8 Cylinder height to cylinder diameter, Ht/D

4.8.1 Introduction

There is a significant difference in water levels during floods and low flows which can be in the order of 10 m. River abstraction works need to perform in both extremes for sustainable design.

Because of this difference in water levels, the effects of cylinder height (Ht) on trapping efficiency were investigated to determine how high the VSB can be constructed. **Table 4-9** below summarises two base model parameters utilised for investigation.

Table 4-9: Influence of cylinder height on sediment removal trapping efficiency base model parameters

Parameter	Symbol and units	Model 1	Model 2
Inlet flow	Qi (l/s)	1	5
Cylinder diameter	D (mm)	480	634
Inlet diameter	Di (mm)	53	156
Cone height	Hc (mm)	250	330
Cylinder height	Ht (mm)	240-1530	250-1000
Outlet height	Ho (mm)	80	80
Inlet height	Hi (mm)	11.5	11.5-800
Underflow/Inflow	Qu/Qi	0.27	0.11
Sediment particle diameter	d50 (µm)	75-112	75-112
Sediment concentration in inflow	C (mg/l)	10,000	10,000

4.8.2 Sediment trapping efficiency

As a result of different model dimensions, the ratio $\frac{\text{cylinder height (Ht)}}{\text{cylinder diameter (D)}}$ was deemed as a suitable parameter for comparison between the efficiencies. The cylinder height was varied, and three sediment particle sizes used in undertaking the tests, namely 75 µm, 100 µm and d50 = 112 µm.

Figure 4-57 shows Model 1 results as a graph of $\frac{\text{Ht}}{\text{D}}$ ratios against numerical and physical modelling trapping efficiency. Due to the destructive nature of testing another model $\frac{\text{Ht}}{\text{D}}$ ratio, only one physical model result is available. However, there is a good correlation between the physical and numerical models. The physical model trapping efficiency for sediment size d50 = 112 µm was found to be 80% against 78% numerical model trapping efficiency.

It was observed in Model 1, with the inlet positioned at 11.5 mm above the base of the cylinder, that the sediment removal efficiency marginally increased with an increase in cylinder height.

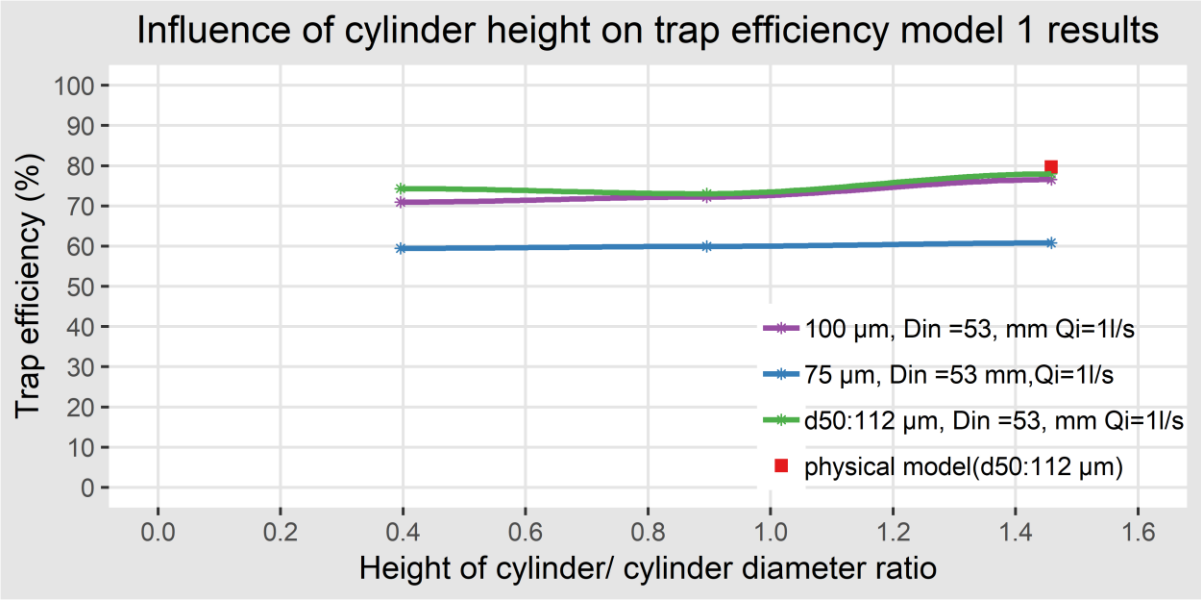

Figure 4-57: Influence of cylinder height on sediment removal efficiency Model 1 numerical (continuous line) and physical model results

In sections **4.6** and **4.2**, it was observed that the underflow and position of the inlet relative to the cylinder height have a significant effect on trapping efficiency. Thus, the ratio $\frac{\mathrm{Hi}}{\mathrm{Ht}} = 0.73$ and the ratio $\frac{\mathrm{Qu}}{\mathrm{Qi}} = 0.11$ were maintained for the Model 2 configuration. **Figure 4-58** shows the results as a graph of $\frac{\mathrm{Ht}}{\mathrm{D}}$ ratios against numerical and physical modelling predictions of sediment trapping efficiency.

The results are not consistent. Depending on the ratio, the height can improve or decrease the trapping efficiency. However, the effects of height are marginal with a ratio of $\frac{\mathrm{Ht}}{\mathrm{D}} = 1.5$ being more desirable. The higher ratios give marginally better trapping efficiencies for 75 µm sediment sizes.

It can be concluded that for South African conditions having offtakes at different elevations will solve the difference in water levels experienced as the influence of cylinder height is minimal.

The design of river abstraction works is site-specific and having towers that can be up to 10 m high does not seem to be a desirable option as compared to having the VSB located above 100 ARI flood level. The 100 ARI option is recommended in this study. The minimum ratio of $\frac{\mathrm{Hi}}{\mathrm{Ht}}$ investigated was limited to 0.5 as reducing it further would lead to short-circuiting of sediments directly to the outlet.

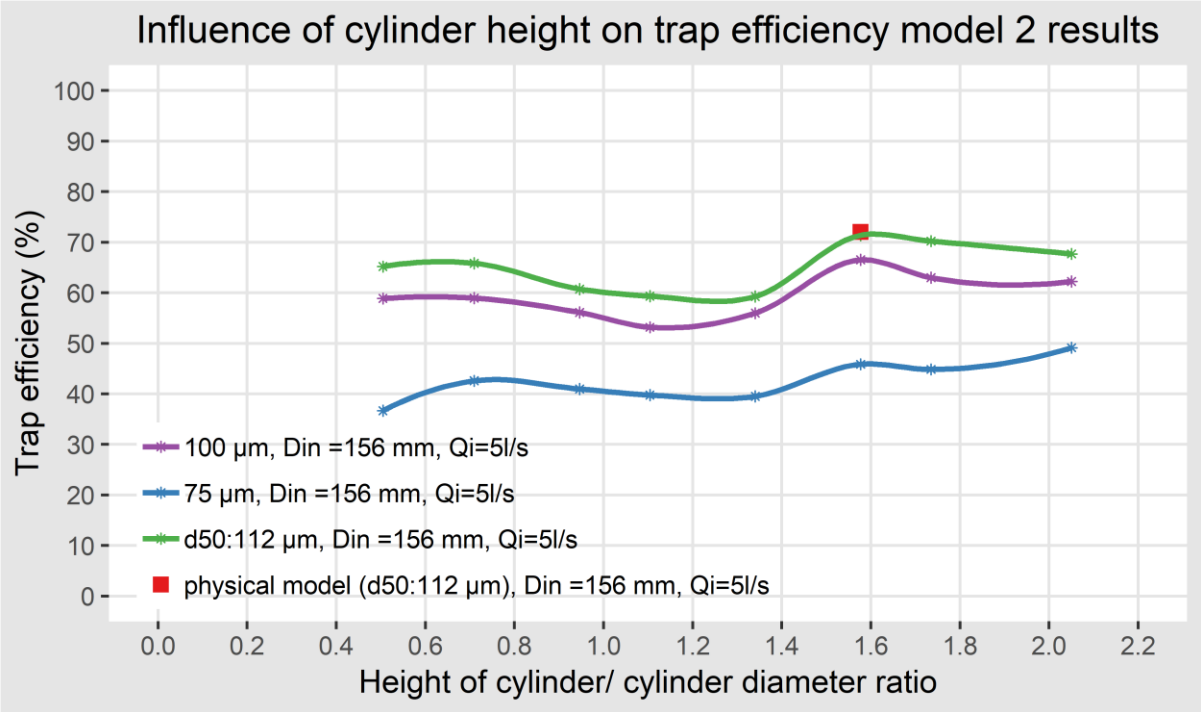

Figure 4-58: Influence of cylinder height on sediment removal efficiency Model 2 numerical results

4.8.3 Conclusion on cylinder height

The Volume of Fluid (VOF) and the Discrete Element Method (DEM) numerical models and physical modelling were conducted to investigate the influence of cylinder height on sediment removal, and it was concluded that:

- The height of the cylinder plays a minor role in sediment control removal.
- Increasing the height of the cylinder marginally improves the trapping efficiency, but the results are inconsistent.
- Sullivan (1972) recommended a ratio $\frac{H_t}{D} > 0.26$ + freeboard if one wants to reduce the construction costs. From this study, a ratio greater than 0.5 is recommended to allow deflector installation discussed in section **4.11** so as to achieve higher efficiency.

4.9 Cone angle

4.9.1 Introduction

As a result of the cohesive nature of South African sediment, a cone needs to be provided to avoid clogging of underflow and resuspension of settled sediment. Previously this has not been an essential consideration in the removal of coarse sediment with a slope of 1:10 (V: H) recommended.

The influence of cone angle Ø on sediment trapping efficiency was studied, and all parameters summarised in **Table 4-10** were kept constant and only the cone Ø was varied.

Table 4-10: Influence of cone angle on sediment removal efficiency base model parameters

Parameter	Symbol and units	Model 2
Inlet flow	Qi (l/s)	5
Cylinder diameter	D (mm)	634
Inlet diameter	Di (mm)	156
Cone height	Hc (mm)	330-549
Cylinder height	Ht (mm)	1000
Outlet height	Ho (mm)	80
Inlet height	Hi (mm)	800
Underflow/Inflow	Qu/Qi	0.11
Sediment particle diameter	d50 (µm)	75-112
Sediment concentration in inflow	C (mg/l)	10,000

4.9.2 Sediment trapping efficiency

Figure 4-59 below illustrates a graph of varying cone angle against trapping efficiency for three sediment particle sizes: 75 µm, 100 µm and d50 =112 µm as predicted by numerical and physical model results. It was observed that the cone angle has minimal influence on the trapping efficiency.

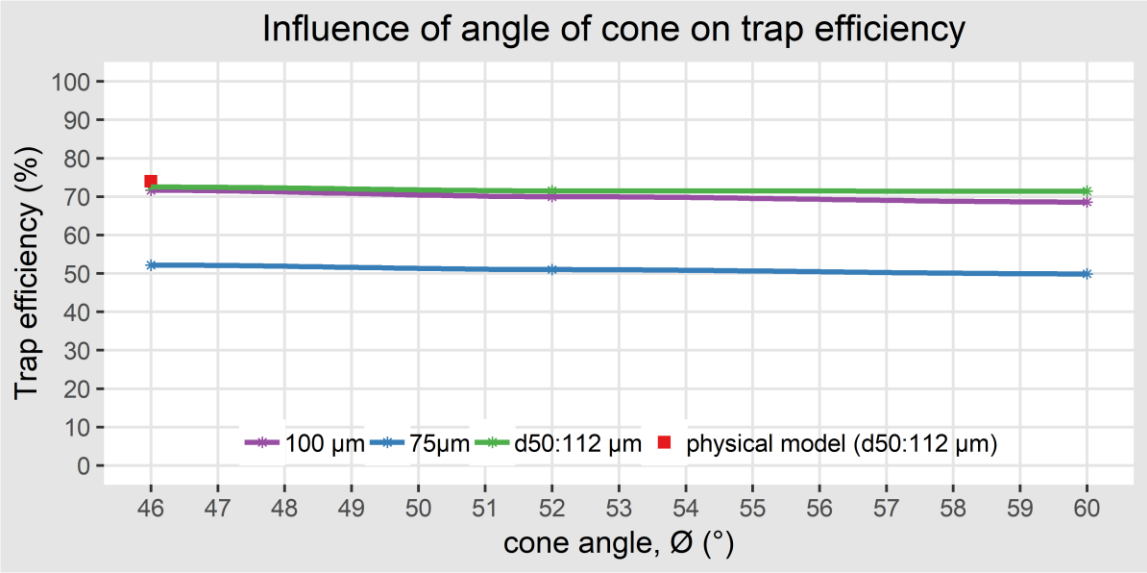

Figure 4-59: Influence of cone angle on sediment removal efficiency Model 2 numerical model results

4.9.3 Conclusion on the cone angle

In the laboratory, the utilised cone with an angle of 46° was self-cleaning. It should be noted that the laboratory sediment was non-cohesive, thus if this angle is used in abstraction works, occasional cleaning in the field will be required.

Figure 4-60 below illustrates the difference in height between a cone that is 60° and 46° to the horizontal. In a 0.634 m diameter cylinder, the difference in height is minimal but can get large with an increase in cylinder diameter.

In conclusion, a cone of 63° (1:2, H: V) is recommended in the field to ensure sustainability; the slope is motivated from the design of hoppers for South African rivers.

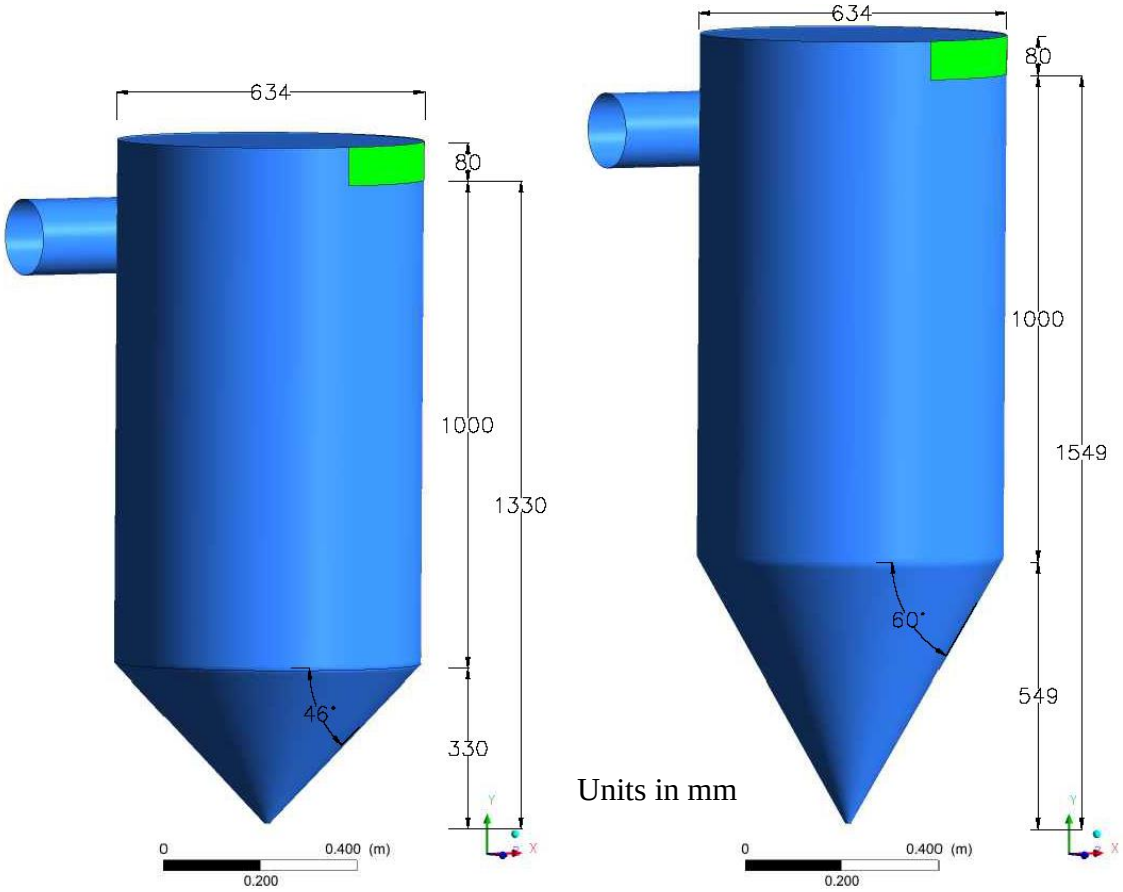

Figure 4-60: An illustration of a 46° (left) and 60° (right) cone influence on the height of VSB

4.10 Cylinder diameter influence, D

4.10.1 Introduction

The effect of cylinder diameter on trapping efficiency was investigated. **Table 4-11** below summarises Models 1 and 2 base model parameters. It should be noted for Model 2, the cylinder height was maintained at 1000 mm that is $\frac{\text{Hi}}{\text{Ht}} = 0.67$.

Table 4-11: Influence of cylinder diameter on sediment removal trapping efficiency base model parameters

Parameter	Symbol and units	Model 1	Model 2
Inlet flow	Qi (l/s)	1-3	3-5
Cylinder diameter	D (mm)	480-1500	480-1500
Inlet diameter	Di (mm)	53/90	120/156
Inlet velocity	Vi (m/s)	0.47-1.40	0.26
Cone height	Hc (mm)	250-1570	240-750
Cone angle	Ø (°)	46	46
Cylinder height	Ht (mm)	750-2344	1000
Outlet height	Ho (mm)	80	80
Inlet height	Hi (mm)	11.5	600
Height of inlet/height of cylinder	Hi/Ht	0.02-0.08	0.67
Underflow/Inflow	Qu/Qi	0.11-0.32	0.11
Sediment particle diameter	d50 (µm)	75-112	75-112
Sediment concentration in inflow	C (mg/l)	10,000	10,000

4.10.2 Sediment trapping efficiency

Figure 4-61 below illustrates Model 1 physical and numerical modelling results investigating the influence of cylinder diameter on sediment trapping efficiency for sediment sizes of 75 µm and d50 = 112 µm. Two inlet diameters were used, 53 mm and 90 mm yielding inflows of 1 l/s and 3 l/s respectively.

It was observed there was a good correlation between the numerical and physical model results. At diameter 480 mm, the trapping efficiency for sediment size d50 = 112 µm was 80% in the physical model against 78% in the numerical model.

Figure 4-62 summarises Model 2 results as a graph of varying cylinder diameter against sediment trapping efficiency as predicted in the physical and numerical models. Two inlet diameters were used; 120 mm and 156 mm yielding inflows of 3 l/s and 5 l/s respectively.

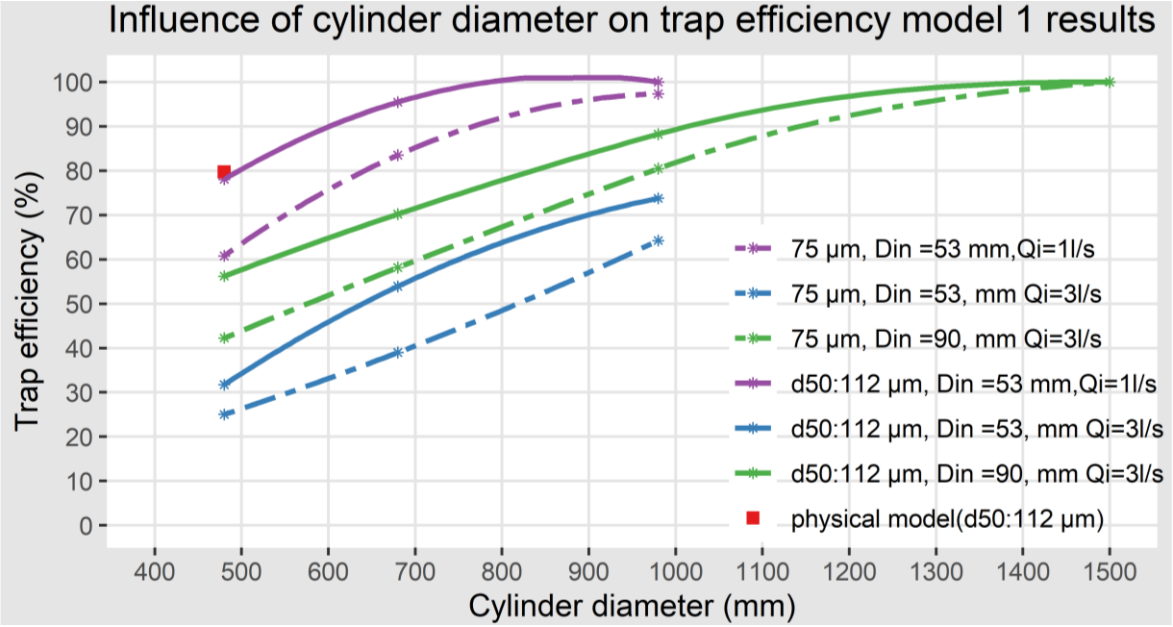

Figure 4-61: Influence of cylinder diameter on sediment removal efficiency model 1 numerical (continuous line) and physical model results

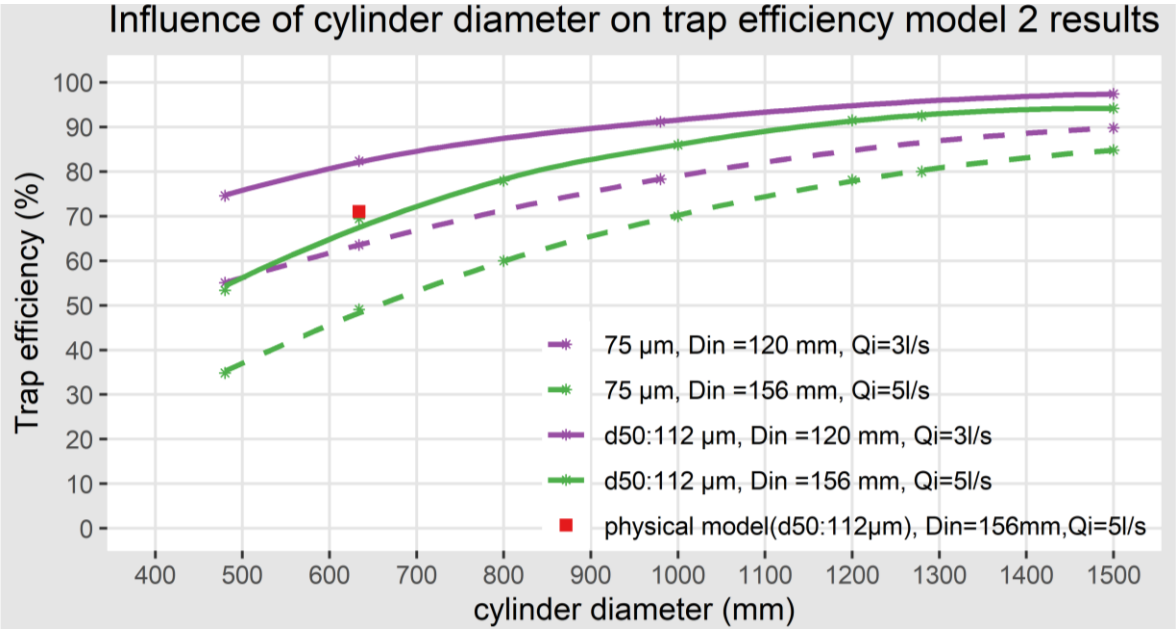

Figure 4-62: Influence of cylinder diameter on sediment removal efficiency Model 2 numerical and physical model results

It was observed that cylinder diameter plays a significant role in sediment removal. Larger cylinders yield higher trapping efficiencies, and this is true for both configurations 1 and 2.

However, under certain flow conditions, that is at a specific flow rate and inlet velocity, there exists a specific small diameter where the system will act like a hydro cyclone or a large diameter where the system behaves like a sand trap. The VSB is in-between the two: it is mainly gravity-driven as explained more in **section 4.4** but takes advantage of hydro cyclone mechanism by allowing higher tangential inlet velocity.

In section **4.8**, it was noted the cylinder height does not play a significant role in controlling sediment removal. The ratio $\frac{\mathrm{Ht}}{\mathrm{D}} > 1.5$ was recommended thus the maximum cut-off diameter for this study was 1.5 m which is approximately about 2.25 m high cylinder.

Abstraction works need to perform even during low flows, and a 1 m height was chosen as a reasonable minimum operating level. The 1 m is inclusive of the cone base. **Figure 4-63** below illustrates the effective height for different cylinder diameters. From this, it is recommended to have a maximum cylinder of 1 m diameter with a cone base height 0.469 m, thus $\frac{\mathrm{Ht}}{\mathrm{D}} = \frac{531}{1000} = 0.531$. In section **4.8** the ratio $\frac{\mathrm{Ht}}{\mathrm{D}} \geq 0.5$ has been recommended.

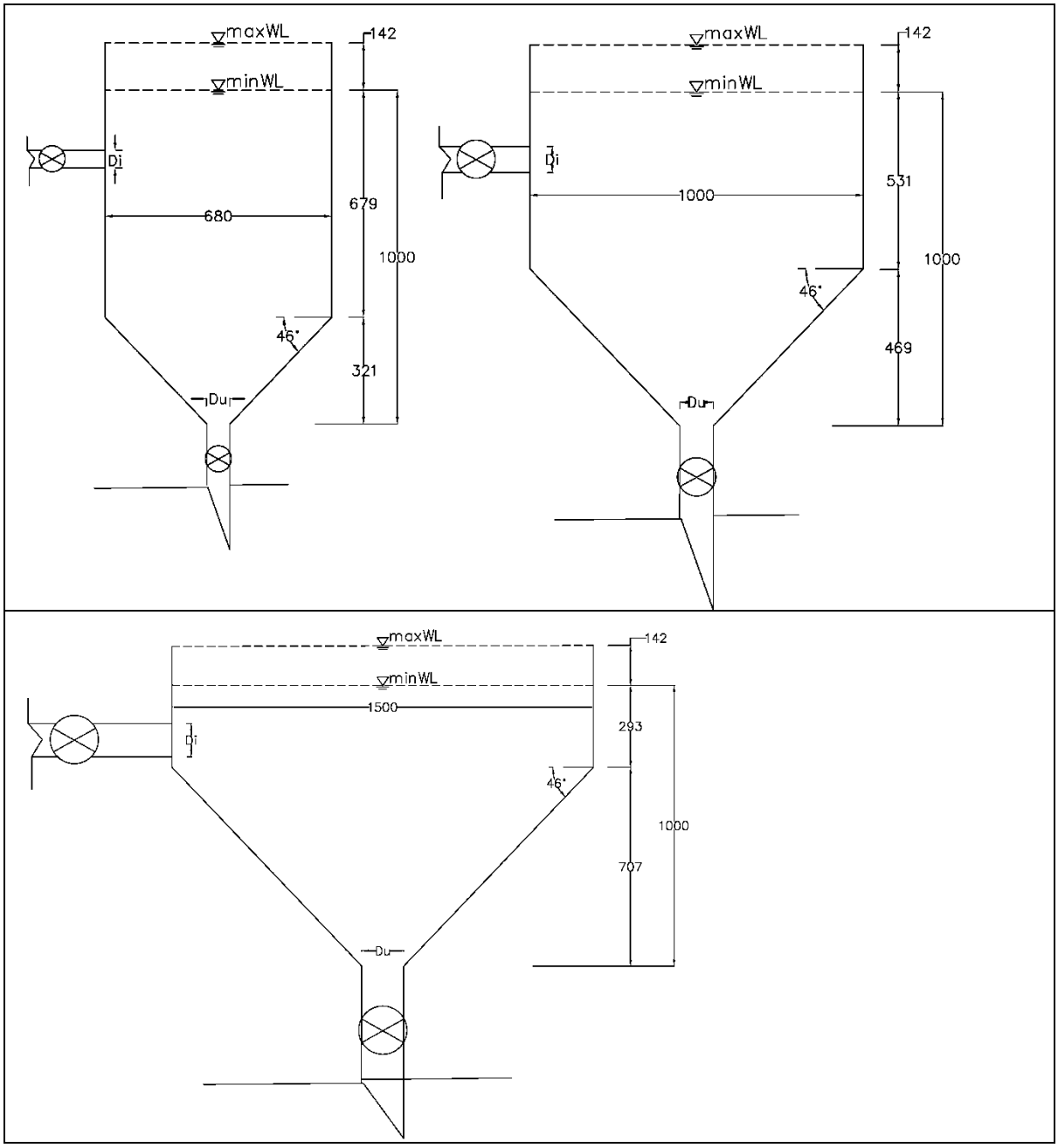

Figure 4-63: Effect of diameter on effective height (all units in mm)

Sullivan (1972) undertook extensive tests for the determination of the applicability of swirl concentrators for combined sewer application. They used a chamber of (3 feet) ≈ 0.9144 m and flow of (0.322 cfs) ≈ 9.118 l/s and, based on Froude's law, scaling was done to yield **Equation 4-4**. The design curve obtained in that study is shown in **Appendix A4**.

$$D = 3 * \left(\frac{Q}{9.118}\right)^{\frac{2}{5}} \qquad \text{Equation 4-4}$$

Where D: cylinder diameter (m), Q: flow rate (l/s).

Design guidelines for the combined sewer are shown in **Appendix A5** and separation efficiency curve in **Appendix A6**. The design curves were based on particle sizes larger than 1000 µm, but of interest in this section, they recommended a ratio of $\frac{D}{Di} = 6$, and this ratio is reviewed for particle sizes greater 75 µm.

Figure 4-64 shows a plot of the influence of the ratio $\frac{\text{Cylinder diameter}}{\text{Inlet diameter}}$ on sediment trapping efficiency and sediment particles residence time in the VSB. The rate of incremental change in residence time is summarised in **Table 4-12**.

It was concluded that, having the ratio $\frac{D}{Di} \geq 8.2$ does not significantly increase the residence time of sediment particles and trapping efficiency, thus, for fine sediment ≈ 75 µm, a value of $\frac{D}{Di} = 8.2$ is recommended.

Table 4-12: Rate of incremental change of residence time with D/Di

Scenario: 75 µm, Di =120 mm, Qi=3 l/s		
D/Di	**Residence time (seconds)**	**Incremental change (seconds)**
4.0	216	
5.3	323	107
8.2	470	147
12.5	506	36
Scenario :75 µm, Di =156 mm, Qi=5 l/s		
D/Di	**Residence time (seconds)**	**Incremental change (seconds)**
3.1	245	
4.0	340	95
5.1	403	63
6.4	476	73
7.7	510	34
8.2	520	10
9.6	536	16

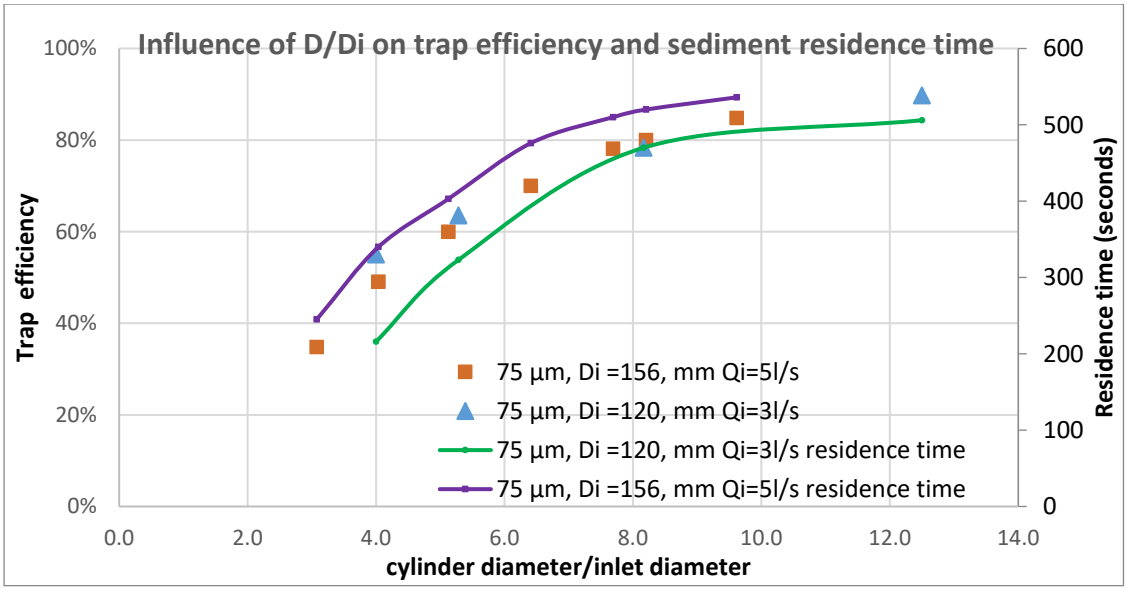

Figure 4-64: Influence of cylinder diameter/inlet diameter on sediment removal efficiency and residence time Model 2 numerical results

4.10.3 Flow field

4.10.3.1 Axial velocity

Figure 4-65 below illustrates the effect of Model 2 diameter variations on numerical model average axial velocity contours on the z-x plane at y =1.073 m, y =1.256 m and y =1.506 m. **Figure 4-66** shows corresponding average axial velocity profiles along lines A-B and C-D. It was observed that:

a) The axial velocity along the crucial inlet zone declines with the increase in diameter consequently an increase in trapping efficiency occurs, this is true as momentum loss increases with diameter increase.

b) A longer path is taken by sediment particles effectively increasing the settling path. Numerical model results in **Figure 4-67** below illustrate this, showing probable paths for 75 µm sediment particles in 10 s and 15 s in the VSB fluid domain.

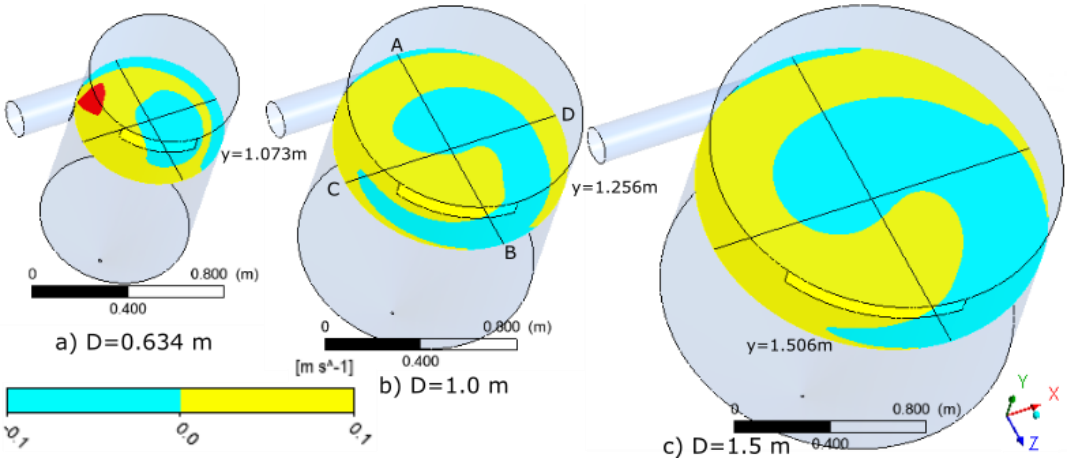

Figure 4-65: Numerical model average axial velocity contours in VSB of diameter: a) 0.634 m b) 1.0 m and c) 1.5 m on the z-x plane at y = 1.073 m, y = 1.256 m and y = 1.506 m

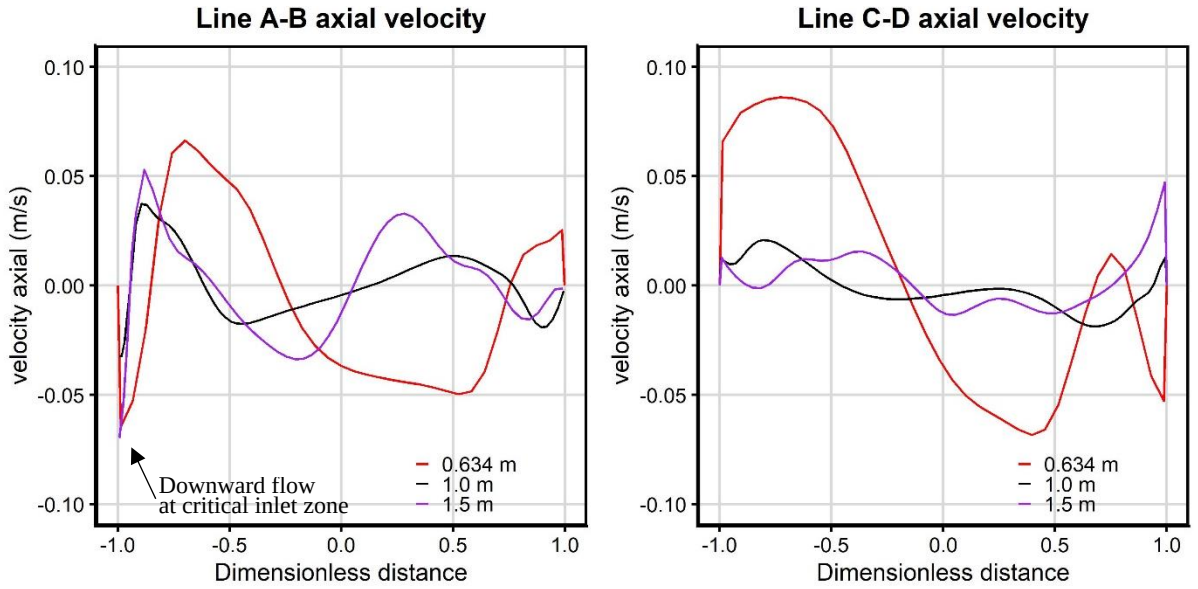

Figure 4-66: Numerical model average axial velocity profile in VSB of diameter: a) 0.634 m b) 1.0 m and c) 1.5 m on the z-x plane along lines A-B and C-D, Note: the dimensionless distance = the distance/ the VSB radius

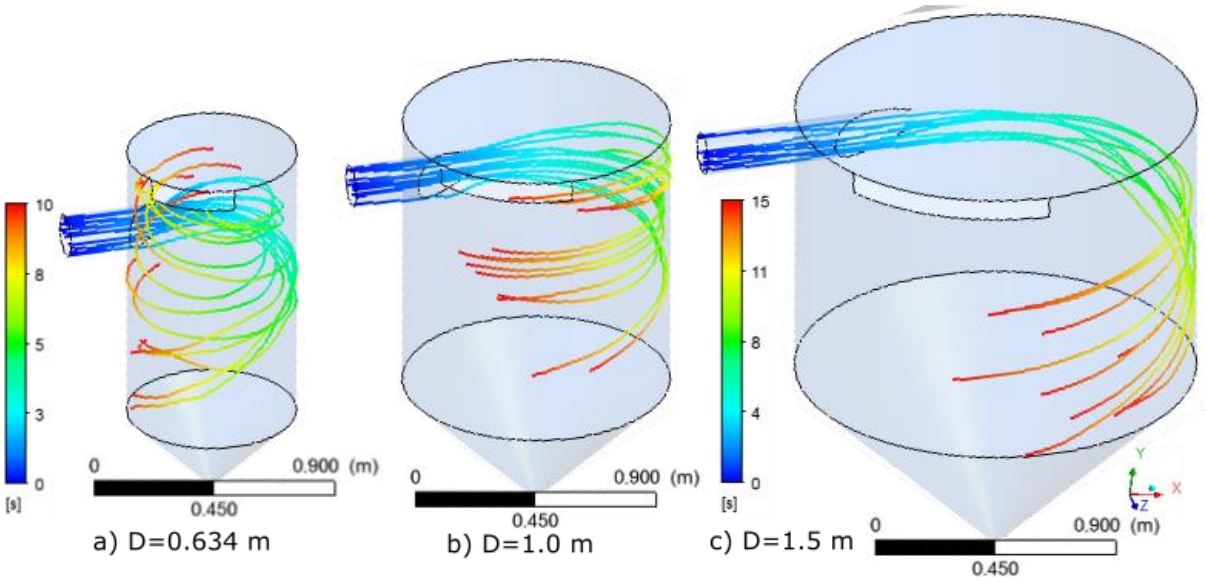

Figure 4-67: Numerical model result showing probable particle path for 75 µm sediment coloured by 10 and 15 seconds hydraulic retention time in VSB with a diameter of: a) 0.634 m b) 1.0 m and c) 1.5 m

4.10.3.2 Tangential and radial velocity

Figure 4-68 below illustrates Model 2 numerical model results for the effect of diameter variations on average tangential velocity contours on the z-x plane at y = 1.073 m, y = 1.256 m and y = 1.506 m and profiles extracted along lines A-B and C-D in **Figure 4-69**. It was observed that:

a) High inlet tangential velocities are recorded near the inlet.
b) A Rankine's type of profile is exhibited.

c) There was not much difference in tangential velocity magnitude near the inlet thus efficiency differences cannot be attributed to tangential forces.
d) The tangential velocity in the VSB domain decreases with an increase in VSB diameter. In scenarios a and b, high tangential velocities are recorded near the wall which ensures that sediment particles are kept near the wall.

Figure 4-70 illustrates Model 2 average radial velocity contours resulting from numerical modelling.

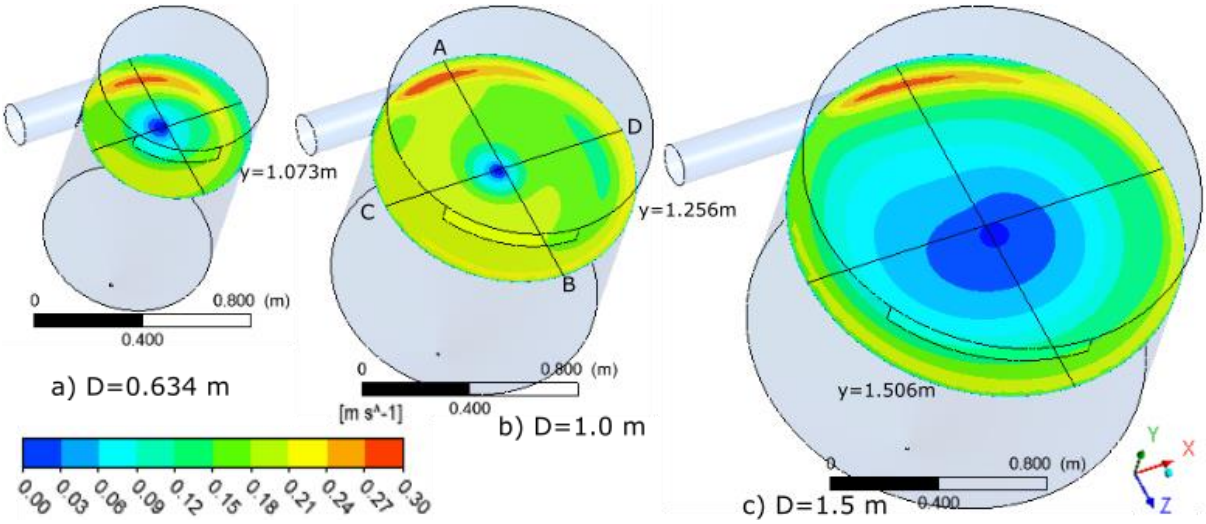

Figure 4-68: Numerical model average tangential velocity contours with VSB diameters of: a) 0.634 m b) 1.0 m and c) 1.5 m, on the z-x plane at y = 1.073 m, y = 1.256 m and y = 1.506 m

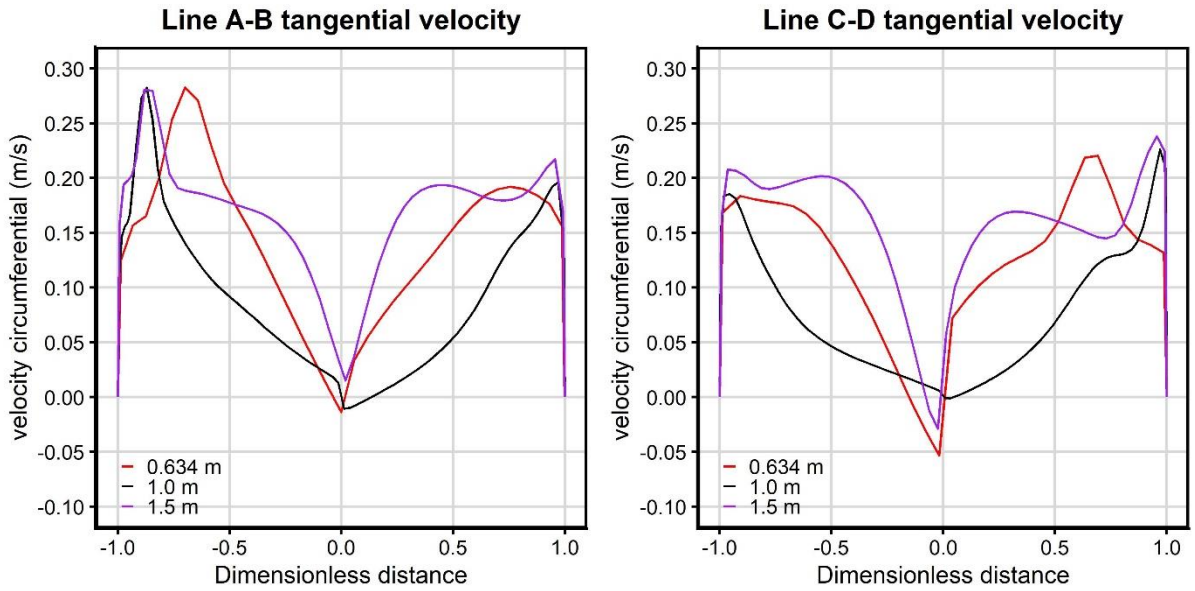

Figure 4-69: Numerical model average tangential velocity profile in VSB of diameter: a) 0.634 m b) 1.0 m and c) 1.5 m on the z-x plane along lines A-B and C-D, Note: the dimensionless distance = the distance/ the VSB radius

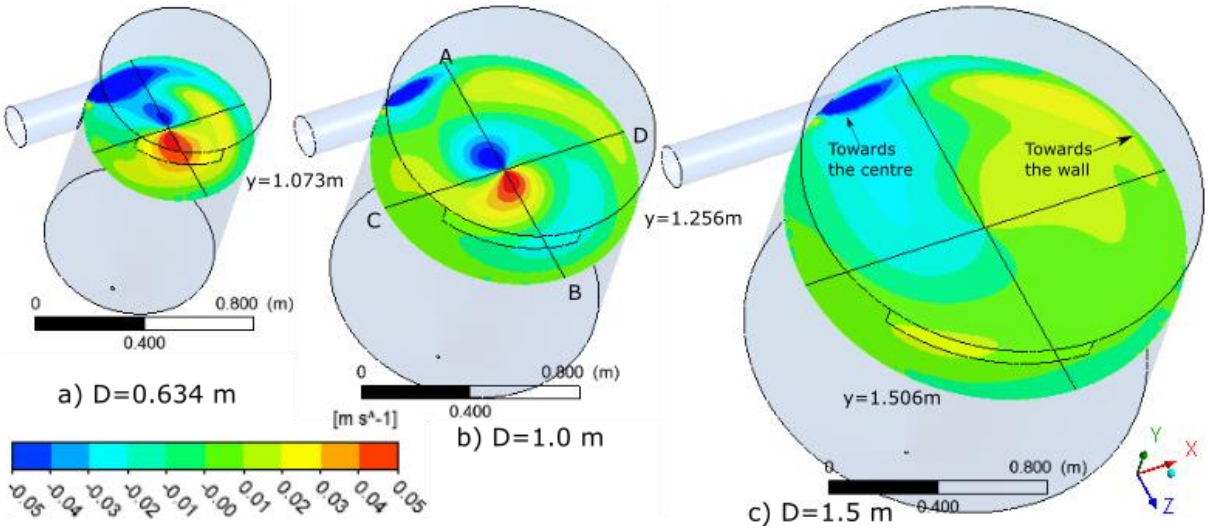

Figure 4-70: Numerical model average radial velocity contours for a VSB of diameter: a) 0.634 m b) 1.0 m and c) 1.5 m on the z-x plane at y = 1.073 m, y = 1.256 m and y = 1.506 m

4.10.3.3 Vorticity

Figure 4-71 below illustrates numerical model velocity vectors and vortex core region plotted at a swirling strength of 0.0021. It was observed that:

a) A swirling core is developed.
b) The swirling strength decreases with increase in diameter but is still adequate to maintain the sediment particles near the wall. The central core is destructive for sediment settling, and this explains why the efficiency is better with an increase in cylinder diameter.

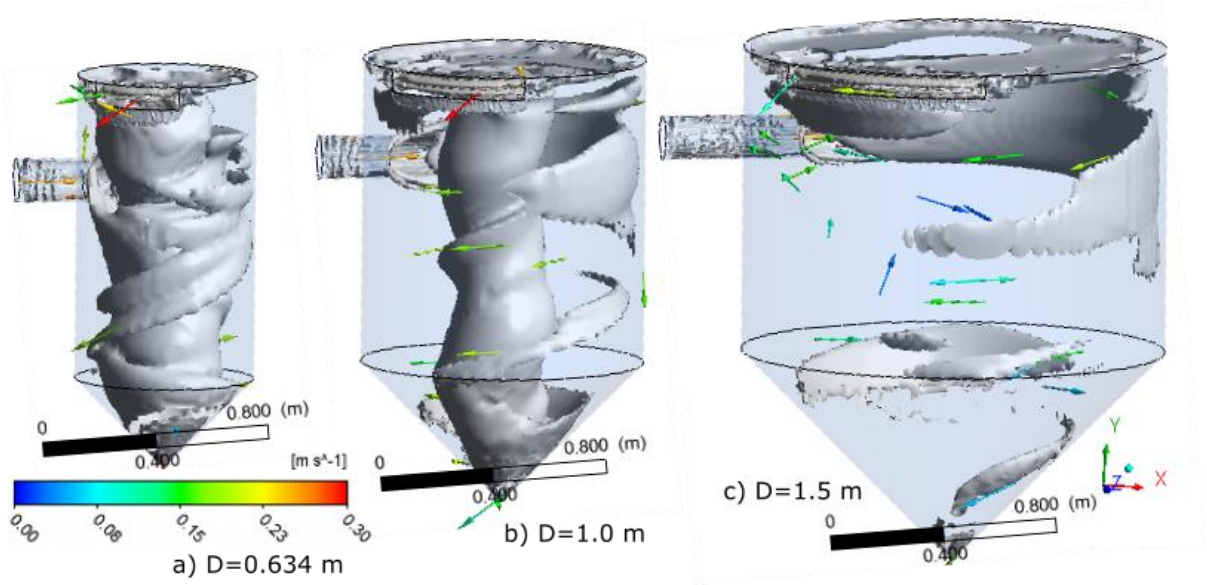

Figure 4-71: Numerical model helical vorticity and velocity vectors for a VSB of diameter: a) 0.634 m b) 1.0 m and c) 1.5 m

4.10.4 Turbulent kinetic energy, TKE

High TKE values indicate low recirculation. **Figure 4-72** below illustrates Model 2 effect of cylinder diameter variations on numerical average TKE contours on the z-x plane at y = 1.073 m, y = 1.256 m and y = 1.506 m. It was observed that:

a) TKE in the fluid domain declines with the increase in diameter, thus there is more secondary current recirculation propagating sediment particles towards the VSB underflow hence greater efficiency.
b) There is high TKE near the wall hence less sediment recirculation at this zone.

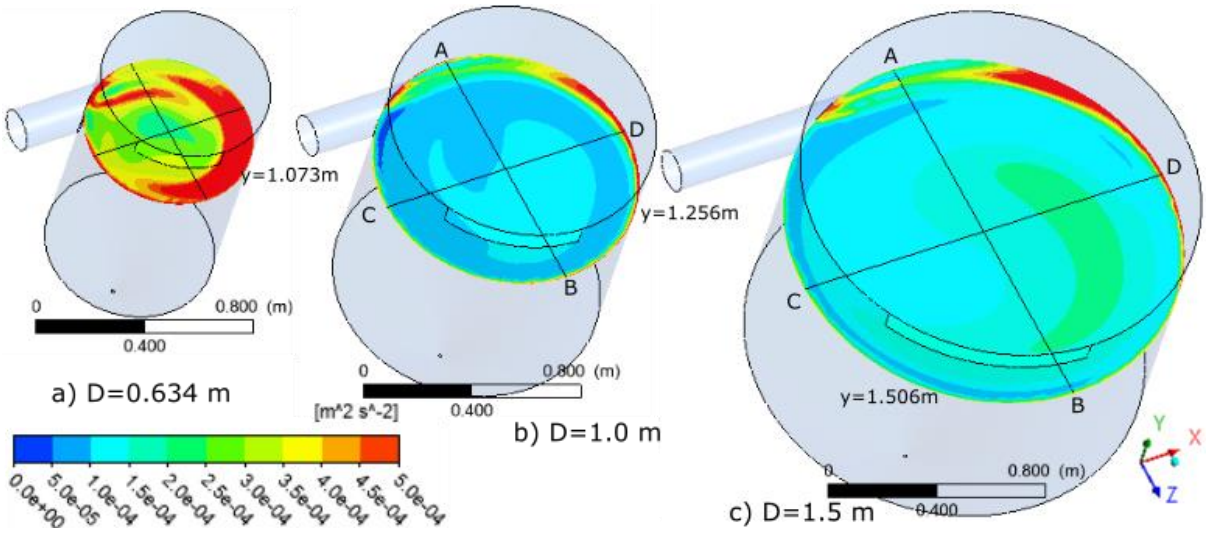

Figure 4-72: Numerical model average turbulent kinetic energy contours for a VSB of diameter: a) 0.634 m b) 1.0 m and c) 1.5 m on the z-x plane at y = 1.073 m, y = 1.256 m and y = 1.506 m

4.10.5 Conclusion on cylinder diameter

The Volume of Fluid (VOF) and the Discrete Element Method (DEM) numerical models and physical modelling were conducted to investigate the influence of VSB diameter on sediment removal. It was concluded that:

- The cylinder diameter plays a significant role in sediment removal efficiency. An increase in diameter increases the sediment trapping efficiency, and it can be attributed to a longer effective settling distance and better loss of momentum thus enhanced settling.
- D = 8.2 Di is recommended for removal of fine sediment as increasing this value does not increase the residence time of particles significantly. It should be noted the inlet diameter should give the recommended inlet velocity of 0.26 m/s.

4.11 Deflectors

4.11.1 Introduction

From literature and in the study of axial velocity, it was noted that deflectors could be used to:

- Increase the residence time of particles in the VSB and
- Avoid short-circuiting increasing the trapping efficiency significantly.

Various configurations, dimensioning and placement have been suggested by various authors as discussed in section 2.4.5, but detailed literature on the placement and dimensioning for design purposes is scarce, and therefore these aspects were studied in detail as described in this section. Numerical modelling formed an excellent basis to test different configurations before validation was undertaken on the physical model. **Table 4-2** summarises the Model 1 base configuration with the only difference being that the ratio $\frac{Qu}{Qi} = 0.08$.

To enable optimisation of deflectors several combinations were tested, and a summary of parameters considered is shown in **Figure 4-73**. ANSYS FLUENT supervised optimisation, particle tracking and use of vectors was used to achieve an optimum configuration, sizing and location of the deflectors. A detailed procedure for the optimisation of each deflector is discussed in this chapter.

It should be noted, Model 1 utilised in this section was discontinued from further study due to:

- Low trapping efficiency at flows > l/s for 75 µm particles,
- Sediment particles settling on the deflectors.

This chapter is included for reporting purposes and the reader can skip the chapter to Model 2 configurations with centroid outlet discussed in section 4.12.

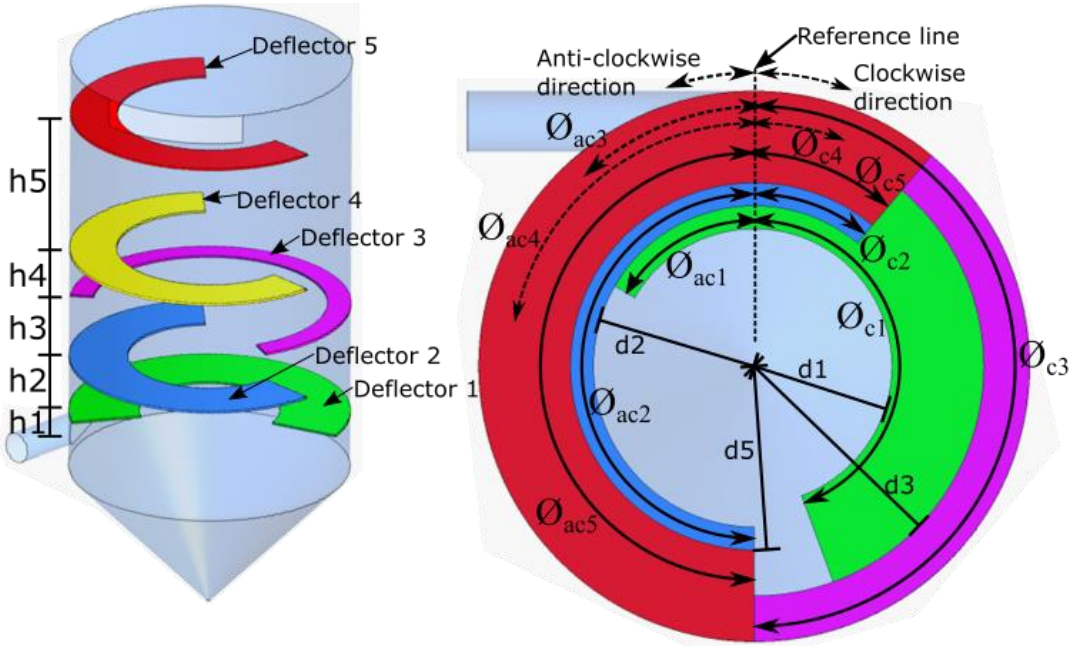

Figure 4-73: Optimization parameters considered
Where h1: length between centre of inflow diameter and deflector 1 (m), h2: length between deflector 1 and 2 (m), h3: length between deflector 2 and 3 (m), h4: length between deflector 3 and 4 (m), h5: length between

deflector 4 and 5 (m), $Ø_{c1}$, $Ø_{c2}$,$Ø_{c3}$, $Ø_{c4}$,$Ø_{c5}$: deflector 1, 2, 3, 4, 5 respectively clockwise angle (°), $Ø_{ac1}$, $Ø_{ac2}$,$Ø_{ac3}$, $Ø_{ac4}$,$Ø_{ac5}$: deflector 1, 2, 3, 4, 5 respectively anti-clockwise angle (°), d1, d2, d3, d4, d5: length of inner deflector 1, 2, 3, 4, 5 radius (m)

4.11.2 Deflector 1 optimisation

Various configurations were considered and based on ANSYS FLUENT supervised optimisation module, particles tracking and use of vectors, optimisation was undertaken. The parameters considered are shown in **Figure 4-74** and results summarised in **Figure 4-75** and **Appendix A8**.

It was observed that there is a good correlation between the numerical and physical models. The base model parameters without deflector are shown in a continuous line. Deflector 1 has a significant impact on trapping efficiency. For test number (4), with d50 =112 µm, an increase from 78% to 87% was observed and for sediment size 75 µm an increase from 55% to 68% was observed**.**

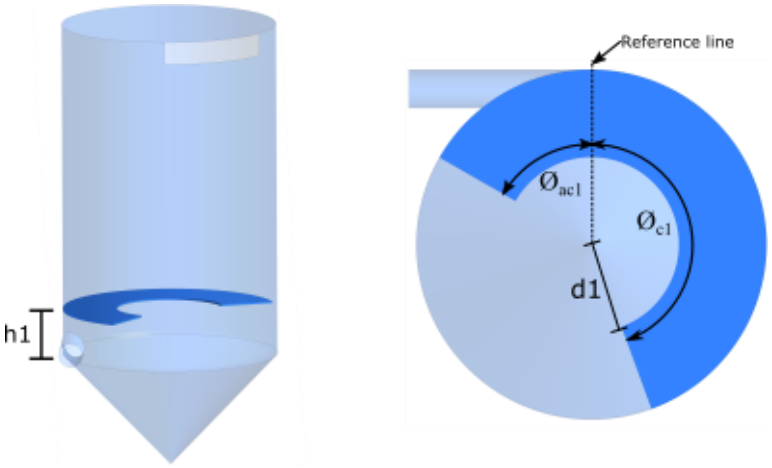

Figure 4-74: Deflector 1 optimisation parameters considered

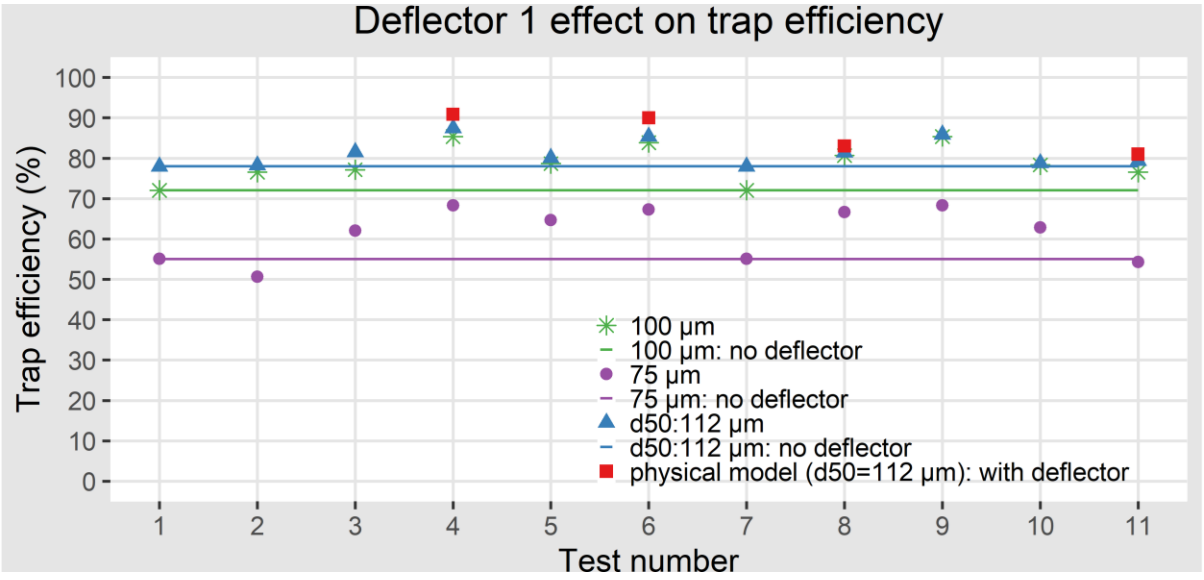

Figure 4-75: Effect of deflector 1 on sediment removal efficiency Model 1 numerical and physical model

4.11.3 Deflector 1-2 optimization

Figure 4-76 shows the general configuration of the parameters optimised and the results summarised in **Figure 4-77** and **Appendix A9**. There was a good correlation between numerical and physical model results, an improvement of trapping efficiency for d50:112 µm was noted from 78% to 92% and 55% to 84% for 75 µm.

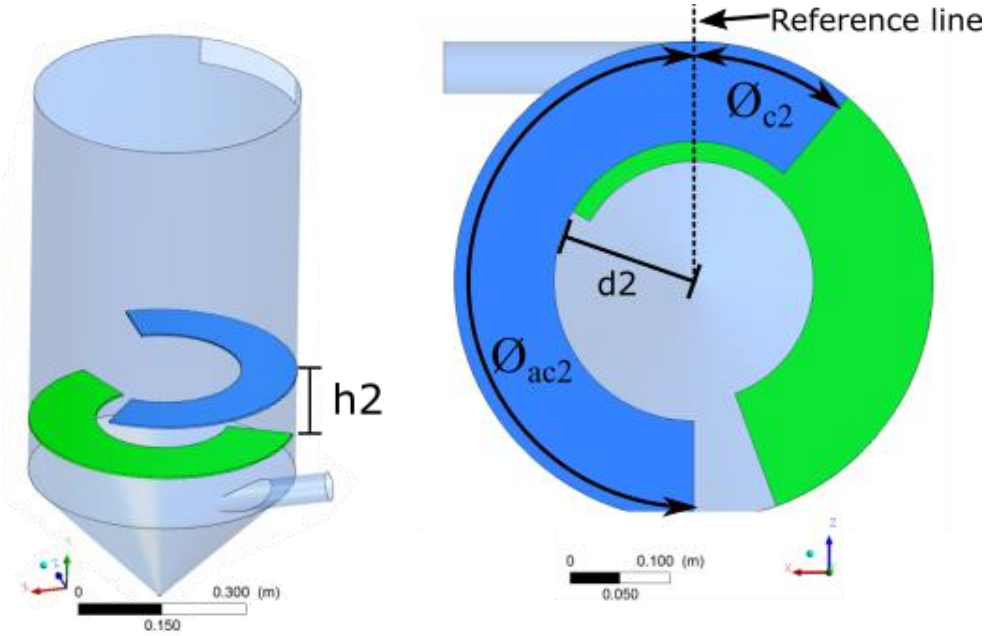

Figure 4-76: Deflector 1 and 2 general layout

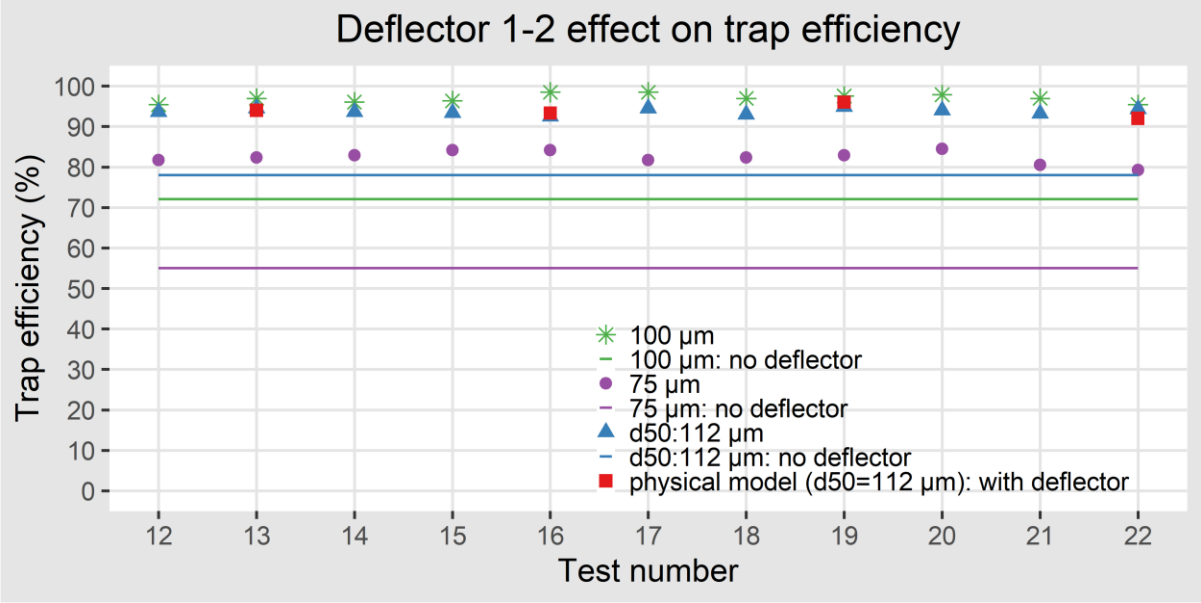

Figure 4-77: Effect of deflector 1-2 on sediment removal efficiency Model 1 numerical and physical model

4.11.4 Deflector 1-2-3 optimization

Figure 4-78 shows the general layout of this setup configuration. It included the optimised deflector 1 and 2, and results are summarised in **Figure 4-79** and **Appendix A10.** A good correlation between the numerical and physical model was observed. An improvement in trapping efficiency for d50:112 µm was noted from 78% to 95% and 55% to 85% for 75 µm.

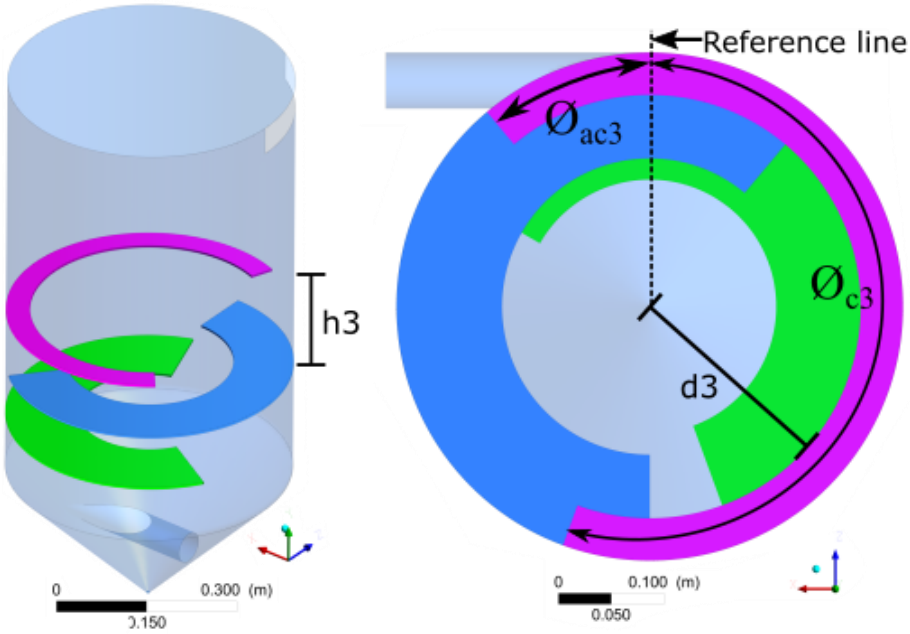

Figure 4-78: Deflector 1, 2 and 3 general layout

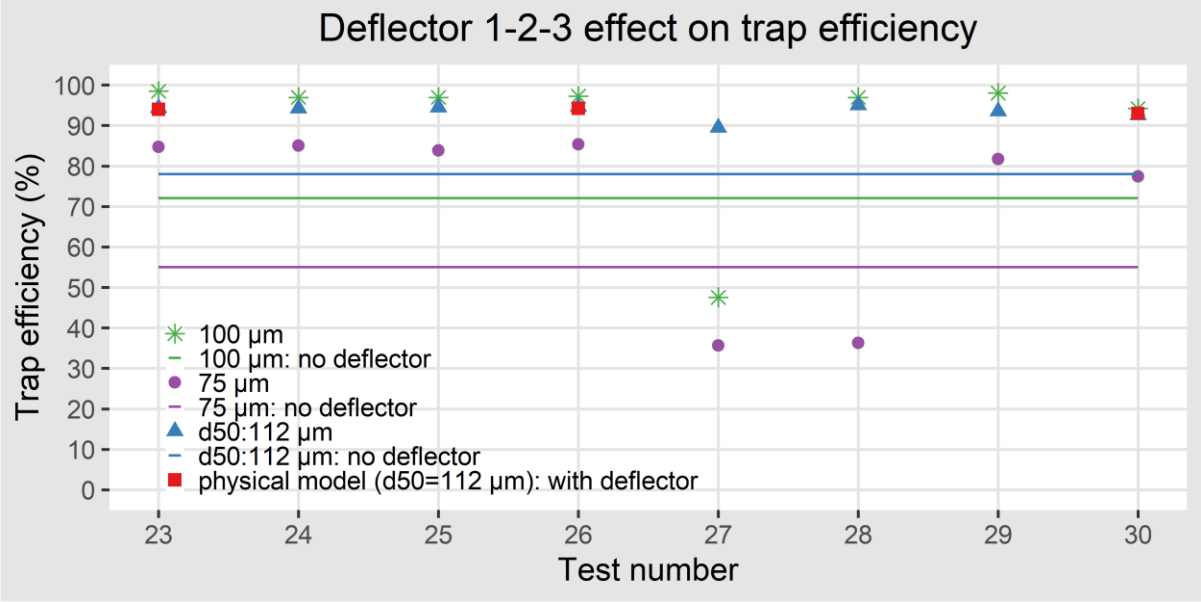

Figure 4-79: Effect of deflector 1-2-3 on sediment removal efficiency Model 1 numerical and physical model

4.11.5 Deflector 1-2-3-4-5 optimization

Figure 4-80 shows the general model layout and parameters optimised. This setup was inclusive of the optimised deflector 1-2-3. Several configurations were tested and optimised. The results are summarised in **Figure 4-81** and **Appendix A11**. There was a good correlation between the numerical and physical models.

From the base control without deflector (continuous line), the trapping efficiency was improved from 78% to 99% for d50:112 µm and 55% to 90% for 75 µm.

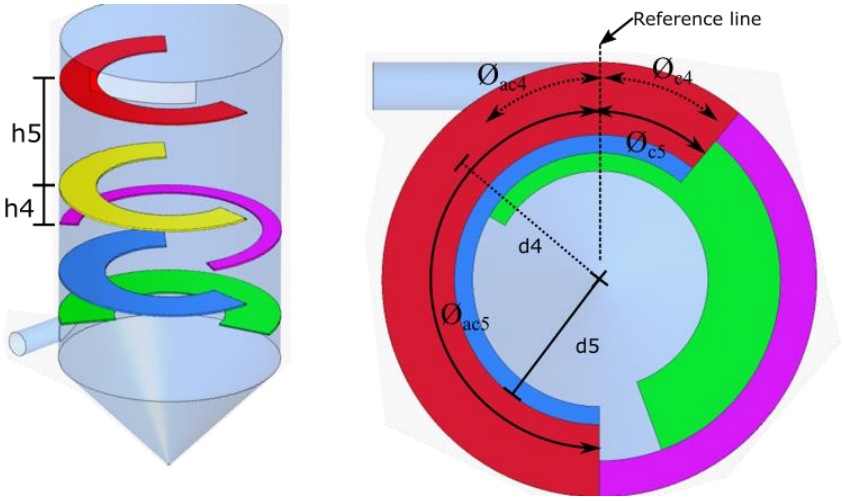

Figure 4-80: Deflector 1-2-3-4 and 5 general layout

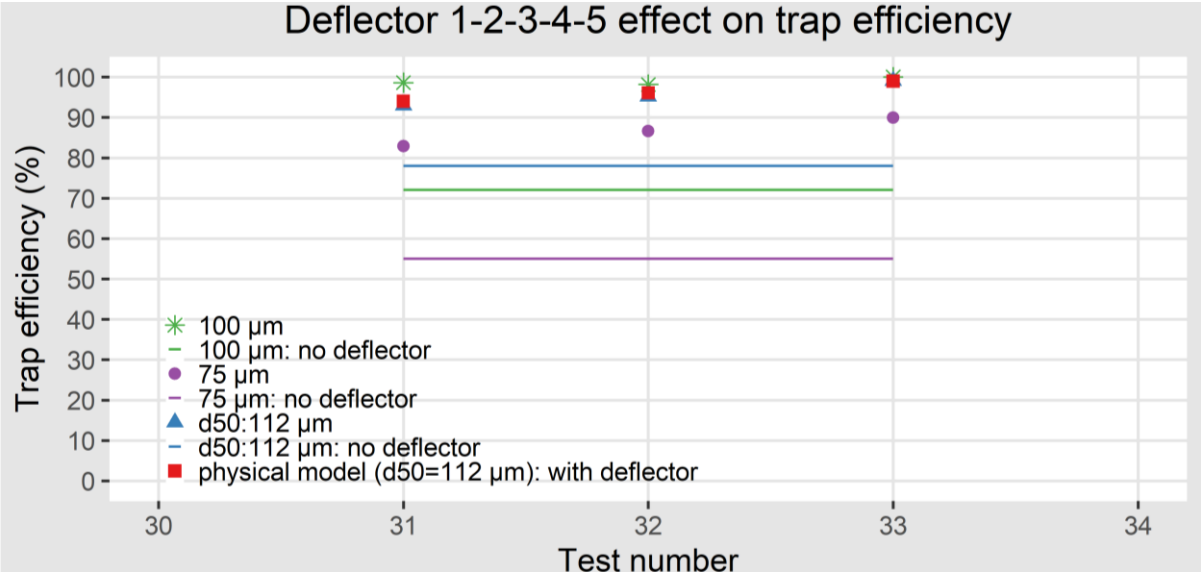

Figure 4-81: Effect of deflector 1-2-3-4-5 on sediment removal efficiency Model 1 numerical and physical model

From this setup, it was noted that:

- Deflectors play a vital role in improving the trapping efficiency. The deflectors help in dispersing the particles across the domain and increasing the distance travelled by the particle thus a notable increase in the residence time; **Figure 4-82** illustrates this. An

increase from 297 s to 1639 s was noted with one deflector only and with five respectively.

- **Figure 4-83** illustrates different sediment concentrations between the various deflectors showing a good correlation between the physical and numerical model.
- The configuration and placement of the deflectors must strictly be followed as different configurations might have destructive secondary currents/turbulent dispersion flows leading to resuspensions of particles towards the outflow.

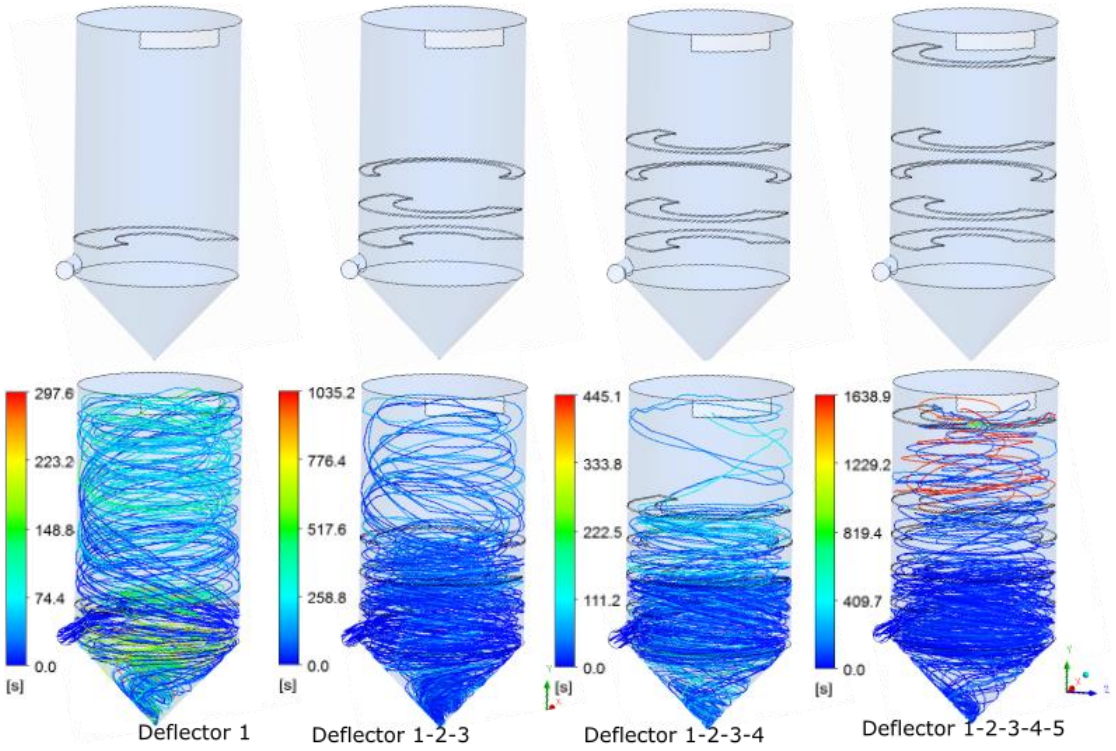

Figure 4-82: Deflectors particle tracking comparison showing different residence times

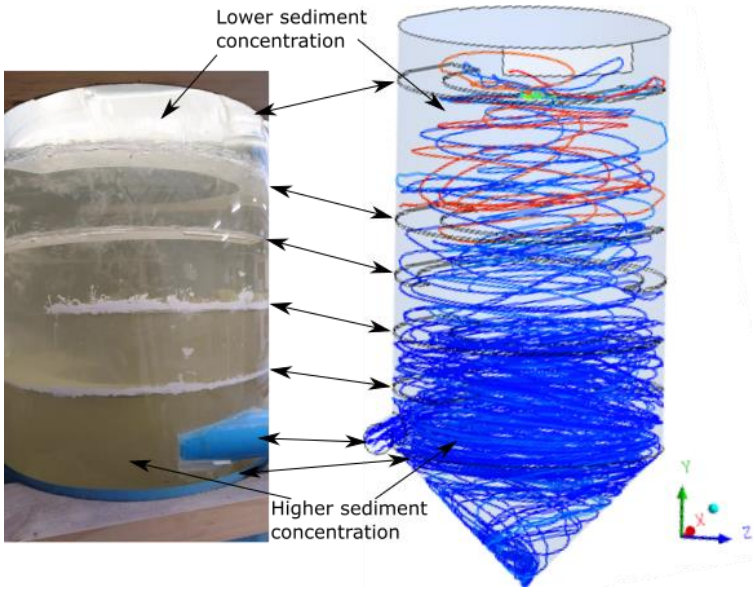

Figure 4-83: An illustration showing sediment concentration comparing physical and numerical models

4.11.6 Limitation of Model 1 configuration

With the optimised Model 1 configuration, the flow was increased to 5 l/s and 75µm sediment trapping efficiency reduced to 36%. Numerical re-optimisation was undertaken but no significant increase in trapping efficiency was realised. The model shortcomings are summarised below:

- Due to the location of the inlet; $\frac{Hi}{Ht} = 0.05$, it was observed that there is a higher percentage of axial velocity moving upwards carrying sediment towards the overflow (see **Figure 4-84**). In section **4.6** it was concluded that a value of $\frac{Hi}{Ht} > 0.7$ is preferred and this motivated the used Model 2 type configuration.

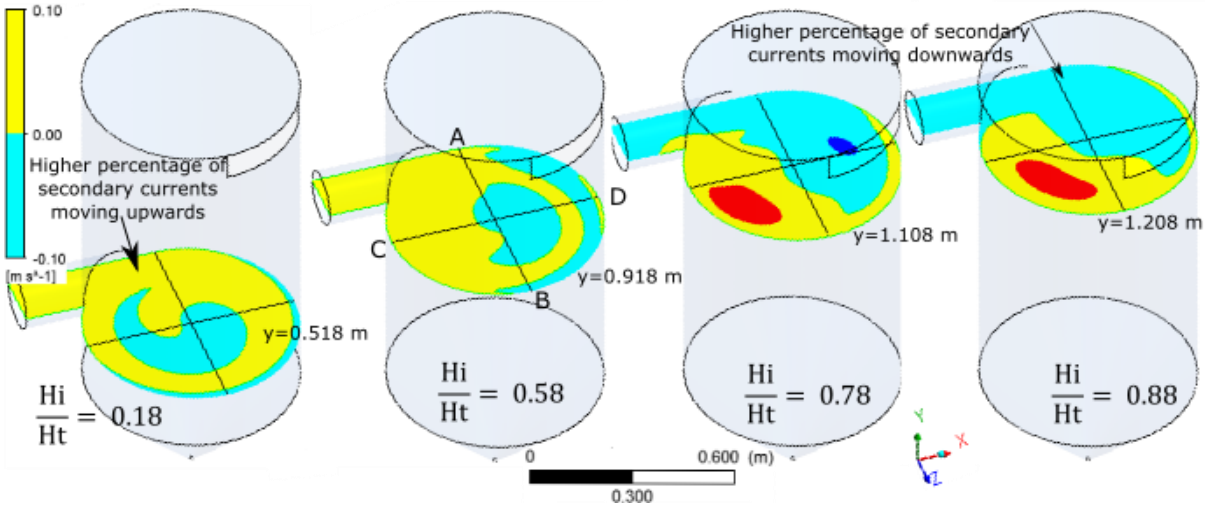

Figure 4-84: Numerical model results showing the effect of inlet location on the plane z-x average axial velocity contour (cyan/blue: downward movement of secondary currents, yellow/red: rising water)

- Sediment was noted to be settling on the physical model deflectors as illustrated in **Figure 4-85**.

Figure 4-85: Physical Model 1 observed sediment settled on the deflectors

4.11.7 Conclusion on Model 1 deflectors

The Volume of Fluid (VOF) and the Discrete Element Method (DEM) numerical models and physical modelling were conducted to investigate the influence of diameter on sediment removal. It was concluded that:

- Depending on the configuration and orientation, deflectors can enhance or be detrimental to sediment removal. In Model 1 configuration deflectors increased the removal of 75 µm from a base value of 55% to 90% at inlet flows of 1 l/s. With increased flows (5 l/s) the sediment trapping efficiency reduced significantly to 36%.
- It was noted Model 1 deflector type configuration has sustainability limitations due to the settling of sediment on the deflectors and the ratio $\frac{\text{Hi}}{\text{Ht}}$ being less than the recommended values in this thesis.

Due to these limitations Model 1 type of configuration was discontinued and not studied further and a different configuration discussed below was explored.

4.12 Outlet structure

4.12.1 Introduction

In sections **4.2** and **4.3**, it was observed that sediment removal by VSB is mainly gravity-driven and weak centrifugal forces mostly help in keeping the particles in suspension near the wall and dispersing the particles in the flow domain. The velocities near the walls and at the bottom central core are smaller leading to a pressure gradient. Secondary currents are formed that tend to carry particles from the outer wall towards the bottom centre of the VSB resulting in a central core that is less concentrated with sediment particles. **Figure 4-86** below shows a sample of Model 2 (configuration I) illustrating lower sediment concentration at the centre.

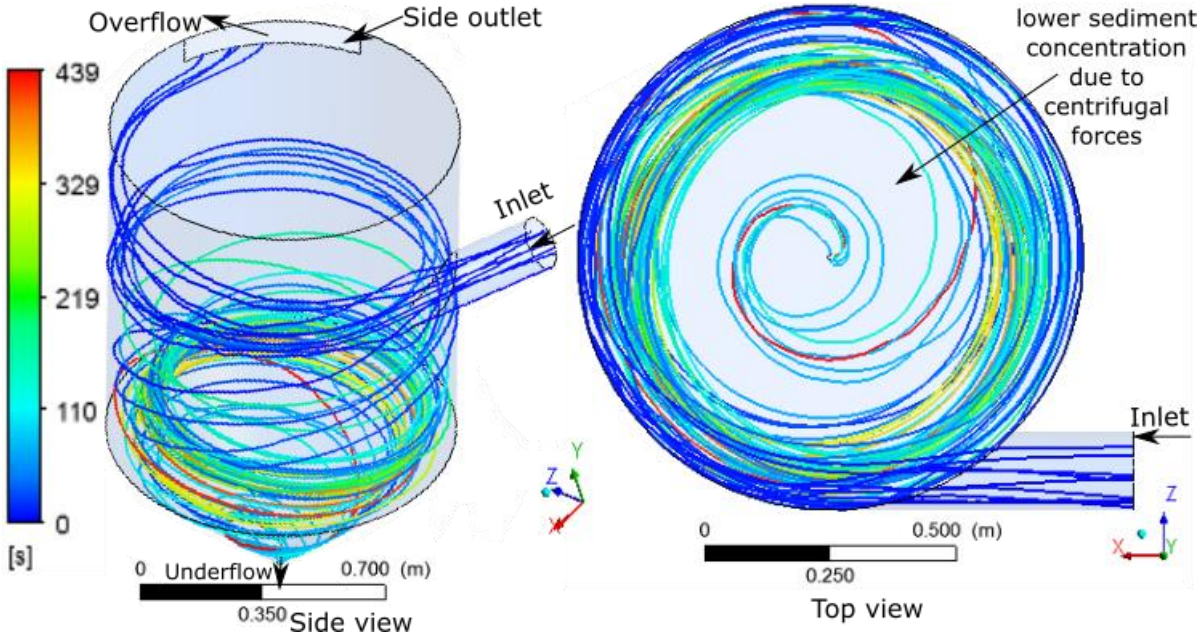

Figure 4-86: Illustration of Model 2 side outlet and sediment particle tracks coloured by hydraulic retention time (configuration I) side and top view

One could take advantage of these secondary currents by placing an outlet at the centre of the VSB. Four different types of configurations were investigated and are discussed below. They were selected based on the following criteria:

- Ensuring the axial velocity is lower than the settling velocity of particles.
- Minimising turbulence in the VSB flow domain.

4.12.2 Configuration II

Figure 4-87 below illustrates the numerical model setup for configuration II. An automatic supervised optimisation was undertaken, and the following parameters were investigated:

- d: outlet pipe diameter
- h1: low weir height
- l: length of the weir
- Ø: orientation of the outlet

The results are discussed further making a comparison with base configuration I (**Figure 4-89** (a1)) whose parameters are summarised in **Table 4-13**.

Table 4-13: Influence of outlet structure on sediment removal trapping efficiency base model parameters

Parameter	Symbol and units	Model 2
Inlet flow	Qi (l/s)	5
Cylinder diameter	D (mm)	634
Inlet diameter	Di (mm)	156
Cone height	Hc (mm)	330
Cylinder height	Ht (mm)	1000
Outlet height	Ho (mm)	80
Inlet height	Hi (mm)	750
Underflow/Inflow	Qu/Qi	0.11
Sediment particle diameter	d50 (µm)	75-112
Sediment concentration in inflow	C (mg/l)	10,000

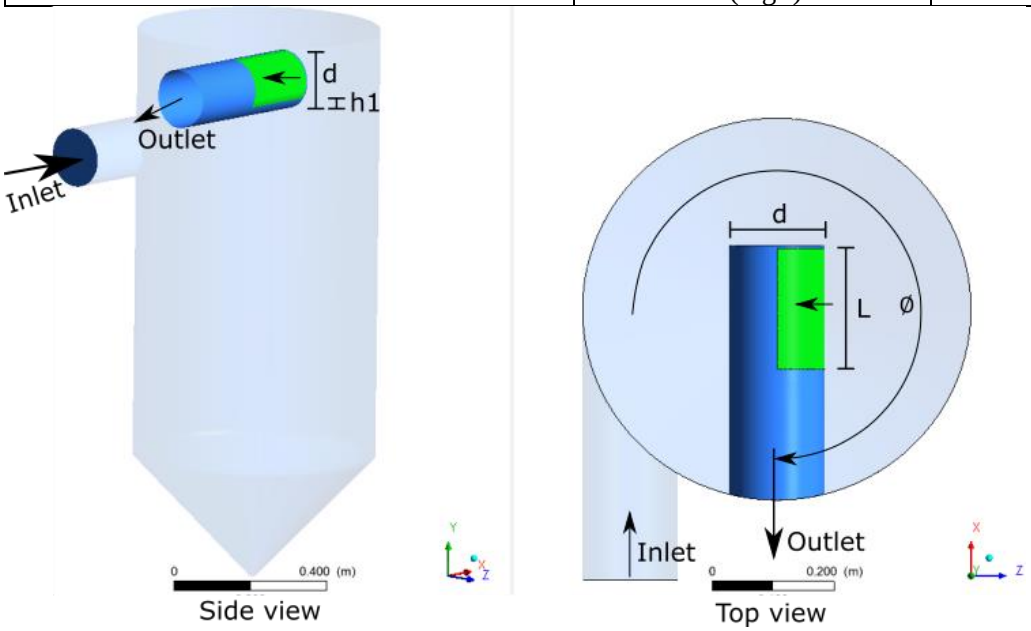

Figure 4-87: Illustration of a central circular outlet with pipe outlet at the top (configuration II) side and top view

4.12.2.1 Sediment trapping efficiency

Table 4-14 below gives a summary of results for the optimised numerical model sediment removal efficiency in configuration II and a plot of the results is given in **Figure 4-88**. It was observed that sediment removal improved from 54 % to 65% for 75 µm in configuration test number (e5) (see **Table 4-14)**. The increase in efficiency is explained by studying the velocity components below.

Table 4-14: Influence of outlet configuration II on sediment removal efficiency optimised numerical model results

Test	Outlet diameter(d) (mm)	L (mm)	h1(mm)	Ø (°)	d50:112 µm	100µm	75µm
e2	90	100x100	35	270	84%	82%	63%
e4	110	100x100	35	270	82%	82%	65%
e5	156	100x100	35	270	82%	83%	65%

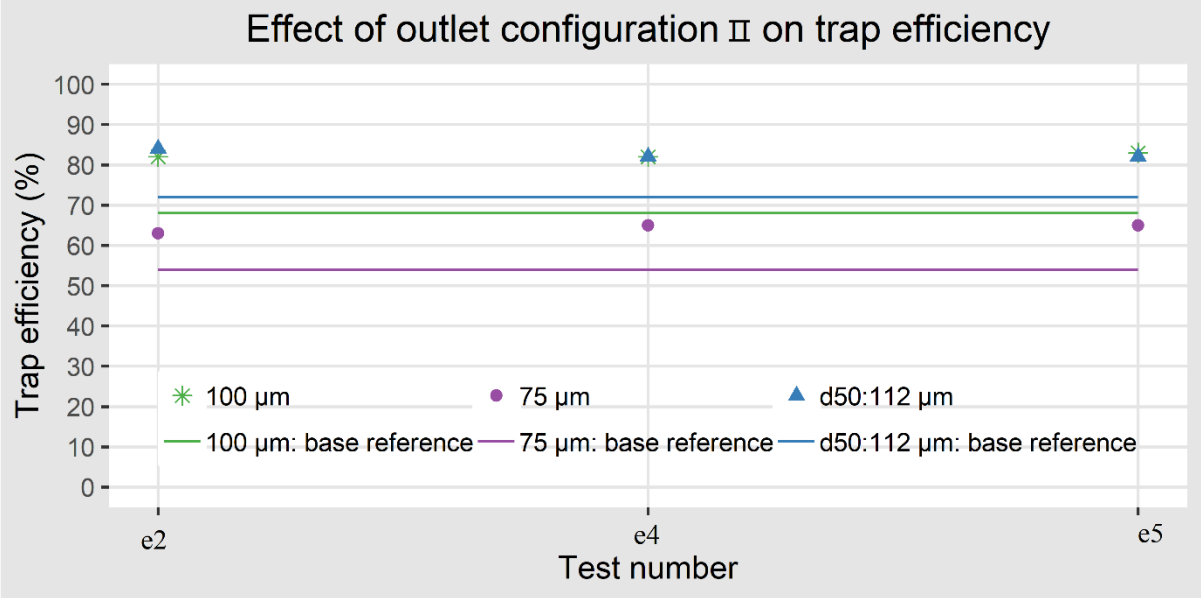

Figure 4-88: Influence of outlet configuration II on sediment removal efficiency optimised numerical model results

4.12.2.2 Axial velocity

Figure 4-89 below illustrates the effect of configuration II on numerical average axial velocity contours on the z-x plane at y = 1.236 m. Negative axial velocity in the y-direction is desirable for a gravity-driven sediment removal mechanism. **Figure 4-90** shows corresponding axial velocity profiles along lines A-B and C-D, and it was observed that:

a) Negative axial velocity along the crucial inlet zone in the y-direction increases with the change in the model configuration. Due to the positioning of the inlet, tangential velocities ensure that sediment particles are dispersed near the wall, and with this zone having a higher negative axial velocity, settling is accelerated thus achieving a higher trapping efficiency.

b) Minimal axial velocity just below the outlet weir was recorded in configuration test number (e5). This explains why this configuration achieves a better trapping efficiency but increasing the diameter (d) further does not have an increase in efficiency.

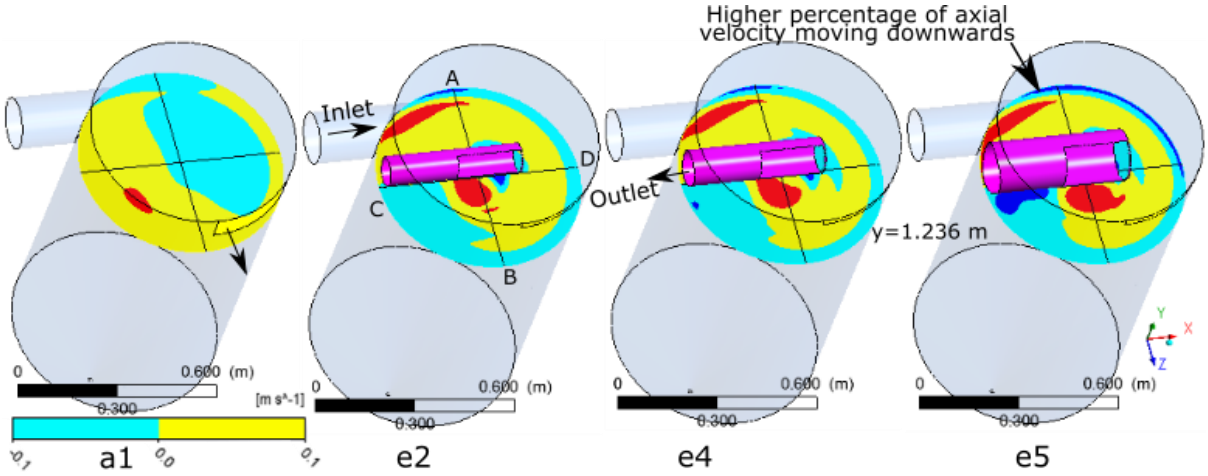

Figure 4-89: Numerical model effect of outlet configuration II on the z-x plane average axial velocity contour (cyan/blue: downward movement of water, yellow/red: rising water)

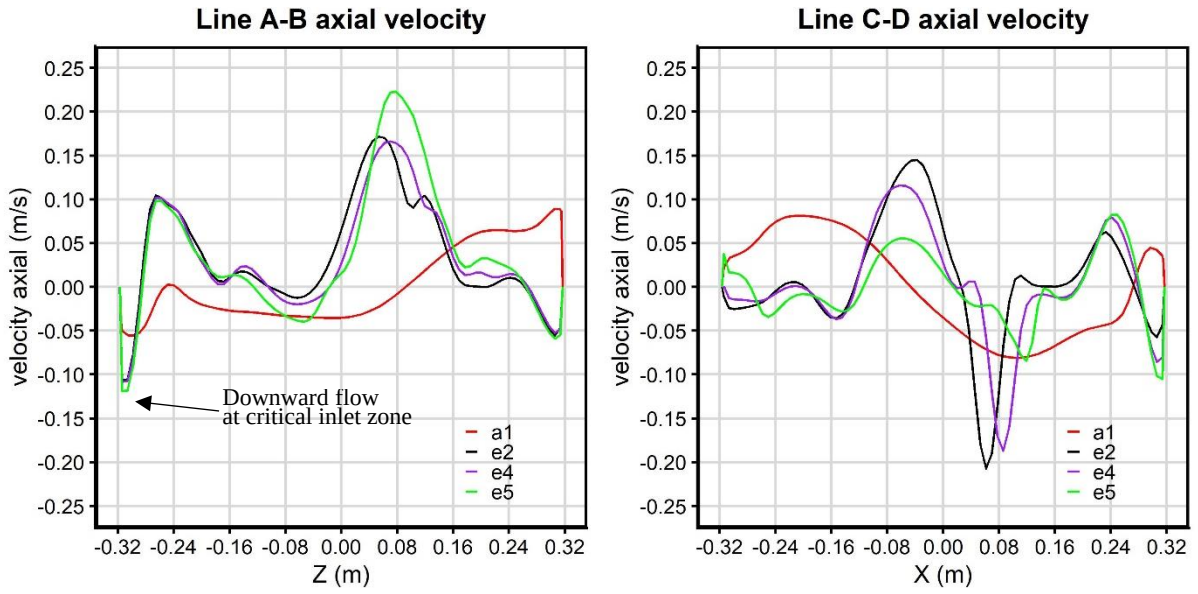

Figure 4-90: Numerical model average axial velocity profile of outlet configuration II on the z-x plane along lines A-B and C-D at y = 1.236 m

4.12.2.3 Tangential velocity

Figure 4-91 below illustrates configuration II effect on numerical average tangential velocity contours on the z-x plane at y = 1.236 m. Tangential velocity influences radial velocity keeping sediment particles near the wall. **Figure 4-92** below illustrates the corresponding average tangential velocity profiles along lines A-B and C-D. It was observed that:

a) Tangential velocity increases with the change of model configuration.
b) Model configuration II experiences a Rankine's type of profile.

c) Tangential velocity in the flow domain rises with an increase in outlet diameter d; thus, sediment particles are kept away from the outlet achieving a better trapping efficiency. This is illustrated in **Figure 4-93** test number (e5) for the 75 µm particle tracking where only five paths are shown for ease of visualisation.

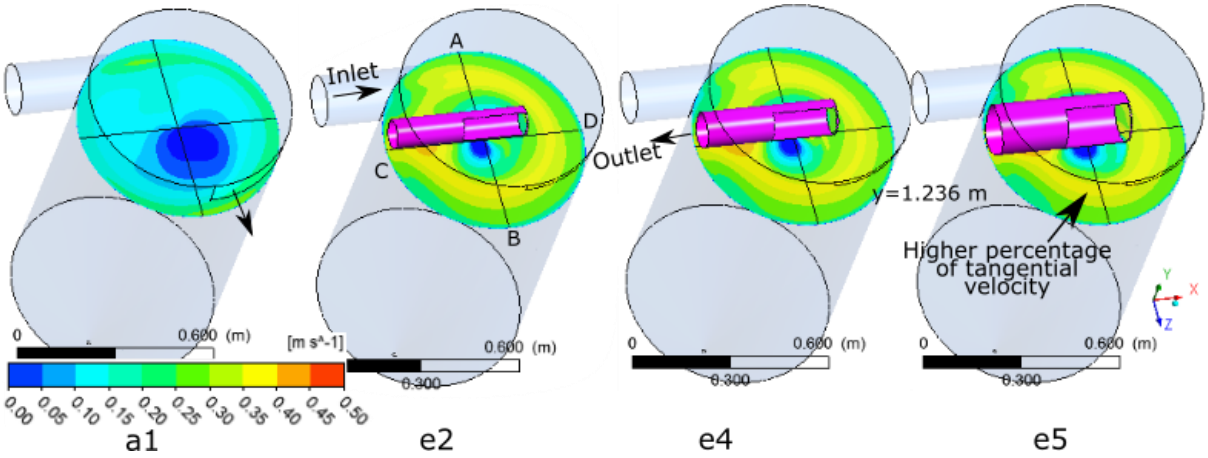

Figure 4-91: Numerical model effect of outlet configuration II on the z-x plane average tangential velocity contour at y = 1.236 m

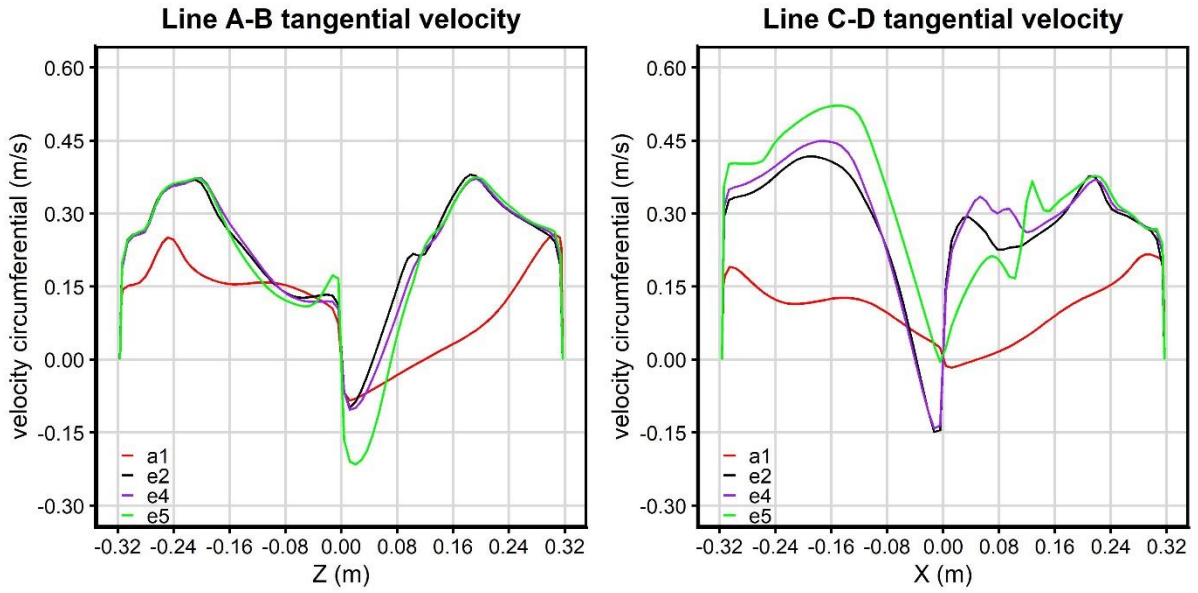

Figure 4-92: Numerical model average tangential velocity profile of outlet configuration II on the z-x plane along lines A-B and C-D at y = 1.236 m

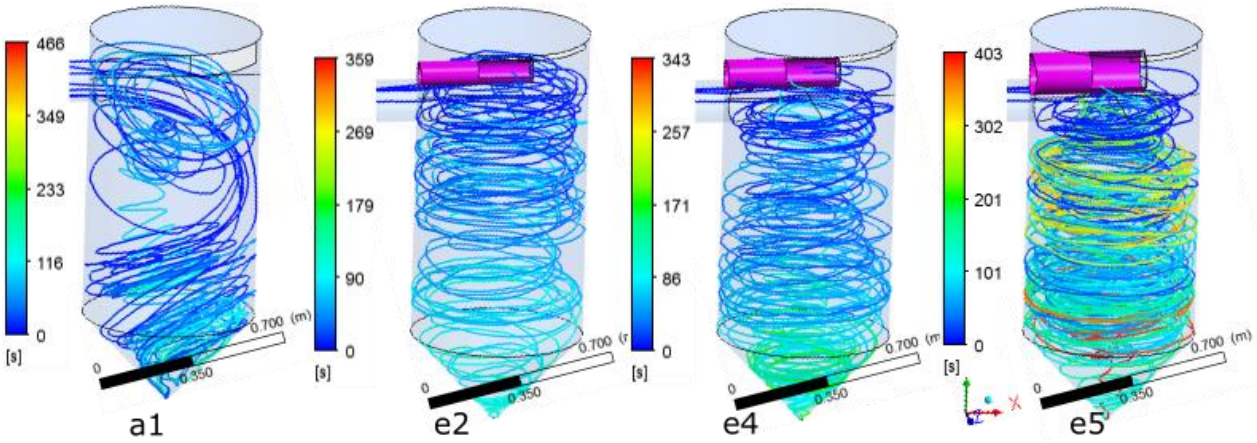

Figure 4-93: Effect of outlet configuration II on 75 µm particle tracking coloured by hydraulic retention time

4.12.2.4 Turbulent kinetic energy, TKE

Figure 4-94 below illustrates configuration II average TKE contours on the z-x plane at y = 1.236 m. It was observed that:

a) By changing the outlet configuration, low TKE is experienced near the wall. Low TKE near the wall leads to secondary currents transporting the sediment particles from the wall surface to the VSB underflow, hence better sediment trappings.
b) Due to locating the outlet on the side, the flow streamlines are affected introducing turbulences at this zone as indicated in test number (e5), altering the path of sediment particles at the wall. To mitigate this, a new configuration III was suggested, and it is investigated further.

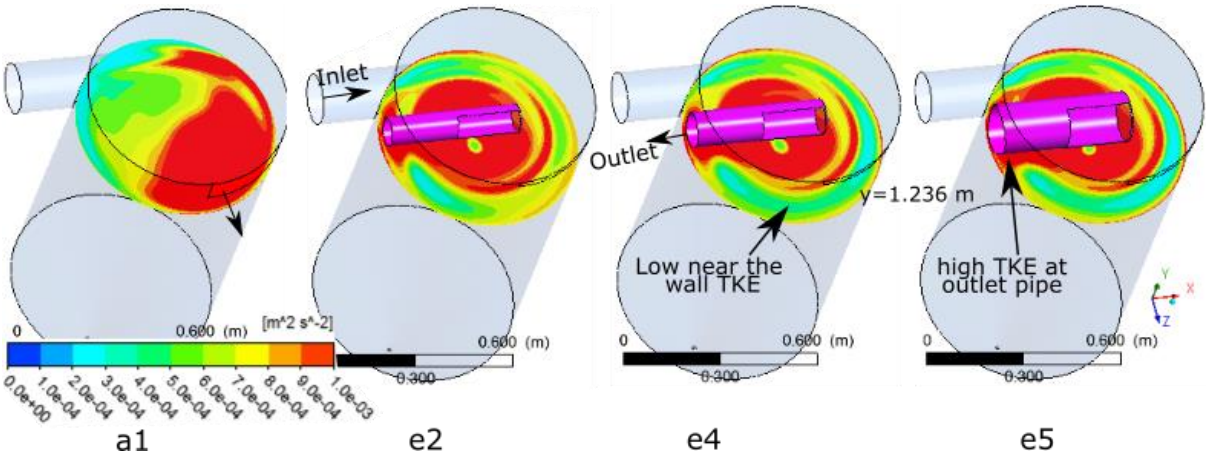

Figure 4-94: Configuration II numerical model turbulent kinetic energy contours on the z-x plane at y = 1.236 m

4.12.3 Configuration III

Figure 4-95 below illustrates configuration III numerical model setup. In the setup the following parameters were investigated:

- L: Length of the weir
- b: breadth of outlet
- h1: low weir height
- Ø: orientation of the outlet
- Do: diameter of the outlet
- Ds: diameter of the outlet shaft

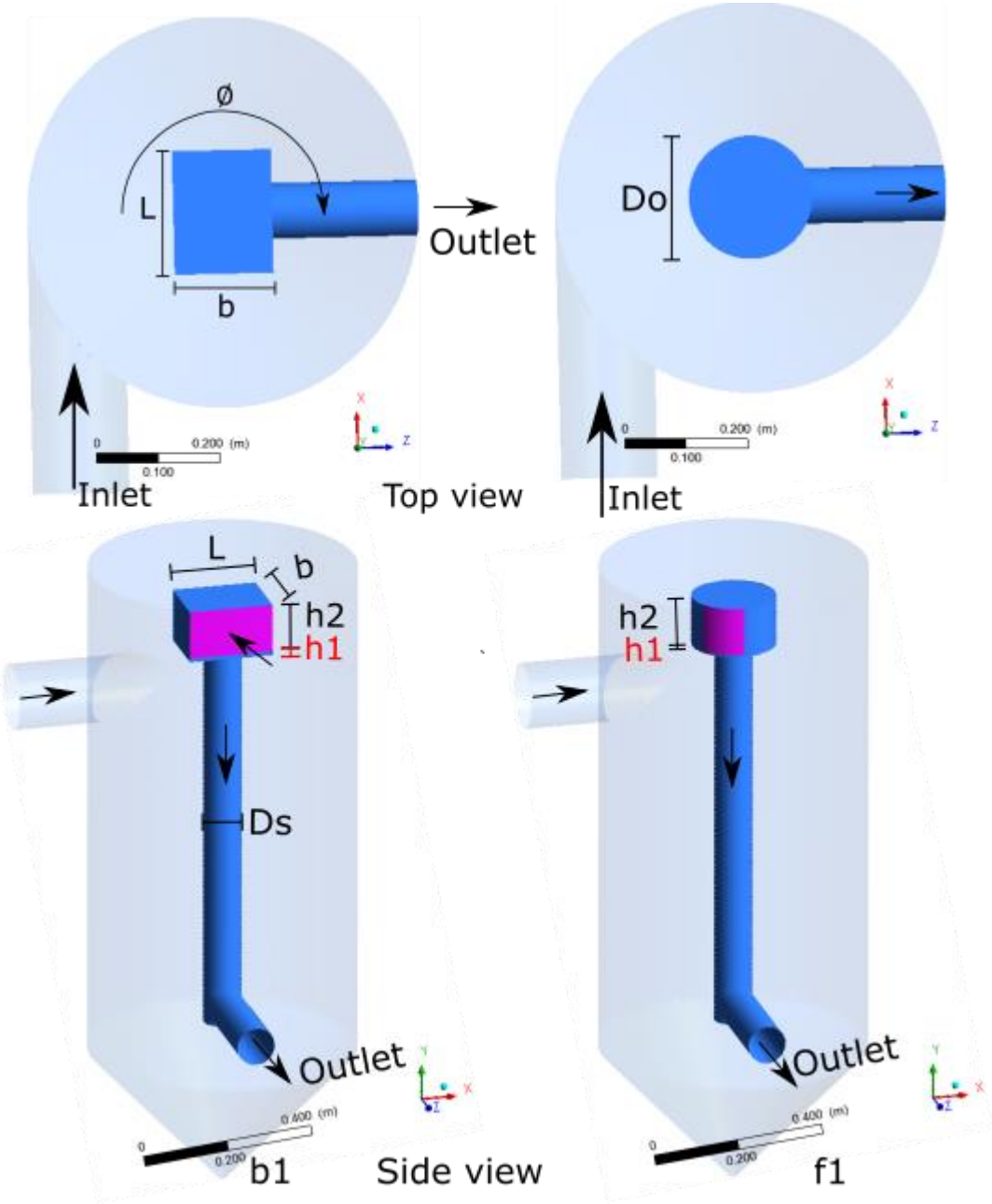

Figure 4-95: Illustration of numerical model central rectangular and circular outlet with pipe outlet at the bottom (configuration III) side and top view

The following design considerations were undertaken before optimisation:

- Submergence depth
- Shaft design
- weir

- Submergence depth, S

The submergence depth (S) is critical to limit vortex formation (**Figure 4-96**), air entrainment and vibrations.

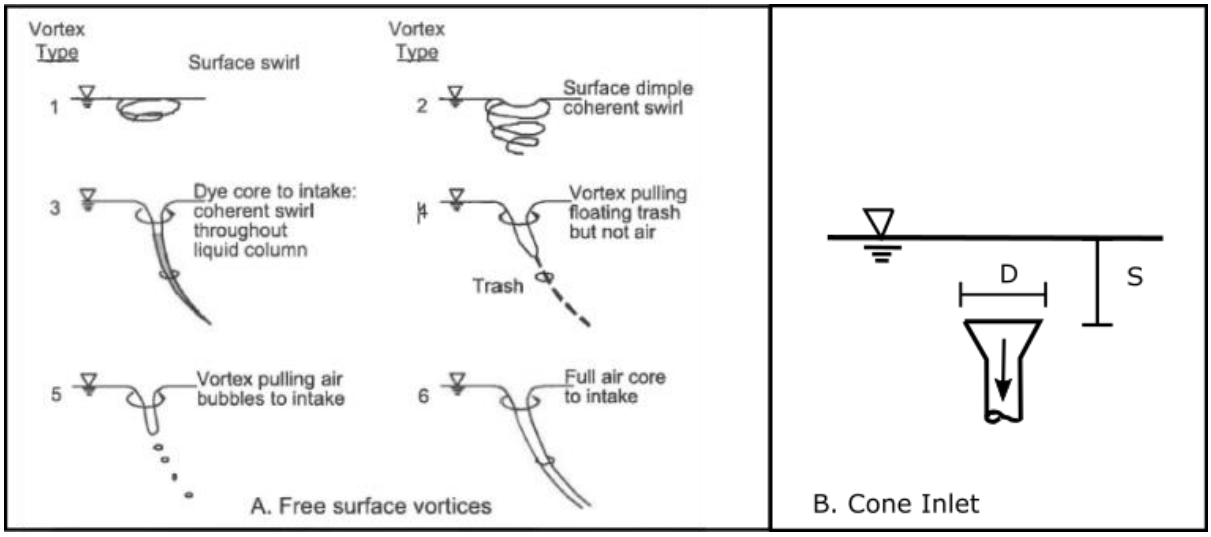

Figure 4-96: Types of free surface vortex classification and definitions of D and S (Hydraulic Institute, 2012)

Knauss (1987) proposed **Equation 4-5** to calculate critical submergence depth where the ratio $\frac{\text{inlet mouth velocity}}{\text{approach velocity}} < 6$. **Table 4-15** below summarises various outlet diameter calculations.

$$S=D\,(0.5+2F_D) \qquad \text{Equation 4-5}$$

Where: S: submergence depth (m), D: diameter of inlet (m), F_D = Froude number = $\frac{\text{velocity at the inlet face}}{\sqrt{gD}}$

Table 4-15: Summary of critical submergence depth required for various outlet diameters according to Equation 4-5

Q (l/s)	4.5	4.5	4.5	4.5	10	10
D (mm)	53	90	120	134	90	120
V (=$Q/\pi D^2/4$) (m/s)	2.04	0.71	0.40	0.32	1.57	0.88
F_d	2.83	0.75	0.37	0.28	1.67	0.82
S_{min} (mm)	327	181	148	142	346	256

- Shaft design

The shaft was designed following section in **Appendix A (9.3)**, and the resulting rating curve illustrated in **Figure 4-97** with the corresponding recommended crest profile in **Figure 4-98**. The D90 mm conduit pipe with a slope of 0.01 m/m flowing 75% full and Mannings roughness

coefficient = 0.01 was found to convey 4.62 l/s at a velocity of 0.9 m/s thus no deposition of sediment occurred in the pipe. Minimum velocities to ensure self-cleaning have been discussed and summarised in **Table 4-5** in section **4.4** (0.6 m/s for 100 µm).

It should be noted that to avoid vibrations and sub-atmospheric pressures; the shaft outlet needs to be designed either for:

a) Fully submerged conditions with full pipe flow or
b) Crest control with a partially full conduit pipe.

The partially full conduit was chosen as a fully submerged outlet reduced the effective cylinder height by values summarised in **Table 4-15** above and the additional turbulence experienced reduced the efficiency.

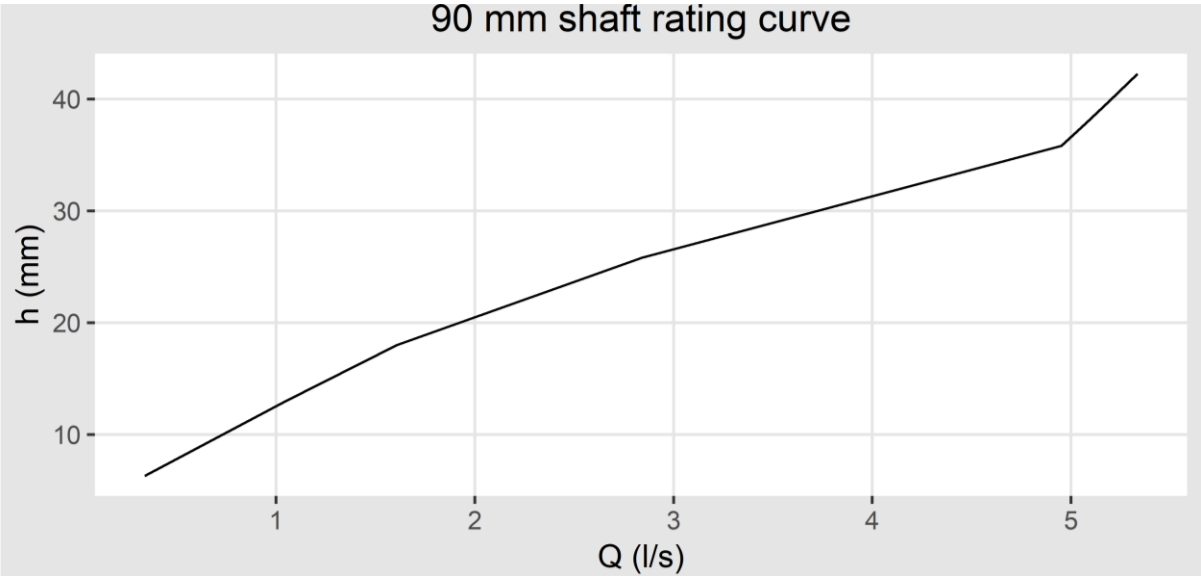

Figure 4-97: 90 mm shaft rating curve

Figure 4-98: 90 mm shaft and inlet mouth outline

From these calculations, it was observed that a self-sustaining central air core was formed as illustrated in **Figure 4-99** for aeration.

Figure 4-99: Illustration of physical model with vortex and aeration core in preliminary analysis

- Weir

To reduce the interaction between the outlet domain section and the VSB a small weir was proposed to be added and it is one of the variables investigated. **Figure 4-100** below illustrates this.

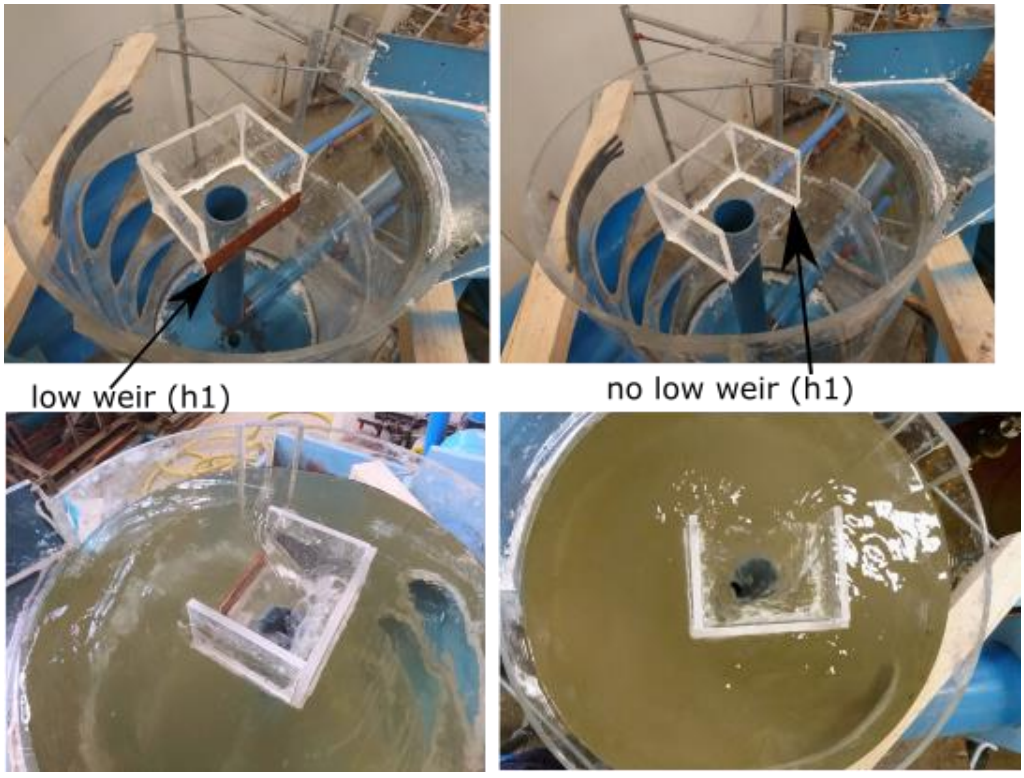

Figure 4-100: Illustration of laboratory physical model outlet configuration II with and without a low weir

The physical model had three inlets which were operated independently and an assumption was made: the inlets do not influence the flow domain. Numerical model supervised automatic optimisation was undertaken on configuration (b1) and (f1) (see **Figure 4-95)** and a possible 50 outcomes investigated. The optimised results for the two configurations were compared to the base model configuration summarised in **Table 4-13** and are discussed below.

4.12.3.1 Sediment trapping efficiency

Table 4-16 below gives a summary of optimised numerical model configuration II and III sediment removal efficiency and a plot of the results in **Figure 4-101.** It was observed that optimised configuration test number (f1) gave the maximum sediment trapping efficiency of 76 % for 75 µm against the base model of 54%. The improvement can be explained by studying the velocity components.

Table 4-16: Influence of outlet configuration III on sediment removal efficiency optimised numerical model results

Test	B (mm)	Ds	L (mm)	Do (mm)	h1 (mm)	Ø (°)	d50:112 µm	100µm	75µm
b1	90	90	100x100		5	180	85%	85%	73%
f1		90		200	5	210	85%	84%	72%

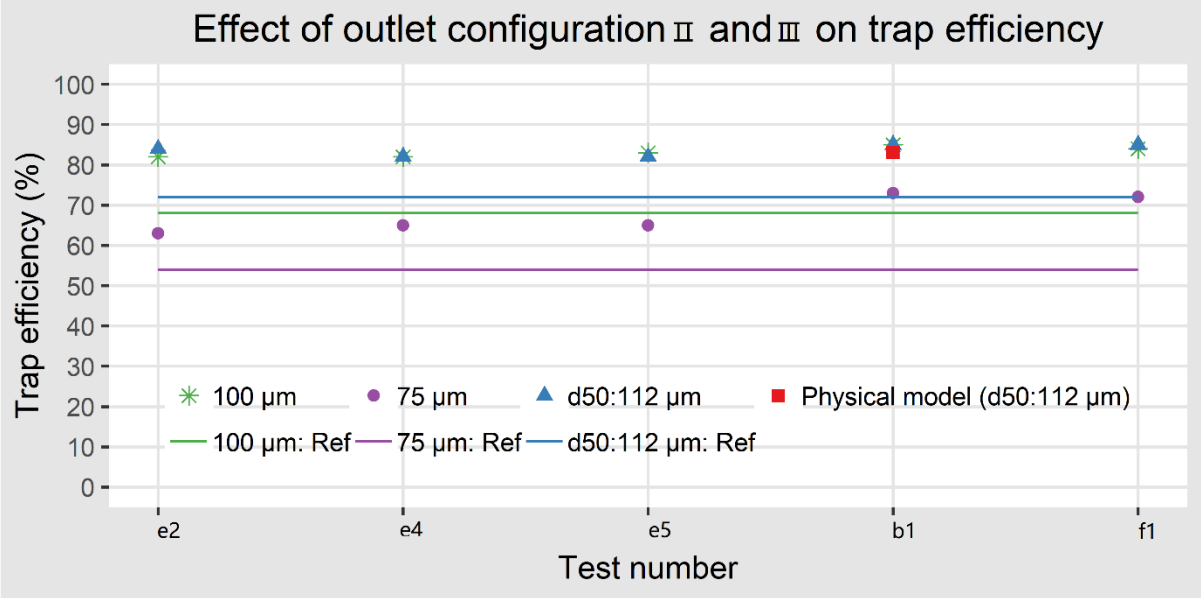

Figure 4-101: Influence of outlet configuration II and III on sediment removal efficiency optimised numerical model results

4.12.3.2 Axial velocity

Figure 4-102 below illustrates the base model and configuration III effect on numerical average axial velocity contours on the z-x plane at y = 1.236 m. Corresponding axial velocity profiles along lines A-B and C-D are shown in **Figure 4-103**. It was observed that:

a) Negative axial velocity along the crucial inlet zone in y-direction increases with the change in model configuration thus assisted settling leading to better trapping efficiency.
b) Overall, minimal axial velocities at critical zones are recorded in configuration test number (f1), but due to the higher axial velocity at the outlet sediment particles are resuspended thus explaining why test number (b1) has better trapping efficiency.

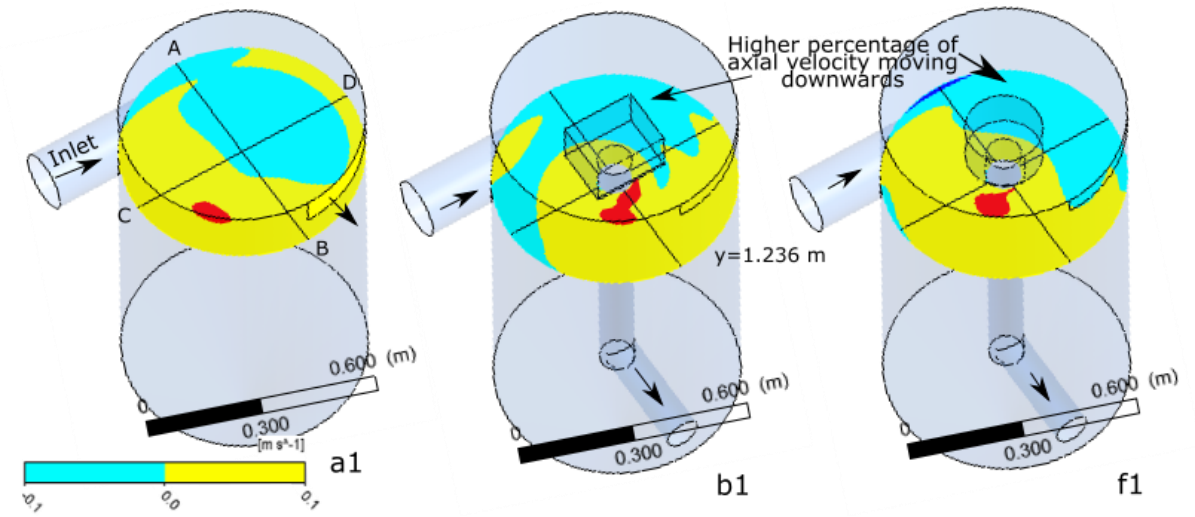

Figure 4-102: Numerical model effect of outlet configuration III on the z-x plane average axial velocity contour (cyan/blue: downward movement of water, yellow/red: rising water)

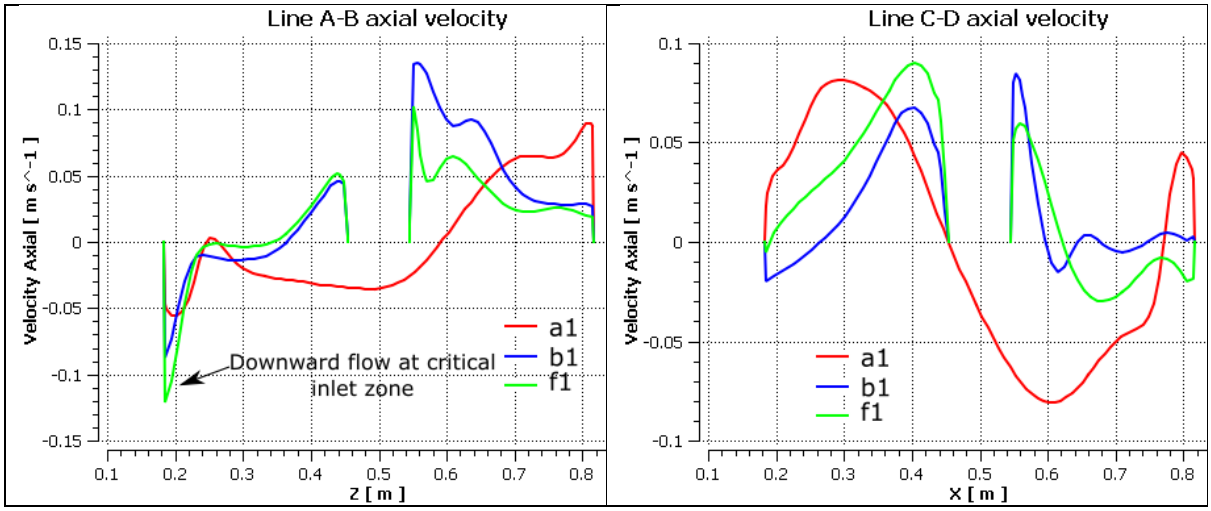

Figure 4-103: Numerical model average axial velocity profile of outlet configuration III on the z-x plane along lines A-B and C-D at y = 1.236 m

4.12.3.3 Tangential velocity

Figure 4-104 below illustrates base model and configuration III effect on numerical average tangential velocity contours on the z-x plane at y = 1.236 m. **Figure 4-105** below shows the corresponding tangential velocity profiles along A-B and C-D. It was observed that:

a) Tangential velocity increases with the change of model configuration.
b) Model configuration III experiences a Rankine's type of profile.

c) Configuration (b1) and (f1) recorded well distributed tangential velocity along the wall thus keeping sediment particles away from the inlet hence the highest sediment trapping.

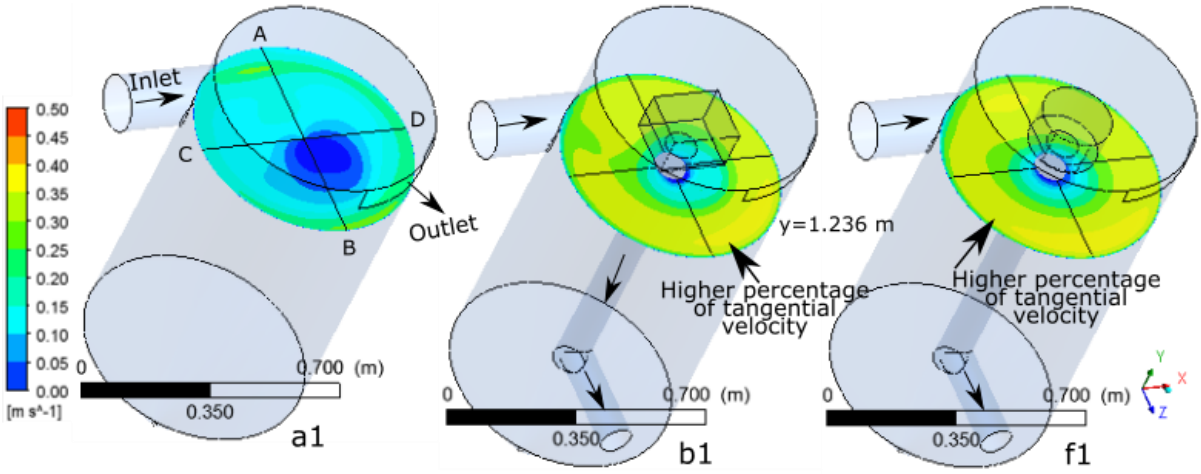

Figure 4-104: Numerical model effect of outlet configuration III on the z-x plane tangential velocity contour at y = 1.236 m

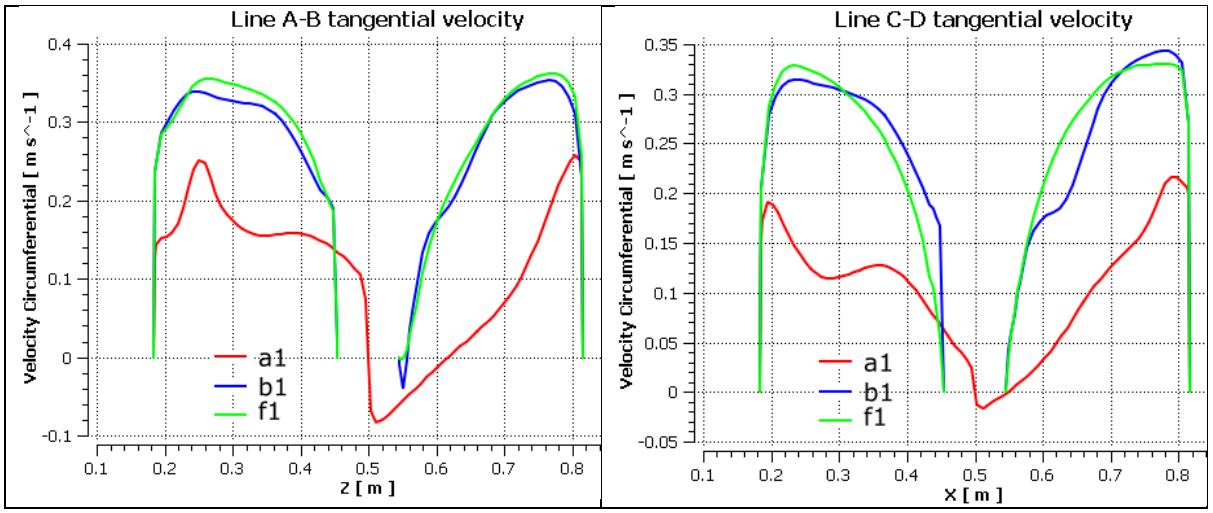

Figure 4-105: Numerical model average tangential velocity profile of outlet configuration III on the z-x plane along lines A-B and C-D at y = 1.236 m

4.12.3.4 Turbulent kinetic energy, TKE

Figure 4-106 below illustrates base model and configuration III average turbulent kinetic energy contours on the z-x plane at y = 1.236 m. It was observed that:

a) By changing the outlet configuration, low TKE is experienced near the wall. Hence currents transporting the sediment particles from the wall surface to the VSB underflow are experienced, thus better sediment trapping occurs.

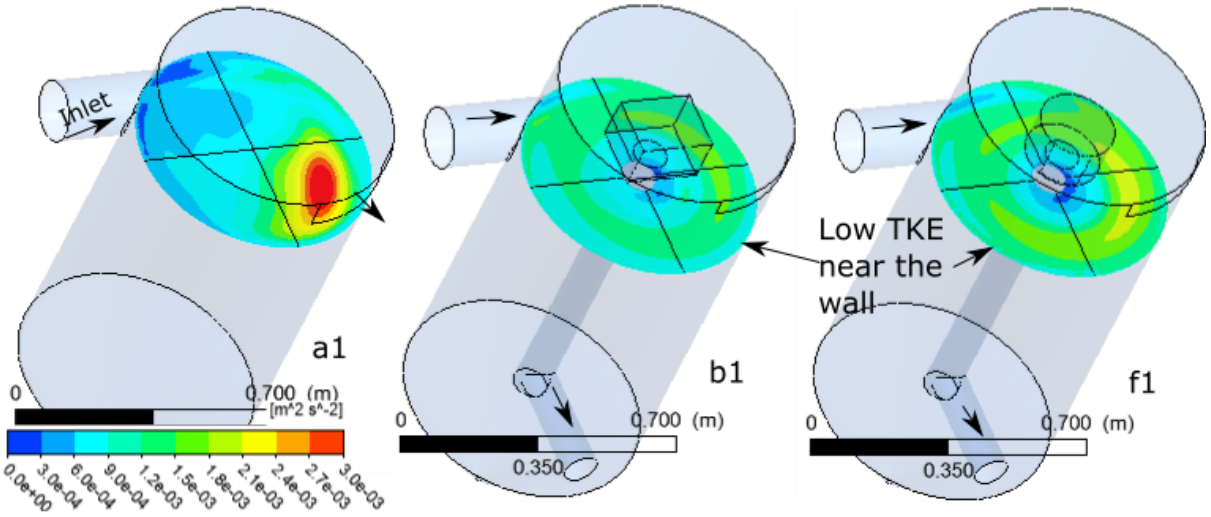

Figure 4-106: Configuration III numerical model turbulent kinetic energy contours on the z-x plane at y = 1.236 m

4.12.4 Conclusion on outlet structure configuration

Physical and numerical modelling were conducted to investigate the effect of placing the outlet structure in the middle of the VSB to take advantage of centrifugal forces. Several configurations were investigated, and it was observed that:

a) Having the outlet structure at the middle yields, a better trapping efficiency with configuration (b1) or (f1) recommended. The dimensions that gave the maximum trapping efficiency are summarised as follows:
   - L = 1.28 Di
   - B = Di
   - h2 = Di
   - Do = 1.28 Di

   Where Di = diameter of the inlet, l = length of the outlet, b = breath of the outlet, h = height of the outlet

b) The outlet shaft should be designed for partially full conditions to minimise vibrations and sub-atmospheric conditions.

5 Proposed layout based on VSB parameter study

5.1 Introduction

Figure 5-2 below shows an overview of this chapter. In chapter 4 it was concluded that , having deflectors increased the sediment trapping efficiency significantly. Horizontal deflectors were optimised for 1 l/s and trappings > 90% for 75 µm was achieved. The model was scaled to flows > 5 l/s, and the trapping efficiency reduced significantly and sediment particles settled on the horizontal deflectors. This design was concluded to be unsustainable and led to an alternative design proposed with a rectangular centroid outlet and shaft. Motivated from the design of hoppers for cohesive sediment in South African Rivers and grit removal in wastewater treatment, inclined deflectors at a slope of 1:2 (H: V) illustrated in **Figure 5-1** were investigated in this chapter. Numerical modelling optimisation was undertaken to yield two final model dimensions (Model 1 with capacity >5 l/s and Model 2 >10 l/s) summarised in **Figure 5-3**, **Figure 5-4** and **Table 5-2**.

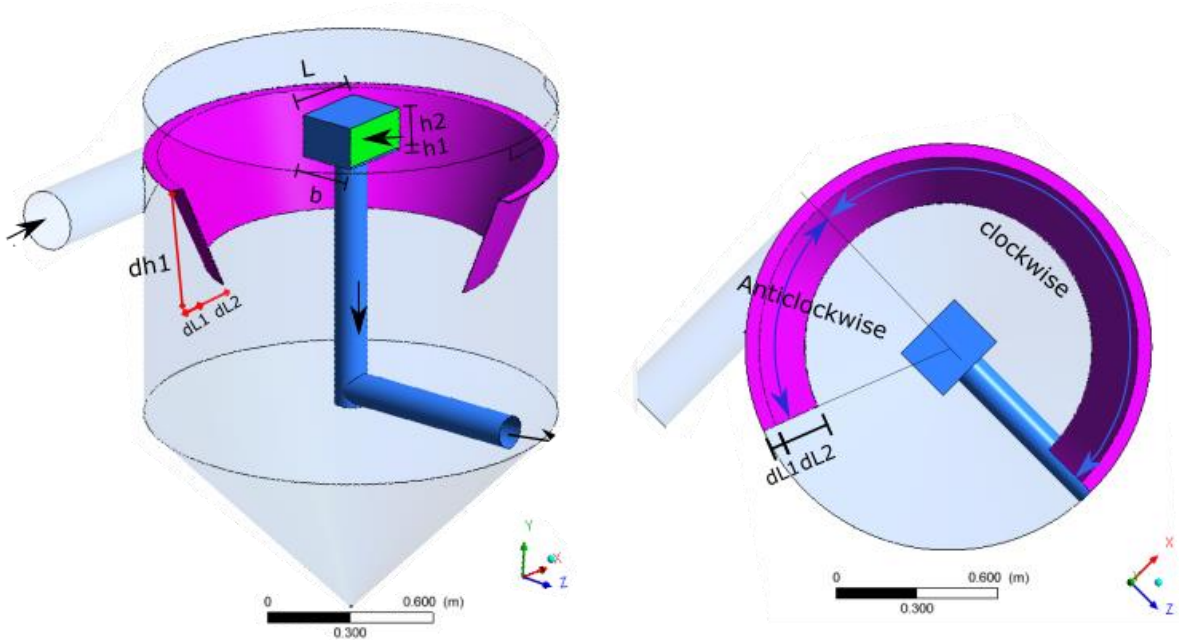

Figure 5-1: Proposed VSB configuration

With optimised models, a flow of 50 l/s was used, and the models compared to:

- Conventional settler designed analytically and verified on ANSYS FLUENT,
- Hydrocyclone designed according to MULTOTEC (2018) catalogue.

It was concluded that VSBs offers a better alternative for small river abstraction works as it achieves high trapping efficiency, small footprint, low energy requirements, no moving parts and no chemical dosing. For applicability in African Rivers, two river abstraction works layouts were suggested:

- Abstraction works with a low weir, gravel trap, trash rack and pumped or gravity flow to VSB,

- Intakes with trash rack, hopper and jet pumped to VSB.

To ensure sustainability, the following performance evaluation and practical consideration were undertaken:

- Trash rack/gravel trap to remove coarse sediment,
- Minimum velocity in the main distribution line suggested to limit clogging,
- Automatic throttle, passing the flow through primary VSB or VSB only used in regions with fine sediment particles to limit clogging of underflow,
- The underflow transport capacity was checked to return the concentrated flow back to the river,
- Performance evaluation under varying sediment loading,
- Performance evaluation under varying sediment sizes,
- Performance evaluation under varying underflow rates,
- Performance evaluation under varying inflow rates.

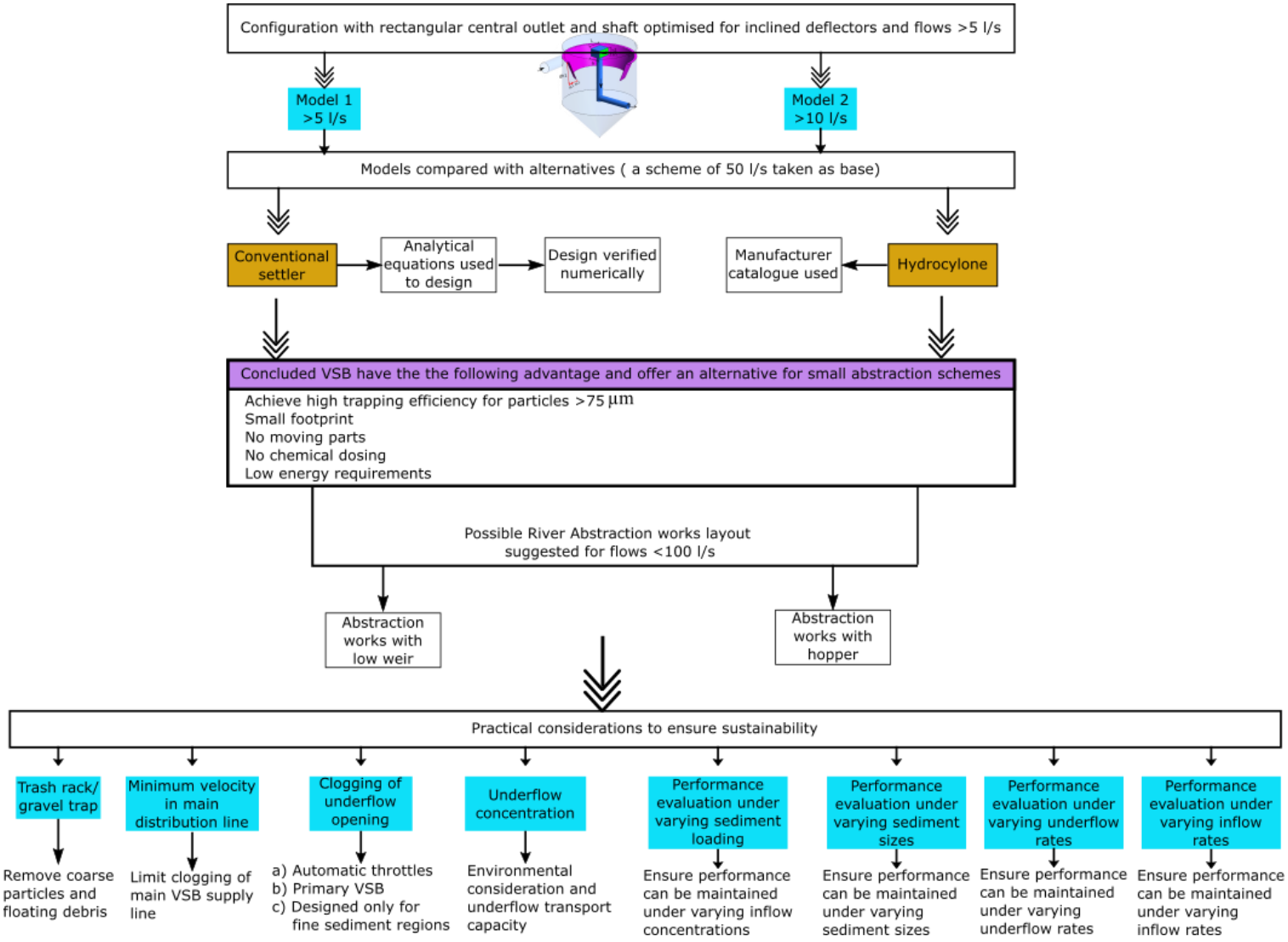

Figure 5-2: Chapter 5 overview

Table 5-1: A comparison of proposed model parameters

Parameters	Recommended in this study	Model 1	Model 2
$\frac{\text{underflow(Qu)}}{\text{inflow(Qi)}}$	0.05-0.1	0.05	0.08
inlet velocity (m/s)	0.26	0.26	0.26
$\frac{\text{position of inlet(Hi)}}{\text{cylinder height (Ht)}}$	0.5-0.88	0.68	0.71
Angle of inlet	0-11.3°	0°	0°
$\frac{\text{cylinder height (Ht)}}{\text{cylinder diameter (D)}}$	>0.5	0.78	0.67
Cone angle	60°	45°/60°	45°/60
$\frac{\text{cylinder diameter(D)}}{\text{inlet diameter (Di)}}$	8.2	8.21	6.82

Table 5-2: Summary of optmised proposed VSB dimension

Parameter	Model 1 base	Model 1	Model 2 base	Model 2
D (mm)	1280	1280	1500	1500
Di (mm)	156	156	220	220
D/Di	8.21	8.21	6.82	6.82
Hc	640	640	750	750
Ht (mm)	1000	1000	1000	1000
Hi (mm)	600	600	600	600
Hi/Ht	0.68	0.68	0.71	0.71
Ht/D	0.781	0.781	0.667	0.667
Qi (l/s)	4.965	4.965	9.870	9.870
Vi (m/s)	0.260	0.260	0.260	0.260
Du (m)	0.116	0.116	0.108	0.108
Qu (l/s)	0.270	0.270	0.789	0.789
Qu/Qi	0.05	0.05	0.08	0.08
Outlet diameter (mm)	90x90	90x90	120x120	120x120
L (mm)		200		280
b (mm)		160		220
h2 (mm)		80		190
h1 (mm)		40		10
angle		180		180
clockwise		180		180
anticlockwise		70		70
dh1		200		400
dL1		20		50
dL2		136		220

Table 5-3: Proposed optimised VSB dimension sediment trapping efficiency

Parameter	Model 1 base	Model 1	Model 2 base	Model 2
d50:122 µm trapping efficiency	89%	99%	91%	97%
100 µm trapping efficiency	99%	100%	93%	98%
75 µm trapping efficiency	96%	99%	77%	91%

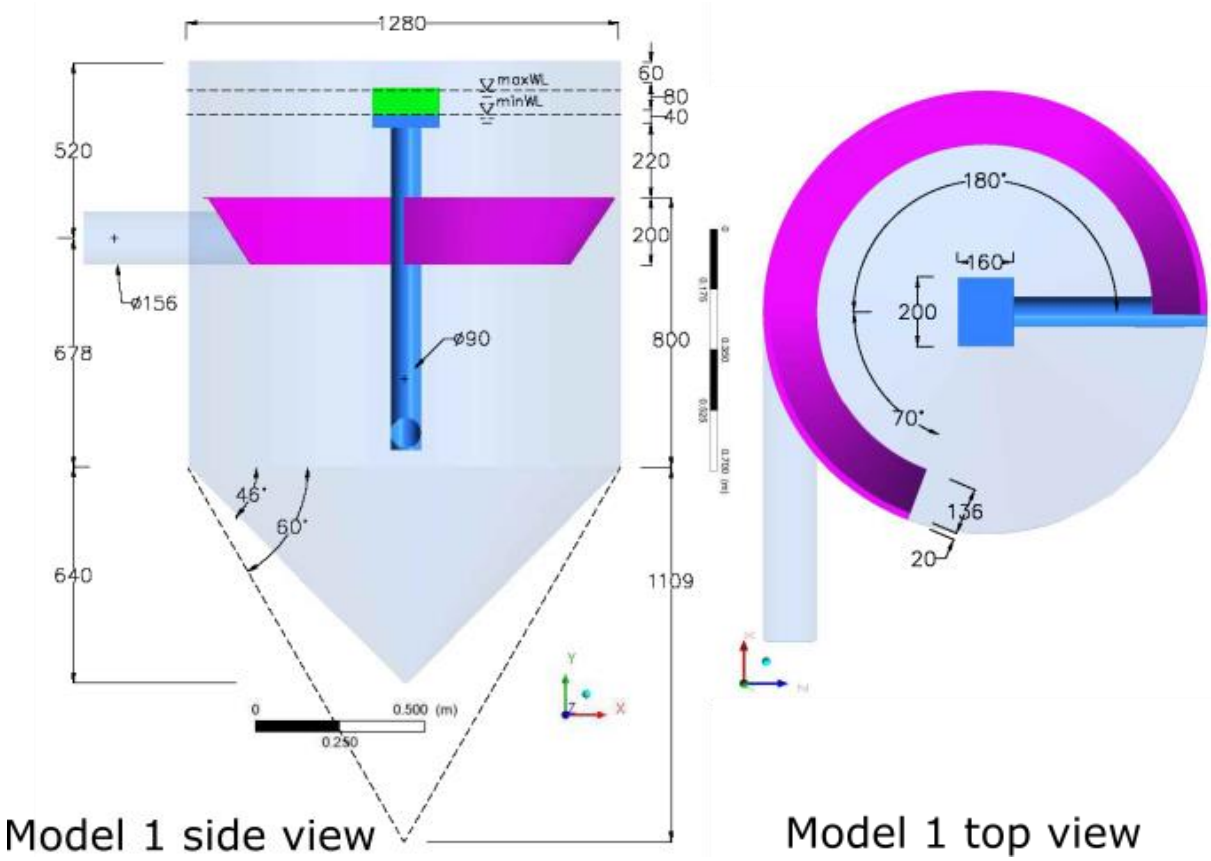

Figure 5-3: Proposed VSB Model 1 dimensions

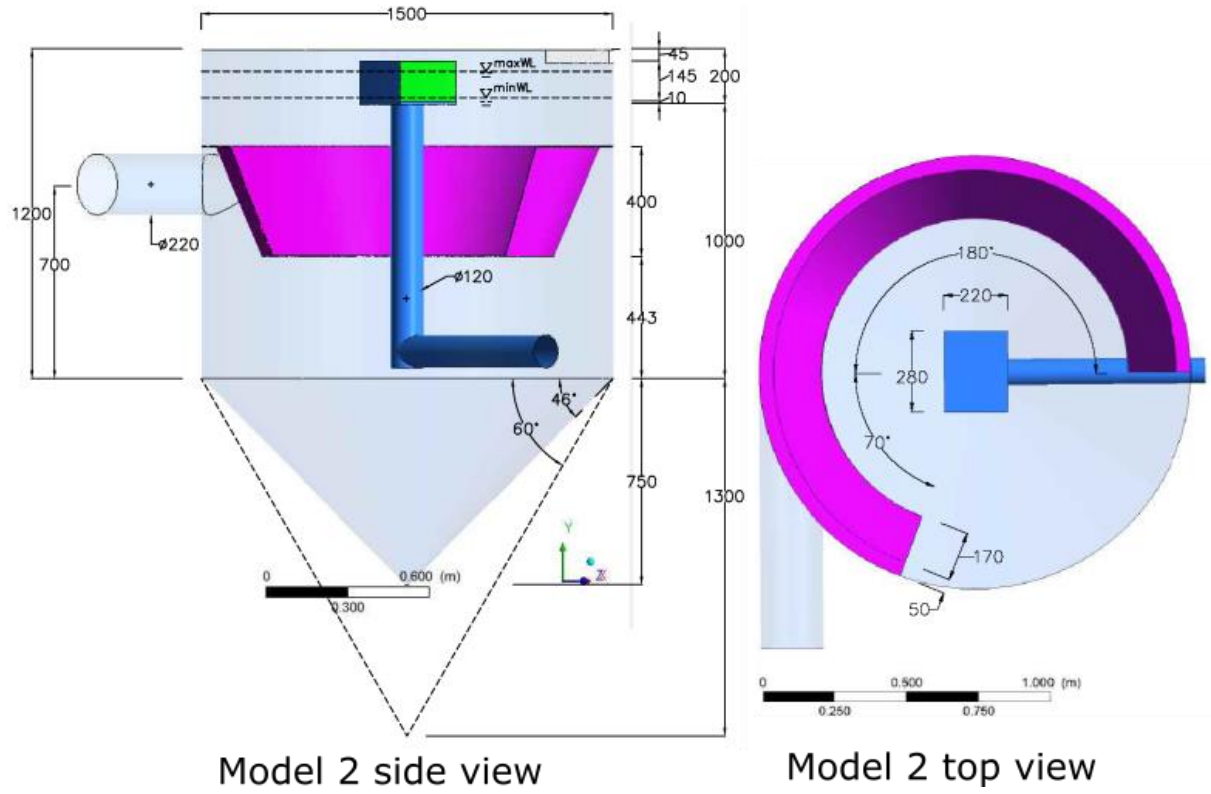

Figure 5-4: Proposed VSB Model 2 dimensions

5.2 Sediment trapping efficiency

The sediment trapping efficiency for Models 1 and 2 is summarised in **Table 5-3**. Model 1 can handle 5 l/s with 5% water loss while realising 99% trapping efficiency for 75 µm and Model 2 can handle 10 l/s with 8% loss while achieving 91% trapping efficiency for 75 µm (Models 1 and 2 at maximum inflow sediment concentration of 10,000 mg/l). A comparison between an equivalent base model without deflectors and with deflectors was undertaken and is discussed below.

5.3 Axial velocity

Figure 5-5 below illustrates Models 1 and 2 numerical average axial velocities contours at cross-section z-x normal to the centre of inlet diameter at y = 1.318 m and y = 1.46 m. **Figure 5-6** shows the corresponding velocity profiles along dimensionless lines A-B and C-D and it was observed that:

a) Two distinct regions occurred; regions with water flowing downwards (cyan and blue) which facilitates settling and regions with water flowing upwards (yellow and red).
b) Deflectors placed at a critical inlet zone acts as a physical barrier increasing flow moving downwards and prevents sediment particles from moving upwards thus increasing the trapping efficiency. **Figure 5-5** shows the probable paths of 75 µm sediment particles for Models 1 and 2 from numerical modelling which illustrates this.

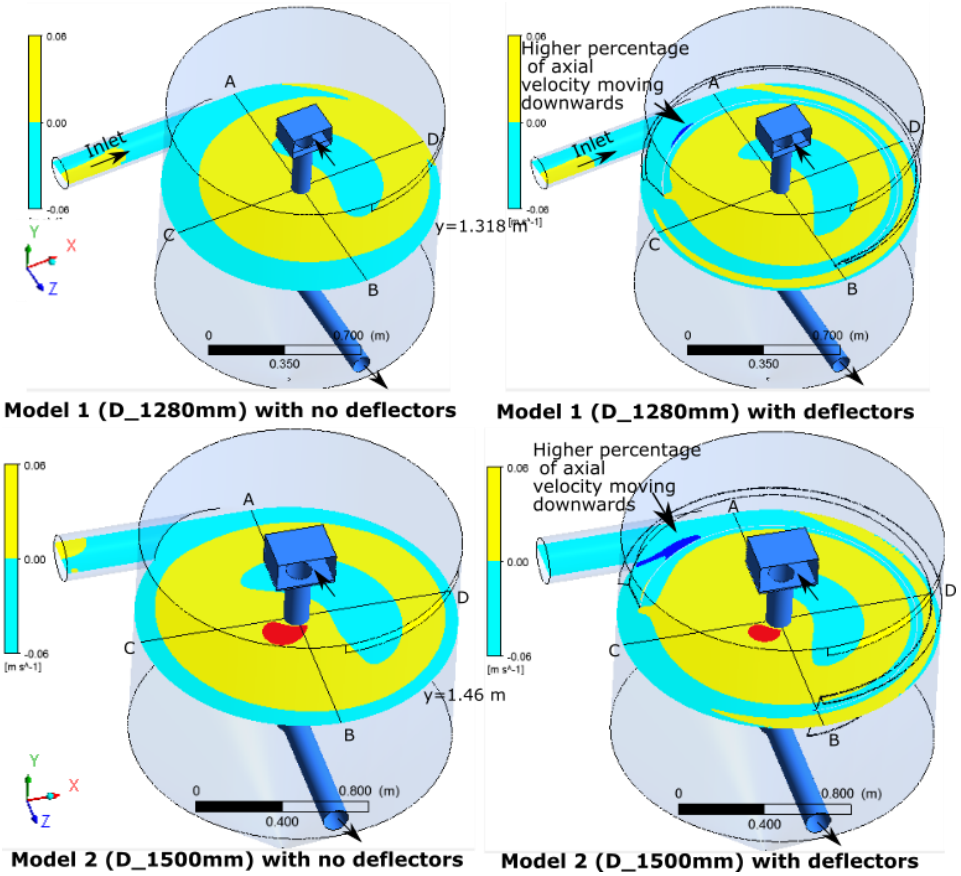

Figure 5-5: Numerical Models 1 and 2 average axial velocity contours on the z-x plane (cyan/blue: downward movement of water, yellow/red: rising water)

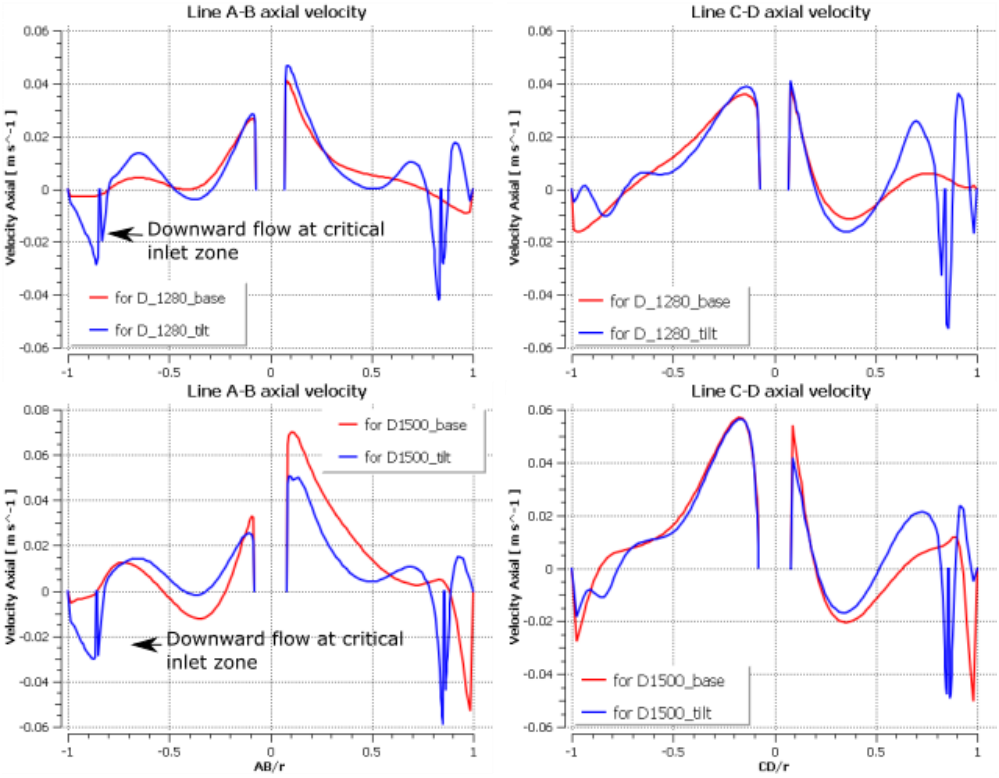

Figure 5-6: Numerical Models 1 and 2 axial velocity profile on the z-x plane along dimensionless lines A-B and C-D

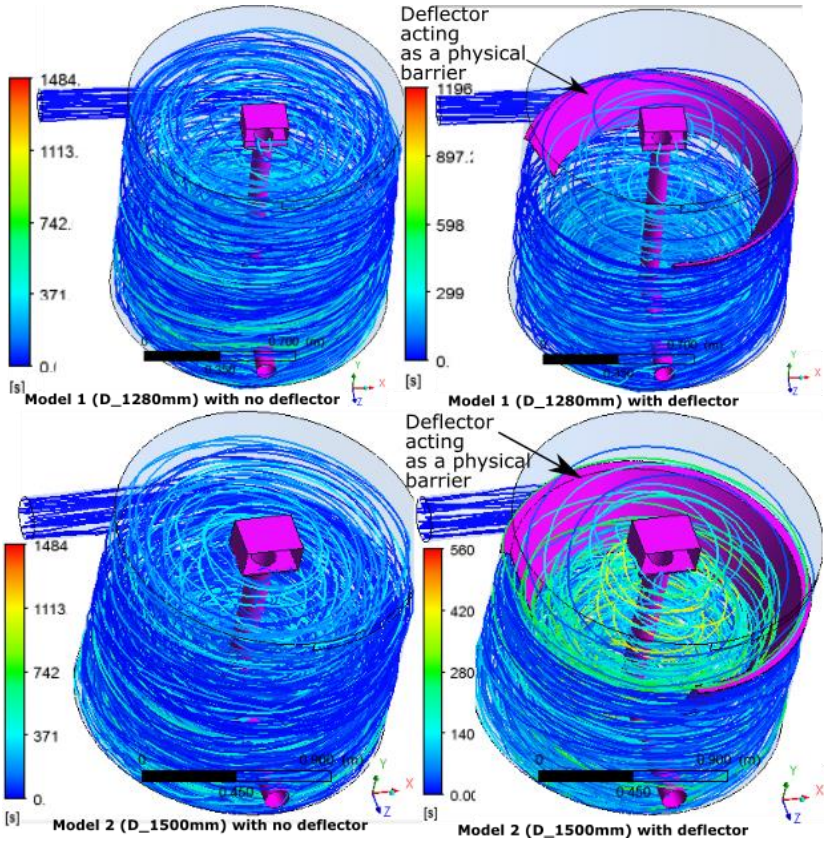

Figure 5-7: Models 1 and 2 numerical 75 µm probable particle path coloured by hydraulic retention time

5.4 Tangential velocity

Figure 5-8 below illustrates Models 1 and 2 numerical model average tangential velocity contours on the z-x plane at y =1.318 m and y = 1.46 m and profiles extracted along a dimensionless lines A-B and C-D in **Figure 5-9**. It was observed that:

a) Near the wall, deflectors do not significantly affect the magnitude of the tangential velocity ensuring sediment particles are suspended near the wall away from the overflow outlet.
b) Deflectors do not have a significant effect on the tangential velocity component but aid in directing the sediment particles.

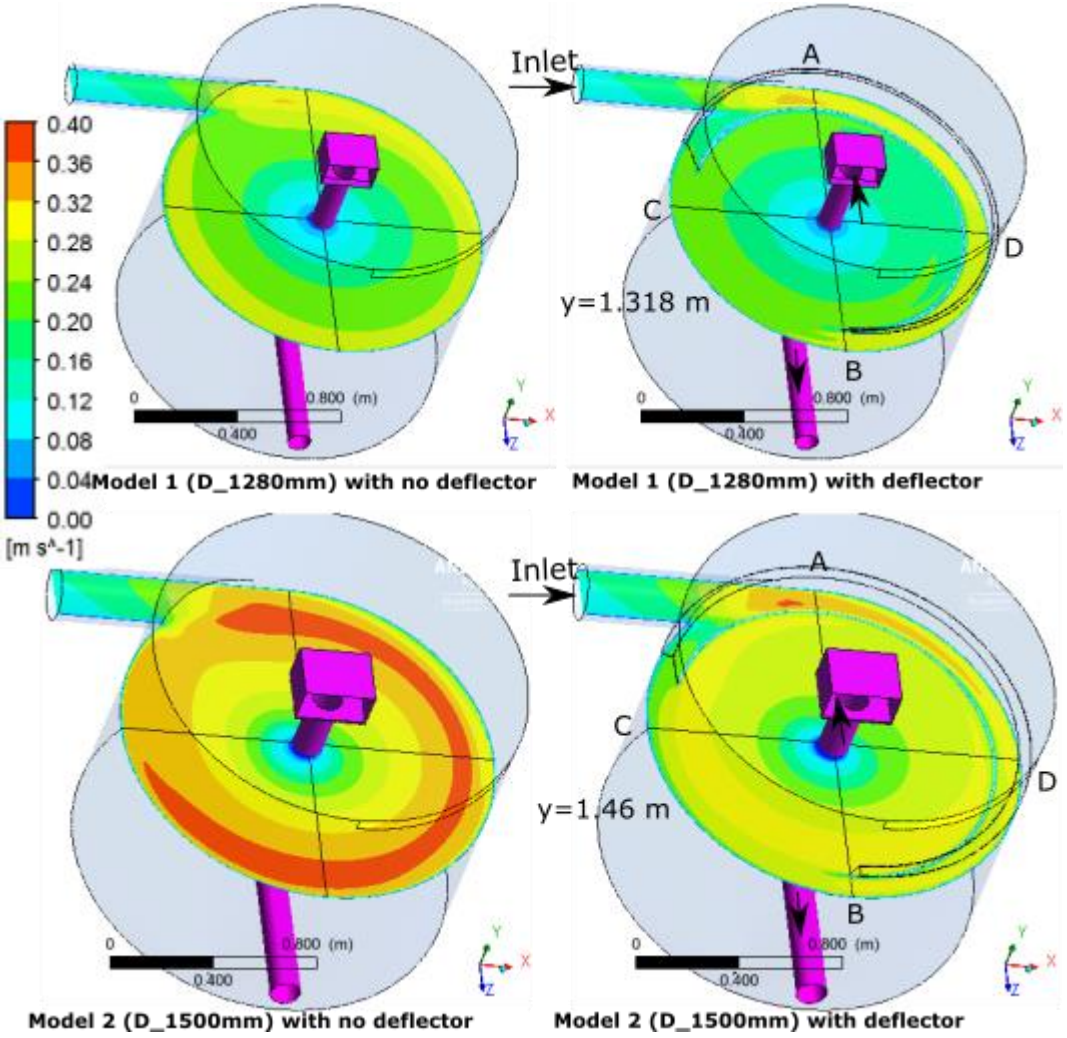

Figure 5-8: Numerical Models 1 and 2 average tangential velocity contours on the z-x plane

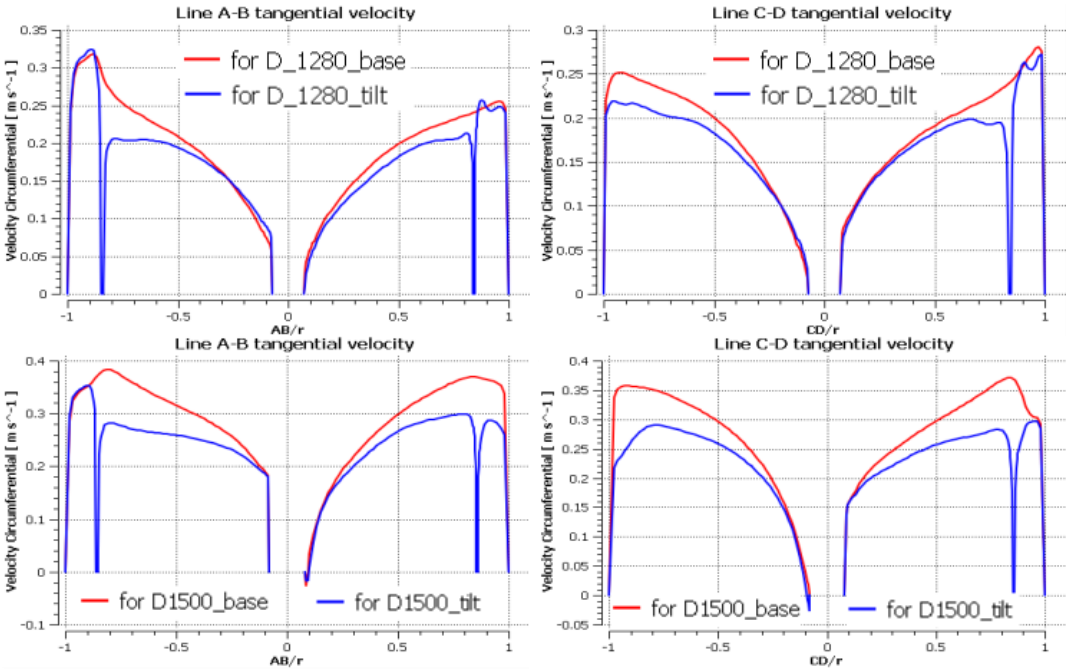

Figure 5-9: Numerical Models 1 and 2 average tangential velocity profile on the z-x plane along dimensionless lines A-B and C-D

5.5 Turbulent kinetic energy, TKE

Figure 5-10 below illustrates Models 1 and 2 numerical model average TKE contours on the z-x plane at y = 1.318 m and y = 1.46 m. At the crucial inlet zone, deflectors reduce the TKE thus higher secondary currents recirculating sediment particles toward VSB underflow occur, hence higher trapping efficiency.

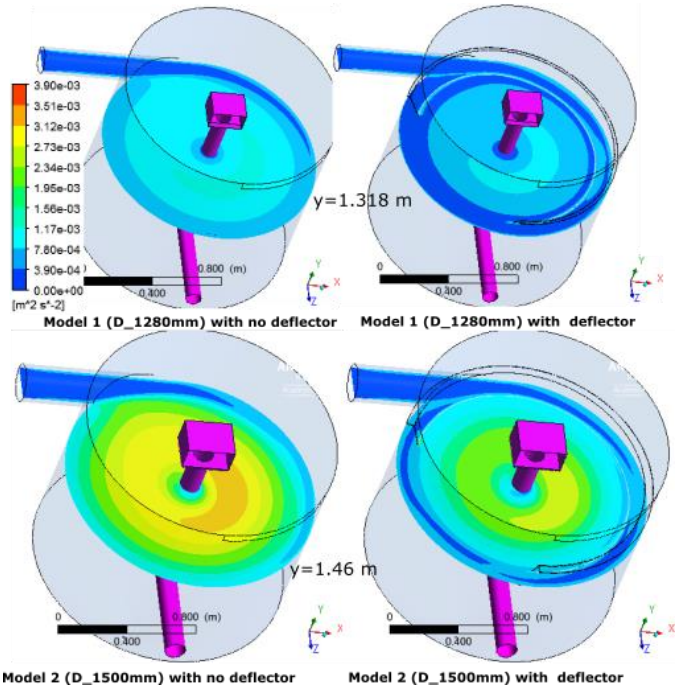

Figure 5-10: Models 1 and 2 numerical model turbulent kinetic energy contours on the z-x plane at y= 1.318 m and y = 1.46 m

5.6 Conclusion on the proposed layout

Based on the preceding investigations, an optimised VSB was refined to handle higher flows of 5 l/s (**Figure 5-3**) with 5% water loss and 10 l/s (**Figure 5-4**) with 8 % water loss while achieving 99 % trapping efficiency and 91 % sediment trapping for a sediment size of 75 µm respectively. To ensure sustainability an inclined cone slope of 1:2 (H:V) was utilised with an outlet in the middle of the VSB.

6 Practical considerations

The VSBs in this study were investigated as an alternative to a conventional settler. For comparison, a throughput of 50 l/s was assumed, and **Table 6-1** below summarises conventional settler and hydro cyclones dimensions required to settle 75 µm sediment particles. The conventional settler was sized with analytical **Equation 2-8**, **Equation 2-9** and **Equation 2-10**. A numerical ANSYS FLUENT model was set up to verify the settler analytical solutions, and **Figure 6-1a** below illustrates the numerical model result for 75 µm probable particle paths with average velocity and TKE contours in **Figure 6-1b** and **c** respectively.

From the ANSYS FLUENT model, it was observed that a 17 m long settler would yield a 97 % sediment trapping efficiency requiring a total surface area of 34 m^2. On the other hand, VSB (5 l/s) yields 99% trapping efficiency requiring a total surface area of 12.9 m^2 and VSB (10 l/s) yields 91% sediment trapping efficiency requiring 8.8 m^2. MULTOTEC (2018) hydro-cyclones need a total surface area of 0.7 m^2. From these calculations, it can be concluded that a VSB needs $\approx \frac{1}{3}$ of settler surface area while achieving a higher sediment trapping efficiency.

For a comprehensive comparison of the energy requirements of the different sediment removal systems, the total energy losses over the respective systems (from inlet to outlet) have to be compared. This was not done for this case, however, the required inlet velocities required for the different systems were used to obtain an indication of energy requirements. The energy requirements of the settler (straight canal type) and VSB are relatively small since their required input and operating velocities have to be small. However, since the input velocity requirement (required input head of 50 kPa = 5.1 m for the case considered) and operating velocity of a hydrocyclone have to be relatively high, the energy loss over it is much higher than that of settlers and VSBs.

Therefore, it can be concluded that, the VSB has the advantage of a small footprint, less energy requirements, no moving parts and no chemical dosing requirement to remove the 75 µm sediment size at relatively high inlet velocities (0.26 m/s) while achieving high sediment trapping efficiency, making the VSB an attractive alternative in the removal of sediment in small river abstraction works.

Table 6-1: Dimensions and energy requirements of a conventional settler, hydro-cyclone and VSB required to settle 75 µm sediment particles at 50l/s

Parameter	Settler	VSB (5l/s)	VSB (10l/s)	MULTOTEC hydro-cyclone (Appendix A1)
Inflow (l/s)	50	50	50	50
Sediment size (µm)	75	75	75	75
Sediment settling velocity, ω (m/s) **(**Equation 2-4**)**	0.0035			
Mean flow velocity, V (m/s)	0.027			
Critical velocity, V_{cr} (m/s) ($V_{cr} = 10\omega R^{1/6}$)	0.031			
Flow depth, h (m)	1.00			
Trap width, B≈2h (m)	2.00			

Minimum length, L_{min} (m) ($l_{min} = V \times \frac{h}{\omega - u^*}$)	15.36			
Trapping efficiency %	97	99	91	100
Diameter (m)		1.28	1.5	0.35
No of VSB/hydro-cyclone required		$50/5 = 10$	$50/10 = 5$	2
Water loss (l/s)		$5\% * 10 * 5l/s = 2.5$	$5\% * 5 * 10l/s = 2.5$	Not known
Total surface area required (m^2)	$2 * 17 = 34$	$\frac{\pi 1.28^2 * 10}{4} = 12.9$	$\frac{\pi 1.5^2 * 5}{4} = 8.8$	2*0.35=0.7
Indication of energy requirements	Relative small inlet velocity head required and small energy head loss due to minor and friction losses			Relatively large inlet head of 50 kPa (5.1 m) required – therefore high energy loss over system

Where u*: shear velocity $u^* = \frac{4.2V}{100} \times \frac{1}{R^{1/6}}$(m/s). recommended: V< V_{cr}, R: hydraulic radius, width ≈ 2h, V≈ 0.07 m/s to remove 100 µ m and 0.35 m/s to remove 300 µm

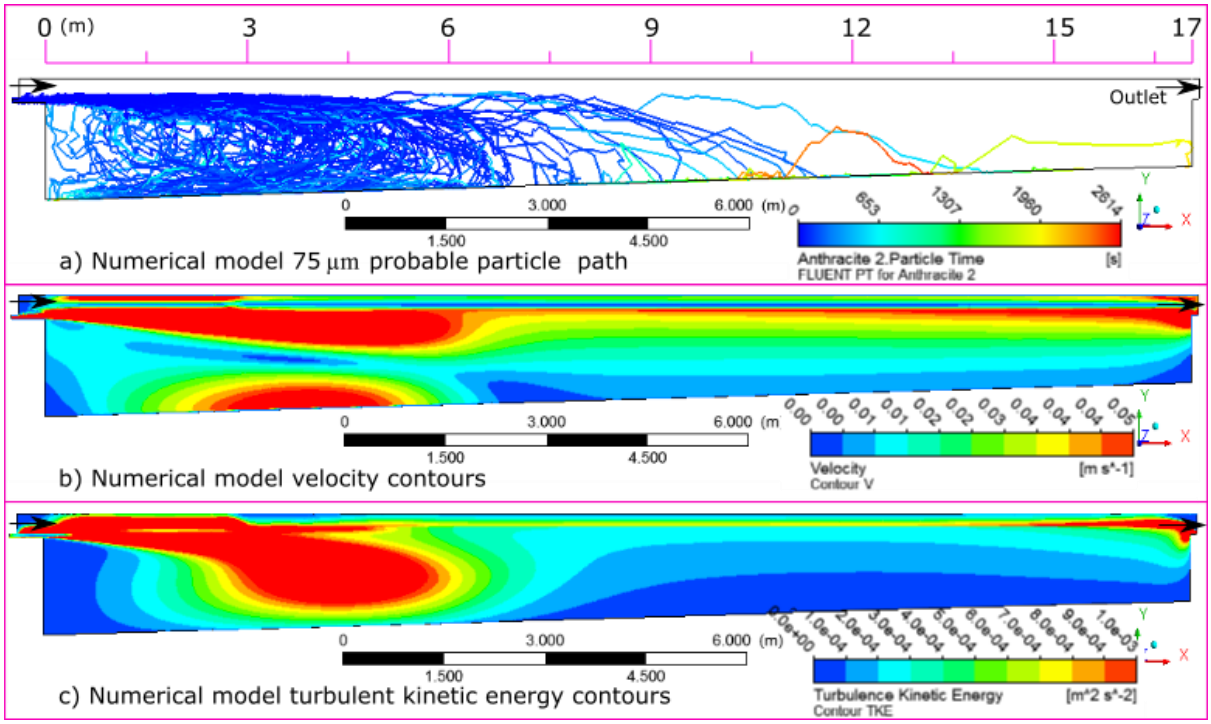

Figure 6-1: Conventional flume/canal type settler numerical model a) 75 µm sediment particle tracking coloured by hydraulic retention time, b) velocity contours and c) turbulent kinetic energy contours

In the river abstraction works two possible layouts are possible:

a) With low weir, gravel trap, trash rack and pumped or gravity flow to VSB
b) Intakes with trash rack, hopper and jet pump flow to VSB

Figure 6-2 below illustrates these configurations and the VSB can be clustered in a parallel configuration to meet the required demand.

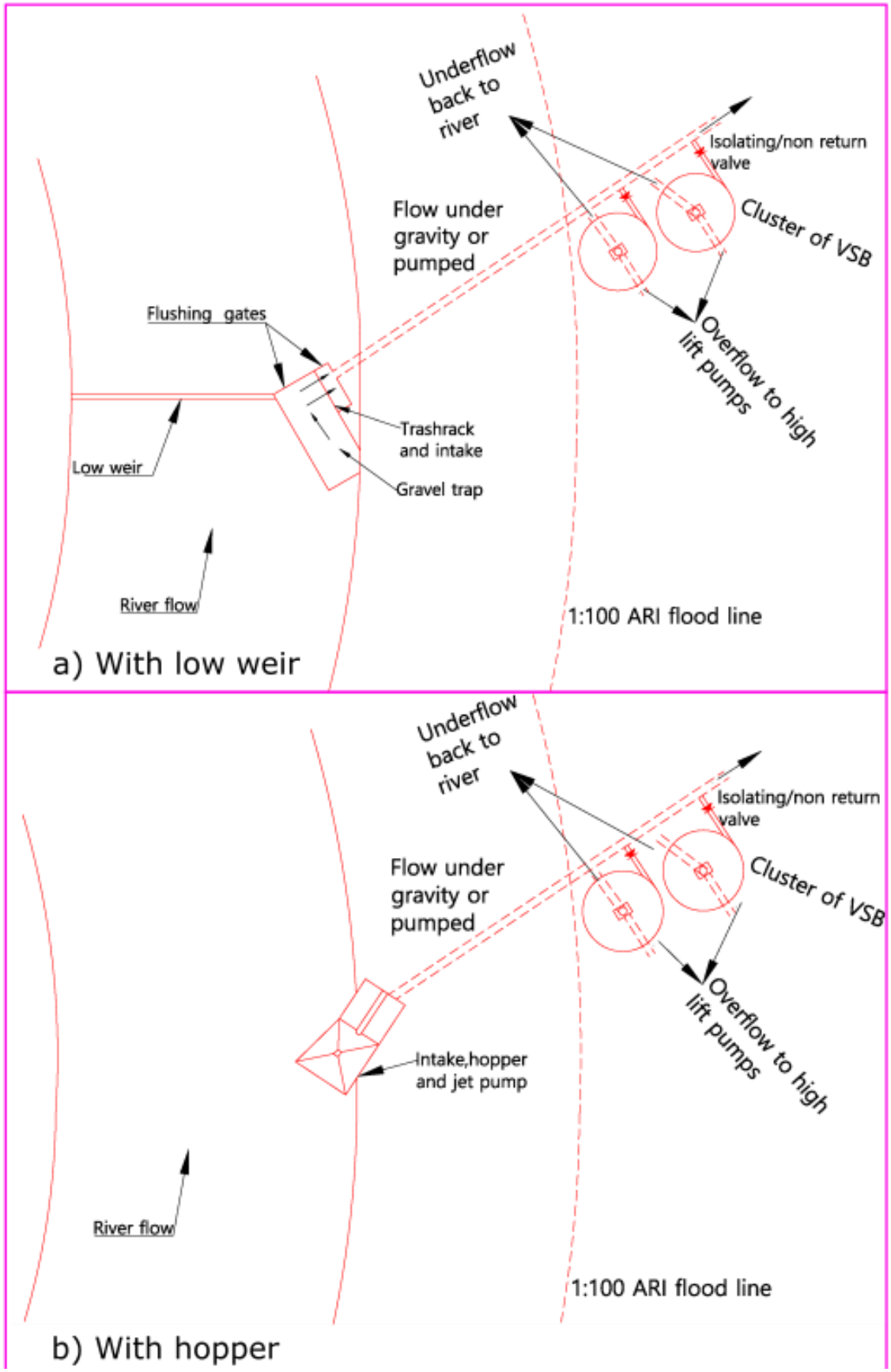

Figure 6-2: Possible river abstraction works layout with VSBs in parallel to meet the required demand

Several practical considerations were considered and are discussed below:

a) Trash rack/gravel trap

To minimise the amount of coarse sediment in the VSB domain, a gravel trap and a trash rack have to be provided. A trash rack of 30 mm x 30 mm with smaller openings is proposed to be utilised.

b) Minimum velocity

The VSB requires a maximum inlet velocity of 0.26 m/s to remove fine sediment adequately, but this velocity in the main distribution line will promote the settling of sediment. As mitigation, taking maximum allowable sediment to be 30 mm, minimum velocity in the distribution line needs to be higher than 0.6 m/s (from **Equation 4-3**).

c) VSB energy requirements

The VSB operates as an open channel flow, and energy requirements can be calculated using Bernoulli's principle. The static head is site-specific, but the minimum velocity head for 1 VSB with inlet velocity of 0.26 m/s is $\frac{0.26^2}{2g} + \text{minor losses}$.

d) Underflow opening

Equation 6-1 below can approximate the underflow opening required and from **Table 5-2** above, it was observed that 11.6 mm and 10.8 mm underflow diameters for VSB (5 l/s), and VSB (10 l/s) respectively are susceptible to clogging. To mitigate this:

- Special automatic throttling valves have to be utilised or
- Flow passed through a primary VSB to remove coarse sediment or
- VSB only used in regions with fine sediment

$$Qu = C_d A\sqrt{2gh} \qquad \text{Equation 6-1}$$

Where Qu: underflow m^3/s, A: underflow area m^2, C_d: coefficient of discharge 0.6-0.9, g: gravitational acceleration (m/s^2), h: water head (m)

e) Underflow sediment concentration

Table 6-2 below summarises the VSB sediment mass balance calculations. Considering a scheme with a throughput of 50 l/s and inlet sediment load of 10,000 mg/l the maximum underflow concentration realised was 198,000 mg/l with an underflow of 2.5 l/s, yielding a volume fraction of 0.075 thus possible to be transported in a solution. Considering a concrete-lined channel, **Table 6-3** below summarises calculations undertaken, and it was observed, a steep channel 1:50 is required to convey the flow adequately. These calculations are site-specific, but if such a slope is not achievable, the underflow can be increased.

Table 6-2: VSB sediment mass balance

Parameters	Model 1 (5l/s)	Model 2 (10l/s)
Inlet sediment concentration (mg/l)	10,000	10,000
Inlet flow (l/s)	50	50
Inlet sediment load (g/s)	500	500
Underflow (l/s)	2.5	2.5
Trapping efficiency (%)	99	91
Underflow sediment concentration (mg/l)	198,000	182,000
Volume by fraction	0.075	0.069

Table 6-3: Concrete channel sediment transport calculations per sediment size based on (Van Rijn, 1993, 2007)

Slope (m/m)	0.02	0.02	0.02
d50(µm)	75	150	300
Water density (kg/m^3)	1000	1000	1000
sand density(kg/m^3)	2650	2650	2650
Channel width (m)	0.1	0.1	0.1
Water depth (m)	0.021	0.021	0.021
Kinematic viscosity (m^2/s)	1.00E-06	1.00E-06	1.00E-06
ks (m)	0.0001	0.0001	0.0001
Velocity (m/s)	1.25	1.25	1.25
Discharge (m^3/s)	0.0026	0.0026	0.0026
Bed load (m^3/s)	0.000008	0.000011	0.000015
Suspended load (m^3/s)	0.000275	0.000161	0.000095
Total load (m^3/s)	0.000283	0.000172	0.000110
Sand transport (kg/s)	0.749036	0.455357	0.290689
Concentration (mg/l)	284,268	172,813	110,320

f) Different sediment loading

Model 1 inlet sediment loading was varied and a Eulerian-Eulerian approach utilised. The method solves coupled sand, water and air mass and momentum equations. **Figure 6-3** below illustrates a) 5,149 mg/l and b) 10,000 mg/l inlet sediment concentration numerical model volume fraction contours on the z-x plane at y = 0.42 m, y = 0.80m and y = 1.318 m. It was observed that the sediment loading rate does not affect VSB trapping efficiency.

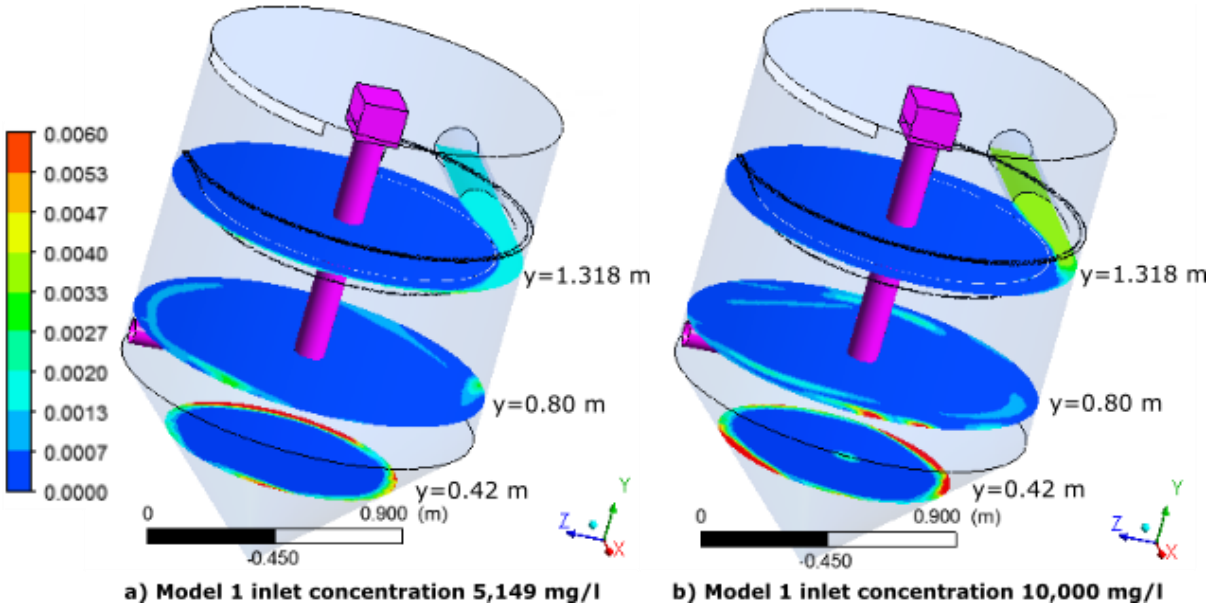

Figure 6-3: Numerical model sand volume fraction at inlet concentration a) 5,149 mg/l and b) 10,000 mg/l at the z-x plane y = 0.42 m, y = 0.80m and y = 1.318 m

g) Performance evaluation over different sediment sizes

Figure 6-4 below illustrates numerical model sediment removal efficiency over varying sediment sizes. Model 1 achieves a 100% trapping efficiency at 90 µm while Model 2 at 110 µm. Model 1 utilises all the recommended settings hence achieves a better trapping efficiency. If a higher flow is needed per single VSB, the methodology and recommendations in this study can be utilised.

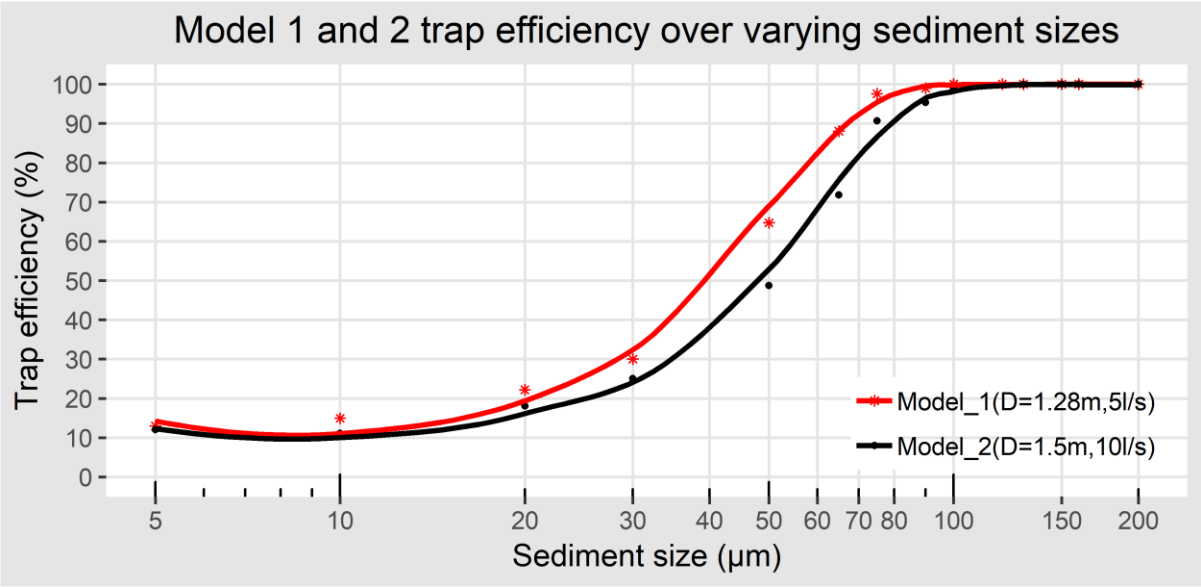

Figure 6-4: Numerical model sediment removal efficiency over varying sediment sizes

h) Performance evaluation for different underflows

All the dimensions in Models 1 and 2 configurations were held constant except the underflow. **Figure 6-5** and **Figure 6-6** illustrates Models 1 and 2 numerical model trapping efficiency over varying sediment sizes and underflow. As it was concluded in section **4.2**, a ratio of $\frac{Q_u}{Q_i} = 0.08$ is the most optimal for sediment removal.

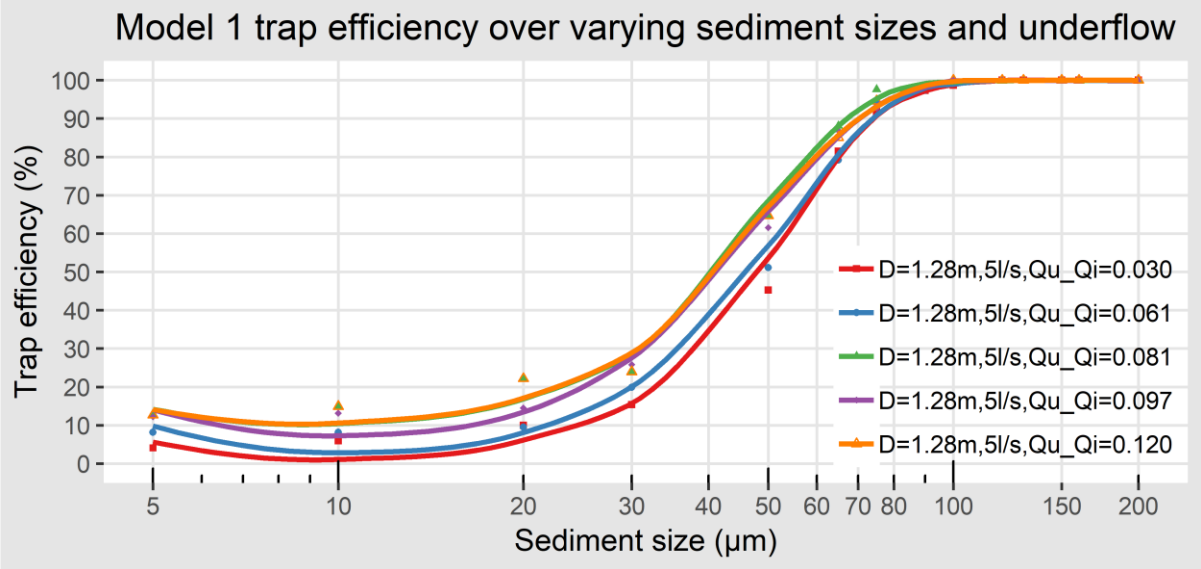

Figure 6-5: Model 1 numerical model sediment removal efficiency over varying sediment sizes and underflow

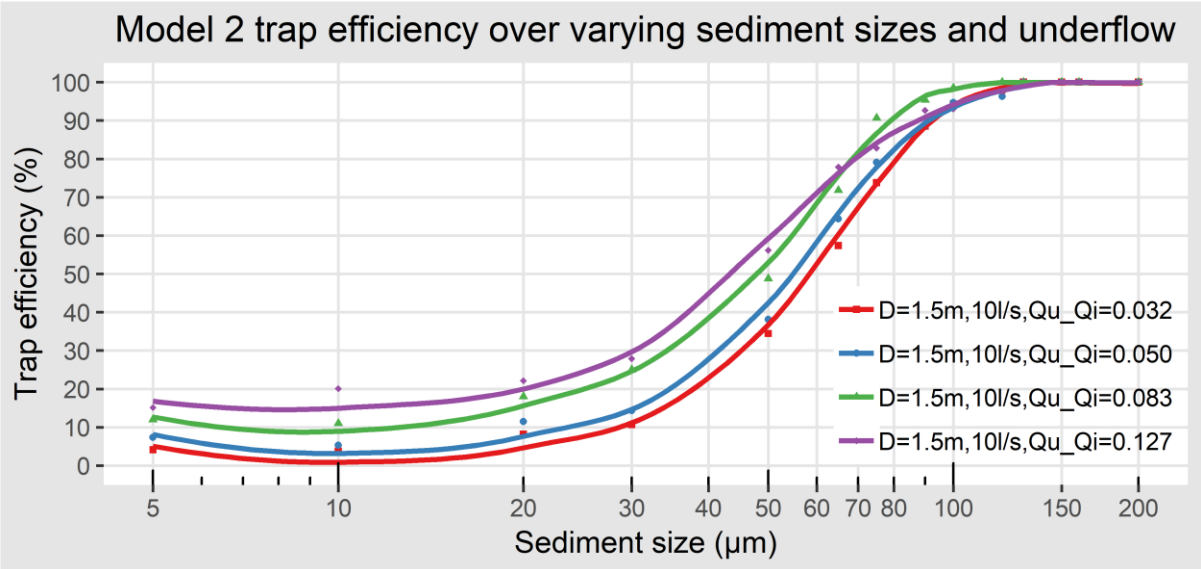

Figure 6-6: Model 2 numerical model sediment removal efficiency over varying sediment sizes and underflow

i) Performance evaluation for varying inflow

Models 1 and 2 dimensions were held constant, and the inflow varied while maintaining a ratio $\frac{Q_u}{Qi} = 0.08$. **Figure 6-7** and **Figure 6-8** below illustrate numerical model sediment trapping efficiency for varying sediment sizes and inflow. It was observed that efficiency reduced with an increase in inflow and to ensure good performance the velocity at the inlet should therefore be maintained at 0.26 m/s.

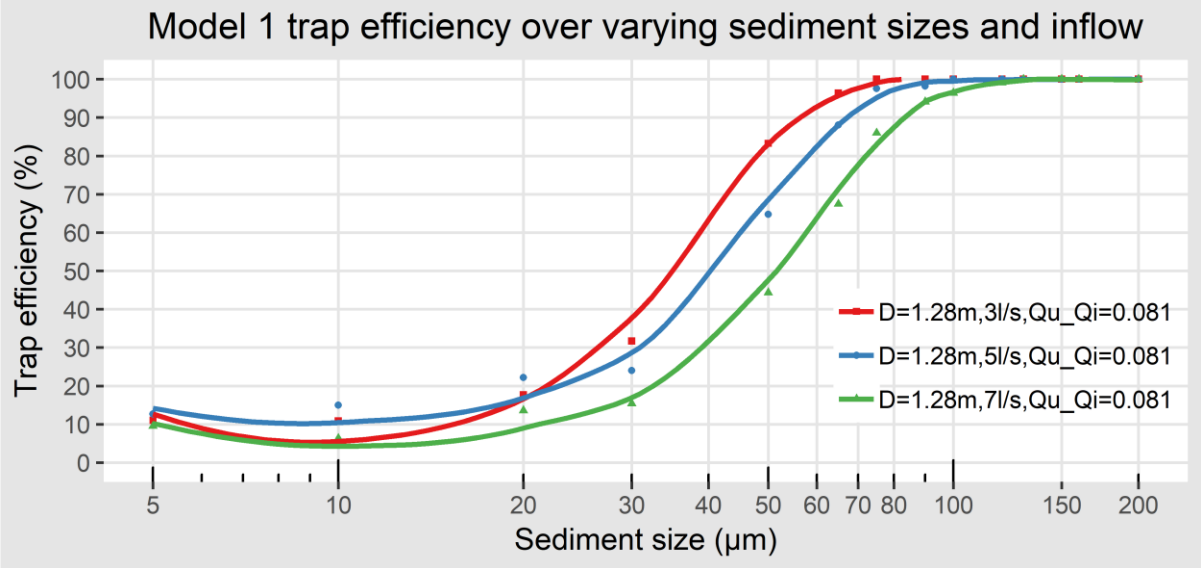

Figure 6-7: Model 1 numerical model sediment removal efficiency over varying sediment sizes and inflow

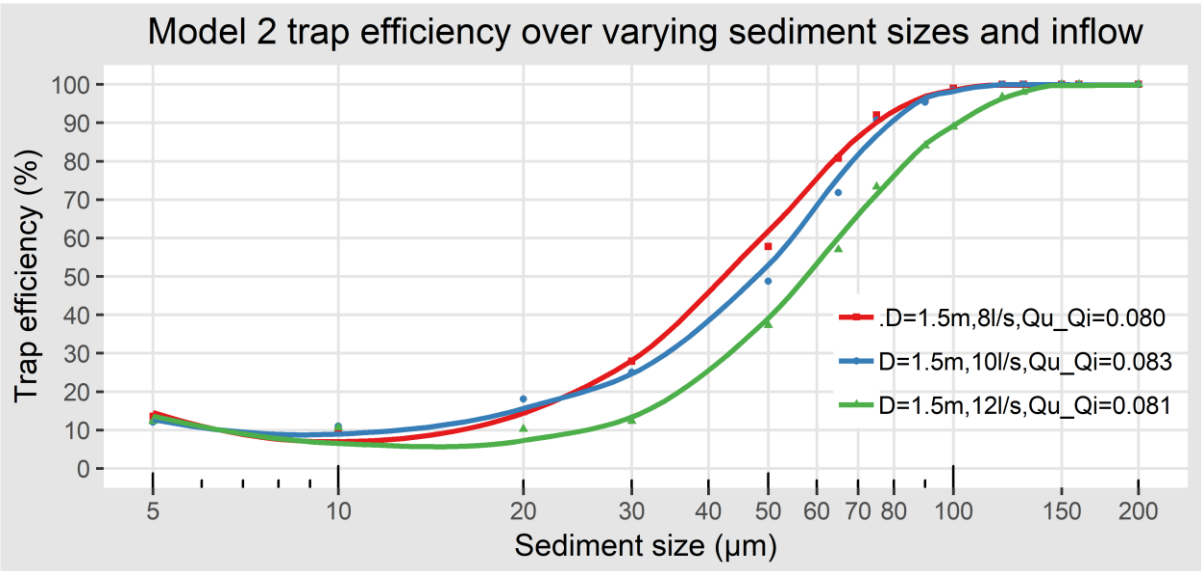

Figure 6-8: Model 2 numerical model sediment removal efficiency over varying sediment sizes and inflow

7 Final conclusion and recommendations

Extensive numerical modelling and physical modelling were undertaken to identify the significant parameters that influence the removal of fine non-cohesive sediment with the aim of incorporating vortex settling basins in very small river abstraction works where the flow rates are less than 100 l/s (7.2 Ml/d at 20 h/d), which is typical for rural potable water schemes in Africa.

The primary objective was achieved, and the findings can be summarised as follows:

- Just as other authors have found out, gravity is the primary driver in sediment removal, and weak centrifugal forces assist in keeping the particles longer in suspension.
- The sediment size affects the settling velocity, and thus VSB cannot effectively remove particles less than 75 µm.
- The VSB diameter plays a major role in sediment removal. Other researchers working on coarse sediment have recommended $\frac{\text{Cylinder diameter(D)}}{\text{Inlet diameter }(D_i)} = 6$ and for the removal of 75 µm, this research recommends $\frac{\text{Cylinder diameter(D)}}{\text{Inlet diameter }(D_i)} = 8.2$. Larger VSB diameters do not significantly increase the resident time of sediment particles and are thus not recommended.
- The tangential inlet velocity should be maintained at 0.26 m/s to ensure centrifugal forces are adequate in dispersing the sediment particles near the wall.
- A ratio of underflow $0.05 < \frac{\text{Underflow}}{\text{Inflow}} < 0.1$ is recommended. Higher ratios lead to water losses without necessarily increasing the sediment trapping efficiencies. Two VSBs can be combined in series with approximately 4% water loss instead of one VSB with 10% to achieve higher efficiency.
- The position of the inlet relative to the cylinder should be $\frac{\text{Height of inlet pipe relative to the cylinder (Hi)}}{\text{Cylinder height (Ht)}} > 0.5$. If combined with a declined deflector a ratio close to one is recommended.
- The cylinder height has a minor impact on the sediment removal and, when varying the cylinder height, trapping efficiency results are inconsistent. In this study a ratio of $\frac{\text{Cylinder height (Ht)}}{\text{cylinder height (D)}} > 0.5$ is recommended to allow installation of deflectors.
- An inlet slope of 1:5 (V:H) is recommended in this study, but the effects on removal efficiency are marginal.
- Due to the cohesive nature of South African sediment, a cone slope 2:1 (V:H) needs to be provided to avoid clogging of the underflow and resuspension of settled sediment. The cone angle has minimal influence on the trapping efficiency.
- Deflectors have a significant impact on sediment removal. Guidelines for placement and sizing are limited from literature; numerically and experimentally this thesis established that a deflector of length = inlet diameter (Di) just above the inlet extending 180° clockwise and 70° anticlockwise inclined at 2:1 (V: H) improves the trapping

significantly. Horizontal deflectors as illustrated in **Figure 4-81** are not recommended due to settling of sediment on the deflectors thus resulting in unsustainable design.

- Several outlet configurations were tested and a rectangular centroid outlet of length = 1.28 Di, width = Di and height = Di located 180° opposite the inlet is the most optimum. The centroid outlet has the shortcoming of vortex-induced air entrainment which can be resolved by using a larger outlet diameter ensuring crest control conditions and a spillway crest at the outlet.
- VSB operates as an open channel and energy requirements are low and can be calculated as $\frac{0.26^2}{2g} + \text{minor losses}$ considering a recommended inlet velocity of 0.26 m/s excluding the site-specific static head.

With these findings two VSB designs are proposed:

a) for an inflow of 5 l/s with 5% water loss at a 99% trapping efficiency for sediment particles as small as 75 µm in diameter and maximum inflow sediment concentration of 10,000 mg/l, and
b) for an inflow of 10 l/s with 8% water loss at a 91% trapping efficiency for sediment particles as small as 75 µm in diameter and maximum inflow sediment concentration of 10,000 mg/l.

A possible river abstraction works layout incorporating VSBs in parallel to cater for the demand is suggested for river abstraction works with a duty pump capacity of less than 100 l/s (7.2 ML/d at 20 h/d) for potable use by rural water schemes in Africa in **Figure 6-2**.

8 References

Alquier, M., Delmas, D., & Pellerej, M. (1982). Improvement of swirl concentrator. *Journal of the Environmental Engineering Division*, *108*(2), 379–390.

Andoh, R. Y. G., & Saul, A. J. (2003). The use of hydrodynamic vortex separators and screening systems to improve water quality. *Water Science and Technology*, *47*(4), 175–183.

ANSYS. (2018). ANSYS Fluent Software: CFD Simulation. Retrieved January 19, 2018, from //www.ansys.com/products/fluids/ansys-fluent

Athar, M., Jamil, M., & Ashfaq, G. (2005). A new relationship for sediment removal efficiency of vortex chamber type sediment extractor. *ISH Journal of Hydraulic Engineering*, *11*(2), 111–131. https://doi.org/10.1080/09715010.2005.10514785

Athar, M., Kothyari, U. C., & Garde, R. J. (2002a). Sediment removal efficiency of vortex chamber type sediment extractor. *Journal of Hydraulic Engineering*, *128*(12), 1051–1059. https://doi.org/10.1061/(ASCE)0733-9429(2002)128:12(1051)

Athar, M., Kothyari, U. C., & Garde, R. J. (2002b). Studies on vortex chamber type sediment extractor. *ISH Journal of Hydraulic Engineering*, *8*(2), 1–16. https://doi.org/10.1080/09715010.2002.10514711

Basson, G. R. (2006). *Considerations for the design of river abstraction works in South Africa Water Research Commission Report No TT 260/06*. Retrieved from http://www.wrc.org.za/wp-content/uploads/mdocs/TT 260-06.pdf

Bosman, D. E., Prestedge, G. K., Rooseboom, A., & Slatter, P. T. (2002). *An investigation into the removal of sediments from water intakes on rivers by means of jet-type dredge pumps Water Research Commission Report No. 1187/1/02*. Retrieved from http://www.wrc.org.za/wp-content/uploads/mdocs/TT 260-06.pdf

Bouvard, M. (1992). *Mobile barrages and intakes on sediment transporting rivers.* Rotterdam: A.A. Balkema.

Boysan, F., Ayers, W. ., & Swithenbank, J. (1982). A fundamental mathematical modelling approach to cyclone design. In *Transactions of the Institution of Chemical Engineers, London, 60(4), 222-230*. Retrieved from https://www.tib.eu/en/search/id/ceaba%3ACEAB1982226977/A-fundamental-mathematical-modelling-approach-to/

Brekke, H., Wu, Y. L., & Cai, B. Y. (2003). *Design of hydraulic machinery working in sand laden water*. https://doi.org/10.1142/9781848160026_0004

Brink, C. J., Basson, G. R., & Denys, F. (2006). *Sediment control at river abstraction works in South Africa* (Vol. 1). Water Research Commission Report No.TT 259/06.

Cecen, K. (1977). Hydraulic criteria of settling basins for water treatment, hydro-power and irrigation. *Proc. 17th Congress of the Int. Assoc of Hydr. Res., BadenBaden, West Germany*, 275–294.

Christian, F. (1999). *Exploratory experimental and theoretical studies of cyclone gasification of wood powder* (Doctoral thesis, Luleå University of Technology, Luleå, Sweden).). Retrieved from http://urn.kb.se/resolve?urn=urn:nbn:se:ltu:diva-25806

Chrysostomou, V. (1983). Vortex-type settling basin (Unpublished master's thesis). University

of Southampton, Southampton, England.

Chu, K. W., Wang, B., Xu, D. L., Chen, Y. X., & Yu, A. B. (2011). CFD–DEM simulation of the gas–solid flow in a cyclone separator. *Chemical Engineering Science*, *66*(5), 834–847. https://doi.org/10.1016/j.ces.2010.11.026

Cullivan, J. C., Williams, R. A., Dyakowski, T., & Cross, C. R. (2004). New understanding of a hydrocyclone flow field and separation mechanism from computational fluid dynamics. *Minerals Engineering*, *17*(5), 651–660. https://doi.org/10.1016/j.mineng.2004.04.009

Curi, K. V., Esen, I. I., & Velioglu, S. G. (1979). Vortex type solid-liquid separator. *Progress in Water Technology*, *7*(2), 183–190.

Gibbs, R. J., Matthews, M. D., & Link, D. A. (1971). The relationship between sphere size and settling velocity. *Journal of Sedimentary Research*, *41*(1), 7–18.

Gimbun, J., Chuah, T. G., Choong, T. S. Y., & Fakhru'l-Razi, A. (2005). A CFD study on the prediction of cyclone collection efficiency. *International Journal for Computational Methods in Engineering Science and Mechanics*, *6*(3), 161–168. https://doi.org/10.1080/15502280590923649

Green, D. D. W., & Southard, D. M. Z. (2019). *Perry's Chemical Engineers' Handbook, 9th Edition* (9th editio). Retrieved from https://www.accessengineeringlibrary.com/content/book/9780071834087

Griffiths, W. D., & Boysan, F. (1996). Computational fluid dynamics (CFD) and empirical modelling of the performance of a number of cyclone samplers. *Journal of Aerosol Science*, *27*(2), 281–304. https://doi.org/10.1016/0021-8502(95)00549-8

GritKing. (2019). Grit King | Hydro International. Retrieved September 3, 2019, from Hydro International website: https://www.hydro-int.com/en/products/grit-king

Gronowska-Szneler, M. A., & Sawicki, J. M. (2014). Simple design criteria and efficiency of hydrodynamic vortex separators. *Water Science and Technology*, *70*(3), 457–463. https://doi.org/10.2166/wst.2014.245

Gronowska, M. A. (2012). Specification of Forces in Rotational Separator. *Archives of Hydroengineering and Environmental Mechanics*, *59*(1–2), 49–62. https://doi.org/10.2478/v10203-012-0004-2

Hoekstra, A. J., Derksen, J. J., & Van Den Akker, H. E. A. (1999). An experimental and numerical study of turbulent swirling flow in gas cyclones. *Chemical Engineering Science*, *54*(13–14), 2055–2065. https://doi.org/10.1016/S0009-2509(98)00373-X

Hydraulic Institute. (2012). *Rotodynamic pumps for Pump Intake Design*. 132. Retrieved from https://webstore.ansi.org/standards/hi/ansihi2018-1730906

Interagency Committee. (1957). *Some fundamentals of particle size analysis: A study of methods used in measurement and analysis of sediment loads in streams. Report No. 12*. Retrieved from https://water.usgs.gov/fisp/docs/Report_12.pdf

Jan, C. D., Hsu, Y. C., Lin, C. H., & Zeng, Y. C. (2011). Experimental study on the effect of deflectors on sediment removal efficiency of a deep-depth vortex chamber type sediment extractor. *Journal of Taiwan Agricultural Engineering*, *57*(4), 84–96.

Jan, C. D., Hsu, Y. C., Lin, C. H., & Zeng, Y. C. (2016). Effect of cylinder heights of a deep-depth vortex chamber type sediment extractor on sediment removal efficiency: Experiments. *Journal of Taiwan Agricultural Engineering*, *62*(2), 64–79.

Keshavarzi, A. R., & Gheisi, A. R. (2006). Trap efficiency of vortex settling chamber for exclusion of fine suspended sediment particles in irrigation canals. *Irrigation and Drainage*, *55*(4), 419–434. https://doi.org/10.1002/ird.263

Knauss, J. (1987). Swirling flow problems at intakes. In *IAHR Hydraulic Structure Design Manual , Vol.1*. Rotterdam: A.A. Balkema.

Luyckx, G., & Berlamont, J. (2004). Removal efficiency of swirl/vortex separators. *Urban Water Journal*, *1*(3), 251–260. https://doi.org/10.1080/15730620410001731991

Mashauri, D. A. (1986). *Modelling of vortex settling chamber for primary clarification of water (Unpublished doctoral dissertation)*. University of Tampere, Tampare, Finland.

Morris, G. L., & Fan, J. (1998). *Reservoir sedimentation handbook: design and management of dams, reservoirs, and watersheds for sustainable use. McGraw Hill Professional*. Retrieved from https://www.hydropower.org/sediment-management/resources/publication-reservoir-sedimentation-handbook

MULTOTEC. (2018). vv-cyclones-brochure-44736.pdf. Retrieved from https://www.multotec.com/public/uploads/fileLibrary/73657-Multotec-VV-Cyclone-2015-09-Rev-02-En-L-Dig-24353.pdf

Novak, P., & Nalluri, C. (1984). Incipient motion of sediment particles over fixed beds. *Journal of Hydraulic Research*, *22*(3), 181–197. https://doi.org/10.1080/00221688409499405

NPTEL. (2018). NPTEL :: Chemical Engineering - Chemical Engineering Design - II. Retrieved November 22, 2018, from https://nptel.ac.in/courses/103103027/20

Ogihara, K., & Sakaguchi, S. (1984). New systems to seperate the sediments from the water flow by using the rotating flow. *4th Congress Asian and Pacific Divison*, 753–766. Chiangmai, Thailand: IAHR.

Paul, T. C. (1988). *Designing circulation chamber sediment extractor. Hydraulics Research Report No. OD 91, Wallingford, United Kingdom.* Retrieved from http://eprints.hrwallingford.co.uk/489/1/OD91.pdf

Paul, T. C., Sayal, S. K., Sakhuja, V. S., & Dhillon, G. S. (1991). Vortex-settling basin design considerations. *Journal of Hydraulic Engineering*, *117*(2), 172–189. https://doi.org/10.1061/(ASCE)0733-9429(1991)117:2(172)

Richardson, J. F., Harker, J. H., & Backhurst, J. R. (2002). Particle Technology and Separation Processes. In *October* (5. ed., re). https://doi.org/10.1016/0009-2509(60)80030-9

Rooseboom, A. (2002). *The extraction of water from sediment-laden streams in Southern Africa*. Retrieved from http://www.wrc.org.za/wp-content/uploads/mdocs/691-2-02.pdf

Rubey, W. W. (1933). Settling velocity of gravel, sand, and silt particles. *American Journal of Science*, *s5-25*(148), 325–338. https://doi.org/10.2475/ajs.s5-25.148.325

Salakhov, F. S. (1975). Rotational design and methods of hydraulic calculation of load-controlling water intake structures for mountain rivers. *Proceedings of Ninth Congress of the ICID, Moscow, Soviet Union*, 151–161.

Singh, G., & Kumar, A. (2016). Performance evaluation of desilting basins of small hydropower projects. *ISH Journal of Hydraulic Engineering*, *22*(2), 135–141. https://doi.org/10.1080/09715010.2015.1094750

Slack, M. D., Prasad, R. O., Bakker, A., & Boysan, F. (2000). Advances in cyclone modelling

using unstructured grids. *Chemical Engineering Research and Design*, *78*(8), 1098–1104. https://doi.org/10.1205/026387600528373

Slattery, J. C. (1999). *Advanced Transport Phenomena (Cambridge Series in Chemical Engineering). Cambridge: Cambridge University Press.* https://doi.org/10.1017/CBO9780511800238

Soo, S. L. (Shao-lee). (1990). *Multiphase fluid dynamics*. Gower Technical Press.

Sullivan, R. (1972). The swirl concentrator as a combined sewer overflow regulator facility. Office of Research and Monitoring U.S. Environmental Protection Agency, Washington, D.C. In *Report No EPA-R2-72-008,*. Retrieved from https://nepis.epa.gov/Exe/ZyPDF.cgi/9100TD0T.PDF?Dockey=9100TD0T.PDF.

Tan, Y. (1996). Design of silt related hydraulic structures. *Int Conf on Reservoir Sedimentation*.

TeaCup. (2019). Tea Cup| Hydro International. Retrieved September 3, 2019, from http://www.hydro-int.com/us/products/stormwater

Truong, N. Q. (2011). *Effect of deflectors on removal efficiency of a deep-depth vortex chamber sediment extractor*. 1–7.

USBR. (1987). *Design of Small Dams. Washington, D.C.: Water resources technical publication.* Retrieved from https://www.usbr.gov/tsc/techreferences/mands/mands-pdfs/SmallDams.pdf

Van Rijn, L. C. (1993). *Principles of sediment transport in rivers, estuaries and coastal seas* (Vol. 1006). Amsterdam: Aqua Publications.

Van Rijn, L. C. (2007). Unified view of sediment transport by currents and waves. I: Initiation of motion, bed roughness, and bed-load transport. *Journal of Hydraulic Engineering*, *133*(6), 649–667. https://doi.org/10.1061/(ASCE)0733-9429(2007)133:6(649)

Veerapen, J. P., Lowry, B. J., & Couturier, M. F. (2005). Design methodology for the swirl separator. *Aquacultural Engineering*, *33*(1), 21–45. https://doi.org/10.1016/j.aquaeng.2004.11.001

Versteeg, H. K., Malalasekera, W. (2007). *An Introduction to Computational Fluid Dynamics*. Harlow, UK: Pearson Education Limited.

Zhiyao, S., Tingting, W., Fumin, X., & Ruijie, L. (2008). A simple formula for predicting settling velocity of sediment particles. *Water Science and Engineering*, *1*(1), 37–43. https://doi.org/10.1016/S1674-2370(15)30017-X

9 Appendix A

9.1 Experimental data

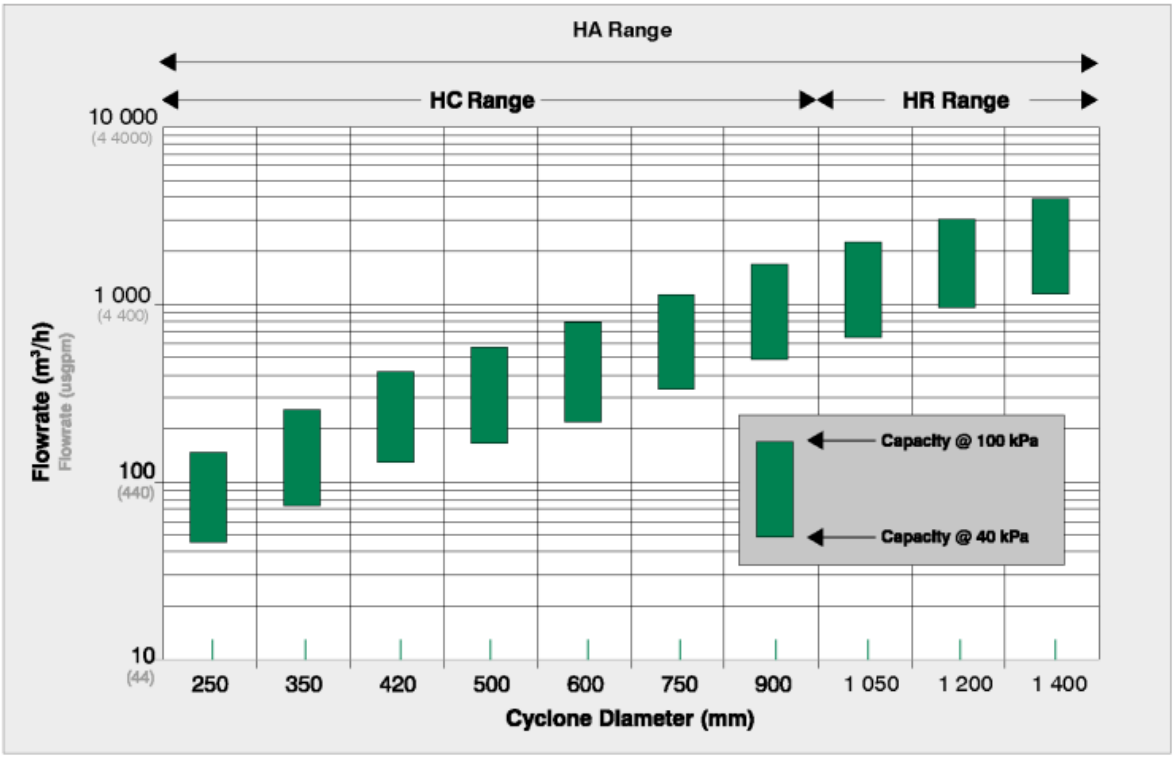

a) MULTOTEC (2018) hydro-cyclone capacity

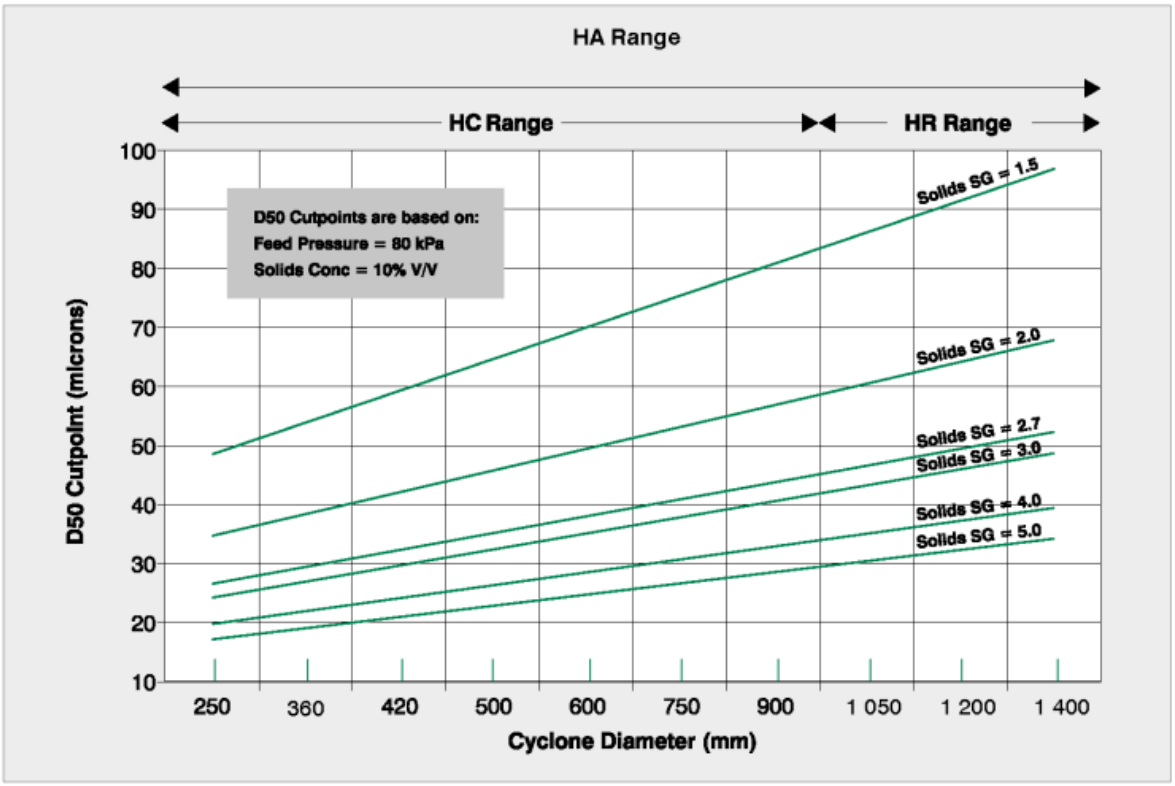

a) MULTOTEC (2018) diameter cut off point

Appendix A1: Illustration of hydro-cyclone selection charts MULTOTEC (2018)

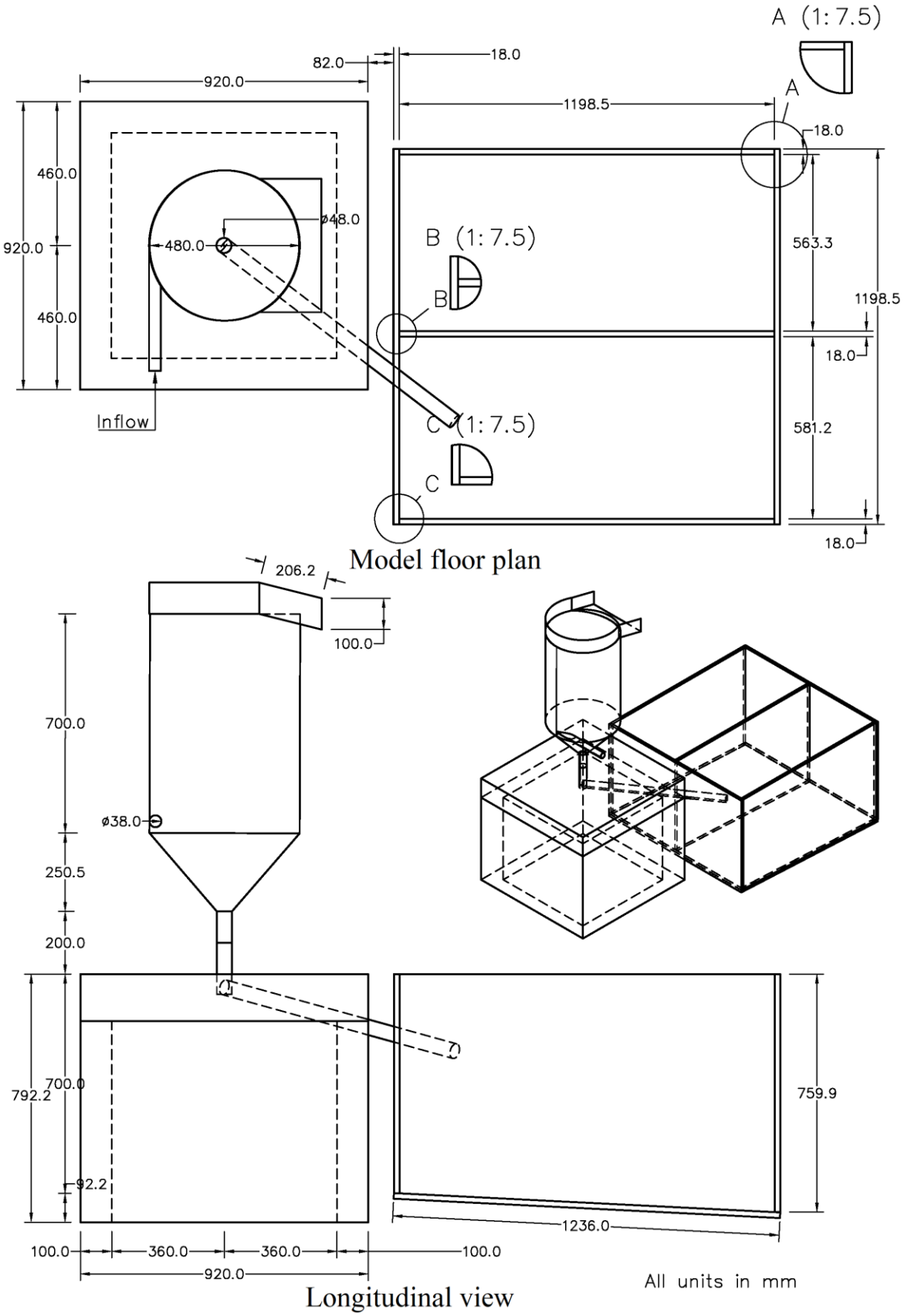

Appendix A2:Detailed Model 1 plan and longitudinal view

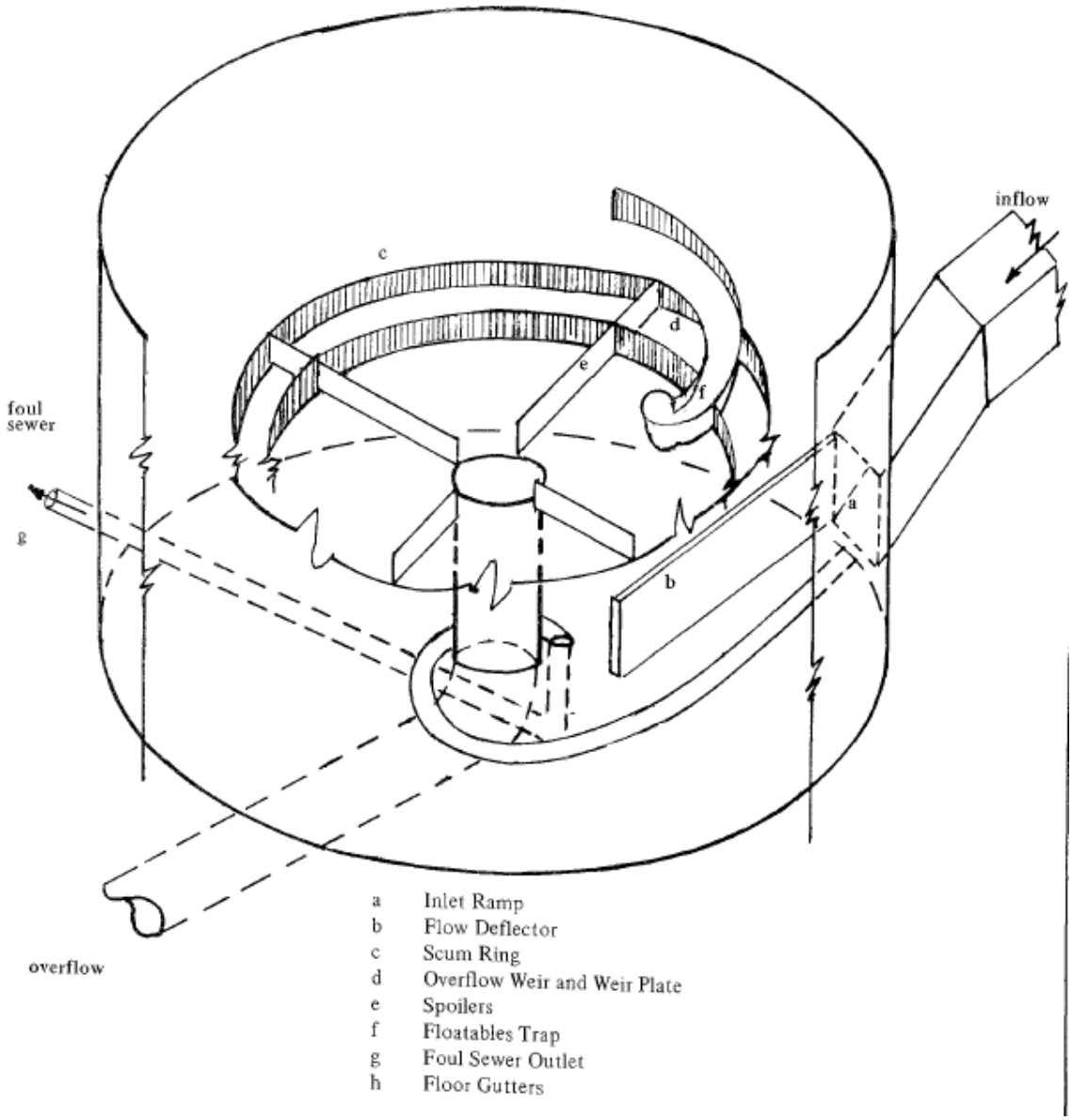

Appendix A3: Isometric view of swirl concentrator (Sullivan, 1972)

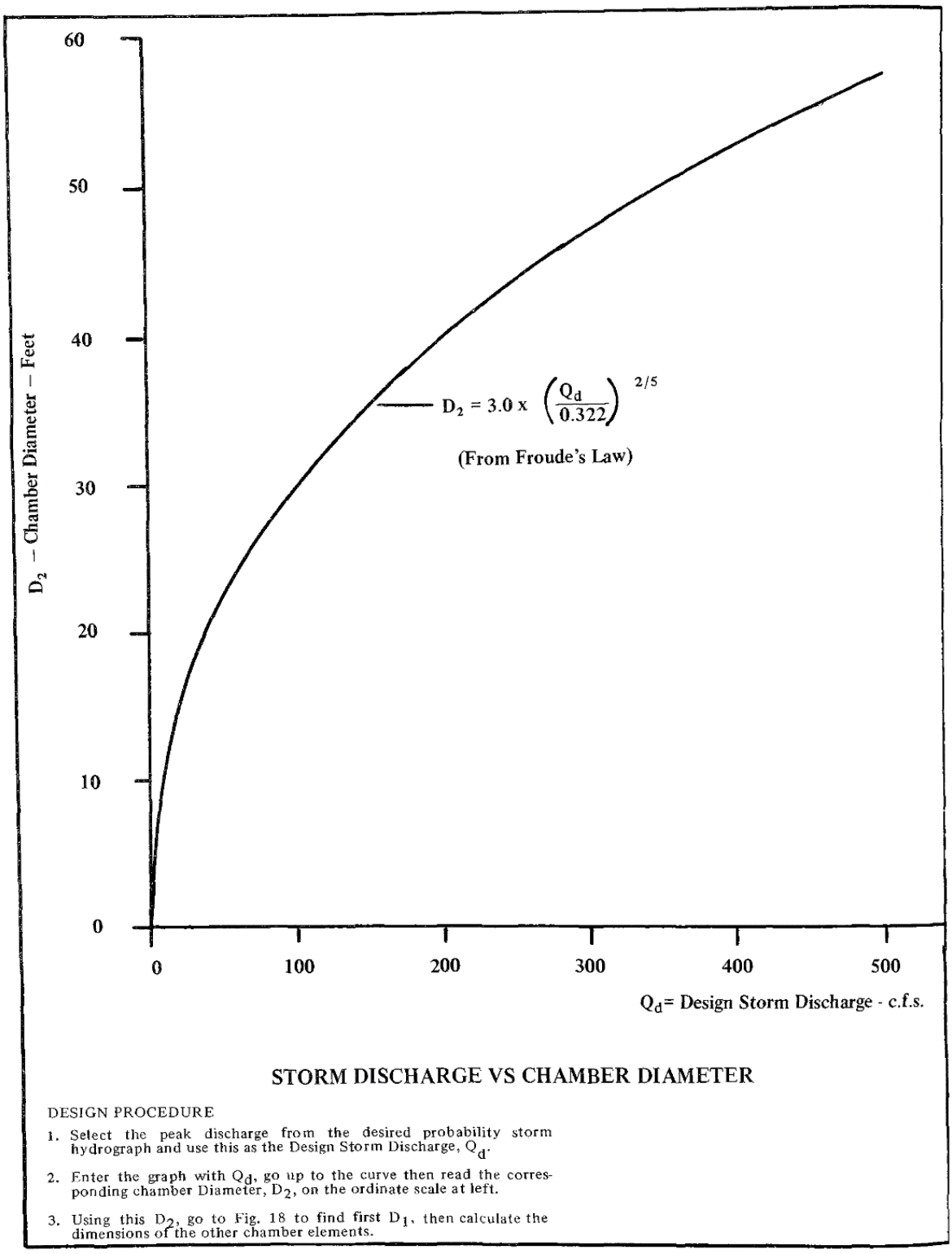

Appendix A4: Storm discharge vs chamber diameter (Sullivan, 1972)

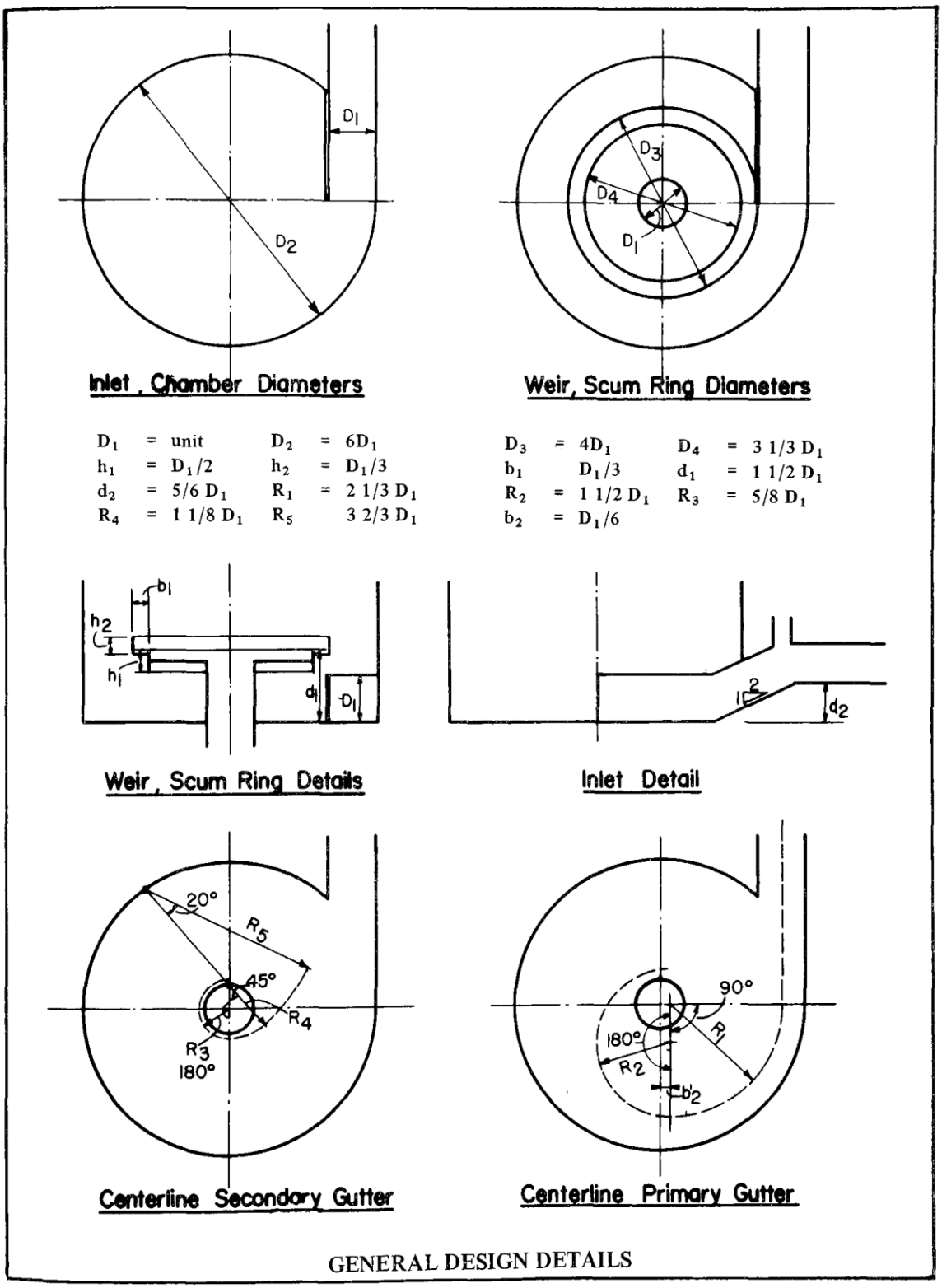

Appendix A5: General design details (Sullivan, 1972)

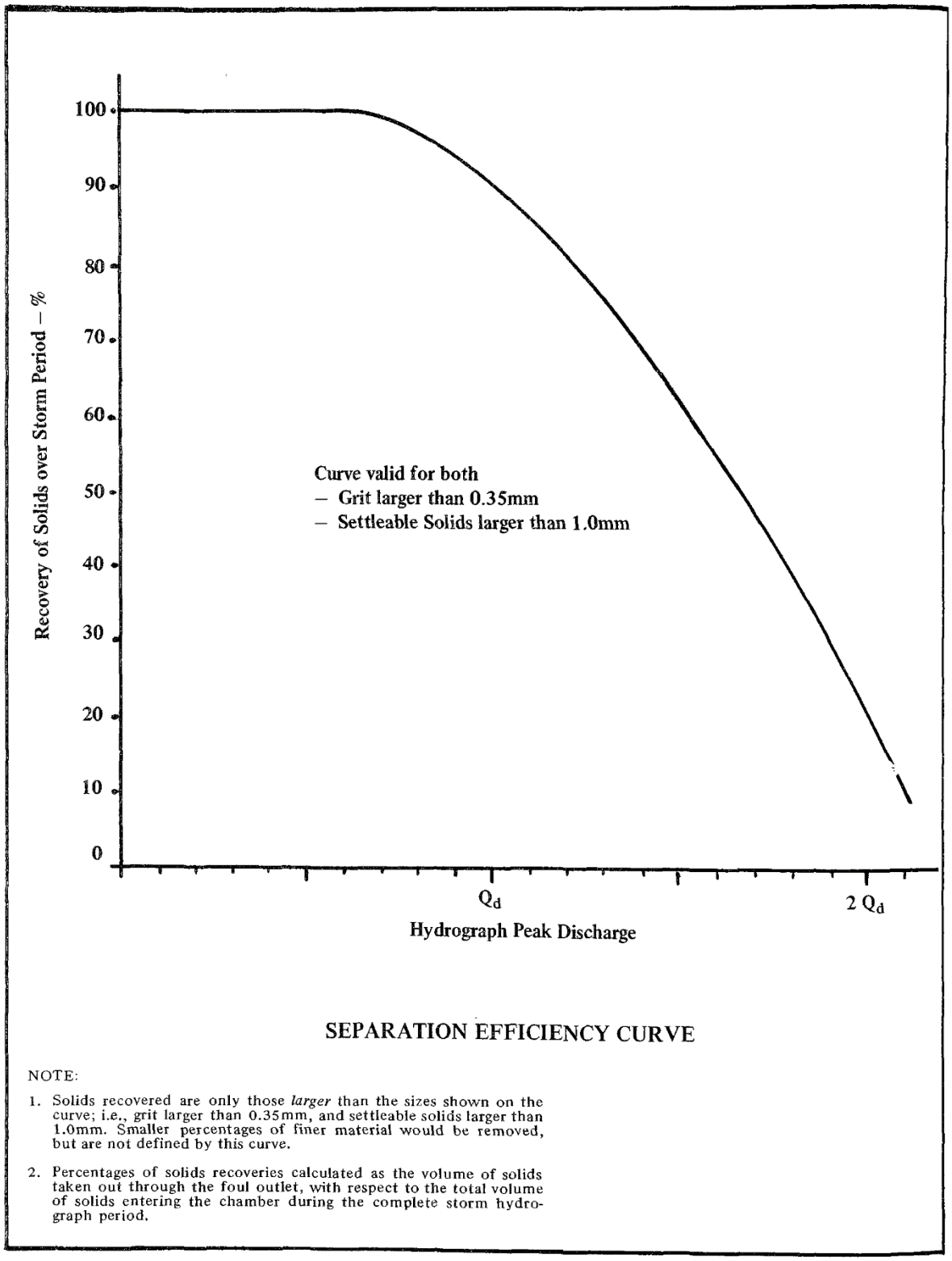

SEPARATION EFFICIENCY CURVE

NOTE:

1. Solids recovered are only those *larger* than the sizes shown on the curve; i.e., grit larger than 0.35mm, and settleable solids larger than 1.0mm. Smaller percentages of finer material would be removed, but are not defined by this curve.

2. Percentages of solids recoveries calculated as the volume of solids taken out through the foul outlet, with respect to the total volume of solids entering the chamber during the complete storm hydrograph period.

Appendix A6: Separation efficiency curve (Sullivan, 1972)

9.2 Experimental data results

Appendix A7: Summary of outlet location influence on sediment removal efficiency Model 1 numerical results

Sediment size	**d50: 112 µm**	**100 µm**	**75 µm**
Outlet angle location variation	**120° sector outlet efficiency (%)**	**120° sector outlet efficiency (%)**	**120° sector efficiency (%)**
250	80	76	60
190	77	74	60
130	77	75	60
70	78	76	61
0	81	78	60
Outlet angle location variation	**60° sector outlet efficiency (%)**	**60° sector outlet efficiency (%)**	**60° sector efficiency (%)**
300	81	77	63
270	78	75	61
240	76	72	61
210	77	77	61
180	76	74	60
150	76	72	59
120	74	68	59
90	76	71	58
60	79	74	61
30	81	76	60
0	83	76	62

Appendix A8: Summary of deflector 1 model parameters

Test	Di (mm)	Du (mm)	Qi (l/s)	Qu (l/s)	Qu/Qi	h1 (mm)	$Ø_{c1}$	$Ø_{ac1}$	d1 (mm)	d50:112 µm	100 µm	75 µm
1	53	5	1.0	0.08	0.08	62	0	60	240	78%	72%	55%
2	53	5	1.0	0.08	0.08	62	120	60	240	78%	77%	51%
3	53	5	1.0	0.08	0.08	62	150	60	240	82%	77%	62%
4	53	5	1.0	0.08	0.08	62	160	60	240	87%	85%	68%
5	53	5	1.0	0.08	0.08	62	170	60	240	80%	79%	65%
6	53	5	1.0	0.08	0.08	62	190	60	240	85%	84%	67%
7	53	5	1.0	0.08	0.08	62	0	60	240	78%	72%	55%
8	53	5	1.0	0.08	0.08	62	60	160	220	81%	81%	67%
9	53	5	1.0	0.08	0.08	62	60	160	240	86%	85%	68%
10	53	5	1.0	0.08	0.08	62	60	160	280	79%	78%	63%
11	53	5	1.0	0.08	0.08	62	60	160	400	79%	77%	54%

Appendix A9: Summary of deflector 1-2 model parameters

Test	Di (mm)	Du (mm)	Qi(l/s)	Qu (l/s)	Qu/Qi	h2 (mm)	$Ø_{c2}$	$Ø_{ac2}$	d2 (mm)	d50:112 µm	100 µm	75 µm
12	53	5	1.0	0.08	0.08	162	40	140	280	94%	95%	82%
13	53	5	1.0	0.08	0.08	162	40	150	280	95%	97%	82%
14	53	5	1.0	0.08	0.08	162	40	160	280	94%	96%	83%
15	53	5	1.0	0.08	0.08	162	40	170	280	93%	96%	84%
16	53	5	1.0	0.08	0.08	162	40	180	280	92%	98%	84%
17	53	5	1.0	0.08	0.08	162	40	190	280	95%	98%	82%
18	53	5	1.0	0.08	0.08	162	40	200	280	93%	97%	82%
19	53	5	1.0	0.08	0.08	162	50	180	280	95%	98%	83%
20	53	5	1.0	0.08	0.08	162	30	180	280	94%	98%	84%
21	53	5	1.0	0.08	0.08	162	40	180	240	93%	97%	80%
22	53	5	1.0	0.08	0.08	162	40	180	320	94%	95%	79%

Appendix A10: Summary of deflector 1-2-3 model parameters

Test	Di (mm)	Du (mm)	Qi(l/s)	Qu (l/s)	Qu/Qi	h3 (mm)	$Ø_{c3}$	$Ø_{ac3}$	d3 (mm)	d50:112 µm	100 µm	75 µm
23	53	5	1.0	0.08	0.08	262	180	40	400	94%	98%	85%
24	53	5	1.0	0.08	0.08	262	180	50	400	94%	97%	85%
25	53	5	1.0	0.08	0.08	262	190	40	400	95%	97%	84%
26	53	5	1.0	0.08	0.08	262	200	40	400	95%	97%	85%
27	53	5	1.0	0.08	0.08	1000	200	40	400	89%	48%	36%
28	53	5	1.0	0.08	0.08	262	40	180	400	95%	97%	36%
29	53	5	1.0	0.08	0.08	262	40	200	400	93%	98%	82%
30	53	5	1.0	0.08	0.08	262	-100	-130	400	93%	94%	77%

Appendix A11:Summary of deflector 1-2-3-4-5 model parameters

Test	Di (mm)	Du (mm)	Qi (l/s)	Qu (l/s)	Qu/Qi	h4 (mm)	$Ø_{c4}$	$Ø_{ac4}$	d4 (mm)	d50:112 µm	100 µm	75 µm
31	53	5	1.0	0.08	0.08	362	60	180	400	93%	99%	83%
32	53	5	1.0	0.08	0.08	362	60	180	320	95%	98%	87%
Test	**Di (mm)**	**Du (mm)**	**Qi (l/s)**	**Qu(l/s)**	**Qu/Qi**	**h5 (mm)**	**$Ø_{c5}$**	**$Ø_{ac5}$**	**d5 (mm)**	**d50:112 µm**	**100 µm**	**75 µm**
33	53	5	1.0	0.08	0.08	612	60	180	320	99%	100%	90%

Appendix A12: Summary of outlet structure Model 2 numerical model results.

Test	Hi (mm)	Outlet diameter (mm)	L (mm)	b (mm)	h2 (mm)	h1 (mm)	angle	Outlet length (mm)	d50:112 µm		100µm	75µm
									Numerical	Physical		
b1	600	90x63	200	160	80	40	180	100x100	86%	84%	87%	69%
b2	600	90x63	200	160	80	5	275	100x100	82%		86%	66%
b3	600	90x83	160	160	80	5	180	80x80	84%		85%	64%
b4	800	90x63	200	160	80	5	180	100x100	85%	83%	86%	70%
c1	600	90	200	160	95	5	90	100x100	74%		65%	49%
c2	600	90	200	160	95	5	0	100x100	75%		68%	51%
d1	600		100x200	80	80	5	90	100x200	74%		66%	48%
d2	600		100x100	80	80	5	90	100x100	74%		65%	48%

Appendix A13: Summary of Model 2 deflector results

Test	Di (mm)	D_u (mm)	Q_i (l/s)	Q_u (l/s)	Qu/Qi	H (mm)	clockwise	anticlockwise	d (mm)	d50:112 µm	100 µm	75 µm
34	156	12	4.965	0.559	0.113	1605	160	70	475	89%	92%	75%
35	156	12	4.965	0.559	0.113	1605	180	70	475	90%	94%	75%
36	156	12	4.965	0.559	0.113	1605	210	70	475	88%	93%	67%
37	156	12	4.965	0.559	0.113	1605	180	70	320	82%	85%	64%

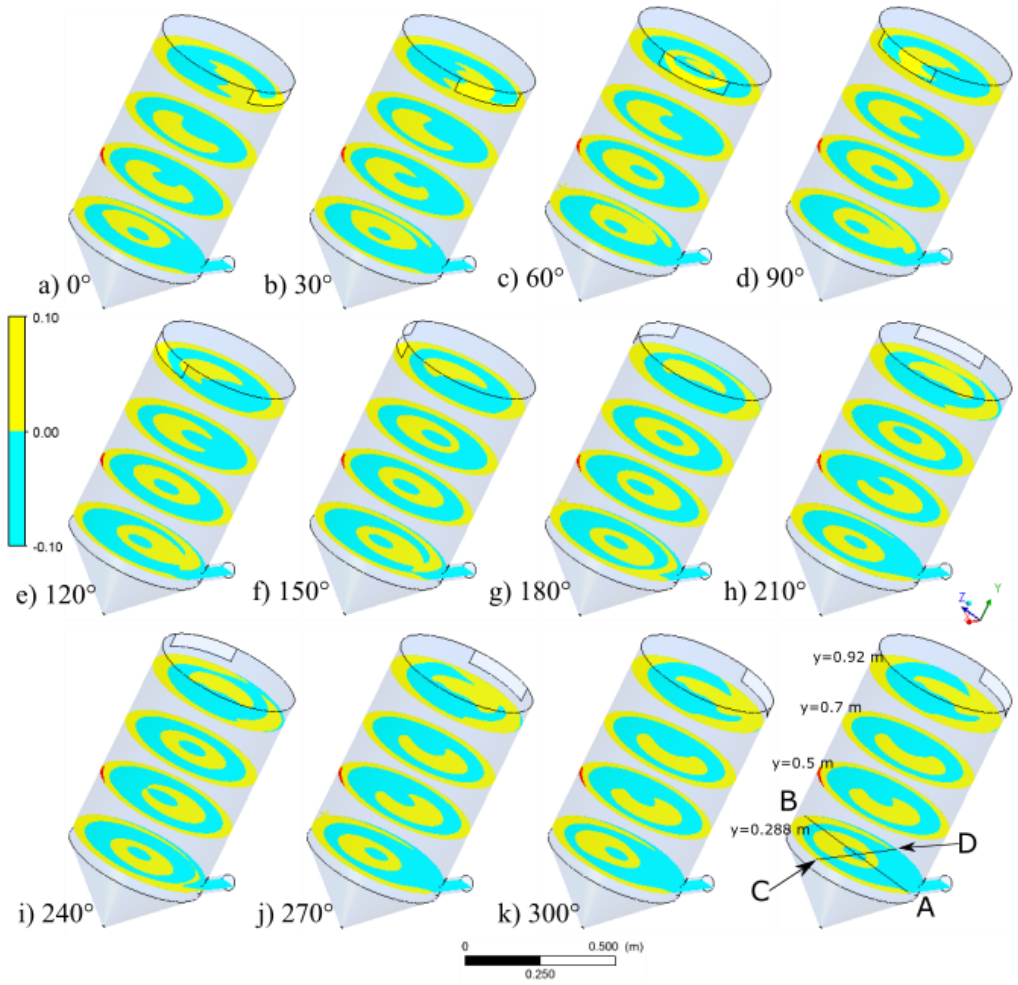

Appendix A14: Model 1 numerical model average axial velocity contours of 60° sector with incremental angle from 0° to 300° on the z-x plane at y = 0.288 m, y = 0.5 m, y = 0.7 m and y = 0.92 m (cyan: downward movement of water, yellow/red: rising water)

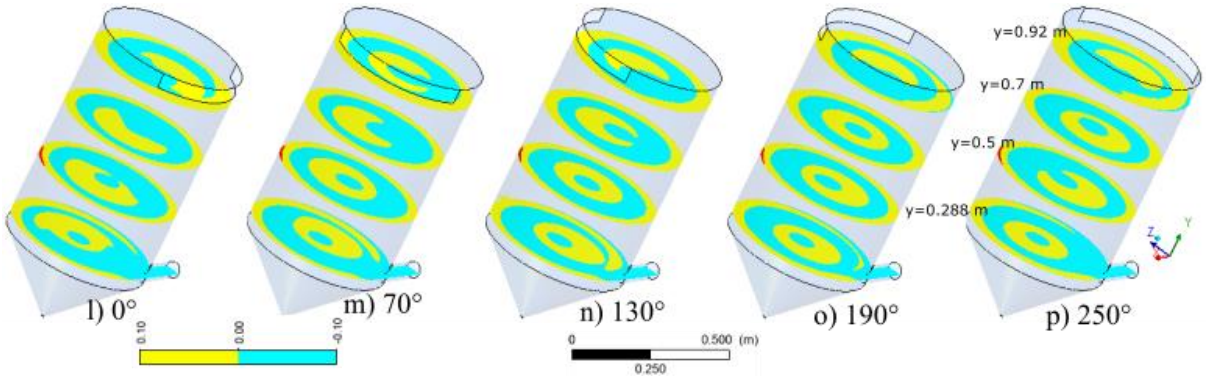

Appendix A15: Model 1 numerical model average axial velocity contours of 120° sector with incremental angle from 0° to 250° on the z-x plane at y = 0.288 m, y = 0.5 m, y = 0.7 m and y = 0.92 m (cyan: downward movement of water, yellow/red: rising water)

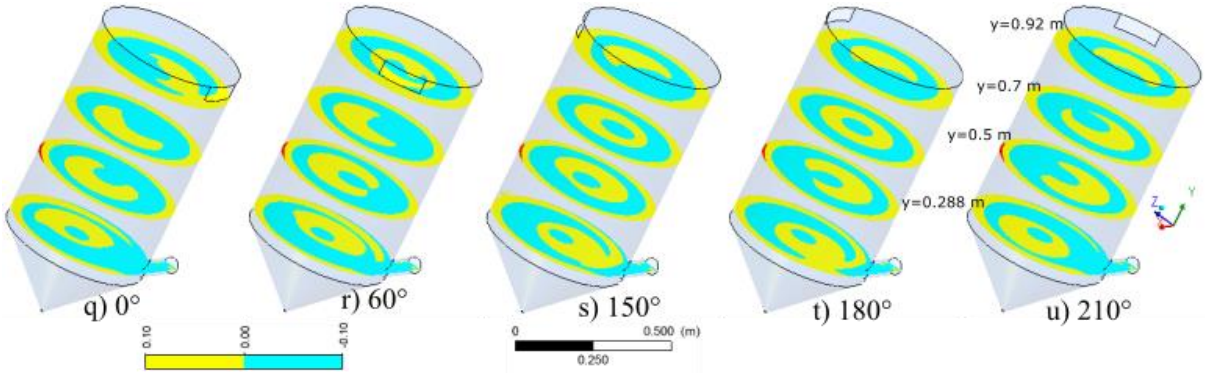

Appendix A16: Model 1 numerical model average axial velocity contours of 35° sector with incremental angle from 0° to 210° on the z-x plane at y = 0.288 m, y = 0.5 m, y = 0.7 m and y = 0.92 m (cyan: downward movement of water, yellow/red: rising water)

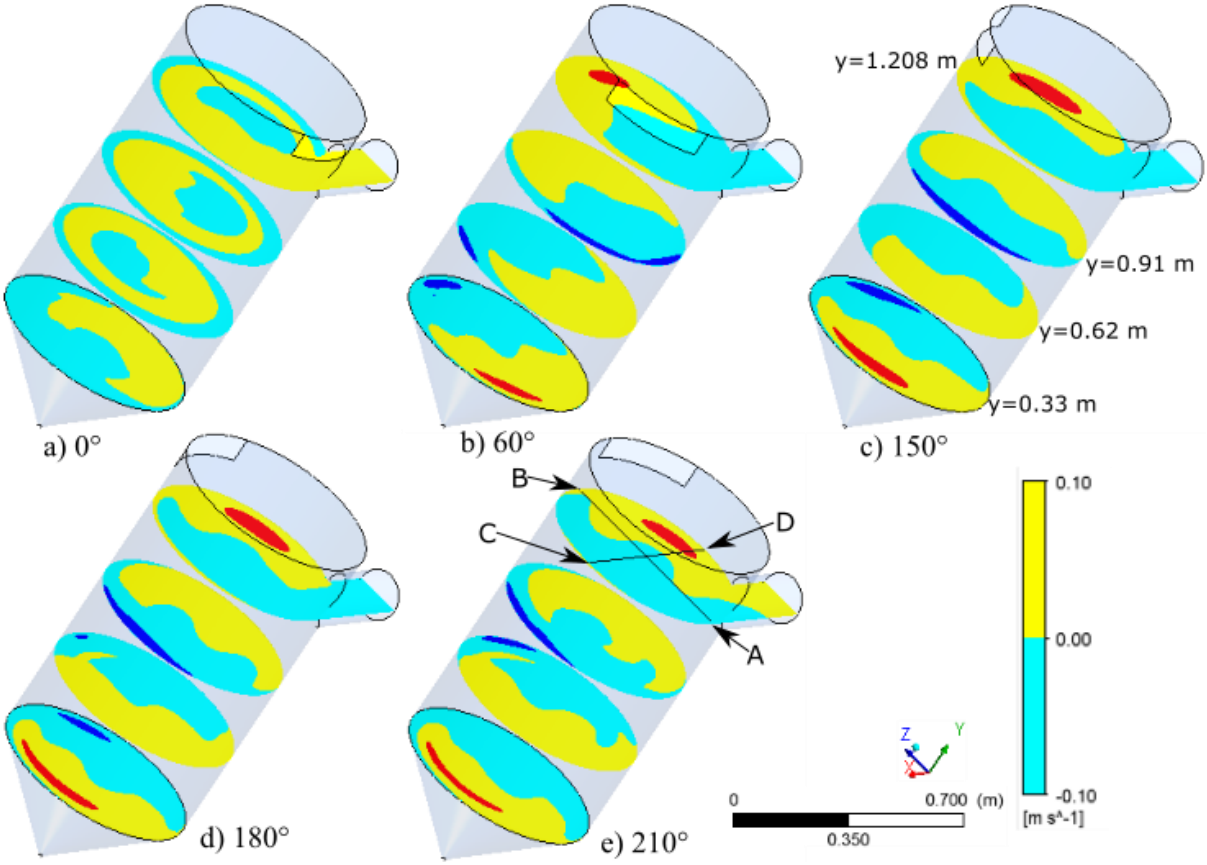

Appendix A17: Model 2 numerical model average axial velocity contours of 60° sector with incremental angle from 0° to 210° on the z-x plane at y = 0.33 m, y = 0.62 m, y = 0.91 m and y = 1.208 m (cyan/blue: downward movement of water, yellow/red: rising water)

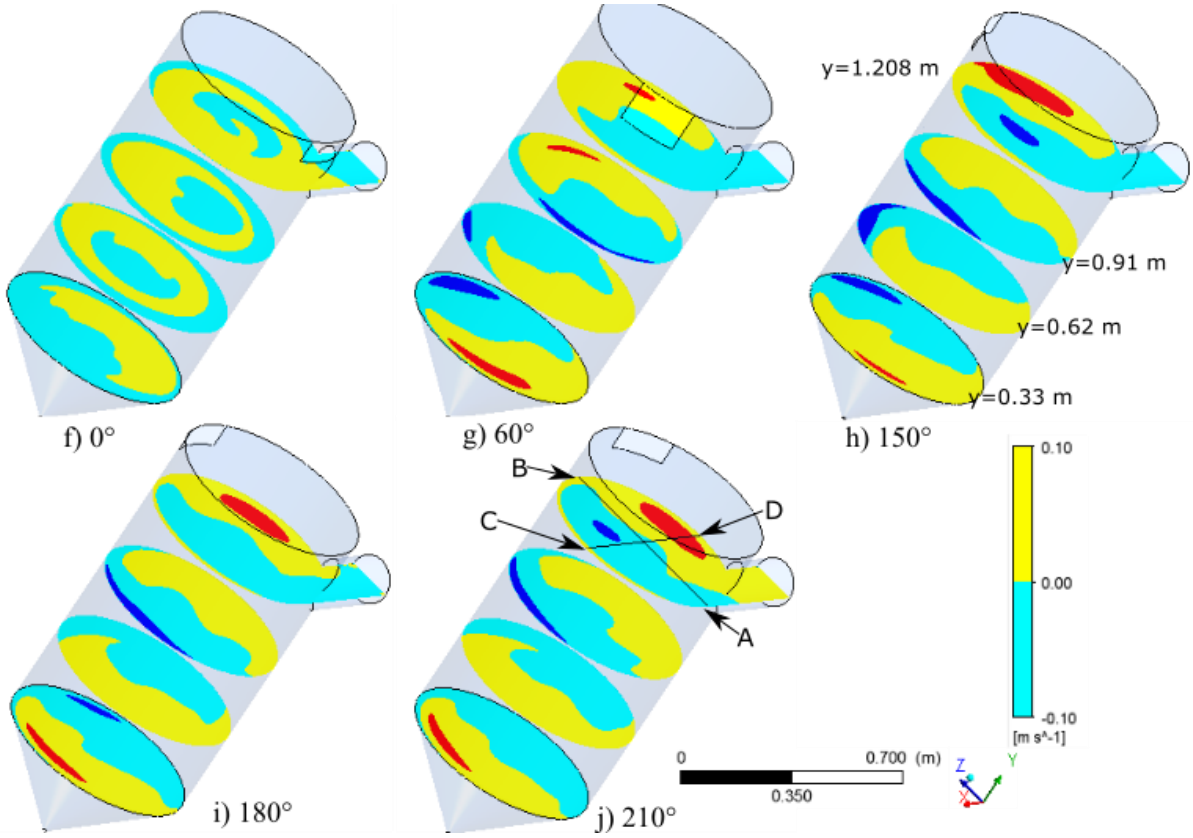

Appendix A18: Model 2 numerical model average axial velocity contours of 35° sector with incremental angle from 0° to 210° on the z-x plane at y = 0.33 m, y = 0.62 m, y = 0.91 m and y = 1.208 m (cyan/blue: downward movement of water, yellow/red: rising water)

9.3 Design of drop inlet

a) By iteration approximate design head H_o and outlet crest radius, Rs from **Appendix A20** and **Appendix A22** to discharge the required flow. For free-flowing flow $\frac{H_o}{R_s}$<0.45 and full submergence for $\frac{H_o}{R_s} \approx 1$. $\frac{H_o}{R_s}$=0.3 is recommended.

b) Determine a discharge rating curve for other heads using **Appendix A23**.

c) Use **Appendix A20**, **Appendix A21** and table **Appendix A24** to determine the nappe profile.

d) Determine throat control using equation **Appendix A19**. Throat control exists when R is greater than shaft radius for a given discharge and Ha

$$R = C_R \frac{Q^{0.5}}{H_a^{0.25}} \qquad \text{Appendix A19}$$

Where R: Radius, C_R=0.275 for metric units and 0.204 for imperial units.

e) Design the outlet conduit for a 75% partially full pipe.

f) Check the water level profile along the pipe using Bernoulli's theorem and re - calculate if necessary.

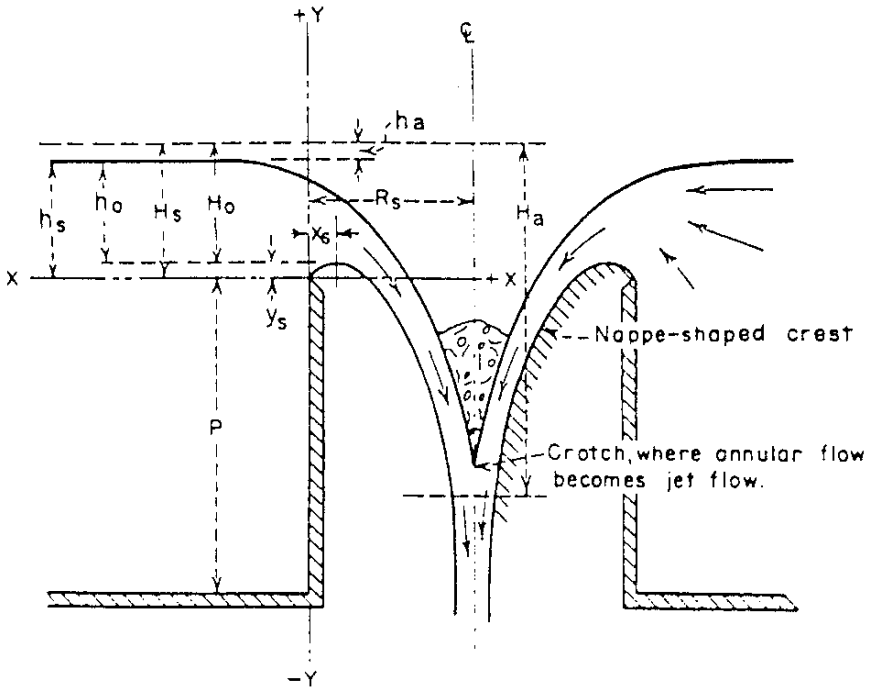

Appendix A20: Elements of nappe-shaped profile for a shaft outlet (USBR, 1987)

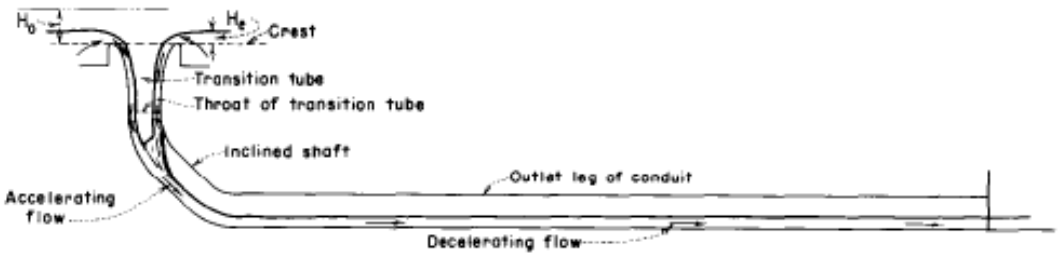

CONDITION 1. CREST CONTROL

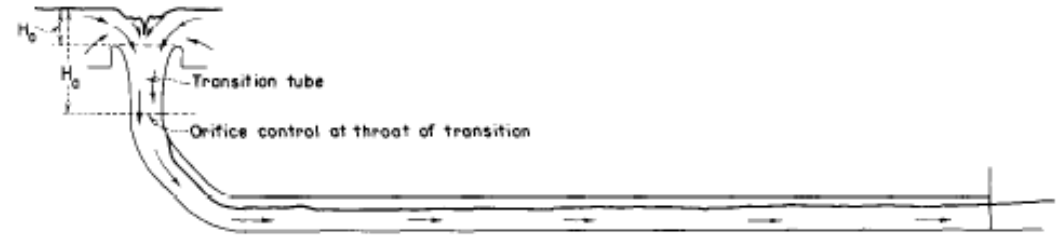

CONDITION 2. TUBE OR ORIFICE CONTROL

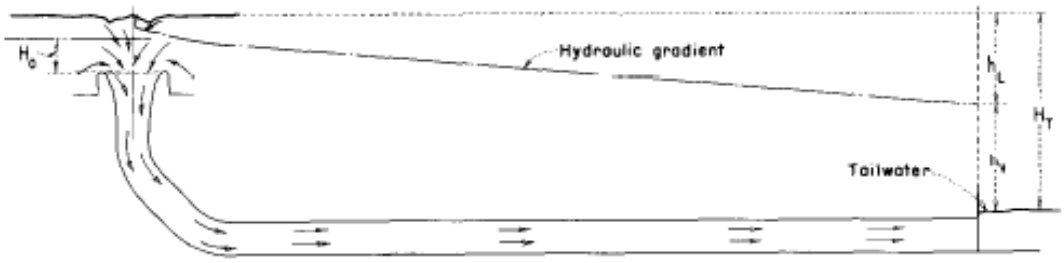

CONDITION 3. FULL PIPE FLOW

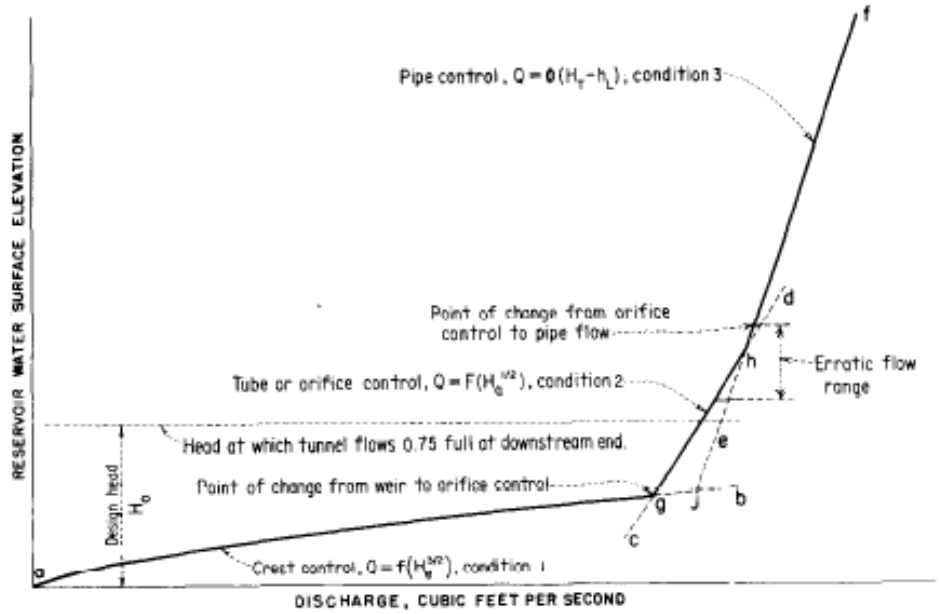

Appendix A21: Discharge characteristics of shaft outlet (USBR, 1987)

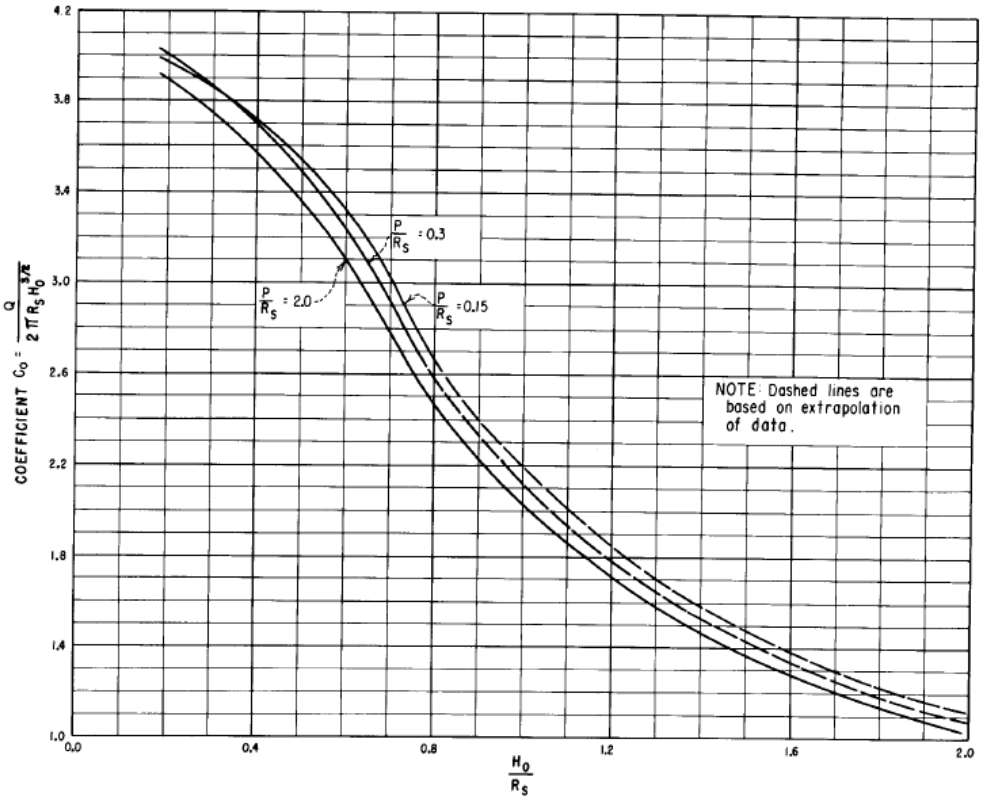

Appendix A22: Circular crest coefficients for a shaft outlet with aerated nappe, Co to be multiplied with 0.552 to convert to metric (USBR, 1987)

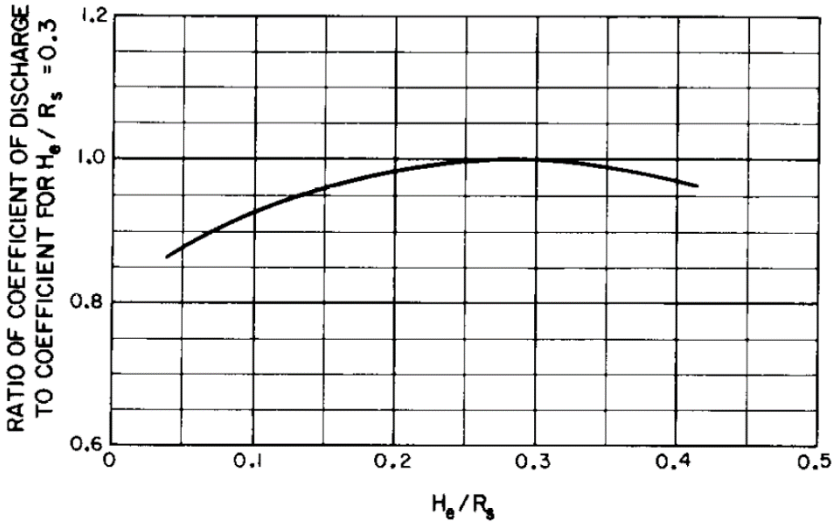

Appendix A23: Circular crest coefficients of discharge for other than design head (USBR, 1987)

Appendix A24: Cordinates of lower nappe surface for different values of H_s/R_s when P/Rs = 0.15 (USBR, 1987)

H_s/R_s	0.20	0.25	0.30	0.35	0.40	0.45	0.50	0.60	0.80
X/H_s	Y/H_s for portion of profile above weir crest								
0.000	0.0000	0.0000	0.0000	0.0000	0.0000	0.0000	0.0000	0.0000	0.0000
.010	.0120	.0120	.0115	.0115	.0110	.0110	.0105	.0100	.0090
.020	.0210	.0200	.0195	.0190	.0185	.0180	.0170	.0160	.0140
.030	.0285	.0270	.0265	.0260	.0250	.0235	.0225	.0200	.0165
.040	.0345	.0335	.0325	.0310	.0300	.0285	.0265	.0230	.0170
.050	.0405	.0385	.0375	.0360	.0345	.0320	.0300	.0250	.0170
.060	.0450	.0430	.0420	.0400	.0380	.0355	.0330	.0265	.0165
.070	.0495	.0470	.0455	.0430	.0410	.0380	.0350	.0270	.0150
.080	.0525	.0500	.0485	.0460	.0435	.0400	.0365	.0270	.0130
.090	.0560	.0530	.0510	.0480	.0455	.0420	.0370	.0265	.0100
.100	.0590	.0560	.0535	.0500	.0465	.0425	.0375	.0255	.0065
.120	.0630	.0600	.0570	.0520	.0480	.0435	.0365	.0220	
.140	.0660	.0620	.0585	.0525	.0475	.0425	.0345	.0175	
.160	.0670	.0635	.0590	.0520	.0460	.0400	.0305	.0110	
.180	.0675	.0635	.0580	.0500	.0435	.0365	.0260	.0040	
.200	.0670	.0625	.0560	.0465	.0395	.0320	.0200		
.250	.0615	.0560	.0470	.0360	.0265	.0160	.0015		
.300	.0520	.0440	.0330	.0210	.0100				
.350	.0380	.0285	.0165	.0030					
.400	.0210	.0090							
.450	.0015								
.500									
.550									
Y/H_s	X/H_s for portion of profile below weir crest								
−0.000	0.454	0.422	0.392	0.358	0.325	0.288	0.253	0.189	0.116
−.020	.499	.467	.437	.404	.369	.330	.292	.228	.149
−.040	.540	.509	.478	.444	.407	.368	.328	.259	.174
−.060	.579	.547	.516	.482	.443	.402	.358	.286	.195
−.080	.615	.583	.550	.516	.476	.434	.386	.310	.213
−.100	.650	.616	.584	.547	.506	.462	.412	.331	.228
−.150	.726	.691	.660	.620	.577	.526	.468	.376	.263
−.200	.795	.760	.729	.685	.639	.580	.516	.413	.293
−.250	.862	.827	.790	.743	.692	.627	.557	.445	.319
−.300	.922	.883	.843	.797	.741	.671	.594	.474	.342
−.400	1.029	.988	.947	.893	.828	.749	.656	.523	.381
−.500	1.128	1.086	1.040	.980	.902	.816	.710	.567	.413
−.600	1.220	1.177	1.129	1.061	.967	.869	.753	.601	.439
−.800	1.380	1.337	1.285	1.202	1.080	.953	.827	.655	.473
−1.000	1.525	1.481	1.420	1.317	1.164	1.014	.878	.696	.498
−1.200	1.659	1.610	1.537	1.411	1.228	1.059	.917	.725	.517
−1.400	1.780	1.731	1.639	1.480	1.276	1.096	.949	.750	.531
−1.600	1.897	1.843	1.729	1.533	1.316	1.123	.973	.770	.544
−1.800	2.003	1.947	1.809	1.580	1.347	1.147	.997	.787	.553
−2.000	2.104	2.042	1.879	1.619	1.372	1.167	1.013	.801	.560
−2.500	2.340	2.251	2.017	1.690	1.423	1.210	1.049	.827	
−3.000	2.550	2.414	2.105	1.738	1.457	1.240	1.073	.840	
−3.500	2.740	2.530	2.153	1.768	1.475	1.252	1.088		
−4.000	2.904	2.609	2.180	1.780	1.487	1.263			
−4.500	3.048	2.671	2.198	1.790	1.491				
−5.000	3.169	2.727	2.207	1.793					
−5.500	3.286	2.769	2.210						
−6.000	3.396	2.800							
H_s/R_s	0.20	0.25	0.30	0.35	0.40	0.45	0.50	0.60	0.80